Causes and Consequences of Centrosome Amplification in Cancer

By

Ryan Austin Denu

A dissertation submitted in partial fulfillment of

the requirements for the degree of

Doctor of Philosophy

(Cellular and Molecular Biology)

at the

UNIVERSITY OF WISCONSIN-MADISON

2018

Date of final oral examination: 04/30/2018

The dissertation is approved by the following members of the Final Oral Committee:

Mark E. Burkard, MD, PhD, Associate Professor, Medicine
Fotis Asimakopoulos, MD, PhD, Associate Professor, Medicine
Joshua Lang, MD, MS, Assistant Professor, Medicine
Gary Lyons, PhD, Professor, Cell and Regenerative Biology
David Wassarman, PhD, Professor, Cell and Regenerative Biology

TABLE OF CONTENTS

ABSTRACT

Causes and Consequences of Centrosome Amplification in Cancer

Ryan A Denu

Under the supervision of Professor Mark E Burkard

At the University of Wisconsin-Madison

The centrosome is the major microtubule organizing center of animal cells and consists of two orthogonally-positioned centrioles surrounded by a complex network of proteins called the pericentriolar material. Centrosome amplification (CA), or the numerical increase of centrosomes, occurs in many human cancers and correlates with worse outcomes. However, the causes and consequences of centrosome amplification in cancer have been underexplored. Herein, I attempt to fill this crucial gap in knowledge.

CA can arise by either centriole overduplication or cell doubling events (e.g. cytokinesis failure or cell-cell fusion). The relative contribution of these mechanisms has been unclear. Herein I attempt to answer this question by assessing centrioles in human cancer tissue. We find that centriole overduplication is the predominant mechanism leading to CA. Given this, we attempt to identify the molecular drivers of centriole overduplication in human cancer. To that end, we investigate genomic and transcriptomic alterations in the 366 known centrosome proteins. We identify the most commonly altered centrosome genes in human cancer using publicly-available data sets and test

these *in vitro*. We find that genomic deletion of MCPH1 is a common and penetrant cause of CA in human cancer.

Given that CA is very specific to cancer cells, it represents a potentially good therapeutic target for treating cancer. To that end, we examined the cellular and physiological consequences of CA. As previously shown, we observe that CA induces mitotic errors, including an increase in multipolar spindles and lagging chromosomes. Furthermore, we find that CA impairs autophagy, the cell's recycling pathway, rendering cells with CA more susceptible to autophagy inhibition.

As PLK4 is a potential driver of CA in human cancer and a potential drug target to better treat human cancer, we engineered a PLK4 analog sensitive human epithelial cell line to interrogate PLK4 signaling. We identify many putative substrates of PLK4, including known substrates CEP152 and PCM1, in addition to unknown substrates. We find that PLK4 phosphorylates CEP131 S78 to control the integrity of centriolar satellites. Centriolar satellites are protein-rich granules that surround the centrosome and regulate protein movement to and from the centrosome. Further, we identify CEP170 and CDK5RAP2 as substrates of PLK4.

Lastly, we explore centriolar satellites in human cancer by assessing genomic and transcriptomic alterations in the 44 known centriolar satellite proteins. We identify genomic deletions. To model this, we engineered PCM1 knockout cells, and find that these cells have greater rates of multipolar spindles and lagging chromosomes. Furthermore, PCM1 knockout cells are more sensitive to autophagy inhibitors, consistent with our findings in cells with CA.

Overall, this work expands our knowledge of centrosome biology and PLK4 signaling at the centrosome. Furthermore, this work has identified some of the major causes and consequences of CA in human cancer.

ACKNOWLEDGEMENTS

This work is mostly a testament to the great people I am so fortunate to have in my life, both professionally and personally.

To my great teachers from the past, who helped me to fall in love with science, helped me to think critically, helped me to write, challenged me, and nurtured me. I thank Peiman Hematti for giving me the opportunity to explore research as an undergraduate and for helping me find the path to the MSTP. I also thank my uncle and mentor, John Denu, for encouraging me to explore research and helping me to think more like a scientist.

To my collaborators, thank you for lending your incredible talents. I have learned so much from you, and your efforts have significantly enriched this thesis.

To our cancer patients at the University of Wisconsin Carbone Cancer Center. Thank you for sharing your stories and allowing me to participate in your care. Thank you for the inspiration and motivation to persevere and to work toward finding better ways to treat cancer.

To my thesis committee: Fotis, Josh, Gary, and David. Thank you for your commitment of time, attention, and rigor. Thank you for instilling in me the importance of focusing and delving deeply into the problem at hand.

To the members of the Mark Burkard Research Group and Beth Weaver Lab, I thank you for your energy and passion, your critiques and advice at lab meetings, the fun times outside of the lab, and for making our lab community an overall enjoyable place to work.

To my advisor, Mark, I will forever be indebted to the opportunity you have afforded me to join the MSTP and to work in your lab. I hope I did not disappoint. Thank you for helping to hone my energy and excitement into focused, deep, and mechanistic projects. Thank you for your optimism, energy, and leadership along the way.

To my parents, Mark and Shirley Denu, and my brother, Andrew Denu, for their unwavering support, devotion, sacrifice, and cheerleading my whole life.

Finally, thank you to my wife, Stefanie, for supporting and refreshing me during graduate school and for teaching me the importance of rest and taking care of myself. I cannot possibly make up for all the time that I have not been with you during this journey, but I will try.

LIST OF ABBREVIATIONS

AS	Analog sensitive
ATP	Adenosine triphosphate
CA	Centrosome amplification
CBB	Coomassie brilliant blue
CIN	Chromosomal instability
CRISPR	Clustered regularly interspaced short palindromic repeats
DAPI	4’,6-diamidino-2-phenylindole
DNA	Deoxyribonucleic acid
GFP	Green fluorescent protein
gRNA	Guide ribonucleic acid
mRNA	Messenger ribonucleic acid
MT	Microtubule
MTOC	Microtubule organizing center
PBD	Polo-box domain
PCM	Pericentriolar material
PI	Propidium iodide
PLK1	Polo-like kinase 1
PLK4	Polo-like kinase 4
RNA	Ribonucleic acid
RNAi	Ribonucleic acid interference
siRNA	Small interfering ribonucleic acid
shRNA	Short hairpin ribonucleic acid

TCGA	The Cancer Genome Atlas
TNBC	Triple negative breast cancer
WT	Wild type

CHAPTER 1: Introduction

Historical Perspectives on the Centrosomes

Ten years after Boveri's death, Maynard Metcalf wrote, "Boveri was the greatest cytologist of his generation … a man so keen, so careful and so cautious that any least suggestion from him deserves most thorough consideration. Boveri's work should be the starting point for any studies of causes, inheritance or cure of cancer." Indeed, Boveri's work has served as the starting point for this thesis. As early as 1887, centrosomes were seen at the poles of the mitotic spindle, which led to their identification as "the organ for cell division" by Boveri and Van Beneden.[1,2] The centrosome was found to direct the formation of the spindle microtubules during mitosis and to organize the interior of the cell during interphase.

Evolutionary History of the Centrosome

The centrosome is the main organizer of the microtubule cytoskeleton in animals, higher fungi and several other eukaryotic lineages. Centrioles and basal bodies are highly similar at the ultrastructural level, and indeed the key factors for centriole assembly are conserved in the genomes of all ciliated organisms.[3] The ancestral function of centrioles was likely to nucleate cilia, as both centrioles and cilia are found in all the major eukaryotic groups.[4] Cilia are involved in locomotion through either beating or gliding motility. Furthermore, cilia have sensory functions in diverse eukaryotes, suggesting an ancient association between motion and sensory perception.[5-7] These observations support the notion that centrioles and basal bodies are related and most probably derive from a centriolar structure present in the last common ancestor of all eukaryotes.

Structure of the Centrosome

There are several differences between the centrosomes and centrioles of different organisms. Centriole structure has been largely studied in one of four major model systems: *Chlamydomonas reinhardtii* (green algae), *Drosophila melanogaster* (fruit flies), *Caenorhabditis elegans* (roundworms), and human cell lines. Centrioles have a unique 9-fold symmetry that are conserved across these systems.[8] However, many differences exist between organisms. For example, yeast centrosomes are called spindle body poles, are always associated with the nuclear envelope, and are structurally different than the animal centrosome.[9] Henceforth, I will focus on the structure and functions of human centrosomes and centrioles.

A human centrosome consists of a pair of orthogonal centrioles surrounded by pericentriolar material (PCM), a protein-rich matrix composed of hundreds of different proteins, including cell cycle regulators, signaling molecules, and mediators of centriole duplication, ciliogenesis, and microtubule nucleation.[10] The centrosome is quite dynamic, and PCM proteins are rapidly exchanged through microtubule trafficking. Centrioles are 450-500nm long and 200-250nm in diameter.[11] Centrioles consist of nine triplets of microtubules arranged in a circle. The tubulins that make up the centrioles are modified by polyglutamylation on γ-carboxyl side chains of glutamic acids in α- and β-tubulin, a reversible post-translational modification that stabilizes microtubules.[12,13] The ninefold symmetry is conferred by a protein called SAS6,[14,15] which makes up a centriolar cartwheel. The basal body, which is found at the base of cilia and flagella, has the same structure as the centriole. They even play similar roles functionally, as the basal body of sperm flagella is incorporated into the centrosome of the fertilized egg.[16] Also, in organisms such as *Chlamydomonas*, the flagellar basal bodies are incorporated into the

centrosome during each round of cell division, and then they revert to their role as flagellar basal bodies during interphase.[17]

Within a centrosome with two centrioles, one of the centrioles is the mother or mature centriole, while the other is the daughter. The mother has distal and subdistal appendages. The distal appendages mainly function in membrane docking and ciliogenesis, while the subdistal appendages anchor microtubules to the centrosome.[18,19] More specifically, the subdistal appendages allow it to attach to γ-tubulin ring complexes (γ-TuRCs), which are anchored to the centrosome by pericentrin[20,21] and serve as the major microtubule-nucleating centers in centrosomes. One major component of γ-TuRCs is γ-tubulin, which is 35% identical to α- and β-tubulins. The other major components are γ-tubulin complex proteins 2-6 (GCP2-6) and GCP-WD.[22,23]

The centrosome is surrounded by centriolar satellites, which are dynamic, protein-rich, cytoplasmic granules.[24] Centriolar satellites are important for recruiting factors involved in microtubule nucleation, ciliogenesis, and centriole duplication.[25,26] Centriolar satellites disassemble during mitosis and reassemble when cells entered interphase.[27-29] Pericentriolar material 1 (PCM1) forms the major structural platform of centriolar satellites and has been used by many to define centriolar satellites.[25,27,30,31]

Functions of the Centrosome

The major function of the centrosome is microtubule organization, and most of its cellular roles rely on this crucial function. In interphase, centrosomes are involved in organizing microtubules for transport, cell shape and size, polarity. In mitosis, centrosomes are involved in organizing the mitotic spindle to help chromosomes partition equally during anaphase. In

addition, entrosomes are involved in ciliogenesis, migration, polarization, and other functions. Other newer functions of the centrosome are still being revealed, such as organization of actin.[32]

With regard to other cellular processes, centrosomes are not entirely dispensable, as they have been shown to be important for primary cilia formation and neural development.[33-35] In G1 or G0 phase of the cell cycle, the centrosome can migrate to the cell periphery, where the older and more mature centriole, called the mother centriole, can dock at the plasma membrane and nucleate a primary cilium. This primary cilium is a non-motile cilium involved in sensory functions, cell–cell signaling, and flow sensing.[3] *Drosophila* flies without centrioles cannot make cilia or flagella and die shortly after birth because their sensory neurons lack cilia.[36] In some cell types, the mother centriole can nucleate a motile cilium or flagellum. This is seen in hair cells of the inner ear and multiciliated respiratory epithelial cells.

A number of studies have cast doubt on the necessity of centrosomes with centrioles for numerous cellular functions, which has been well reviewed.[10,37] Regarding mitosis, it appears that centrioles are not universally required. Several cell types divide without centrioles, with the classic examples being those of higher plants and oocytes,[38] the planarian flatworm *Schmidtea mediterranea*,[39] and *Myxozoa*.[40] Additionally, genetically engineered *Drosophila* lines without centrioles are able to develop with near normal timing into morphologically normal adults,[36,41] and the first few divisions of a mouse embryo use microtubule organizing centers (MTOCs) that lack centrioles.[42] However, other cells depend on centrioles for accurate cell division, such as embryos, neural progenitor cells, and spermatocytes from a variety of species.[38,43,44] In humans, inherited mutations in several centrosome proteins cause microcephaly,[45,46] suggesting that neural progenitor cell divisions are particularly dependent on centrioles.[47] Further evidence from human cells suggest that loss of centrioles causes chromosomal instability (CIN) and

aneuploidy.[48] Therefore, in human cells, centrioles are not required for mitosis or cytokinesis but do increase mitotic fidelity.

The Centriole Duplication Cycle

Similar to DNA, centrioles duplicate once per cell cycle. Centriole duplication has gained tremendous interest in recent years, evidenced by a number of excellent reviews on this topic.[11,45,49-51] Genetic studies in *C. elegans* initially revealed that just five genes are strictly required for centriole formation:[52] SPD-2, ZYG-1, SAS-4, SAS-5, and SAS-6; the human analogs are CEP192, PLK4, CPAP, STIL, and SASS6, respectively. Additional studies confirmed the findings of this screen.[53-60]

Centriole number is tightly controlled in human cells, and disruptions in centriole duplication can have several consequences, including mitotic errors and disrupted cilia formation and signaling.[37,61] Centriole duplication is regulated by Polo-like kinase 4 (PLK4).[62,63] In late G1 and early S phase, CEP152 and CEP192 recruit PLK4 to the proximal end of the parent centriole. PLK4 then recruits and phosphorylates STIL, which allows SAS6 recruitment.[64] The nine-fold symmetry of centrioles is conferred by nine homodimers of SAS6.[14,15,65] PLK4 exists as a homodimer and engages in trans-autophosphorylation, causing SCF-βTrCP-mediated ubiquitination and subsequent degradation of PLK4; this process tightly regulates the levels of PLK4, which helps to limit centriole duplication to once per cell cycle.[66-70] The nascent centrioles then elongate, which is dependent on SAS-4 (also known as CPAP or CENPJ), [71-73] POC5, [74] OFD1,[75] and CP110.[72,76,77] Further, additional PCM proteins are recruited as the cell nears M phase, which is dependent on PLK1[78,79] and Aurora A.[80] Some proteins are recruited specifically to the new mother centriole in the new centrosome, including distal and subdistal

appendage proteins. The recruitment of some of these proteins allows for the massive increase in microtubule nucleation required for form the mitotic spindle in mitosis. These two centrosomes are physically attached by a tether between the two parent centrioles that is composed of CNAP1, rootletin, and others.[81] At the onset of mitosis, this tether is cleaved to allow centrosome separation, which is dependent on NEK2.[82]

At the end of mitosis, separase cleaves pericentrin to allow for centriole disengagement,[83] and the cartwheel is removed from the procentriole, a process dependent on CDK1;[84] these events relieve the block to reduplication of the parental centriole. The procentriole also depends on PLK1 and CDK1 to become licensed for centriole duplication, a process known as centriole-to-centrosome conversion.[85,86]

Polo-Like Kinase 4 Signaling at the Centrosome

Humans have five Polo-like kinases (PLK1-5).[87] PLK1-4 are implicated in cell cycle processes, such as centriole duplication (PLK2 and PLK4); DNA replication (PLK3); centrosome separation and maturation (PLK1); mitotic entry (PLK1); spindle formation, chromosome segregation and cytokinesis (PLK1). On the other hand, PLK2 and PLK5 (and probably PLK3) are involved in non-proliferative functions, such as neuron differentiation (PLK2 and PLK5) and synaptic homeostasis (PLK2).

PLK4 is the master regulator of centriole duplication and is a low abundance protein with a short cellular half-life.[88] In contrast to PLKs 1-3, PLK4 possesses a unique central region called the “cryptic polo box.” PLK4 has two tandem homodimerized polo boxes, PB1-PB2, that form a unique winged architecture in addition to a third C-terminal PBD (PB3).[89] This entire triple PBD structure is required for PLK4 localization, centriole duplication, and trans-

autophosphorylation and subsequent destruction.[63,89,90]

To coordinate centriole duplication, PLK4 has been shown to phosphorylate the following: STIL/Ana2 [64,91,92], SAS6 [93], FBXW5 [94], GCP6 [95], CEP135 [96], CPAP [97], CP110 [98], and CDC6.[99] Additionally, as mentioned before, PLK4 autophosphorylates itself in *trans* to regulate its proteolytic degradation and abundance.[66,67,70,100]

Additional non-canonical roles of PLK4 have also been identified. PLK4 is implicated in other critical roles in centrosome biology independent of its role in centriole duplication, such as ciliogenesis[101,102] and centriolar satellite maintenance.[103] Regarding the latter, PLK4 phosphorylates PCM1 which partly regulates the integrity of centriolar satellite integrity.[103] These data support a role for PLK4 in other centrosome functions, but a comprehensive list of substrates or functions is not available. This is a crucial gap that exists in the centrosome field.

Although centriole duplication occurs in early S phase, PLK4 levels actually do not reach their peak until mitosis.[70] However, a role of PLK4 in mitosis (independent of its role in duplicating centrioles) has not been described. This is another crucial gap that exists in the centrosome field.

Centrosomes in Human Disease

The role of centrosomes in human disease has been extensively reviewed.[50] Centrosome aberrations cause human diseases including ciliopathies that arise from mutations in genes encoding centrosome components, such as primary ciliary dyskinesia, autosomal recessive primary microcephaly, polycystic kidney disease, and Bardet-Biedl disease.[50]

Autosomal recessive primary microcephaly (MCPH) is caused by bi-allelic null mutations in any of the several following genes that localize to the centrosome: MCPH1,

CDK5RAP2, ASPM, CPAP, PLK4, TUBGCP6, and STIL.[46,101] Many of these MCPH proteins are involved in spindle positioning, suggesting that this process could be imperative for disease development.[36,104] In addition, mutation of either *PLK4* or its interacting partner *CEP152,* causes Seckel Syndrome, a disorder associated with dwarfism, microcephaly, and abnormal eye, jaw, ear, and sometimes, spinal development.

An open question in this field is why mutations in centrosome genes have a disproportionate effect on brain size, especially because they are ubiquitously expressed and required for proper mitosis. One hypothesis is that neural progenitor cells are exquisitely dependent on proper coordination of symmetric and symmetric cell divisions.[105] Another hypothesis is that neural progenitor cells disproportionately depend on mitosis in general, given their high rates of proliferation in neurogenesis, a process that occurs during a restricted developmental time frame.[101] Lastly, aberrant mitosis could promote cell death specifically in neural progenitor cells more so than other cells.[101,106]

Centrosomes are also dysregulated in human cancer, with the major defect being centrosome amplification (CA).

Centrosome Amplification in Human Cancer

Theodor Boveri first established a link between centrosome abnormalities and cancer more than 100 years ago by proposing that an abnormal increase in centrosome number could lead to abnormal mitotic spindles and cause chromosome instability, leading to cancer.[2] Indeed, CA and other centrosome defects have been reported in nearly all human cancers, both solid and hematological.[107-113 107,114] In breast cancer, centrosome aberrations are common, and CA correlates with higher tumor grade,[111,115,116] metastasis,[117-119] and negative hormone receptor

status.[120,121] It is thought that CA is an early and potentially initiating event, as mice overexpressing PLK4 spontaneously generate more tumors.[122] Furthermore, CA can be seen in pre-malignant lesions, such as DCIS. Yet the causes and consequences of CA in cancer remain obscure; this remains a critical gap in the centrosome field.

There are several major alternative mechanisms by which CA can arise,[107,114] which we divide into two categories: (1) cell doubling from cytokinesis failure, cell-cell fusion, or endoreduplication resulting in both genome and centrosome doubling; and (2) centrosome duplication independent of cell doubling, either *de novo* or due to dysregulation of the centriole cycle. The relative contributions of these mechanisms of CA to human cancer are unclear.

CA has a number of unwanted consequences. First, cells with supernumerary centrosomes generate genetic diversity through asymmetric cell divisions on abnormal spindles with chromosome missegregation.[108,111,123] Consistent with this, CA correlates with aneuploidy and CIN in cancer.[109,124] CA also causes decreased cilia signaling, altered regulation of Rho GTPases, and increased microtubule-directed polarization.[114,125-127] Furthermore, CA can behave like an oncogene, increasing cell migration and invasiveness by enhancing Rac1 activity.[121,126] These ideas suggest that CA may directly promote tumor cell invasion and metastasis without requiring altered genome content. However, all the consequences of CA in human cancer remain unclear.

As mentioned, CA is a key mechanism of CIN, the perpetual gain or loss of whole chromosomes during cell division. Cells with CA can undergo aberrant mitoses with multipolar spindles, resulting in CIN.[108,111,123] CIN leads to large karyotypic diversity among cancer cells, and this genetic diversity provides an enhanced opportunity for selection of highly aggressive clones.[128,129] Thus, CA can partly explain the karyotypic diversity of breast cancer.[130] However,

CA is unlikely to be necessary or sufficient for CIN because CIN can arise from other pathways.[131,132] Furthermore, cells with CA cluster centrosomes into a pseudo-bipolar spindle under some conditions, allowing them to avoid CIN induced by multipolar division;[133] nevertheless, these divisions with pseudo-bipolar spindles are more likely to have merotelic attachments (chromatid attached by microtubules to both spindle poles) and subsequent lagging chromosomes and chromosome bridges in anaphase.[134] Prior work has suggested CA is at least partly responsible for CIN in a small cohort of breast cancers,[124] but the extent of CA as a cause of CIN is unknown.

Scope of Project

Overall, I have delved into uncovering the causes and consequences of CA in human cancer. I attempt to answer whether CA is mostly due to centriole overduplication or cell doubling events and delve into the potential clinically relevant molecular mechanisms underlying CA in human cancer. Further, I engineer a chemical genetic system to interrogate signaling of PLK4, the master regulator of centriole duplication, to identify novel substrates and potentially novel functions of PLK4. Furthermore, I examine the consequences of CA on cellular physiology, focusing on microtubule-dependent pathways. I find that cells with CA are exquisitely dependent on autophagy, the cell's recycling pathway. Lastly, I explore alterations in centriolar satellite genes in human cancer, determine how the most common alteration affects cell physiology, and try to identify potential vulnerabilities amenable to therapeutic targeting.

Gap 1: Causes of CA in human cancer

Here I seek to determine the contributions of the two principal mechanisms of CA: centriole overduplication versus cell doubling events (e.g. cytokinesis failure or cell-cell fusion). Staining for CEP170 can distinguish between these two mechanisms of CA. CEP170 marks mother centrioles and is recruited to centrosomes in late G2. If centriole overduplication is the predominant mechanism leading to CA, we expect extra centrosomes with only one co-staining with CEP170; conversely, if cell doubling events were predominant, then we expect all centrosomes would have mature centrioles, as identified by CEP170. Herein, I utilize this method to ascertain the major cause of CA.

Gap 2: Consequences of CA in human cancer

Firstly, I explore the clinical consequences of CA in a large cohort of breast cancer patients. I test the hypothesis that CA is a prognostic biomarker in breast cancer. Heretofore, the impact of CA on patient survival has not been reported.

CA is known to have several consequences, including mitotic aberrations, increased cellular invasiveness, increased Rac and Rho GTPase activity, altered cilia signaling, and altered polarity.[114] However, all the potential cellular consequences of CA have not been elucidated. Herein, I delve into a series of microtubule-dependent pathways and assess whether CA alters these pathways. I focus on autophagy, the cell's recycling pathway, which is exquisitely dependent on autophagosome movement along microtubules to reach lysosomes for clearance of autophagic cargo.

Gap 3: PLK4 phosphoproteomics and identification of substrates and functions

The entire phosphoproteome of PLK4 has not been elucidated. Furthermore, the entire mechanism of PLK4-mediated centriole duplication has not been elucidated. Other roles of PLK4 have been reported, such as ciliogenesis and regulation of centriolar satellite integrity. Herein, I set out to map the phosphoproteome of PLK4 using a novel chemical genetic system of PLK4 inhibition coupled with a multiplex mass spectrometry experiment.

Gap 4: Role of centriolar satellites in human cancer

There have been no reports of centriolar satellites in human cancer. However, there are reports of certain centriolar satellite proteins being important for genomic integrity. Therefore, I hypothesized that dysregulation of centriolar satellites could be a driver of genomic instability in human cancer. Herein, I conduct an unbiased bioinformatic analysis of the 44 known centriolar satellite genes using publicly-available cancer datasets.

CHAPTER 2: Centrosome amplification induces high grade features and is prognostic of worse outcomes in breast cancer

Work in this chapter was adapted from:

Centrosome Amplification Induces High Grade Features and is Prognostic of Worse Outcomes in Breast Cancer

Ryan A. Denu, Lauren M. Zasadi, Craig Kanugh, Jennifer Laffin, Beth A. Weaver, Mark E. Burkard

BMC Cancer. 2016 Jan 29;16(47). PMID: 26832928

Abstract

Introduction:

Centrosome amplification (CA) has been reported in nearly all types of human cancer and is associated with deleterious clinical factors such as higher grade and stage. However, previous reports have not shown how CA affects cellular differentiation and clinical outcomes in breast cancer.

Methods:

We analyzed centrosomes by immunofluorescence and compared to ploidy and chromosomal instability (CIN) as assessed by 6-chromosome FISH in a cohort of 362 breast cancers with median clinical follow-up of 8.4 years. Centrosomes were recognized by immunofluorescence using antibodies for pericentriolar material (PCM; pericentrin) and centrioles (polyglutamylated tubulin). CA was experimentally induced in cell culture by overexpression of polo-like kinase 4 (PLK4).

Results:

CA is associated with reduced all-cause and breast cancer-specific overall survival and recurrence-free survival. CA correlates strongly with higher stage and grade, and the prognostic nature of CA can be explained largely by these factors, suggesting that CA may cause aggressive tumor characteristics. A strong correlation between CA and high tumor ploidy demonstrates that chromosome and centrosome doubling often occur in concert. Intriguingly, some high-risk tumors have more acentriolar centrosomes, suggesting PCM fragmentation as another mechanism of CA. CA is proposed to be a method of inducing CIN via aberrant mitotic cell divisions. Consonant with this, we observed a strong correlation between CA and CIN in breast cancers. However, some CA tumors had low levels of CIN, indicating that protective

mechanisms are at play, such as centrosome clustering during mitosis. *In vitro* induction of CA in two non-transformed human cell lines (MCF10A and RPE) demonstrated that CA induces a de-differentiated cellular state and features of high-grade malignancy, supporting the idea that CA intrinsically causes high-grade tumors.

Conclusions: Greater CA is associated with deleterious clinical factors and outcomes in breast cancer. Cell doubling events are the most prevalent causes of CA in cancer, although PCM fragmentation may be a secondary cause. CA promotes high-risk breast cancer in part by inducing high-grade features. These findings highlight the importance of centrosome aberrations in the biology of human breast cancer.

Introduction

The centrosome consists of a pair of attached centrioles surrounded by proteinaceous pericentriolar material (PCM) and functions as the major microtubule organizing center in human cells.[37] During interphase, centrosomes organize cytoplasmic microtubules to control cell shape, polarity, and motility; during mitosis, centrosomes separate to form poles of the mitotic spindle. Centrosome aberrations cause human diseases including ciliopathies that arise from mutations in genes encoding centrosome components, such as primary ciliary dyskinesia, autosomal recessive primary microcephaly, polycystic kidney disease, and Bardet-Biedl disease.[50] Furthermore, structural and functional defects of centrosomes are found in cancer, with the most commonly reported being a numerical excess, known as centrosome amplification (CA).[107]

Over a century ago, Theodor Boveri proposed that supernumerary centrosomes can cause cancer.[2] Indeed, CA and other centrosome defects have been reported in diverse cancer types.[107,114] In breast cancer, centrosome aberrations are common, and amplification correlates with higher tumor grade,[111,115,116] metastasis,[117-119] and negative hormone receptor status[120,121] in small patient cohorts. Yet the causes and consequences of CA in breast cancer remain obscure.

There are several major alternative mechanisms by which CA can arise,[107,114] which we divide into three categories: (1) cell doubling from cytokinesis failure cell-cell fusion, or endoreduplication resulting in both genome and centrosome doubling; (2) centrosome duplication independent of cell doubling, either *de novo* or due to dysregulation of the centriole cycle; and (3) PCM fragmentation. The relative contributions of these mechanisms of CA to human breast cancer are unclear, but can be addressed with a large cohort of tumor samples. For instance, if polyploidy correlates with CA, this would support genome doubling over centrosome

duplication or PCM fragmentation. Moreover, PCM fragmentation is distinguished from duplication in that it is predicted to cause acentriolar centrosomes. Here we evaluate these to provide insight into mechanisms of CA in a large cohort of breast cancers.

The consequences of CA in human cancer also remain unclear. CA is a key mechanism of chromosomal instability (CIN), the perpetual gain or loss of whole chromosomes during cell division. Cells with CA can undergo asymmetric cell division with multipolar spindles, resulting in CIN.[108,111,123] CIN leads to large karyotypic diversity among cancer cells, and this genetic diversity provides an enhanced opportunity for selection of highly aggressive clones.[128,129] Thus, CA can partly explain the karyotypic diversity of breast cancer.[130] However, CA is unlikely to be necessary or sufficient for CIN because CIN can arise from other pathways.[131,132] Furthermore, cells with CA cluster centrosomes into a pseudo-bipolar spindle under some conditions, allowing them to avoid CIN induced by multipolar division.[133] Prior work has suggested CA is at least partly responsible for CIN in a small cohort of breast cancers,[124] but the extent of CA as a cause of CIN is unknown.

In addition to CIN, CA can yield aggressive tumor phenotypes via other mechanisms. For instance, CA causes decreased cilia signaling, altered regulation of Rho GTPases, and increased microtubule-directed polarization.[114,125-127] Furthermore, CA can behave like an oncogene, increasing cell migration and invasiveness by enhancing Rac1 activity.[121,126] These ideas suggest that CA may directly promote tumor cell invasion and metastasis without requiring altered genome content. If these preclinical findings operate in human breast cancer, then we would anticipate CA to correlate with altered cancer cell physiology and worse clinical outcomes, independent of CIN.

Here, we assess CA and other centrosome abnormalities and correlate these with FISH data for 6 chromosomes in 362 human breast cancers with a median 8.4 years of clinical follow-up. We find that CA portends worse clinical outcomes, and is most prevalent in high-risk breast cancer. The data suggest that multiple mechanisms contribute to the development of supernumerary centrosomes, and that CA promotes aneuploidy. There is a strong correlation between CA and tumor grade, providing a potential mechanism for the aggressive behavior of high-grade tumors. Accordingly, in cell models, induced CA promotes expression of cellular markers of de-differentiation and induces high-grade phenotypes. These findings provide important insight into how CA arises in human cancer and how it imparts high-grade phenotypes and worse clinical outcomes in human breast cancer. Moreover, our findings suggest that pharmacologic interventions on CA or its downstream effects could improve outcomes for patients with centrosome-amplified cancer.

Results

Centrosome amplification is associated with adverse clinical factors and worse survival

We initially characterized the distribution of centrosome abnormalities and clinical characteristics seen in our breast cancer samples. Patient characteristics are shown in Supplemental Table 2-1. Centrosomes were assessed in each sample using pericentrin, a PCM marker. The normal mammary gland is composed of terminal ductal lobular units, and polarity is well defined, as indicated by luminal positioning of the centrosome and basal positioning of the nucleus (Figure 2-1A, top). However, this organization is disrupted in carcinoma samples (Figure 2-1A, bottom). Furthermore, the median centrosome number from all the tumor samples was almost double that of the normal breast samples (1.8 vs. 1.0, p=0.001), and 84% (305 of 362) of breast cancer samples had a mean centrosome value higher than that of the normal breast samples. Additionally, the average centrosome number per cell and the percent of cells with greater than 2 centrosomes were both significantly greater in breast cancers compared to normal breast (Figure 2-1B-C). To demonstrate that this is not simply due to a greater proliferative rate in the tumors (as centrosomes are duplicated at G1/S and are expected to increase in G2), we correlated average centrosome number with Ki67, a marker of proliferative index. Although there is a partial correlation a significant portion of samples have high centrosome number with low Ki67 (Figure 2-1D). Because of the partial correlation, an elevated average centrosome number between 1 and 2 could indicate increase in the percent of tumor cells in G2. Hence, we used a strict cutoff of >2 centrosomes for subsequent analyses of centrosome amplification. Breast cancers also showed a wider distribution of mean centrosome number per cell compared to normal breast (range 0.5-5.9 and 0.23-2.77, respectively), consistent with CA occurring in a variable fraction of cells within a tumor. The distribution of centrosomes in breast cancer was

unimodal with right skew, while the distribution of centrosomes in normal breast samples was normal (Supplemental Figure 2-1).

We stratified patients based on stage, grade, subtype, regional node status, and recurrence site. Patients with higher stage and grade also had a higher average number of centrosomes per cell (Figure 2-2A-B). Furthermore, CA was more marked in triple negative and HER2 amplified subtypes (Figure 2-2C); in general, estrogen/progesterone receptor-positive breast cancers have a more favorable prognosis than HER2 amplified or triple negative cancers.[135]

A tumor was considered to have CA if the mean number of pericentrin foci per cell exceeded 2. Using this definition, CA was found in 35.1% of breast tumors and 13.3% of normal breast samples. It was most common in triple negative breast cancers (61.4%) and less frequent in HER2-positive (41.2%) and hormone-sensitive/HER2-negative subgroups (29.2%). We next assessed how CA correlated with clinical outcomes. Patients with CA had significantly worse overall survival (OS, $P=0.002$; Figure 2-2D) and recurrence-free survival (RFS, $P<0.001$; Figure 2E) than those without CA. Furthermore, these patients also had worse breast cancer-specific mortality ($P=0.003$; Figure 2-2F). Our findings led us to hypothesize that high-CA tumors may provide useful prognostic data in addition to providing a biologic reason for aggressive breast cancers. To be clinically useful, CA would need to indicate risk that is not captured with currently available clinical factors such as tumor stage, grade, and subtype. To test this, we performed Cox proportional hazards modeling (Supplemental Table 2-2). This analysis demonstrated that stage and hormone receptor status were the strongest predictors of OS and RFS. When corrected for these, CA is not an independent predictor of OS or RFS. Although CA does not provide a clinical factor independent of known risk factors, it nevertheless may provide a biological explanation for how tumors advance in grade and stage.

To survey additional centrosome defects, we observed aberrations in centrosome shape, size, and patterning (Supplemental Figure 2-2). Centrosome clustering was observed in 58% of tumors versus 13% of normal samples. Centrosome speckling (clusters with >5 centrosomes) was observed in 23% of tumors versus 7% of normal samples, and irregular centrosome shapes in 41% of tumors versus 20% of normal samples (this relatively high incidence of abnormal shapes in normal samples likely represents staining artifact). What we term centrosome speckling has been described by others as sand-like centrosomes.[120] We did not observe worse clinical outcomes with atypically shaped centrosomes or centrosome speckling, although centrosome clustering correlated with significantly worse OS (P=0.009) and RFS (P=0.030). Centrosome clustering has been proposed as a mechanism by which cells with CA are able to divide with pseudo-bipolar spindles,[136,137] although it is unclear whether the interphase clustering observed here would correspond with clustering during mitosis.

Doubling events as a common cause of centrosome amplification

One potential mechanism leading to CA is cell-doubling events (e.g. cytokinesis failure, cell-cell fusion). If cell doubling represented the primary cause of CA in breast cancer, we would expect a strong correlation between CA and increased cell ploidy. Therefore, we evaluated how CA correlates with high tumor ploidy, as determined by 6-chromosome FISH in 354 breast tumors. Ploidy ranged from 1.43 to 8.75 with a median of 2.08. We find that CA strongly correlates with ploidy (P=0.006; Figure 2-3A). Further, after dividing patients by CA (defined as >2 centrosomes per cell), tumors with CA had significantly greater ploidy (Figure 2-3B). To verify these findings, analyses were repeated using a more stringent definition for centrosomes: the overlap of pericentrin and polyglutamylated tubulin, which represents the overlap of PCM

and centriole markers, respectively.[13,138] Using these criteria, CA still correlated with ploidy (Supplemental Figure 2-3). These data provide evidence that CA and whole genomic amplifications occur in concert in incipient tumor cells, suggesting that genome doubling events occur commonly in breast cancer oncogenesis.

To estimate what percentage of CA events arise from doubling events, we calculated the percent of tumors with CA (average centrosome number >2) that also had elevated ploidy (>3). This revealed that at least 15% of CA events arose from doubling events (Figure 2-3C). However, this method is likely to underestimate the true percentage of CA events that arise from doubling events because cells that originate after genome doubling can subsequently lose chromosomes.[134,139]

Centrosome amplification as a common cause of chromosomal instability

CA can lead to multipolar cell division or lagging chromosomes through induction of merotelic attachments on focused bipolar spindles, resulting CIN.[134] Therefore, we examined the relationship between CA and CIN. CIN was calculated as the percent of cells within a tumor with a non-modal number of chromosomes, averaged for 6 chromosomes. 44.7% of breast tumors have CIN compared to 9.1% of normal breast samples. Patients whose tumors displayed CIN had worse breast cancer-related overall survival (Supplemental Figure 2-3). CA correlated positively with CIN (Figure 2-3D, $P<0.001$). After dividing the patients into two groups based the presence of CA, as done for survival analyses, tumors with higher CA had significantly elevated CIN (Figure 2-3E). These data support the hypothesis that CA is a common cause of CIN in breast cancer. In addition, we found a strong positive correlation between ploidy and CIN (Figure 2-3F).

Pericentriolar material fragmentation is a marker of aggressive tumors

As done above for CA and ploidy analysis, we repeated other analyses using the more stringent definition of pericentrin and polyglutamylated tubulin overlap. Similar to our analysis based on pericentrin staining alone, CA defined by the overlap of pericentrin and polyglutamylated tubulin was more pronounced in triple negative breast cancer and cancers with higher histological grade (Supplemental Figure 2-4A-D). Patients with CA had worse overall and recurrence-free survival (Supplemental Figure 2-4E-G). Furthermore, CA as defined by these criteria also demonstrated a significant correlation with ploidy and CIN (Supplemental Figure 5A-D). In summary, we observed similar findings whether centrosomes were defined using solely pericentrin or using the overlap of pericentrin and polyglutamylated tubulin.

Although centrioles are surrounded by PCM in normal cells, ~1/3 of cells in normal samples had PCM without detectable centrioles, suggesting that only a subset of centrioles were labeled with the polyglutamylated tubulin antibody. However, compared with normal samples, tumors more frequently had pericentrin foci that lacked co-staining with polyglutamylated tubulin. An average of 78% of pericentrin foci contained this centriolar marker in normal samples compared to an average of 46% in breast tumors. 302 out of 362 breast cancer cases had a percentage lower than 78%, suggesting a true loss of this centriole marker in some breast tumors. These findings suggest that either these tumor centrioles lack polyglutamylated tubulin, or that acentriolar centrosomes are a *bona fide* characteristic of many human breast cancers. Acentriolar centrosomes have been reported previously in cancer cells and are thought to result from PCM fragmentation.[131,140] Additionally, acentriolar centrosomes were more common in the triple-negative breast cancer subtype and correlated with advanced stage and grade (Figure 2-4A-

C), although there was no significant correlation with worse clinical outcomes (Figure 2-4D-E; P=0.202 for overall survival and P=0.133 for recurrence-free survival). Nevertheless, these findings indicate that PCM fragmentation is potentially a marker of more aggressive tumors.

Centrosome amplification causes high-grade features

Because there was a strong correlation of CA with poorly differentiated tumors (grade 3) in our study and others,[111,115,116] we hypothesized that CA induces cellular de-differentiation. To test this, we utilized doxycycline-inducible PLK4 in MCF10A and RPE cell lines,[126,141] in which the overexpression of PLK4 results in CA (Figure 2-5A,D). Breast cancer cells that express less CD24 and more CD44 are more de-differentiated and more stem cell-like.[142-144] These cells may also have enhanced metastatic potential.[145] We analyzed CD24 and CD44 by flow cytometry after inducing CA in MCF10A cells, and found that this significantly decreased CD24 and increased CD44 (Figure 2-5B-C). To ensure this was not an effect of doxycycline or of PLK4 expression independent of centrosome amplification, we employed a doxycycline-inducible $PLK4^{1-608}$ cell line in which this kinase is expressed without amplifying centrosomes due to lack of a critical localization domain. We did not observe markers of de-differentiation with doxycycline in this control (Figure 2-5C). To validate this finding, we employed a second cell line, immortalized retinal pigment epithelial (RPE) cells, for which cytokeratin profiles can reveal differentiation status. More de-differentiated cells express excess cytokeratins 7 and 19 and less cytokeratin 18.[146-149] We assessed expression of these 3 cytokeratins by qRT-PCR, finding that RPE cells with CA express more cytokeratins 7 and 19, but less cytokeratin 18 (Figure 2-5E), which is consistent with a de-differentiated state.

The Nottingham grading scale uses the following three criteria to determine the differentiation status of a tumor: (1) the amount of gland formation, (2) nuclear pleomorphisms, and (3) mitotic figures.[150,151] To address whether CA is sufficient to impart these characteristics, we first observed which tumors demonstrated glandular/tubular structures in at least two of three histologic regions examined. Indeed, tumors from the TMA without tubule formation had greater CA (Figure 2-5F). With regard to the second criterion, previous work has shown cells with CA can exhibit multipolar spindles and other nuclear pleomorphisms, and this is seen *in vitro* as well (Figure 2-5G). For the third criterion, it has already been demonstrated that cells with CA proliferate more slowly,[67,126] which would tend to cause lower grade tumors; however, numerical CA positively correlates with Ki67 status in our data set (Pearson $r = 0.3106$, $p<0.001$, Figure 2-1D) suggesting that CA does not cause tumor cells to exit the cell cycle. Furthermore, it has been demonstrated that cells with CA take longer to complete mitosis due to multipolar spindle formation,[152] which could explain why more mitotic figures are seen in tumors with CA. Taken together, these data support the idea that CA directly or indirectly imparts high-grade features to tumors, leading to worse clinical outcomes.

Discussion

Our findings provide important insight into the origin, frequency, and the clinical correlates of CA in human breast cancer. CA was previously reported in small sample sizes to be a hallmark found in diverse cancer types,[107] and often is found early in carcinogenesis, including in precursor lesions of breast cancer.[124] Likewise, we find that CA is common in our cohort of 362 breast cancer patients. CA correlates with increasing grade and stage, and CA was more pronounced in triple negative and HER2 amplified subtypes, consistent with past observations in smaller patient cohorts.[111,115-121] Further, CA confers worse OS and RFS, which can be explained by the aggressive characteristics of cancers with CA, including advanced stage and grade. Intriguingly, CA is sufficient to induce high-grade phenotypes in human epithelial cells, including those of breast origin. This can explain why tumors that originate with CA have de-differentiated phenotypes that presage worse clinical outcomes. Additionally, CA can cause CIN, leading to rapid evolution of tumors into more aggressive phenotypes.

Our data provide the first evidence for the origin of CA in breast cancer. The data indicate that at least 15% of cases of CA in human breast cancer arose by a doubling event, such as cytokinesis failure or cell-cell fusion. However, our method likely underestimated the true percentage of CA from doubling events because the supernumerary centrosomes lead to a loss chromosomes, and tetraploidy buffers the risk of haploinsufficiency;[134,139] hence some CA cancers with near-diploid genome could have originated in a doubling event. To more definitively answer this question regarding the relative contributions of mechanisms leading to CA, a large tumor cohort could be probed for a marker of mature centrioles, such as CEP170. Cells with *de novo* centrosome amplification should have a single CEP170-positive centrosome,

whereas tumor cells with multiple CEP170-positive centrosomes are more consistent with doubling events, in which two mature centrosomes would be inherited.

PCM fragmentation has been proposed as a mechanism by which CA can occur.[110,131,140] Indeed, we found centrioles absent from a sizeable proportion of centrosomes in the tumor samples in our TMA. This suggests that the regulation of recruitment of centrosome proteins is just as important as the regulation of centriole duplication for proper centrosome function. Excess PCM or PCM fragmentation may result in cells that are likely to undergo multipolar mitoses and generate daughter cells with altered karyotypes. Many of these daughter cells generated from multipolar divisions will not be viable but will promote diversity for evolutionary selection. We found that an increased percentage of acentriolar centrosomes correlated with adverse clinical features, suggesting that PCM fragmentation is more common in more aggressive tumors.

Previous studies have provided conflicting information about how centrosome number and size correlate with aneuploidy and CIN in breast cancer, with some studies supporting the relationship,[124] and others finding no association.[153] Here we quantified a greater number of chromosomes with FISH on a larger patient cohort and found a strong correlation between CA and both CIN and aneuploidy. This is consistent with mechanistic studies that illustrate that CA can cause CIN and aneuploidy.[108,111,123] The strong correlation between CA and ploidy suggests that CA can occur in many breast cancers from prior cell doubling events, although it is unclear whether this originates from failed cell division, cell-cell fusion, or other mechanism such as endoreduplication. Furthermore, we found a strong positive correlation between ploidy and CIN, consistent with the previous suggestion that cells with higher ploidy can better tolerate CIN and buffer the deleterious effects of CIN.[139] However, there were a number of cases (approximately

18%) in which CIN did not correlate with CA. First amongst these was a high CA, low CIN group, in which centrosome clustering may be occurring; clustering has been described previously as a way that the cell prevents multipolar spindle formation,[133,136,154] although this can still result in chromosome missegregation.[134] In a second group with low CA and high CIN, another mechanism of generating CIN is operating, such as impaired checkpoint function.[131-133]

Advantages of our methods include a large cohort of breast tumor samples with survival data, evaluation of 6 chromosomes by FISH for analysis of aneuploidy and CIN, and use of the overlap of PCM and centriole markers to characterize acentriolar centrosomes and PCM fragmentation. This allowed us to establish how CIN and ploidy correspond with centrosome number in several hundred breast tumors. A potential limitation to this study is dependence on single-section analysis of histological samples, which underestimate CA and overestimate CIN through sectioning artifact. However, the inclusion of triplicate punch biopsies per patient and normal breast samples help to alleviate this concern. It is possible that larger cancer cells could suffer disproportionate underestimation of CA than normal cells; however this does not explain our finding that CA is commonly found in larger high-grade tumor cells. Nevertheless, our results provide quantitative comparisons among breast cancer types and shed important insight into the causes and consequences of CA in human breast cancer.

In conclusion, CA is a common feature of human breast cancers that presages worse clinical outcomes but is not an independent predictor of survival. CA arises by multiple mechanisms, most predominantly by doubling events and PCM fragmentation. PCM fragmentation may represent a marker of high-risk cancers. In human cancer CA is associated with a high-grade phenotype and loss of genetic stability. These factors lead to the aggressive phenotypes of cancers with high CA. It may be possible to interrupt these phenotypes with

specific drugs targeting centrosome amplification, such as recently discovered inhibitors of PLK4.[155-157]

Materials and Methods

Patients, Tissues, Ethics, and Consent

The breast cancer tissue microarray (TMA) used in this analysis has been described previously.[158] Briefly, samples were obtained from primary breast tumor blocks obtained at time of surgery for stage I-III breast cancer patients seen at the University of Wisconsin Carbone Cancer Center under protocol OS10111. The University of Wisconsin Health Sciences Institutional Review Board approved the TMA creation and approved use of the TMA and the de-identified coded data set (IRB approval 2010-0405). As this study used de-identified data, the IRB waived the need for patient consent. The TMA contains three 0.6mm punch biopsies from each patient's tumor, and 15 normal breast controls from mammoplasty are included in the array. All cases had at least 5 years of follow-up or recurrence or death within 5 years. Clinical information includes age at diagnosis, ethnicity, tumor size, lymph node involvement, stage, estrogen receptor (ER), progesterone receptor (PR), and HER2 status, type of surgery, adjuvant breast cancer treatments, and follow-up data, including any recurrence and death. Clinical data was obtained from the UW Hospital and Clinics Cancer Registry and manual chart review. ER, PR, and HER2 immunohistochemistry were also performed on the completed TMAs and interpreted by a breast pathologist. If ER/HER2 clinical data was not available, the clinical pathologic data from the original tumor sample was used for analysis. Patients with unknown or equivocal values were excluded from these analyses of subtype and CA. For subtype analysis, the following groups were used based on their clinical relevance [159,160]: ER or PR positive and HER2-nonamplified; HER-amplified; and triple negative.

Immunohistochemistry

Breast cancer TMAs were sectioned at 5 μm thickness, deparaffinized, and rehydrated. Antigen retrieval was performed in a pressure cooker at 250°F with citrate buffer (pH 6) for 4 minutes. Blocking was done for 1 hour in 10% fetal bovine serum (FBS) in PBS. Tissues were probed with anti-pericentrin (Abcam, ab4448, 1:200) and anti-polyglutamylated tubulin (Adipogen, GT335, 1:100) antibodies diluted in 1% FBS and 0.1% triton X in PBS overnight in a humidified chamber at 4°C. Pericentrin and polyglutamylated tubulin are *bona fide* markers of centrosomes.[13,138,161] The TMAs were then incubated with anti-rabbit Alexa 488 and anti-mouse IgG1 Alexa 647 secondary antibodies (Jackson ImmunoResearch Laboratories, West Grove, PA) for 1 hour at room temperature. Slides were washed 3 times after primary and secondary antibody incubations. Slides were counterstained for DNA with 4',6-diamidino-2-phenylindole (DAPI) and mounted with ProLong Gold antifade reagent (Life Technologies). Scoring of centrosome phenotypes was performed using a Nikon Eclipse Ti inverted microscope, 100x objective, and CoolSNAP HQ2 charge-coupled device camera (Photometrics). The observer was blinded to clinical data and analyzed centrosomes in a minimum of 30 cells per case from 3 different tumor regions. The number of distinct pericentrin foci as well as foci that overlapped with polyglutamylated tubulin were counted. Cell boundaries were visualized by nonspecific background staining with the polyglutamylated tubulin antibody. Average centrosome number per cell was calculated for each case. Centrosome sizes were measured in at least 15 representative centrosomes per case from three different tumor regions using the pericentrin marker, and an average was calculated for each case. For survival analysis, the median centrosome size (0.99 μm) was used as the cutoff for large versus small centrosomes. In addition to number and size, we also noted any unusual centrosome phenotypes such as centrosome clustering, centrosome speckling, and atypical shapes.

A small fraction of samples in the TMA were not evaluable due to loss of tissue, insufficient cellularity, or other technical issues and were excluded from analysis. Centrosome data were linked to de-identified clinical data by sample number and position on the TMA and sorted for analysis using Microsoft Excel.

Fluorescence In Situ Hybridization

Fluorescence in situ hybridization (FISH) was performed using standard techniques, as reported elsewhere [162]. Briefly, chromosomes 4, 10, and 17 were probed on one section, and chromosomes 3, 7, and 9 on another section. Chromosomes were counted by observers blinded to patient conditions in a minimum of 10 cells per case. A small fraction of samples were not evaluable due to loss of tissue, insufficient cellularity, or other technical issues and were excluded from analysis. Similarly a subset of samples had a single probe that was not well visualized, but if at least five chromosomes were available, it was included in further analyses. FISH data were linked to de-identified clinical data by sample number and position on the tissue microarray and sorted for analysis using Microsoft Excel. Ploidy was determined by the average chromosome number for all 6 probes combined. CIN was determined as the average percentage of cells that deviated from the modal number for each of the 6 chromosomes assessed by FISH. Samples were considered to have CIN if this value exceeded 45%, a cutoff that yielded appropriate percentages of normal samples and tumors with CIN.

Cell Culture

The doxycycline-inducible $PLK4^{WT}$ and $PLK4^{608}$ MCF10A and RPE cell lines were a kind gift from Dr. David Pellman. Cells were cultured and centrosome amplification was

induced as previously described.[126,163] For assays, cells were treated with 2 μg/mL doxycycline for 48 hours and subsequently harvested for qRT-PCR and flow cytometry. Immunofluorescence was performed as previously described using the following antibodies: anti-pericentrin (Abcam, ab4448), anti-gamma tubulin (Abcam, ab27074), anti-alpha tubulin (Millipore, MAB1864), and Alexa fluorophore-conjugated secondary antibodies (Jackson).

Quantitative Reverse Transcriptase Polymerase Chain Reaction (qRT-PCR)

RNA was isolated from cells using the RNeasy Micro Kit (Qiagen, Valencia, CA), and converted to cDNA using the Quantitect Reverse Transcription Kit (Qiagen). qRT-PCR was performed using EvaGreen master mix (MidSci, St. Louis, MO) and a StepOne Plus instrument (Applied Biosystems). Quantification of cytokeratins 7, 18, and 19 (*KRT7, KRT8, KRT19*) expressed as mRNA level was normalized to the mRNA of three housekeeping genes (*RRN18S, GAPDH and ACTB*). Primers sequences are provided in Supplemental Table S3. Fold changes in gene expression were assessed using the 2^-ΔΔCt method.[164]

Flow Cytometry

A total of 50,000 events were acquired for each sample using an Accuri C6 flow cytometer (Accuri, Ann Arbor, MI) equipped with multicolor analysis, and data were analyzed with Flow Jo 7.0 (Tree Star, Ashland, OR). Samples were run in triplicate in at least 3 independent experiments. The following antibodies were used: CD24-PE, CD44-PE, and mouse IgG1 isotype control (BD Biosciences). Mean channel fluorescence of FL2 was used to quantitatively compare conditions.

Statistical Analysis

R (version 3.1.1, R Core Team, Vienna, Austria) statistical software was used for survival analysis. A total of 362 patients were included in survival analyses. The clinical outcomes analyzed in this study were recurrence-free survival (RFS) and overall survival (OS). RFS was defined as the time from initial breast cancer diagnosis to recurrence or death. OS was defined as the time from diagnosis to the date of death or last follow-up. RFS and OS were plotted using the Kaplan–Meier method, and log-rank tests were used to compare patients with tumors with CA versus tumors with no CA using 2 centrosomes per cell as a cutoff. Sensitivity analyses were also performed using the average of all the normal breast samples in the TMA as the cutoff for defining CA. Cox proportional hazards model included centrosome amplification, stage, tumor grade, hormone receptor status, and HER2 status. Associations between these factors and either RFS or OS were analyzed and presented as hazard ratios (HR) with 95% confidence intervals (CI). For centrosome size, an average size was calculated for each case. The median of all cases was used as the cutoff for the large versus small centrosome groups. The correlations of CA with ploidy and CIN were assessed with Spearman's correlation. The correlations between centrosome amplification and grade or stage were performed by stratifying patients by grade or stage and comparing the mean centrosome number among the groups by Kruskal-Wallis tests. Non-parametric tests were used because the distribution of average centrosome number was right skewed (Supplemental Figure 2-1). Two-sided, unpaired statistical tests were used throughout. $P < 0.05$ was considered statistically significant for all statistical tests.

Figure 2-1

Centrosome amplification in breast cancer.

(A) Representative single plane images of normal breast and breast cancer from the tissue microarray taken using the 100x objective. Blue = DNA, green = pericentrin. Scale bar = 5 μm. **(B)** The average centrosome number per cell (as assessed by pericentrin staining) is significantly greater in breast tumors than in normal breast samples included in the TMA ($p=0.0012$ from unpaired, two-tailed t-test). **(C)** The percentage of tumors with an average of > 2 centrosomes per cell is significantly greater than the percentage of normal breast samples with > 2 centrosomes per cell in the TMA ($p=0.049$). **(D)** Scatterplot demonstrating the correlation between average centrosome number and proliferation, as assessed by Ki67 staining.

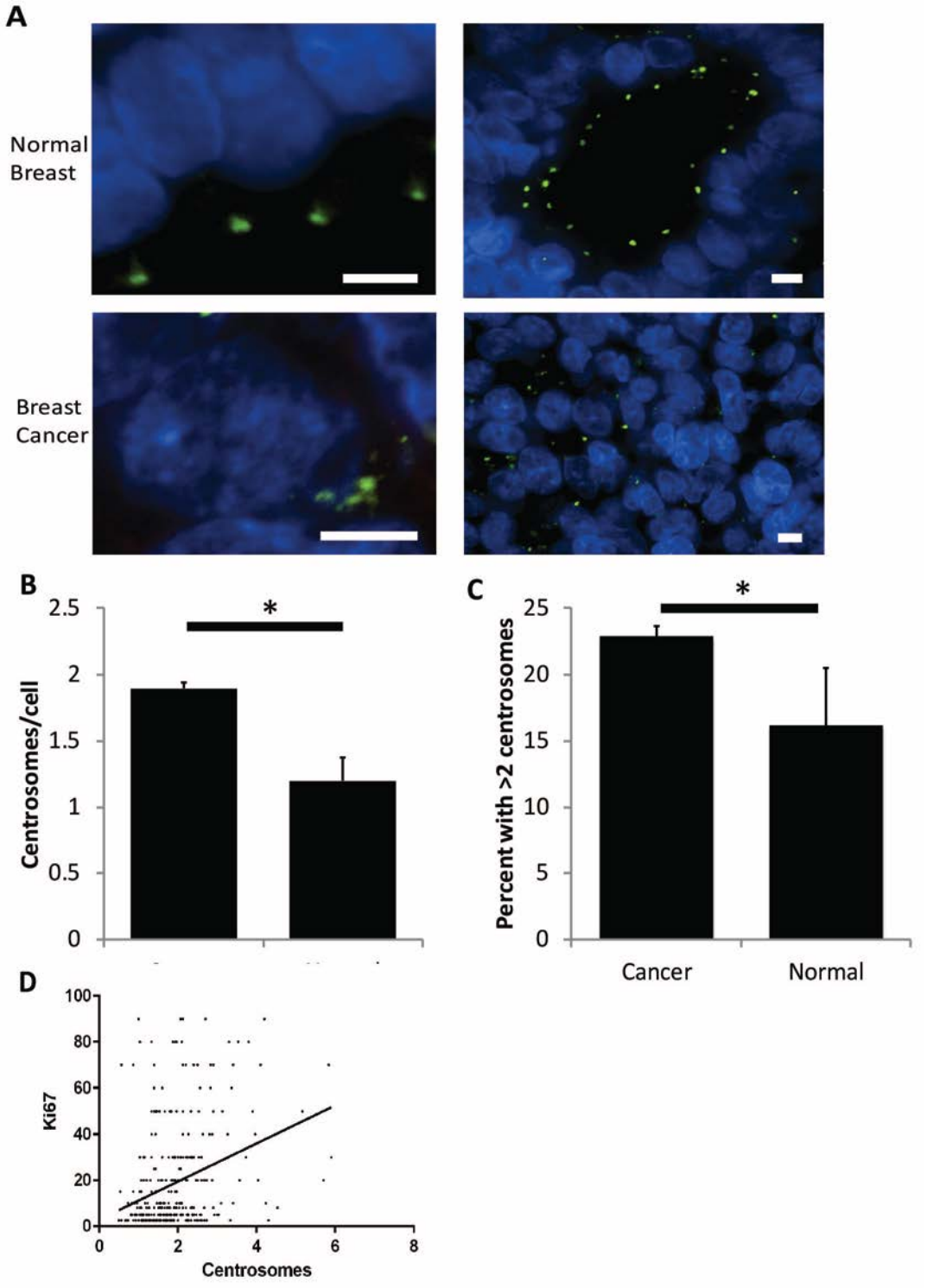
A
Normal Breast
Breast Cancer
B
Centrosomes/cell
2.5
2
1.5
1
0.5
0
*
C
Percent with >2 centrosomes
25
20
15
10
5
0
*
Cancer
Normal
D
Ki67
100
80
60
40
20
0
0
2
4
6
8
Centrosomes

Figure 2-2

Centrosome amplification is associated with adverse clinical factors.

(A-C) Centrosome amplification correlates with stage (A; p<0.01), grade (B; p<0.01), and subtype (C; p<0.01). Dots represent each patient with bars representing the average ± SE. HR = hormone receptor. **(D-F)** Tumors were considered to have CA if the average number of centrosomes per cell, as assessed by pericentrin staining, was greater than 2. Centrosomes were assessed with pericentrin staining. All-cause overall survival **(D),** recurrence-free survival **(E),** and breast cancer-specific overall survival **(F)** are reduced in patients whose tumors demonstrated CA compared to those that did not. Log rank tests were used to calculate p-values.

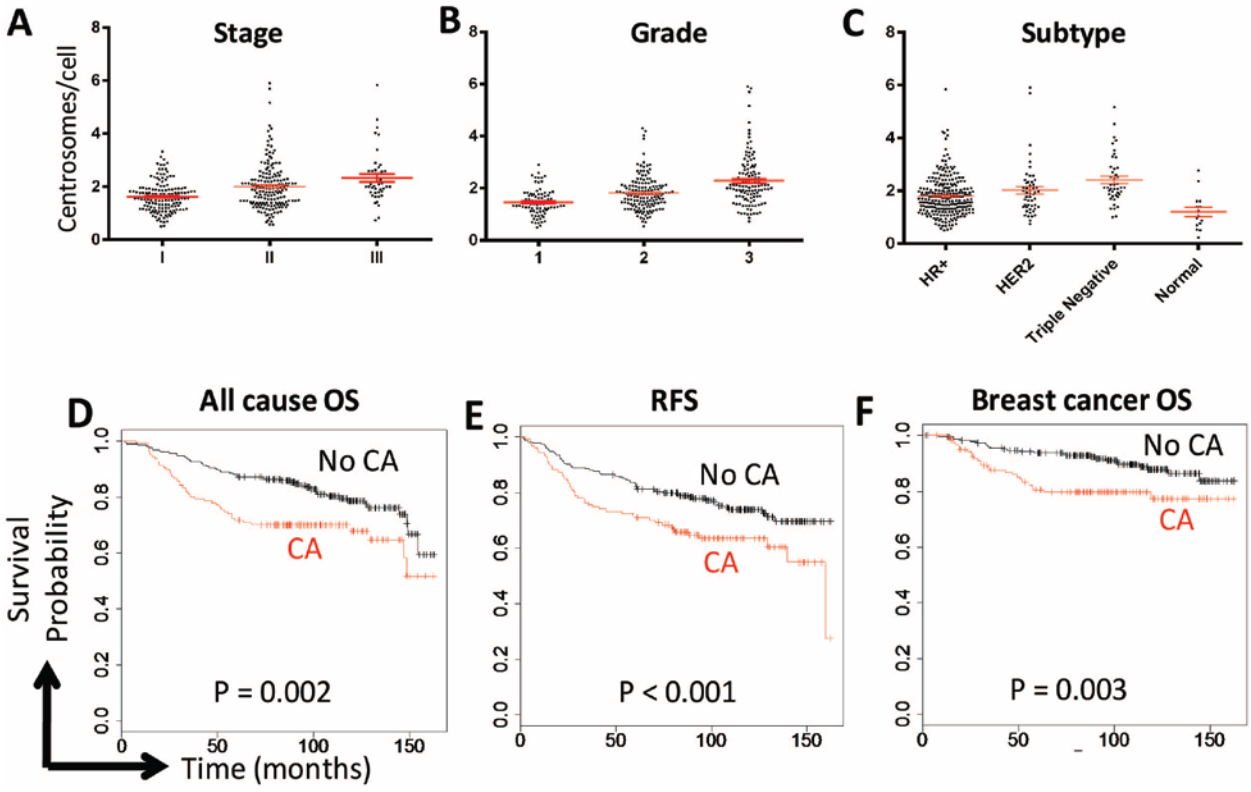

Figure 2-3

Centrosome amplification correlates with high ploidy and high CIN.

(A) Centrosome number correlates with ploidy. **(B-C)** Breast tumors were divided into two groups based on the presence or absence of CA, which was defined as having an average of >2 centrosomes per cell, as in Figure 2. Tumors with CA had higher average ploidy, as assessed by 6-chromosome FISH **(B),** and more polyploidy **(C)**. **(D)** CIN was assessed by the average non-modal chromosome number from FISH and correlated with average centrosome number. (E) CIN was higher in CA versus non-CA tumors. **(F)** Correlation of ploidy with CIN. P values displayed on the scatterplots are from Pearson's correlations. Bars represent means ±SD. **P value < 0.01.

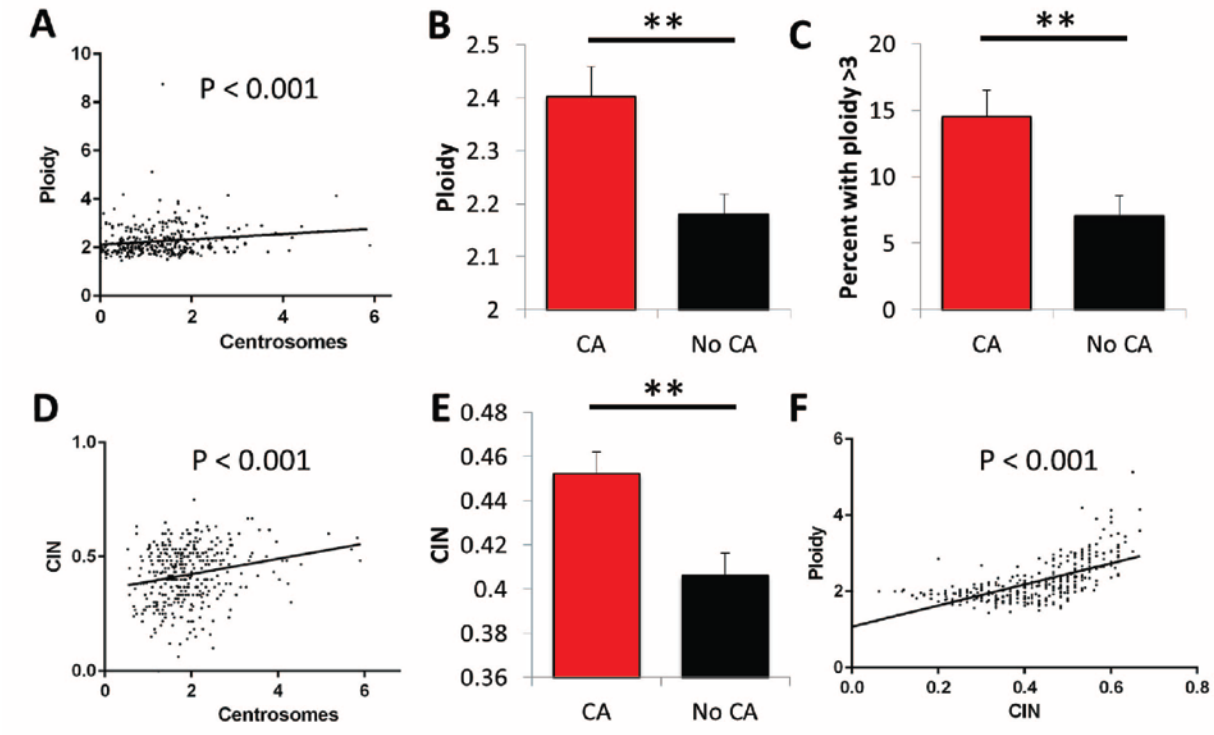

Figure 2-4

Pericentriolar material (PCM) fragmentation is more prevalent in advanced tumors.

(A-C) The average percent of centrosomes (as indicated by pericentrin) without centrioles (as indicated by polyglutamylated tubulin) were plotted based on subtype **(A),** stage **(B)**, and grade **(C).** In panel A, T-tests were used to compare averages for each breast cancer subtype to normal breast. HR+ = hormone receptor (ER and/or PR) positive and HER2 nonamplified; HER2+ = HER2 amplified; TNBC = triple negative breast cancer. In panels B-C, ANOVA was used to analyze differences across stage and grade; the asterisk indicates $P<0.05$ for these statistical tests. **(D-E)** Overall survival **(D)** and recurrence-free survival **(E)** were plotted using the Kaplan Meier method with the cutoff being the median percentage of centrosomes without centrioles. Log rank tests were used to determine P values.

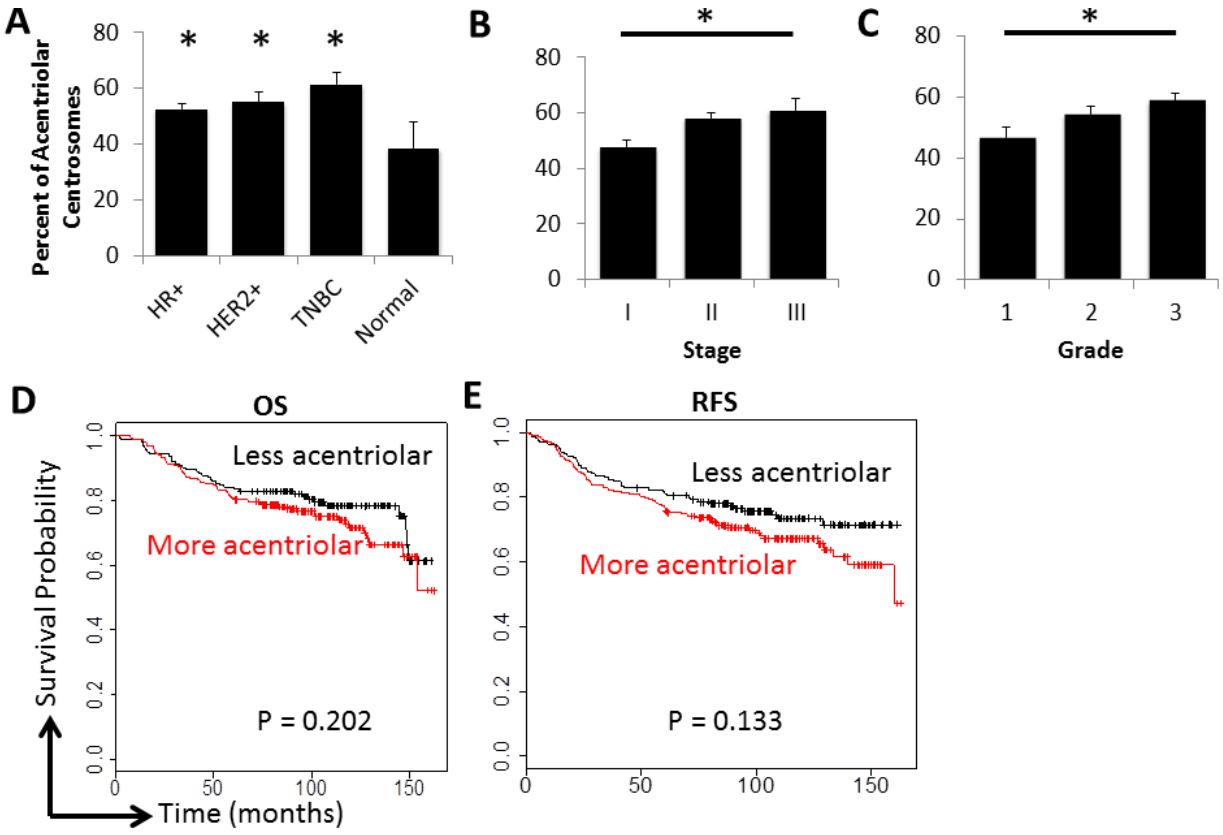
A
Percent of Acentriolar Centrosomes
80
60
40
20
0
*
*
*
HR+
HER2+
TNBC
Normal
B
*
80
60
40
20
0
I
II
III
Stage
C
*
80
60
40
20
0
1
2
3
Grade
D
OS
Survival Probability
Less acentriolar
More acentriolar
P = 0.202
0.0
0.2
0.4
0.6
0.8
1.0
0
50
100
150
Time (months)
E
RFS
Less acentriolar
More acentriolar
P = 0.133
0.0
0.2
0.4
0.6
0.8
1.0
0
50
100
150

Figure 2-5

Centrosome amplification induces dedifferentiation.

(A) Overexpression of PLK4 using doxycycline-inducible MCF10A cell line [126] results in CA after 48 hours of doxycycline treatment. $PLK4^{608}$ overexpresses a truncated form (amino acids 1-608) that contains the kinase domain but does not result in CA. Blue = DNA, yellow = overlap of pericentrin and gamma tubulin. **(B,C)** Flow cytometry analysis of CD24 and CD44 expression in MCF10A cells using PE-conjugated antibodies after 48 hours of doxycycline treatment. **(B)** Mean channel fluorescence (FL2) was normalized within cell lines (i.e. either $PLK4^{WT}$ or $PLK4^{608}$). **(C)** Bars represent the average ± SE of 3 independent experiments. **(D)** Overexpression of PLK4 using doxycycline-inducible RPE cell line [141] results in CA. **(E)** qRT-PCR analysis of cytokeratins 7, 18, and 19 normalized to 3 housekeeping genes (*RRN18S, GAPDH, ACTB*) in RPE cells. Bars represent average values of 2^-ΔΔCt from 3 independent experiments. **(F)** Tumors in the TMA with tubule formation in 2 of the 3 tumor regions examined were compared to tumors without tubule formation. Representative images demonstrate how the scoring was performed. Blue = DNA, green = pericentrin. **(G)** Representative images of normal and pleomorphic nuclei seen in RPE and MCF10A cell lines treated with doxycycline. The bar graphs demonstrate the average percent of pleomorphic nuclei in each condition from 3 independent experiments. Blue = DNA, green = pericentrin. *$P<0.05$. Scale bars = 5 μm.

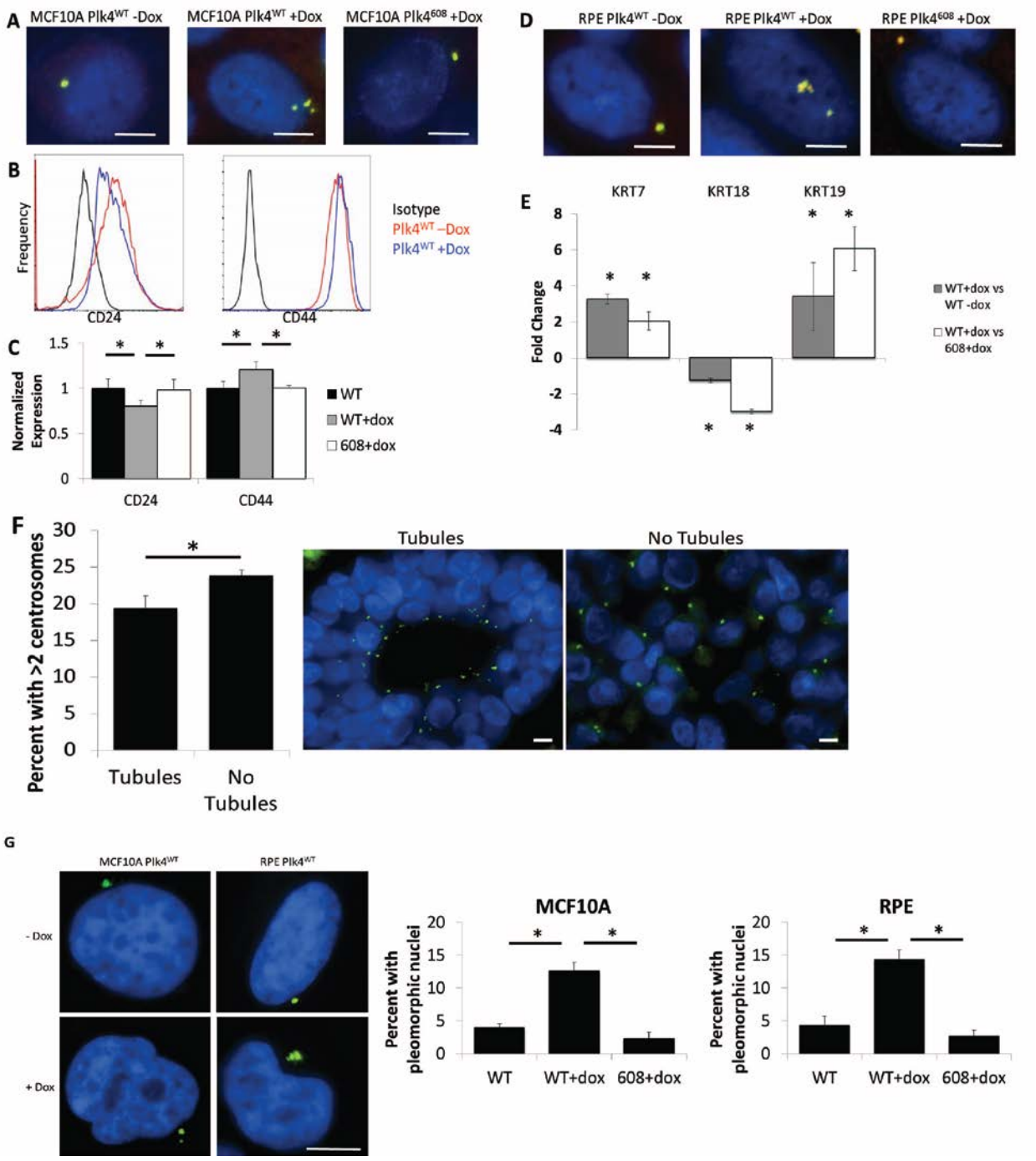
A
MCF10A Plk4WT -Dox
MCF10A Plk4WT +Dox
MCF10A Plk4608 +Dox
B
Frequency
CD24
CD44
Isotype
Plk4WT –Dox
Plk4WT +Dox
C
Normalized Expression
WT
WT+dox
608+dox
CD24
CD44
D
RPE Plk4WT -Dox
RPE Plk4WT +Dox
RPE Plk4608 +Dox
E
KRT7
KRT18
KRT19
Fold Change
WT+dox vs WT -dox
WT+dox vs 608+dox
F
Percent with >2 centrosomes
Tubules
No Tubules
G
MCF10A Plk4WT
RPE Plk4WT
- Dox
+ Dox
Percent with pleomorphic nuclei
MCF10A
RPE
WT
WT+dox
608+dox

Supplemental Table 2-1

Patient characteristics

Characteristic	**Number**	**Percent**
Race		
Caucasian	348	96.1%
Black	6	1.7%
Asian	3	0.8%
Hispanic	2	0.6%
Unknown/Other	3	0.8%
Sex		
Female	362	100.0%
Male	0	0.0%
Age at diagnosis		
<40	37	10.2%
40-49	101	27.9%
50-59	96	26.5%
60-69	64	17.7%
70-79	44	12.2%
>=80	20	5.5%
Histology		
Ductal or ductal subtype	301	83.1%
Lobular	33	9.1%
Mammary	26	7.2%
Phyllodes	1	0.3%
Adenoid cystic	1	0.3%

Histological Grade		
1	83	22.9%
2	149	41.2%
3	124	34.3%
Unknown	6	1.7%
Stage		
I	147	40.6%
II	170	47.0%
III	45	12.4%
Hormone Receptor Status		
ER+ and/or PR+	296	81.8%
ER/PR negative	65	18.0%
Unknown	1	0.3%
HER2 Status		
Positive	51	14.1%
Negative	295	81.5%
Unknown	16	4.4%
Regional Node Status		0.0%
Positive	149	41.2%
Negative	213	58.8%
Type of Surgery		
BCS	189	52.2%
Mastectomy	171	47.2%
No surgery	2	0.6%
Recurrence		
Local	13	3.6%
Distant	63	17.4%

No recurrence	285	78.7%
Unknown	1	0.3%
Vital Status		
Death due to breast cancer	50	13.8%
Death due to other cause	42	11.6%
Alive	268	74.0%

Supplemental Table 2-2

Hazard ratios from multivariate analysis.

	OS		**RFS**	
	HR	**P-Value**	**HR**	**P-Value**
High centrosomes (vs low)	1.20 (0.76-1.90)	0.427	1.25 (0.82-1.90)	0.297
Stage II (vs I)	1.50 (0.87-2.60)	0.143	1.69 (1.03-2.76)	0.039
Stage III (vs I)	3.25 (1.69-6.24)	<0.001	3.30 (1.79-6.09)	<0.001
HR positive (vs negative)	0.43 (0.25-0.73)	0.002	0.56 (0.34-0.92)	0.021
HER2 positive (vs negative)	0.63 (0.33-1.18)	0.151	0.68 (0.38-1.21)	0.185
Grade 2 (vs 1)	1.38 (0.70-2.72)	0.355	1.37 (0.75-2.53)	0.308
Grade 3 (vs 1)	1.61 (0.77-3.37)	0.207	1.68 (0.87-3.25)	0.125

Supplemental Table 2-3

Sequences of primers used for qRT-PCR.

Gene	**Forward Sequence**	**Reverse Sequence**
RRN18S	GTAACCCGTTGAACCCCATT	CCATCCAATCGGTAGTAGCG
GAPDH	GGAGCGAGATCCCTCCAAAAT	GGCTGTTGTCATACTTCTCATGG
ACTB	CATGTACGTTGCTATCCAGGC	CTCCTTAATGTCACGCACGAT
KRT7	TCCGCGAGGTCACCATTAAC	GCTCTGTCAACTCCGTCTCAT
KRT18	GGCATCCAGAACGAGAAGGAG	ATTGTCCACAGTATTTGCGAAGA
KRT19	AACGGCGAGCTAGAGGTGA	GGATGGTCGTGTAGTAGTGGC

Supplemental Figure 2-1

Distribution of average centrosome number per cell in the breast cancer patients represented in our TMA.

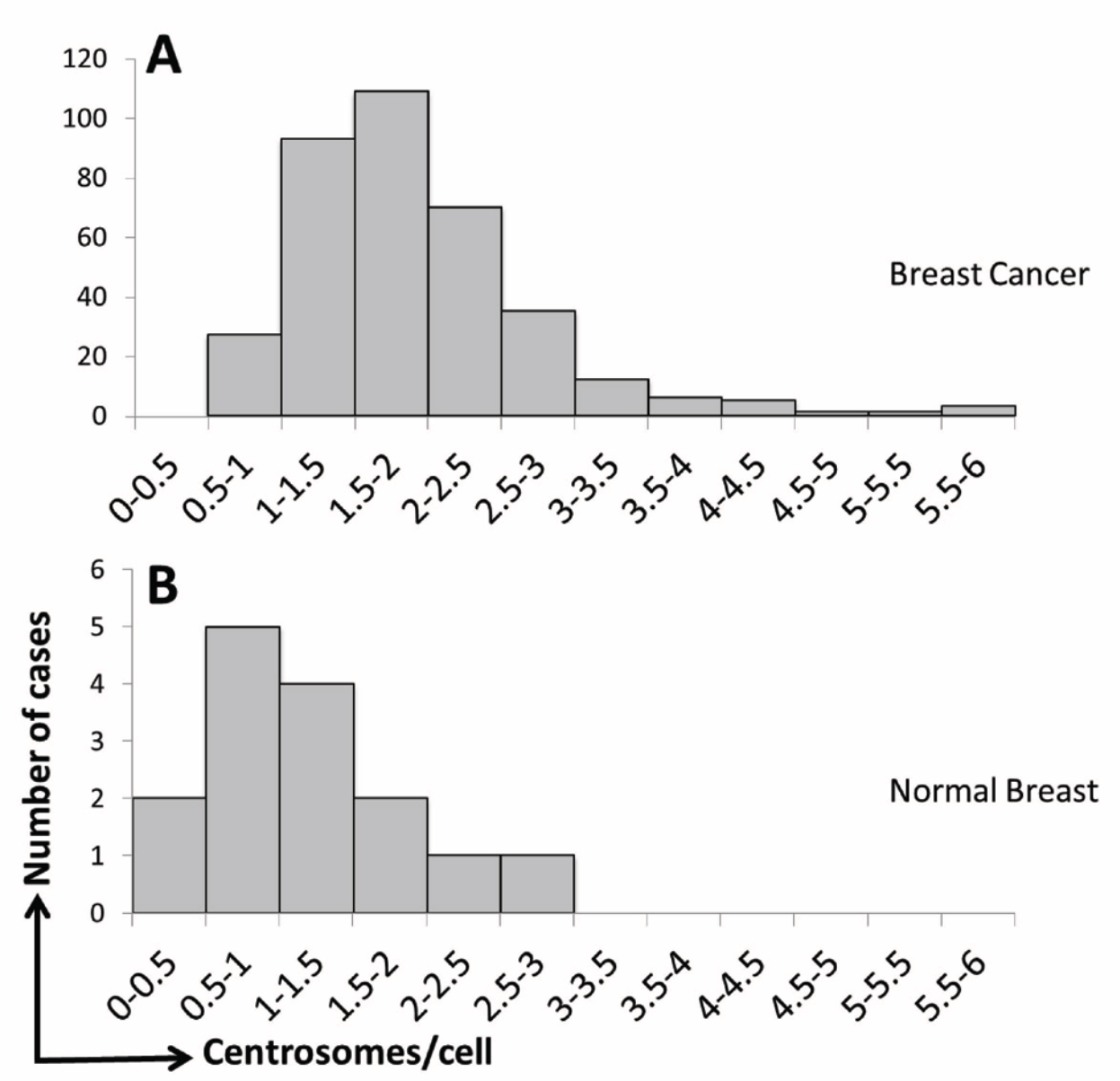

Supplemental Figure 2-2

Correlations between centrosome amplification and nodal status, patient age, and tumor size.

CA was defined as an average of greater than 2 centrosomes (marked by pericentrin staining) per cell across the 3 tumor regions for each patient. **(A)** Bars represent percentage of patients with positive nodes ± standard error of proportion. **(B-C)** Bars represent average values ± SE.

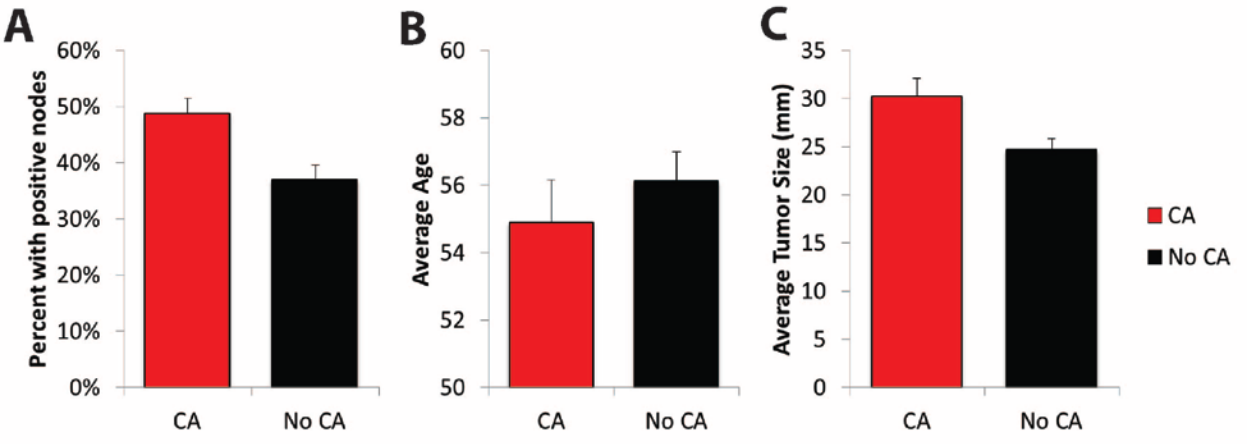

Supplemental Figure 2-3

Centrosome clustering but not structural abnormalities correlate with worse outcomes in breast cancer.

Numbers and percentages in the left column indicate tumors containing centrosomes with atypical shapes, clustering, specking, and increased size. Tumors were considered to have atypical centrosome shapes if these were observed in more than 1 of the cells counted in at least 2 of the 3 tumor regions investigated; this same criterion was used for analysis of centrosome clustering and speckling. Clustering was defined as more than 2 distinct pericentrin foci together. Speckling was defined as more than 5 distinct pericentrin foci, which were smaller than typical centrosomes. For size, patients were divided into two groups (small versus large centrosomes) using the median centrosome size (0.99 μm) as the cutoff; therefore, half of cases fall into each group. Overall survival and recurrence-free survival are plotted using the Kaplan Meier method, and log rank tests were used to determine p values. Blue = DNA, green = pericentrin. Scale bar = 5 μm.

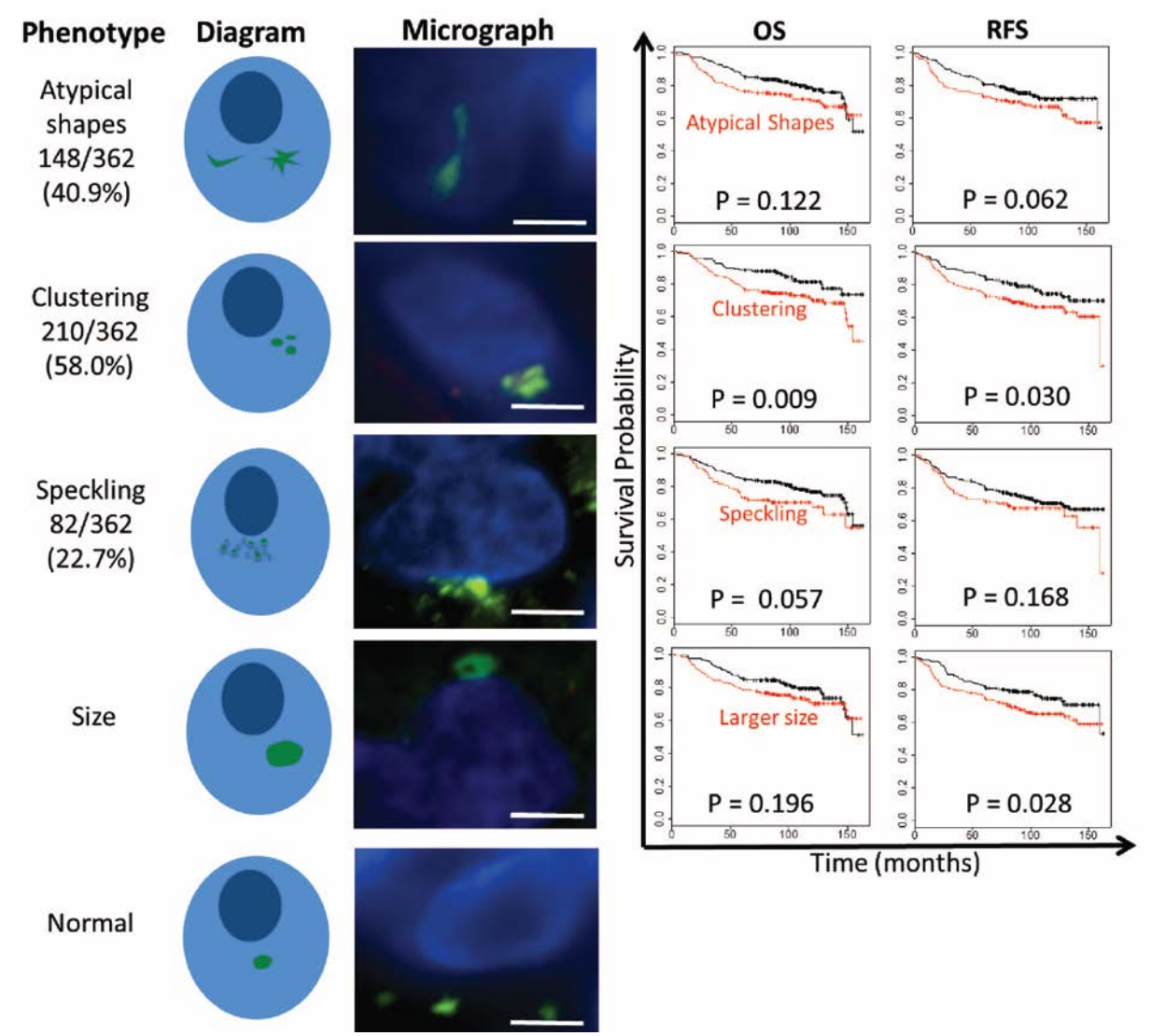
Phenotype
Diagram
Micrograph
OS
RFS
Atypical shapes 148/362 (40.9%)
Clustering 210/362 (58.0%)
Speckling 82/362 (22.7%)
Size
Normal
Atypical Shapes
P = 0.122
P = 0.062
Clustering
P = 0.009
P = 0.030
Speckling
P = 0.057
P = 0.168
Larger size
P = 0.196
P = 0.028
Survival Probability
Time (months)

Supplemental Figure 2-4

CIN is prognostic of worse breast cancer-related survival.

All-cause overall survival **(A),** recurrence-free survival **(B),** and breast cancer-specific survival **(C)** were assessed based on the presence of CIN. Displayed p-values are from log rank tests.

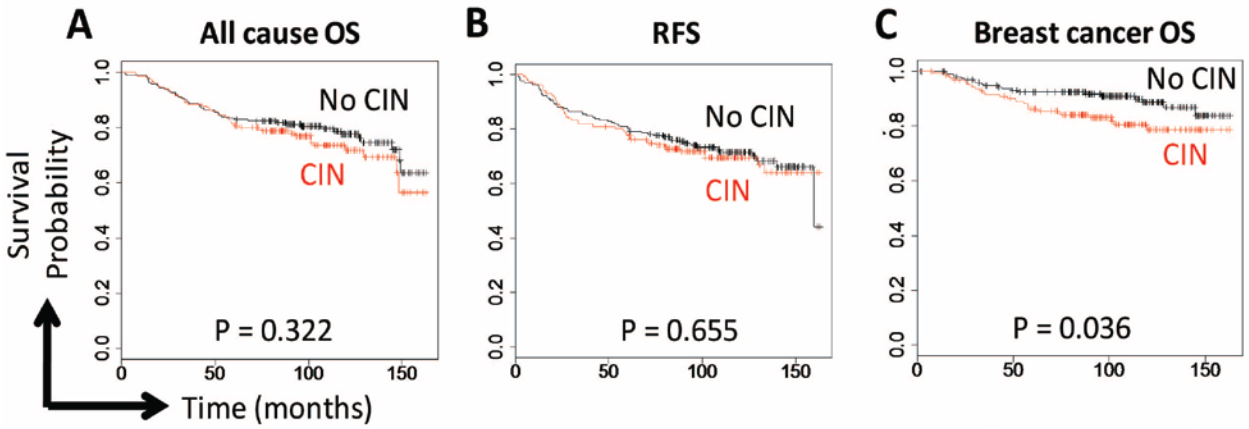

Supplemental Figure 2-5

Centrosome amplification correlates with adverse clinical factors.

(A) These analyses used the overlap of pericentrin and polyglutamylated tubulin markers to define centrosomes. The pericentrin and polyglutamylated tubulin images are enlarged from the boxed region in the merged image. Scale bar = 2 μm. Blue = DNA, green = pericentrin, red = polyglutamylated tubulin. **(B-D)** Dot plots show the average centrosome number per cell in each tumor based on stage **(B),** grade **(C),** and subtype **(D)**. Bars show averages ± SE. **(E,F)** Patients were divided into two groups (CA versus no CA) using an average of 2 centrosomes per cell as the cutoff. All-cause overall survival **(E),** recurrence-free survival **(F),** and breast cancer-specific survival **(G)** were assessed using the median centrosome value as a cutoff for low centrosomes versus high centrosomes. Displayed p-values are from log rank tests.

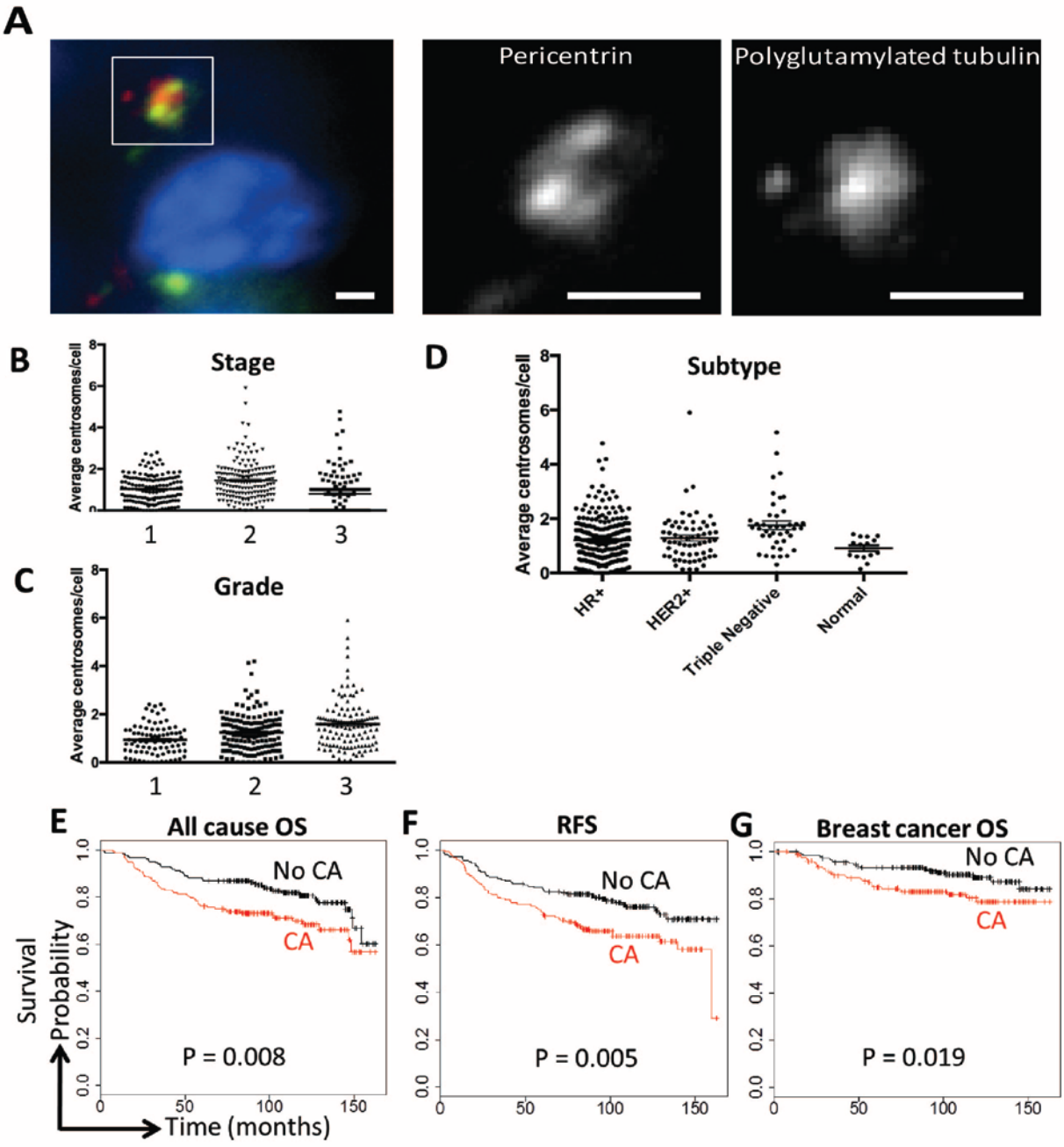
A
Pericentrin
Polyglutamylated tubulin
B
Stage
Average centrosomes/cell
1
2
3
C
Grade
D
Subtype
HR+
HER2+
Triple Negative
Normal
E
All cause OS
No CA
CA
P = 0.008
Survival Probability
Time (months)
F
RFS
P = 0.005
G
Breast cancer OS
P = 0.019

Supplemental Figure 2-6

CA correlates with higher ploidy and CIN.

These analyses were performed by defining centrosomes as the overlap of pericentrin and polyglutamylated tubulin. **(A, B)** Patients were divided into two groups based on whether their average centrosome number was above or below 2. Ploidy was determined using 6-chromosome FISH. CIN was determined as the average non-modal chromosome number for each of the 6 chromosomes assessed by FISH. Bars indicate averages ± SE. **(C,D)** Scatterplots demonstrating the correlation of CA with ploidy and CIN.

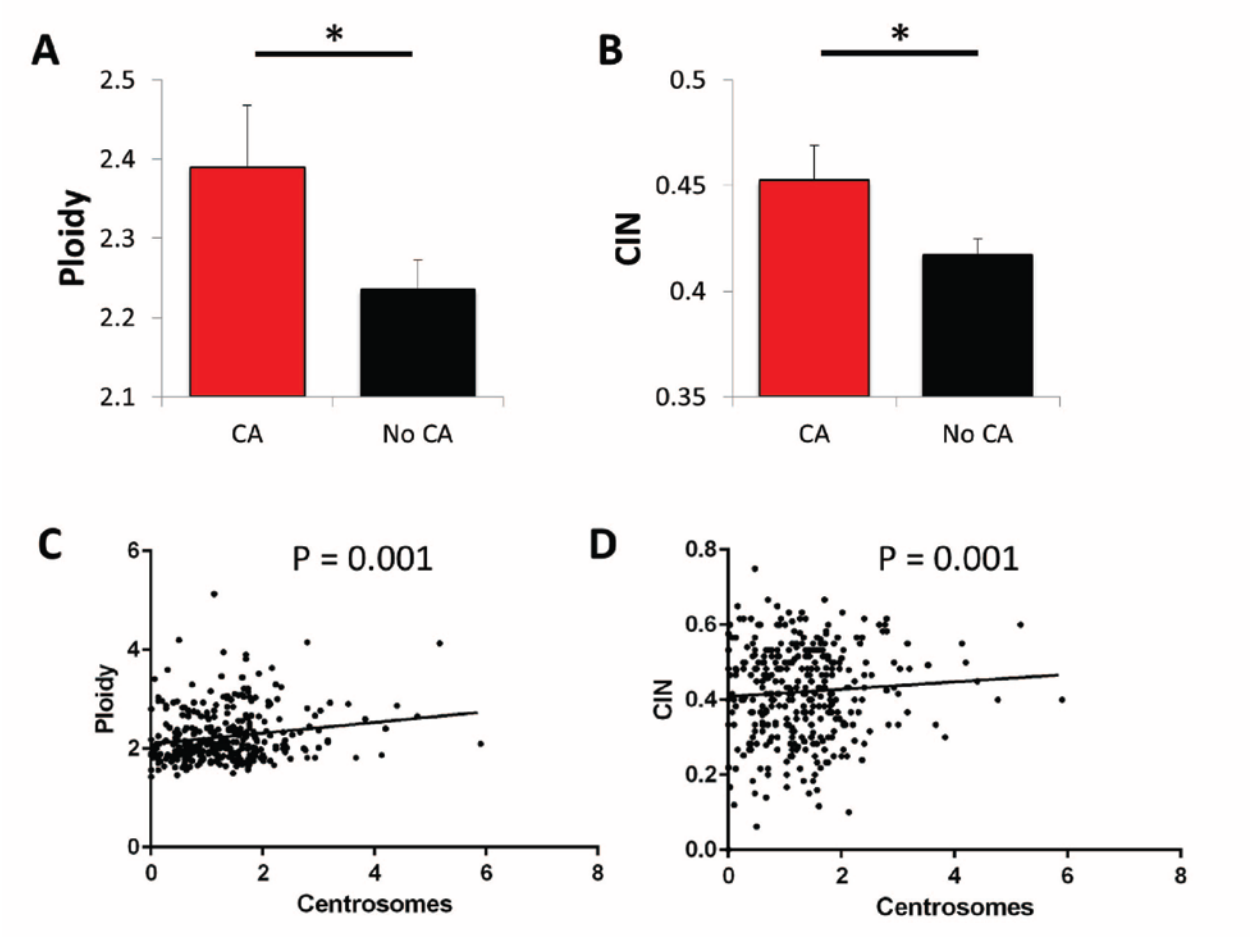

Acknowledgements

This project is supported by R01 GM097245 to MEB and R01 CA140458 to BAW and and UWCCC grant P30 CA014520. RAD is in the University of Wisconsin Medical Scientist Training Program (T32GM008692). LMZ was supported by T32CA9135-37. The authors thank Dr. David Pellman for cell lines; Dr. Monica Bettencourt Dias for helpful discussion; and the University of Wisconsin Translational Research Initiatives in Pathology laboratory for use of its facilities and services; Sandeep Saha for help with statistical analyses; and Rob Lera and Amber Lasek for reviewing the chapter.

CHAPTER 3: Centrosome amplification is predominantly caused by centriole overduplication

Work in this chapter was adapted from:

Centriole Overduplication is the Predominant Mechanism Leading to Centrosome Amplification in Melanoma

Ryan A. Denu, Maria Shabbir, Minakshi Nihal, Chandra K. Singh, B. Jack Longley, Mark E. Burkard, Nihal Ahmad

Mol Cancer Research, 2018 Jan 12, PMID 29330283

Abstract

Centrosome amplification (CA) is common in cancer and can arise by centriole overduplication or by cell doubling events, including the failure of cell division and cell-cell fusion. To assess the relative contributions of these two mechanisms in melanoma, we examined the number of centrosomes with mature/mother centrioles by immunofluorescence in a tissue microarray (TMA) of 79 melanomas and 17 benign nevi. CEP170 was used to identify centrosomes with mature centrioles; this is expected to be present in most centrosomes with cell doubling, but on fewer centrosomes with overduplication. Using this method, we find that the majority of CA in melanoma can be attributed to centriole overduplication rather than cell doubling events. Since polo-like kinase 4 (PLK4) is the master regulator of centriole duplication, we tested the hypothesis that PLK4 overexpression contributes to centriole overduplication. We found that PLK4 is significantly overexpressed in melanoma compared to benign nevi and in a panel of human melanoma cell lines (A375, Hs294T, G361, WM35, WM115, 451Lu, SK-MEL-28) compared to normal human melanocytes. However, PLK4 expression does not correlate well with CA in most cases. Nevertheless, treatment of melanoma cells with a selective small molecule PLK4 inhibitor, centrinone B, resulted in a significant decrease in the cell proliferation in melanoma cell lines. The observed anti-proliferative effects of centrinone B are accompanied by induction of apoptosis. Based on the data, we suggest that PLK4 should be further evaluated as a potential therapeutic target for human melanoma.

Introduction

Centrosomes, the major microtubule organizing centers of the cell, are composed of two orthogonal centrioles embedded in a protein-rich pericentriolar material (PCM). During interphase, centrosomes organize cytoplasmic microtubules and anchor cilia. In mitosis, centrosomes organize the mitotic spindle. Structural and functional defects of centrosomes are associated with cancer.[107,165] Among these, the most common is centrosome amplification (CA), the numerical increase in centrosome number, which has been reported in nearly all human cancers, both solid and hematological,[107-113] and in some contexts is sufficient for tumorigenesis [122]. CA has a number of unwanted consequences. First, cells with supernumerary centrosomes generate genetic diversity through asymmetric cell divisions on abnormal spindles with chromosome missegregation.[108,111,123] Consistent with this, CA correlates with aneuploidy and chromosomal instability in cancer.[109,124] In addition, CA enhances invasiveness, attenuates cilia signaling, increases activity of Rac and Rho GTPases, induces de-differentiation, and increases microtubule-directed polarization.[109,114,126]

Polo-like kinase 4 (PLK4) is the master regulator of centriole duplication.[62,63,166] When overexpressed, PLK4 can induce CA through the generation of multiple procentrioles adjoining each parental centriole,[76,167] and can enhance cancer cell migration via actin reorganization.[168] PLK4 inhibition impairs centriole duplication and enhances genomic instability of cancer cells, leading to cell death.[169] Based on recent research, PLK4 is emerging as a potential target for cancer treatment. PLK4 is overexpressed in colorectal cancer tissue compared with the adjacent normal intestinal mucosa.[170] Additionally, PLK4 is overexpressed in breast cancer, correlates with worse outcomes,[171] and predicts resistance to taxane-based chemotherapy.[172] However, the role of PLK4 in melanoma and its association with CA are not known.

Melanoma is one of the most aggressive human cancers with approximately 87,110 new melanoma cases and 9,730 melanoma-related deaths predicted in the U.S. in 2017.[173] The role of CA in melanoma and its underlying causes have not been well-studied. The activating mutation *B-RAF*^{V600E} can induce CA by abrogating a negative feedback regulation loop that disrupts centrosome duplication ;[174,175] however, CA does not correlate with *B-RAF* mutations in melanoma cell lines,[176] suggesting that other mechanisms are responsible. The two possible mechanisms leading to CA are cell doubling events (cytokinesis failure or cell-cell fusion) and centriole overduplication.[114] The relative contribution of these mechanisms has yet to be determined.

In this study, we evaluated the prevalence and mechanism of CA in melanoma, and the possible role of PLK4 overexpression and CA and as therapeutic targets.

Results

Centrosome amplification is prevalent in melanoma

To determine the frequency of CA in melanoma, we analyzed centrosomes by immunofluorescence staining of a melanoma TMA for pericentrin (Figure 3-1A). We analyzed CA in 79 melanomas and 17 benign nevi (Figure 3-1B). The mean centrosome number was 2.0 (median 1.9) in melanoma compared to 1.1 (median 1.2) in benign tissue (Figure 3-1C). We also analyzed CA by calculating the percentage of tumor cells within each sample that had greater than 2 centrosomes (Figure 3-1D), as proliferating cells in late G2 can have duplicated and separated centrosomes without CA. The rate of CA ranged from 0-83.3% with a mean of 33.5% (median 31.4%) for melanomas compared to benign samples which had a range of 0-20.0% with mean 6.5 (median 3.3). Of 79, 35 melanoma samples had an average of greater than 2 centrosomes per cell compared to 0/17 benign samples. There was no significant difference based on stage (p-value = 0.40) or comparing primary to metastatic samples (p-value = 0.33) (Figure 3-1E). We conclude that CA is common in malignant melanoma but does not appear to have a strong correlation with disease progression.

Centrosome amplification arises predominantly from centriole overduplication

Next, we sought to determine the contributions of the two principal mechanisms of CA: centriole overduplication versus cell doubling events (e.g. cytokinesis failure or cell-cell fusion). CEP170 marks mother centrioles and is recruited to centrosomes in late G2 [177]. If centriole overduplication is the predominant mechanism leading to CA, we expect only one centrosome to co-stain with CEP170; conversely, if cell doubling events were predominant, then we expect all centrosomes would have mature centrioles, as identified by CEP170 (Figure 3-2A). Staining for

CEP170 can distinguish between these two mechanisms of CA (Figure 3-2B) [177]. Before employing this strategy, we confirmed this by assessing CEP170 in cells that failed cytokinesis compared to cells that overexpressed PLK4 to cause centriole overduplication. (Supplemental Figure 1). In the TMA, we assessed the percent of centrosomes in each melanoma cell (determined by tyrosinase expression, see Supplemental Figure 3-2) that co-stained for CEP170 (Figure 3-2C). The mean percentage of centrosomes with CEP170 was 18.0% for melanoma compared to 56.8% for benign samples. This demonstrates that the majority of centrosome amplified melanomas arise from overduplication rather than cell doubling events.

PLK4 overexpression is associated with centrosome amplification in clinical melanoma cases

Given that centriole overduplication is the dominant cause of CA, we next investigated underlying mechanisms. *B-RAF*^{V600E} mutations do not adequately explain all cases of CA in melanoma.[176] Given that PLK4 is the master regulator of centriole duplication, we hypothesized that its overexpression could be responsible for overduplication. To test this, we quantified PLK4 expression in the same melanoma TMA and co-stained with two centrosome markers, pericentrin and γ-tubulin (Figure 3-3A). We empirically tested 4 different antibodies before choosing the best (Supplemental Figure 3-3). To validate the PLK4 antibody used in this study, we first stained untreated and PLK4-overexpressing cell lines by immunofluorescence and also embedded formalin-fixed cell lines in paraffin for fluorescence immunohistochemistry; indeed, this antibody labels centrosomes (Supplemental Figure 3-4). Furthermore, we utilized RPE PLK4 floxed conditional knockout cell lines (See Chapter 7). These cells were treated with Cre recombinase to cause deletion of exons 3 and 4 of PLK4, then the efficiency of PLK4 knockout

was assessed by qRT-PCR, followed by immunofluorescent staining with the PLK4 antibody. We find that knockout of PLK4 was accomplished and resulted in reduced PLK4 staining by this antibody (Supplemental Figure 3-4), and therefore proceeded to stain the melanoma TMA.

In the TMA, melanoma samples had significantly greater PLK4 expression at the centrosomes compared to benign nevi (Figure 3-3B). However, PLK4 expression did not correlate well with CA (Figure 3-3C-D). Because PLK4 overexpression is known to drive CA via centriole overduplication, we correlated PLK4 expression with our CEP170 mature centriole analysis. Interestingly, many of the melanomas with high PLK4 expression demonstrated a low percent of centrosomes with CEP170, suggesting that PLK4 overexpression may be responsible for centriole overduplication-induced CA in these 15% (10/66 cases) of melanomas (Figure 3-3E, outlined by dotted rectangle).

We then assessed the correlation between PLK4 expression and survival in the TCGA melanoma dataset. Interestingly, PLK4 expression varied among tumors by nearly 7 log expressions (Supplemental Figure 3-5A). While there was a trend toward worse survival with higher PLK4 expression, the differences were not significant (Supplemental Figure 3-5B-C). We conclude that PLK4 expression is the best candidate as a principal driver of centriole overduplication in melanoma but is not itself prognostic.

There are two scores to determine CA in clinical samples that have previously been reported: the centrosome index (CI)[178,179] and the centrosome amplification 20 (CA20).[180] Both of these scores are calculated from mRNA expression values of certain genes required for centriole duplication. We assessed whether or not these scores correlated with PLK4 expression and whether they were prognostic in the melanoma TCGA cohort. Both scores trended toward correlating with worse overall survival and disease-free survival in this cohort. Overall survival

was significantly worse in patients with both high CI and CA20. CA20 and CI significantly correlated with each other, although with limited strength ($r = 0.23$, $P < 0.001$). CA20 also correlated strongly with PLK4, but CI did not. Next, we assessed the p53 status of tumors overexpressing PLK4, since loss of p53 has been shown to permit the growth of cells with CA, which would otherwise arrest.[67] Of the 20 melanomas with increased PLK4 expression, 4 had mutant or deleted p53. Taken together, these melanoma TCGA data suggest that PLK4 overexpression may explain some cases of CA in melanoma.

Inhibition of PLK4 exerts anti-proliferative effects and deplete centrioles in human melanoma cells

To evaluate the potential of PLK4 as a drug target in melanoma, we first examined its expression profile in a series of human melanoma cell lines (A375, Hs294T, G361, WM35, WM115, 451Lu, and SK-MEL-28) and compared to normal adult human epidermal melanocytes (HEMa). All of these cell lines have intact p53 activity except for SK-MEL28. Compared to HEMa, melanoma cell lines showed a significantly higher level of PLK4 protein and mRNA (Figure 3-4A-B). We also assessed centriole numbers in these cell lines and correlated with PLK4 expression. While the data suggest a positive trend, the correlation is not statistically significant (Figure 3-4C-F).

Next, melanoma cells were treated with a small molecule inhibitor of PLK4, centrinone B,[157] and we assessed cells viability. First we confirmed that centrinone B depleted centrioles in these cell lines by immunofluorescent staining of centrioles (Figure 3-4C, D, G). For A375 and Hs294T cell lines, treatment with centrinone B resulted in a marked decrease in cell viability (Figure 3-4H). Interestingly, normal human melanocytes (HEMa) were much less sensitive to

centrinone B (Figure 3-4H). Our data demonstrate that treatment of human melanoma cell lines with centrinone B reduces cell proliferation.

To ensure that the observed effects of centrinone B on these melanoma cell lines is dependent on centrinone B targeting PLK4, we overexpressed a centrinone B-resistant allele of PLK4 (G95L mutation)[157] in these cell lines (Supplemental Figure 3-6). We find that overexpression of $PLK4^{G95L}$ makes the cell lines more resistant to centrinone B, suggesting that the observed effects of centrinone B on the melanoma cell lines is dependent on inhibiting PLK4.

We hypothesized that CA is a biomarker for sensitivity to PLK4 inhibition. To test this hypothesis, we correlated centriole numbers with sensitivity to centrinone B in the aforementioned melanoma cell lines. Furthermore, we utilized inducible-PLK4 overexpression in RPE-1 and MCF10A immortalized, non-transformed human cell lines to model CA and treated these cells with a range of concentrations of centrinone B. By both crystal violet staining and assessment of cell viability, we find no difference in centrinone B sensitivity in cells with CA compared to controls (Supplemental Figure 3-7).

PLK4 inhibition induces apoptosis in human melanoma cells.

Reduced cell viability in response to centrinone B could be attributable to slowed proliferation, apoptosis, or to other mechanisms of cell death. To assess apoptosis, centrinone B-treated cells were stained with Annexin V and propidium iodide (PI) and examined by flow cytometry. The number of Annexin V and PI-stained cells exhibited a significant concentration-dependent increase in A375 and Hs294T cells, indicating an increase in apoptosis following PLK4 inhibition; however, this increase in apoptosis was not observed in normal melanocytes (Figure 3-5A-B). Also, PARP cleavage was assessed in centrinone B-treated cells, as this is a

hallmark of cellular apoptosis. Cleaved PARP bands are seen in centrinone B-treated A375 and Hs294T cells, but these cleaved PARP bands are not as pronounced in HEMa (Figure 3-5C). We conclude that PLK4 inhibition by centrinone B reduces cell viability and induces apoptosis in human melanoma cell lines.

Discussion

A century ago, Theodor Boveri proposed that increased centrosome numbers can cause cancer.[2] This is supported by evidence demonstrating that CA is found in precursor lesions and could be an early or even initiating event in carcinogenesis.[124,152,181] Further, CA is elevated in higher tumor stages and grades, is a prognostic biomarker,[109] and may predict paclitaxel resistance.[182] Therefore, it is important to understand the underlying mechanisms leading to CA.

Our findings address several important questions regarding CA in human melanoma. Our analysis of a melanoma TMA demonstrated that 44.3% of melanomas display CA. Herein, we have proposed that most of CA is due to centriole overduplication, while a minority of CA is due to doubling events. There are some limitations to this analysis using a mother centriole marker. First, if cells with centriole overduplication progressed through late G2 when CEP170 is recruited to the nascent mature centriole,[177] we would underestimate the amount of CA due to centriole overduplication and overestimate the amount of CA due to doubling events. However, we actually observed a decrease in the percentage of centrosomes containing CEP170 in melanomas compared to benign controls, suggesting that this has not had a substantial impact on our analysis. Another limitation is the difficulty in assessing centrioles in formalin-fixed paraffin-embedded tissue. There are instances where the pericentrin staining may underestimate the number of centrioles present in a sample; therefore, there may be instances where we have underestimated the degree of CA. Additionally, a cell's centrosomes may not be present in the analyzed tissue section, and this sectioning artifact can also contribute to an underestimation of CA. There are also instances where we may have overestimated CA, as not every pericentrin focus may represent a real centrosome with centrioles.

We hypothesized that overexpression of PLK4, the master regulator of centriole duplication, was responsible for most of these overduplication events. Our results suggest that PLK4 is required for centriole overduplication, as inhibition of PLK4 with centrinone B reduces CA in melanoma cell lines; however, overexpression of PLK4 does not appear to be the driver of most cases of centriole overduplication in melanoma, and there may be other mechanisms at play. One previously reported mechanism is *B-RAF*^{V600E} mutation,[174,175] but the relative contribution of this mechanism to CA in melanoma is unclear [176]. Further study of these other drivers of centriole overduplication is warranted. *In vitro* experimental evidence has suggested that overexpression of PLK4,[126] SAS6,[183] STIL,[184] and pericentrin,[185] to name a few, can result in centriole overduplication. There is a dearth of reports of the main centrosome components being genetically altered in cancer and leading to CA. We analyzed melanoma TCGA data and also found a no obvious causative mutations, copy number variations, or expression changes in the 366 proteins known to localize to the centrosome (data not shown).

Our results show that PLK4 is significantly overexpressed in clinical human melanoma tissues compared to nevi tissues, and in human melanoma cell lines compared with normal primary melanocytes. Previous reports have similarly found increased PLK4 expression in medulloblastoma, breast, colorectal, prostate, and ovarian cancers [155,170-172,186,187]. Further, we find that PLK4 inhibition reduces cellular growth and viability and increases apoptosis in human melanoma, suggesting a potent pro-proliferative function of PLK4.In some melanoma cell lines, the PLK4 mRNA and protein levels did not correlate well. This may suggest some additional post-transcriptional and/or post-translational regulation of PLK4 that has heretofore been undetermined for PLK4, such as the presence of upstream open reading frames,[188,189] and represents a potentially interesting area of future research.

CA from PLK4 overexpression causes invasive acini formation and greater cell invasiveness in *in vitro* cell-based assays,[126,190] so we hypothesized that metastatic melanoma samples would have higher CA compared to primary melanoma samples. However, there was not a clear difference in CA between primary and metastatic samples in our TMA we analyzed. This study was not adequately powered to reject the hypothesis that CA is more common in metastatic disease, and further investigation comparing CA in primary versus metastatic patient samples is warranted.

PLK4 has grown in interest as a therapeutic target to treat cancer.[155,157] One PLK4 inhibitor, CFI-400945,[155] has completed phase 1 clinical trial for advanced cancer.[191] However, it is important to note that this compound has also demonstrated activity against the Aurora kinases, so it is difficult to determine whether the potential clinical efficacy of this drug is due to inhibition of PLK4, the Aurora kinases, or both. Given the data presented herein, we suggest that CFI-400945 or other PLK4 inhibitors be studied in a cohort expansion of melanoma patients. A remaining question to be answered is what biomarker predicts sensitivity to PLK4 inhibitors. It appears that CA does not independently predict sensitivity to PLK4 inhibition; however, our data suggest that PLK4 may be a potential biomarker, and further study will be required to answer this question. In conclusion, our data suggest that CA is prevalent in human melanoma, CA predominantly arises by overduplication of centrioles, and PLK4 is a potential biomarker and drug target in melanoma.

Materials and Methods

Tissue Microarray (TMA) and Immunohistochemical (IHC) Analysis

A melanoma TMA was purchased from US Biomax (ME1004c, 100 cases/cores), containing 62 cases of malignant primary melanoma, 20 metastatic melanomas, and 18 nevus tissues. IHC was carried out as previously described.[109,192] Briefly, the slide was heated at 60 °C for 30 min to melt the paraffin, deparaffinized with xylenes (10 minutes x 3) and rehydrated with serially diluted ethanol washes (100%, 95%, 80%, 50%, 2 minutes each) followed by water. Antigen retrieval was performed in a pressure cooker at 121 °C with citrate buffer (pH 6.0) for 5 minutes. Blocking was done for 1 hour in 10% fetal bovine serum (FBS) in PBS. Tissues were probed with anti-PLK4 (Abcam, ab137398, 1:200), anti-pericentrin (Abcam, ab4448, 1:200), anti-CEP170 (Life Technologies, 72-413-1, 1:100), anti-γ-tubulin (Abcam, ab27074), and anti-tyrosinase (Thermo Scientific, MS-800, 1:200) antibodies diluted in 1% FBS and 0.1% triton-X in PBS overnight in a humidified chamber at 4°C. The slide was then incubated with Alexa fluor-conjugated secondary antibodies (Jackson ImmunoResearch Laboratories) for 1 hour at room temperature. Slides were washed 3 times after primary and secondary antibody incubations with PBS + 0.1% triton-X. Slides were counterstained with 4',6-diamidino-2-phenylindole (DAPI) and mounted with ProLong Gold antifade reagent (Life Technologies). Scoring of centrosome phenotypes was performed using a Nikon Eclipse Ti inverted microscope, 100x objective, and CoolSNAP HQ2 charge-coupled device camera (Photometrics). The observer was blinded to clinical data and analyzed centrosomes in an average of 29.7 cells per case from at least 3 different regions of the tumor core. We examined the number of pericentrin foci as well as foci that overlapped with CEP170 in cells expressing tyrosinase, a melanocyte marker (Supplemental Figure 2). A focus was defined as a region of signal intensity that exceeded a set

threshold. Tyrosinase staining also allowed for delineation of individual cells. Tissue quality was poor for 3 melanomas and 1 benign sample, so these were excluded from analysis.

To quantify PLK4 expression, the TMA was imaged using a Vectra automated quantitative pathology imaging system (PerkinElmer Life Sciences) with a 40x objective. Tissue images were segmented and scored using inForm (version 1.4.0). We quantified total PLK4 expression and PLK4 expression co-localizing with pericentrin in tyrosinase-positive cells.

Cell Culture

The human melanoma cell lines A375, Hs294T, G361, WM35, WM115, 451Lu, and SK-MEL-28 and adult human epidermal melanocytes (HEMa) cells were obtained from American Type Culture Collection (ATCC). The HEMa cells were cultured in Dermal Cell Basal Medium supplemented with Melanocyte Growth Kit (ATCC). The melanoma cell lines were maintained in specified media supplemented with 10% FBS (Sigma-Aldrich) in a humidified chamber with 5% CO_2 at 37 °C. G361 was maintained in McCoy's 5a medium, A375 and Hs294T in Dulbecco's Modification of Eagle's Medium (DMEM) and 451Lu, WM35, WM115, and SK-MEL-28 in Minimum Essential Medium (MEM), procured from Corning Cellgro. Melanoma cells were authenticated by STR analysis using the Promega PowerPlex 16 HS System kit (DC2101) at the University of Wisconsin Translational Research Initiatives in Pathology laboratory (TRIP Lab). The cells were routinely tested for mycoplasma using the Mycoplasma Detection Kit (Lonza) according to the vendor's protocol. The effects of PLK4 inhibitor centrinone B (Tocris Biosciences) were analyzed at multiple concentrations for 48 hours.

To make PLK4 resistant to centrinone B, we used Phusion site-directed mutagenesis of pcDNA3XFLAG-PLK4 vector to introduce the G95L mutation [157]. $PLK4^{G95L}$ was transfected

into melanoma cell lines using Lipofectamine 2000 (Thermo). Cells were plated in 6-well plates and transfected at 60% confluency. DNA lipid complex was prepared using 4 µg plasmid in 250 µl serum free medium and 10 µl Lipofectamine 2000 in 250 µl serum free medium. Each was mixed separately for 5 minutes then combined together and incubated for 20 minutes at room temperature. During incubation, medium was remove from wells, rinsed once with PBS, and replaced with 2 mL of serum free medium and 500 µl of DNA-Lipofectamine 2000 complex to appropriate wells. Cells were incubated for 24 hours, removed transfection media and replaced with regular media. Selection of stable clones was done using 2 µg/ml G418.

Immunoblotting

Control and treated cell pellets were lysed in 1X RIPA buffer (EMD Millipore Corp.) containing 10 µL/mL protease inhibitor cocktail (Thermo Fisher) and 1 mM PMSF (Amresco, LLC) and protein was isolated. For western blot analysis, 40 µg protein was electrophoresed on SDS-PAGE, transferred to a nitrocellulose membrane, blocked with 5% non-fat dry milk, incubated with primary antibodies PLK4 (Abcam ab56752), PARP (Cell Signaling 9542), and β-actin (Cell Signaling 4970S), followed by incubation with secondary HRP-conjugated antibody and chemiluminescent detection using Kodak Image Station 4000 MM (Carestream Health).

Quantitative Real-Time Reverse Transcription PCR (qRT-PCR)

RNA was extracted from the cells using RNeasy Mini Kit (Qiagen) and cDNA was transcribed with M-MLV reverse transcriptase (Promega). qRT-PCR was performed using StepOnePlus PCR system (Life Technologies) and SYBR Premix Ex Taq II (TaKaRa). PLK4 primer pair was procured from Sigma-Aldrich and GAPDH primer pair was selected from the

PrimerBank database [193]. Relative quantification was analyzed using GAPDH as endogenous control and ΔΔCT algorithm to assess PLK4 mRNA level.

Flow Cytometry

Detection of apoptotic cells in centrinone B-treated samples were carried out using Vybrant Apoptosis Assay Kit (Molecular Probes). Briefly, A375 and Hs294T cells (10^5) were plated in 6-well plates and treated the next day with centrinone B (25, 50 and 100 nM) for 48 hours. Cells were trypsinized and resuspended in Annexin V binding buffer followed by incubation with Annexin V- FITC for 15 min at 4 °C in the dark. Cells were further stained with 5 µl of propidium iodide (PI) for another 5 min at 4 °C in the dark. Apoptotic cells were evaluated immediately on a flow cytometer (BD Biosciences) and analyzed with FlowJo software.

Cell Proliferation and Viability Assays

The effect of centrinone B on melanoma cell line and normal melanocyte viability was determined using the CytoTox-Glo assay (Promega). Briefly, cells were counted and plated in a 96-well plate and next day, treated with centrinone B for 48 hours, followed by incubation for 15 min with AAF-Glo substrate (alanyl-alanylphenylalanyl-aminoluciferin), which determines a distinct intracellular protease activity related with cytotoxicity (dead-cell protease) via a luminescent signal. Cell viability was determined by subtracting the luminescent signals of dead cells (due to centrinone B) from total dead cells (after addition of digitonin to lyse remaining viable cells). Data are represented as relative light units (RLU) for viable cells.

To assess whether CA sensitizes to centrinone B, we utilized RPE-1 and MCF10A (two immortalized, non-transformed human epithelial cell lines) with doxycycline-inducible PLK4. These cell lines were a kind gift from Dr. David Pellman. 1000 cells in 100 μL media were plated per well in 96 well plates. Cells were allowed to attach overnight, then doxycycline was added the next morning to a concentration of 2 μg/mL. Centrinone B was added the following day. After 4 days of incubation with centrinone B, CCK-8 vital stain (Biotool) was added to each well, incubated for 1 hour at 37 °C, and absorbance was analyzed with a spectrophotometer. From each experimental absorbance value, we subtracted the absorbance value of wells with media plus CCK-8 reagent (indicating background absorbance without cells). To further assess proliferation, we utilized crystal violet staining in 24-well plates. For crystal violet staining, cells were plated at a density of 5000/well. Doxycycline was added the next day, and centrinone B was added the following day. Cells were incubated for 4 days after addition of centrinone B, then stained with crystal violet.

Immunofluorescence (IF) and Microscopy

IF and imaging were carried out as previously described [194,195]. Cells were seeded on glass coverslips in 24-well plates and fixed with 100% ice-cold methanol for 15 min. Fixed cells were then blocked for 30 min in 3% bovine serum albumin (BSA) and 0.1% triton X-100 in PBS (PBSTx + BSA). Primary antibodies were incubated in PBSTx + BSA for 1 hour at room temperature and washed three times in PBSTx, followed by secondary antibody incubation in PBSTx + BSA for 30 min at room temperature and two washes with PBSTx. Primary antibodies used were: pericentrin (Abcam, ab4448), centrin (Millipore, 04-1624), γ-tubulin (Abcam, ab27074), CEP170 (Life, 72-413-1). Alexa Fluor-conjugated secondary antibodies were used at

1:350 (Invitrogen). Cells were counterstained with DAPI and mounted on glass slides with Prolong Diamond antifade medium (Invitrogen). Images were acquired on a Nikon Eclipse Ti inverted microscope using a 100x objective; and CoolSNAP HQ2 charge-coupled device camera (Photometrics). Optical sections were taken at 0.2-μm intervals and deconvolved using Nikon Elements. Images were processed and analyzed using Nikon Elements software. The observer was blinded to information about each sample in the TMA.

Statistical Analysis

ANOVA and T-tests were used to compare means. The correlation of centrosomes with PLK4 expression was assessed with Pearson's correlation. Dunnett's multiple comparison and Fisher's least significant difference tests were used to compare the control with all the treatment groups for experiments involving centrinone B treatment. Two-sided, unpaired statistical tests were used to calculate statistical differences. P value <0.05 was considered statistically significant for all statistical tests. Indications are made in the figures and legends for statistical significance.

Figure 3-1

Figure 1. Centrosome amplification is prevalent in melanoma.

(A) Micrographs demonstrating centrosome amplification in melanoma but not in benign melanocytes from a melanoma TMA (US Biomax TMA# ME1004c). Blue = DNA/DAPI, red = pericentrin, scale bar = 5 μm. **(B)** Dot plot demonstrating the number of pericentrin foci observed in each individual cell in every sample in the TMA. Melanoma samples are demonstrated with black circles and benign samples are demonstrated with gray triangles. Each dot represents one cell. **(C)** The data from panel B are combined to demonstrate aggregate differences in CA between melanoma and benign samples. **(D)** Dot plot quantifying the percent of cells displaying centrosome amplification, defined as having more than 2 pericentrin foci, in melanoma samples (n=79) versus benign samples (n=17). **(E)** Dot plot demonstrating differences in centrosome amplification based on primary melanoma tumors of stage I-IV (n=59) versus metastatic tissue (n=20) versus benign tissue (n=17). Bars represent means ±SD. Statistical significance is indicated as *$p<0.05$. T tests were used in C and D, and an ANOVA was used in E.

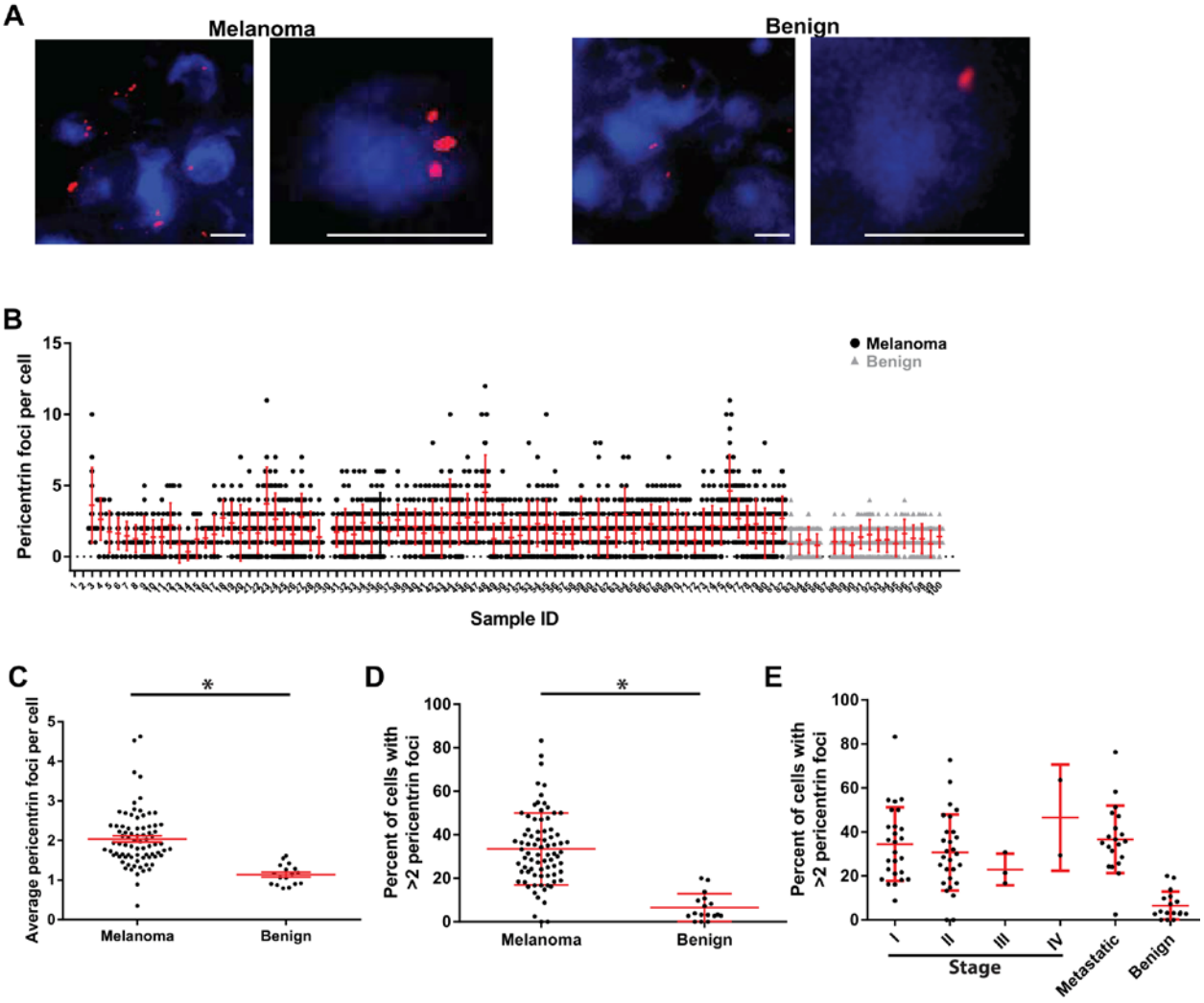
A
Melanoma
Benign
B
Pericentrin foci per cell
Melanoma
Benign
Sample ID
C
Average pericentrin foci per cell
Melanoma
Benign
D
Percent of cells with >2 pericentrin foci
Melanoma
Benign
E
Percent of cells with >2 pericentrin foci
I
II
III
IV
Stage
Metastatic
Benign

Figure 3-2

Centrosome amplification arises predominantly from centriole overduplication.

(A) Normally cells have one centrosome during G1 with one mother centriole expressing CEP170, two centrosomes after duplication in early S phase, and CEP170 is recruited to one centriole in each centrosome late in G2. If centriole overduplication was predominant, then one would expect many centrosomes with only one staining for CEP170. Conversely, if doubling events predominated, then one would expect many centrosomes that all stain for CEP170. **(B)** Micrographs demonstrating centrosomes lacking CEP170 (low overlap, more consistent with centriole overduplication hypothesis) versus centrosomes expressing CEP170 (high overlap, more consistent with cell doubling hypothesis). Blue = DNA/DAPI, green = CEP170, red = pericentrin, scale bar = 5 μm. **(C)** Dot plot quantifying the percent of centrosomes staining for CEP170 in melanoma samples (n=79) versus benign samples (n=17). **(D)** Dot plot demonstrating differences in the percent of centrosomes staining for CEP170 based on primary melanoma tumors of stage I-IV (n=59) versus metastatic tissue (n=20) versus benign tissue (n=17). Bars represent means ±SD. Statistical significance is indicated as *$p<0.05$. A T test was used in C.

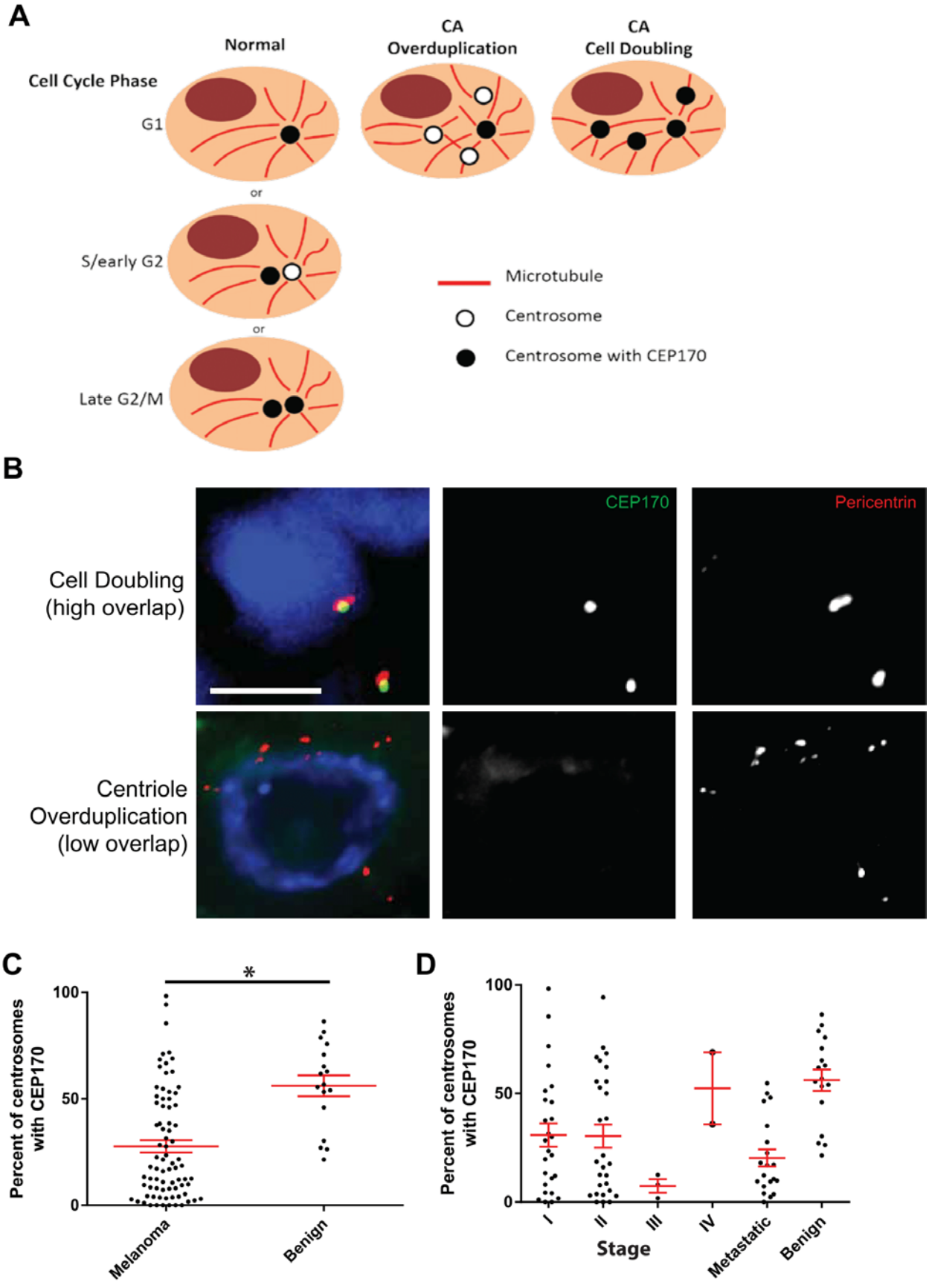
A
Normal
CA
Overduplication
CA
Cell Doubling
Cell Cycle Phase
G1
or
S/early G2
or
Late G2/M
Microtubule
Centrosome
Centrosome with CEP170
B
CEP170
Pericentrin
Cell Doubling
(high overlap)
Centriole
Overduplication
(low overlap)
C
*
Percent of centrosomes
with CEP170
100
50
0
Melanoma
Benign
D
Percent of centrosomes
with CEP170
100
50
0
I
II
III
IV
Metastatic
Benign
Stage

Figure 3-3

PLK4 is required for centriole overduplication but its overexpression does not drive most instances of centrosome amplification in human melanoma.

(A) Representative micrograph of a melanoma immunostained using PLK4, pericentrin, and γ-tubulin antibodies Scale bar = 10 μm. **(B)** Quantification of PLK4 expression that overlapped with pericentrin. Bars represent means ± SD with statistical significance *$p<0.05$. **(C)** Correlation of PLK4 expression with centrosomes (average pericentrin foci per cell in each sample). **(D)** Correlation of PLK4 expression with centrosome amplification, defined as the percent of cells with greater than 2 centrosomes (Pearson R for melanomas = 0.26, P value = 0.04). **(E)** Correlation of PLK4 expression with the average percent of centrosomes expressing CEP170 in each sample (Pearson R for melanomas = -0.22, P value = 0.07). The dotted rectangle indicates cases where we hypothesize that PLK4 overexpression caused CA by centriole overduplication.

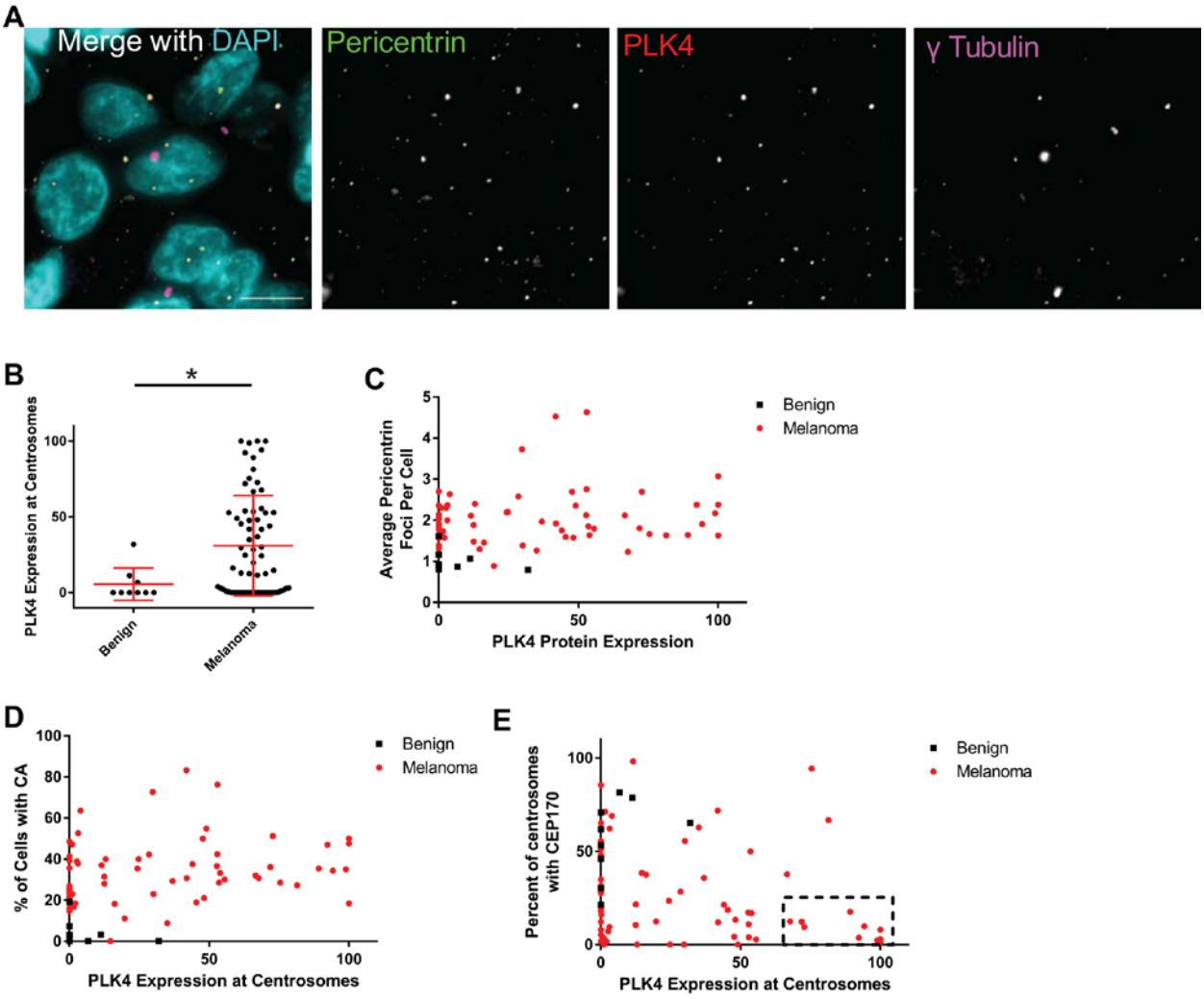
A
Merge with DAPI
Pericentrin
PLK4
γ Tubulin
B
*
PLK4 Expression at Centrosomes
100
50
0
Benign
Melanoma
C
Average Pericentrin Foci Per Cell
5
4
3
2
1
0
0
50
100
PLK4 Protein Expression
Benign
Melanoma
D
% of Cells with CA
100
80
60
40
20
0
0
50
100
PLK4 Expression at Centrosomes
Benign
Melanoma
E
Percent of centrosomes with CEP170
100
50
0
0
50
100
PLK4 Expression at Centrosomes
Benign
Melanoma

Figure 3-4

PLK4 is overexpressed in human melanoma cell lines, and its inhibition with small molecule inhibitor centrinone B significantly reduces cell viability human melanoma cells. **(A)** Western blot and **(B)** qRT-PCR analysis of PLK4 expression in normal adult human epidermal melanocytes (HEMa) and seven human melanoma cell lines (A375, Hs294T, G361, WM35, WM115, 451Lu, and SK-MEL-28). (C) Centrioles were assessed before and after centrinone B treatment by immunofluorescence. Representative images of A375 and Hs294T melanoma cells with or without centrinone B treatment (100 nM for 48 hours). Centrin labels individual centrioles while pericentrin labels the entire centrosome or PCM. Scale = 5 μm. **(D)** Quantification of centrioles in each cell line before and after treatment with centrinone B. **(E)** Correlation of centrioles with PLK4 protein expression in the melanoma cell lines. PLK4 expression was normalized to actin. Pearson R = 0.47, P value = 0.24. **(F)** Correlation of centrioles with PLK4 mRNA expression in the melanoma cell lines. Pearson R = 0.05, P value = 0.90. **(G)** Quantification of the percent of centrioles with <4 centrioles before and after treatment with centrinone B. **(H)** The anti-proliferative potential of PLK4 inhibitor centrinone B (treated for 48 hours) was assessed using CytoTox-Glo assay in A375,Hs294T, G361, and SK-MEL-28 melanoma cell lines as well as in normal human melanocytes. All the data are representative of at least three independent experiments. Quantitative results are presented as means ± SEM. Statistical significance are indicated as *$p<0.05$, **$p<0.1$, ***$p<0.001$.

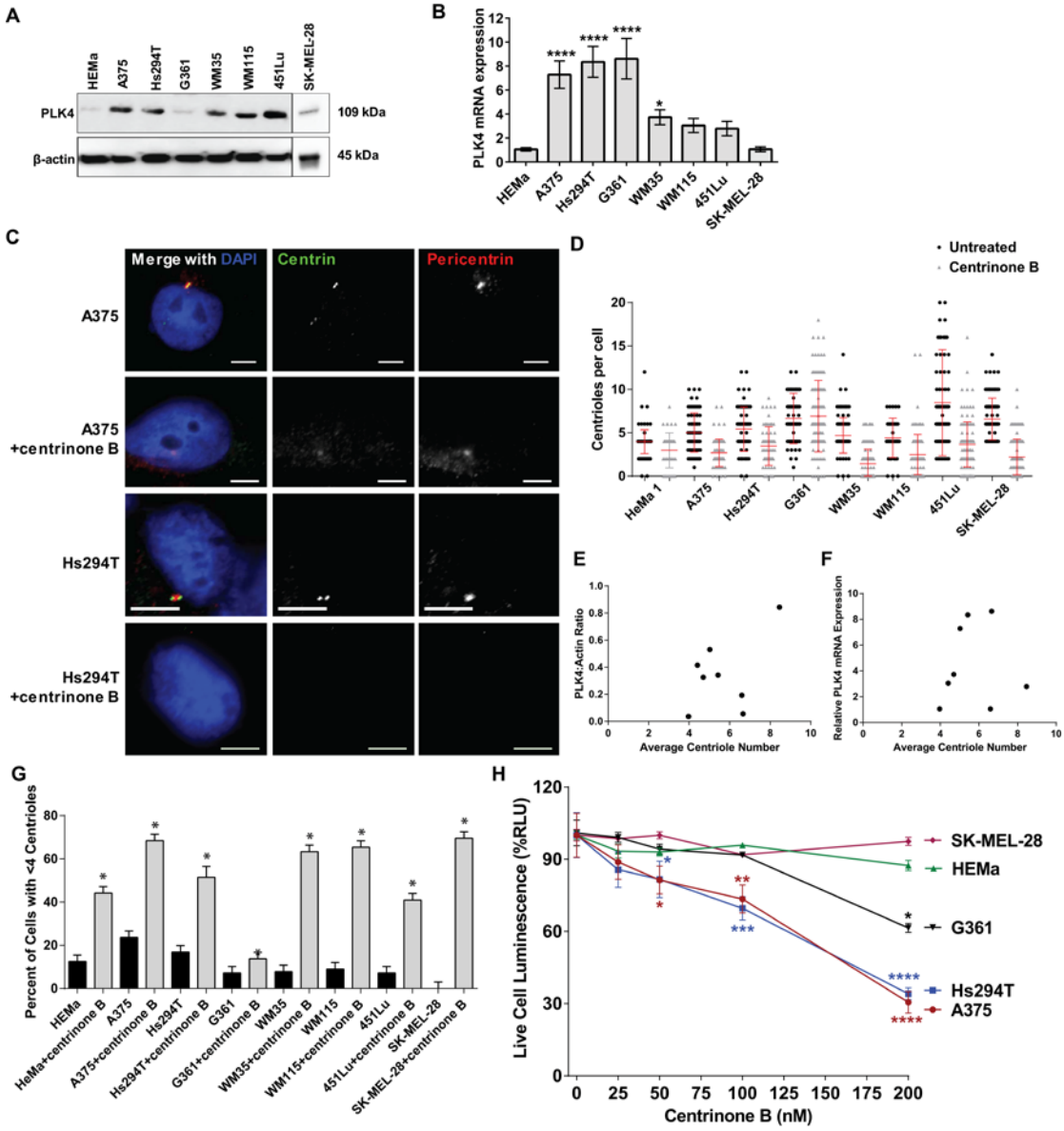
A
HEMa
A375
Hs294T
G361
WM35
WM115
451Lu
SK-MEL-28
PLK4
109 kDa
β-actin
45 kDa
B
PLK4 mRNA expression
HEMa
A375
Hs294T
G361
WM35
WM115
451Lu
SK-MEL-28
C
Merge with DAPI
Centrin
Pericentrin
A375
A375 +centrinone B
Hs294T
Hs294T +centrinone B
D
Untreated
Centrinone B
Centrioles per cell
HeMa 1
A375
Hs294T
G361
WM35
WM115
451Lu
SK-MEL-28
E
PLK4:Actin Ratio
Average Centriole Number
F
Relative PLK4 mRNA Expression
Average Centriole Number
G
Percent of Cells with <4 Centrioles
HEMa
HeMa+centrinone B
A375
A375+centrinone B
Hs294T
Hs294T+centrinone B
G361
G361+centrinone B
WM35
WM35+centrinone B
WM115
WM115+centrinone B
451Lu
451Lu+centrinone B
SK-MEL-28
SK-MEL-28+centrinone B
H
Live Cell Luminescence (%RLU)
Centrinone B (nM)
SK-MEL-28
HEMa
G361
Hs294T
A375

Figure 3-5

PLK4 inhibition with centrinone B causes apoptosis in human melanoma cells.

(A) Melanoma cells were grown to 70% confluency, then treated for 48 hours with 25, 50, 100 nM of centrinone B. The number of apoptotic cells was assessed by flow cytometric analysis of annexinV/propidium iodide (PI) staining. Representative two-dimensional dot plots of annexinV-FITC and PI fluorescence are shown here. **(B)** Total Annexin V-positive and propidium iodide-positive (apoptotic) cells are plotted. Data represent means ± SEM of three replicates. Statistical significance is indicated as *$p<0.05$, **$p<0.1$, ***$p<0.001$, ****$p<0.0001$. (C) Western blot analysis of PARP cleavage in centrinone B-treated A375, Hs294T, and HEMa cells. β-actin was used as a loading control.

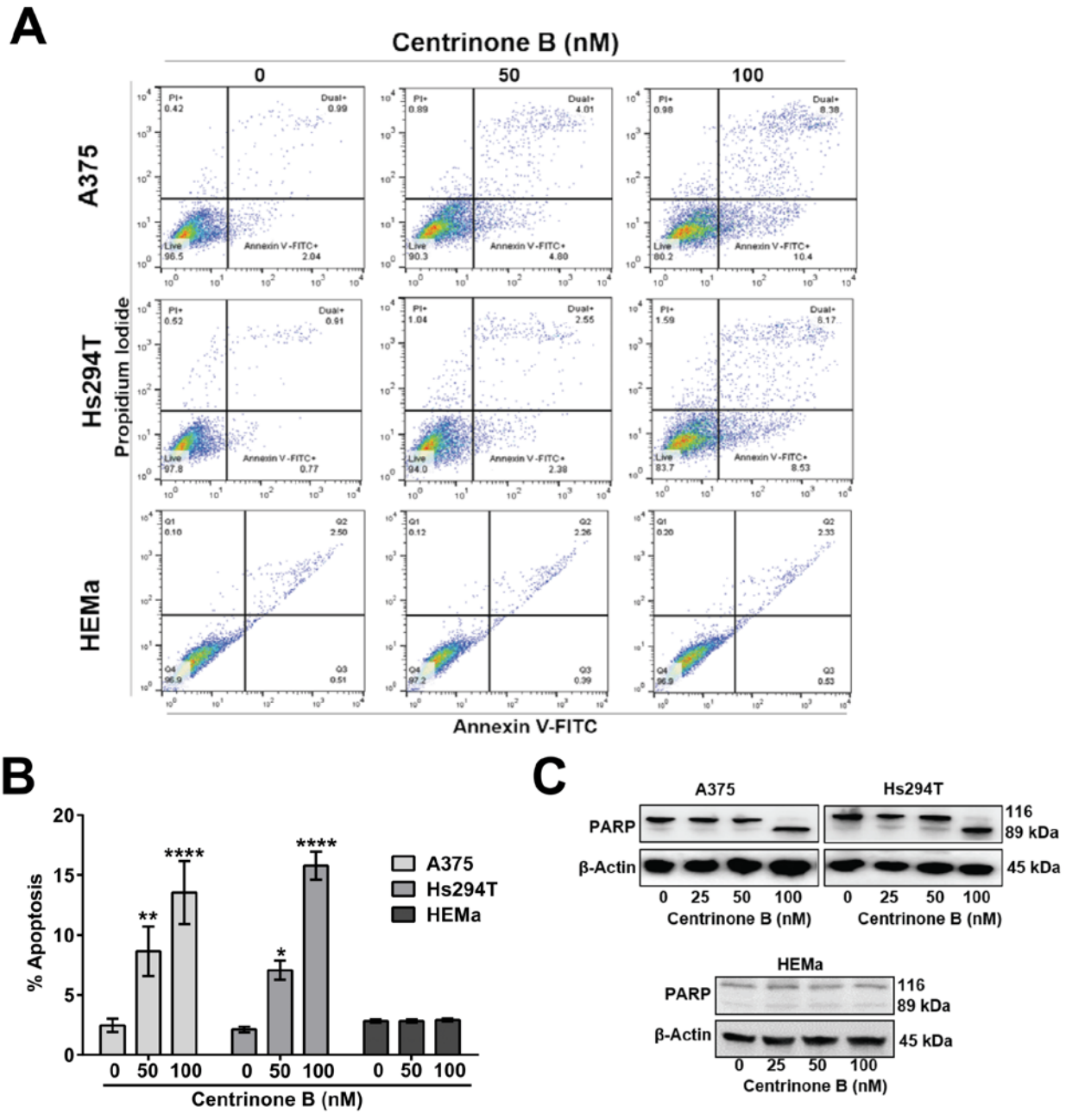
A
Centrinone B (nM)
0
50
100
A375
Hs294T
HEMa
Propidium Iodide
Annexin V-FITC
B
% Apoptosis
A375
Hs294T
HEMa
Centrinone B (nM)
C
A375
Hs294T
PARP
β-Actin
116
89 kDa
45 kDa
Centrinone B (nM)
HEMa

Supplemental Figure 3-1

Validation of CEP170 staining in overduplication- versus cell doubling-induced centrosome amplification.

(A) Representative images of CEP170 staining in retinal pigment epithelium (RPE) cells. Overexpression of PLK4 was used to simulate centriole overduplication. Cytochalasin D was used to induce cytokinesis failure and simulate doubling. Blue = DAPI/DNA, white = centrin, red = CEP170, scale bar = 5 μm. The insets show magnified images of the boxed area. **(B)** Quantification of the percent of centrioles co-staining with CEP170. Only cells with ≥4 centrioles were included in the Centriole Overduplication category. Bars represent mean percentages ± SEM. **(C)** Representative images of CEP170 staining in RPE cells. This experiment was conducted exactly as in panel A, except we co-stained with pericentrin to more closely mimic what we did with the melanoma TMA. Blue = DAPI/DNA, green = pericentrin, red = CEP170, scale bar = 5 μm. The insets show magnified images of the boxed area. **(D)** Quantification of the percent of centrosomes (defined by pericentrin foci) co-staining with CEP170. Only cells with >2 centrosomes were included in the Centriole Overduplication category. Bars represent mean percentages ± SEM.

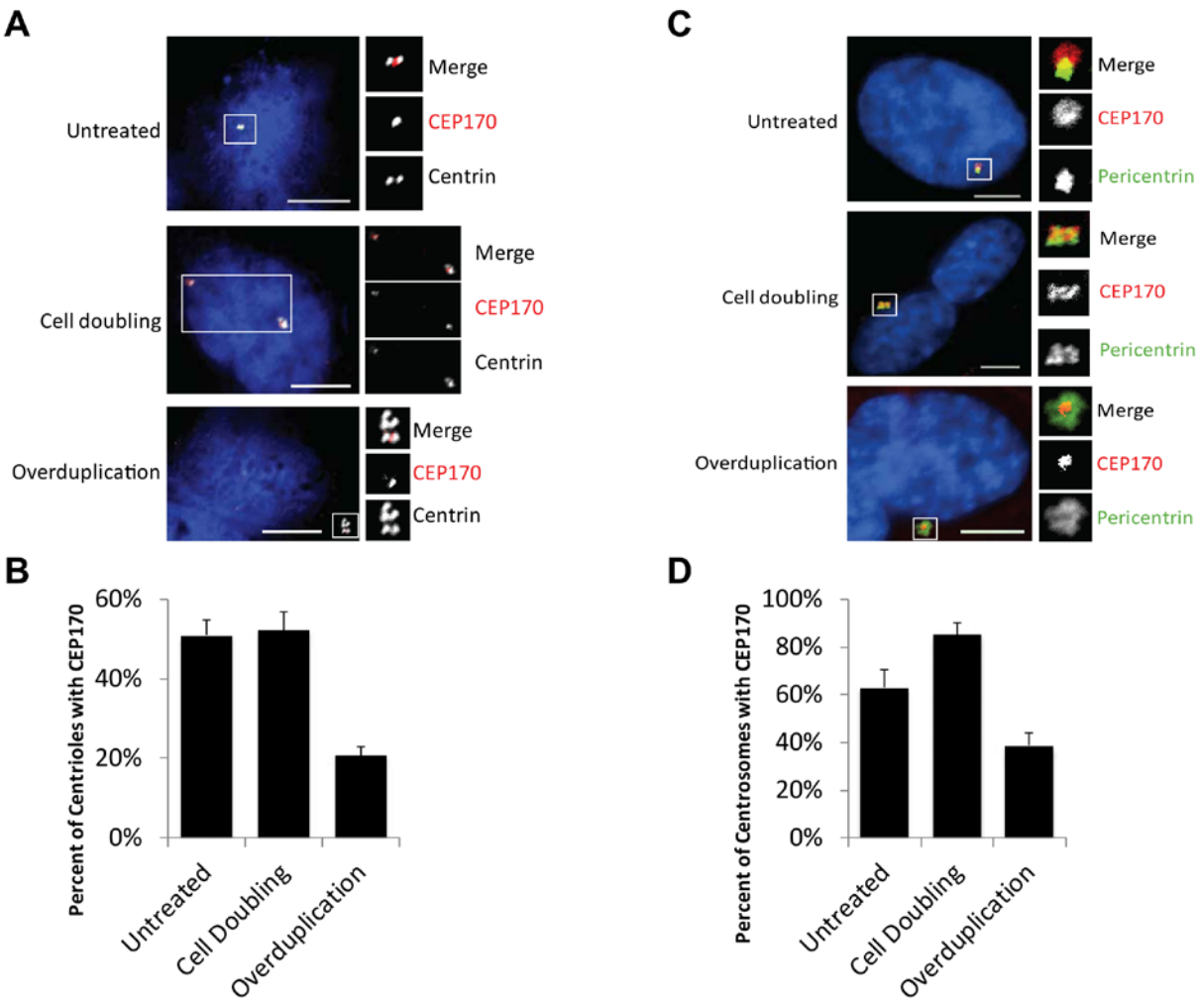
A
Untreated
Merge
CEP170
Centrin
Cell doubling
Merge
CEP170
Centrin
Overduplication
Merge
CEP170
Centrin
C
Untreated
Merge
CEP170
Pericentrin
Cell doubling
Merge
CEP170
Pericentrin
Overduplication
Merge
CEP170
Pericentrin
B
Percent of Centrioles with CEP170
60%
40%
20%
0%
Untreated
Cell Doubling
Overduplication
D
Percent of Centrosomes with CEP170
100%
80%
60%
40%
20%
0%
Untreated
Cell Doubling
Overduplication

Supplemental Figure 3-2

Validation of tyrosinase staining to identify melanocytes

(A) Representative image of tyrosinase staining in a FFPE melanoma sample. **(B)** Representative image of tyrosinase staining in FFPE breast tissue. Blue = DAPI/DNA, red = tyrosinase, scale bar = 10 μm.

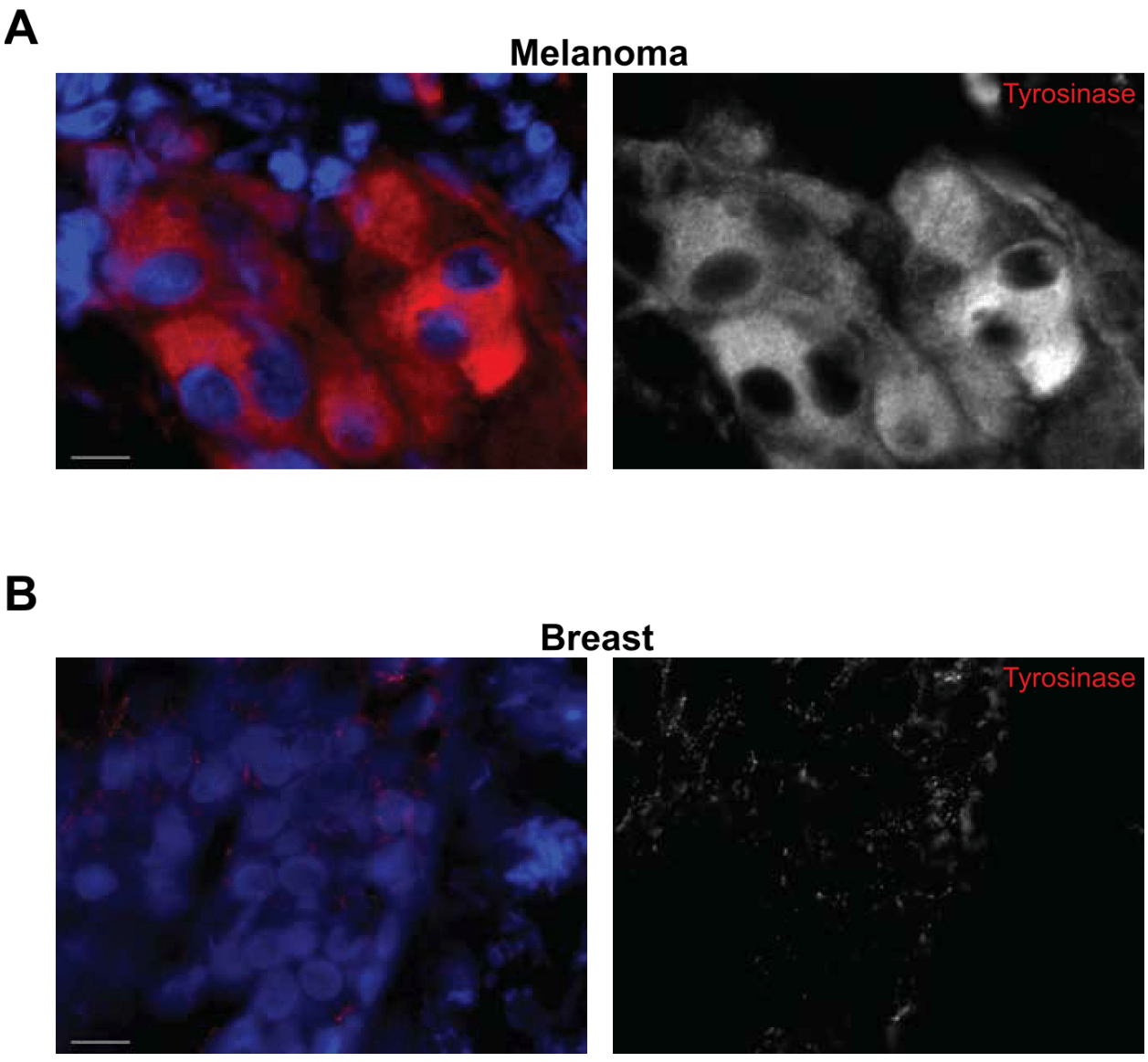

Supplemental Figure 3-3

Testing of four different PLK4 antibodies

Representative images of PLK4 staining in RPE-1 cells, either untreated (WT) or overexpressing PLK4 (PLK4 OE). The antibodies used are as follows: Abcam ab137398, Abgent AP13934b, Cell Signaling Technology (CST) 3248, and Epitomics (S2547). Blue = DAPI/DNA, green = centrin, red = PLK4, purple = γ-tubulin, scale bars = 10 μm.

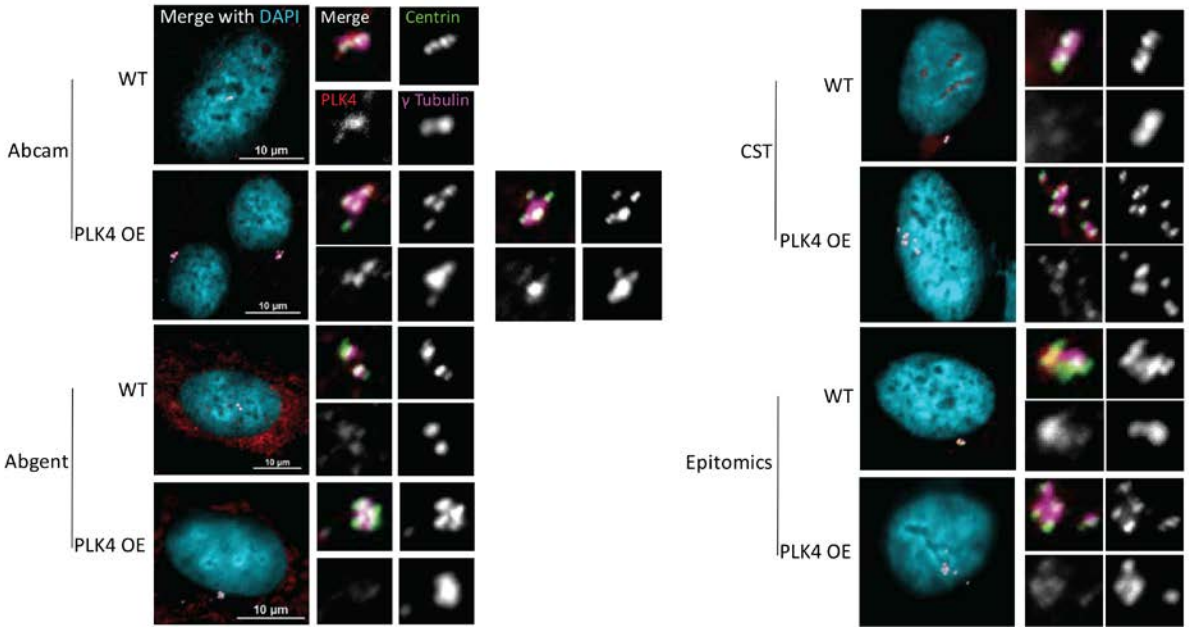

Supplemental Figure 3-4

Validation of PLK4 antibody in cell lines.

(A) RPE-1 cells were fixed with ice-cold methanol and stained for PLK4 (red), centrioles (centrin, green, Millipore, 04-1624), and pericentriolar material (γ-tubulin, purple, Abcam, ab27074). **(B)** RPE-1 cells were suspended in agar, fixed with formalin, embedded in paraffin, and stained for PLK4 (red) and pericentriolar material (pericentrin, green, Abcam ab4448). Immunohistochemistry was carried out as described in Materials and Methods for the melanoma TMA. The centrosomes (white box in merged images) are magnified for the adjacent single-channel images. OE = overexpression. Scale bar sizes are indicated on the images. **(C)** To further validate the antibody, we utilized PLK4 conditional knockout cell lines. The efficiency of PLK4 depletion was quantified by quantitative reverse transcription polymerase chain reaction (qRT-PCR). **(D)** PLK4 was assessed by immunofluorescent staining of conditional knockout cell lines treated with either AdGFP (control) or AdCre (to excise PLK4). The centrosomes (white box in merged images) are magnified for the PLK4 and centrin single-channel images on the far right column of the image panel.

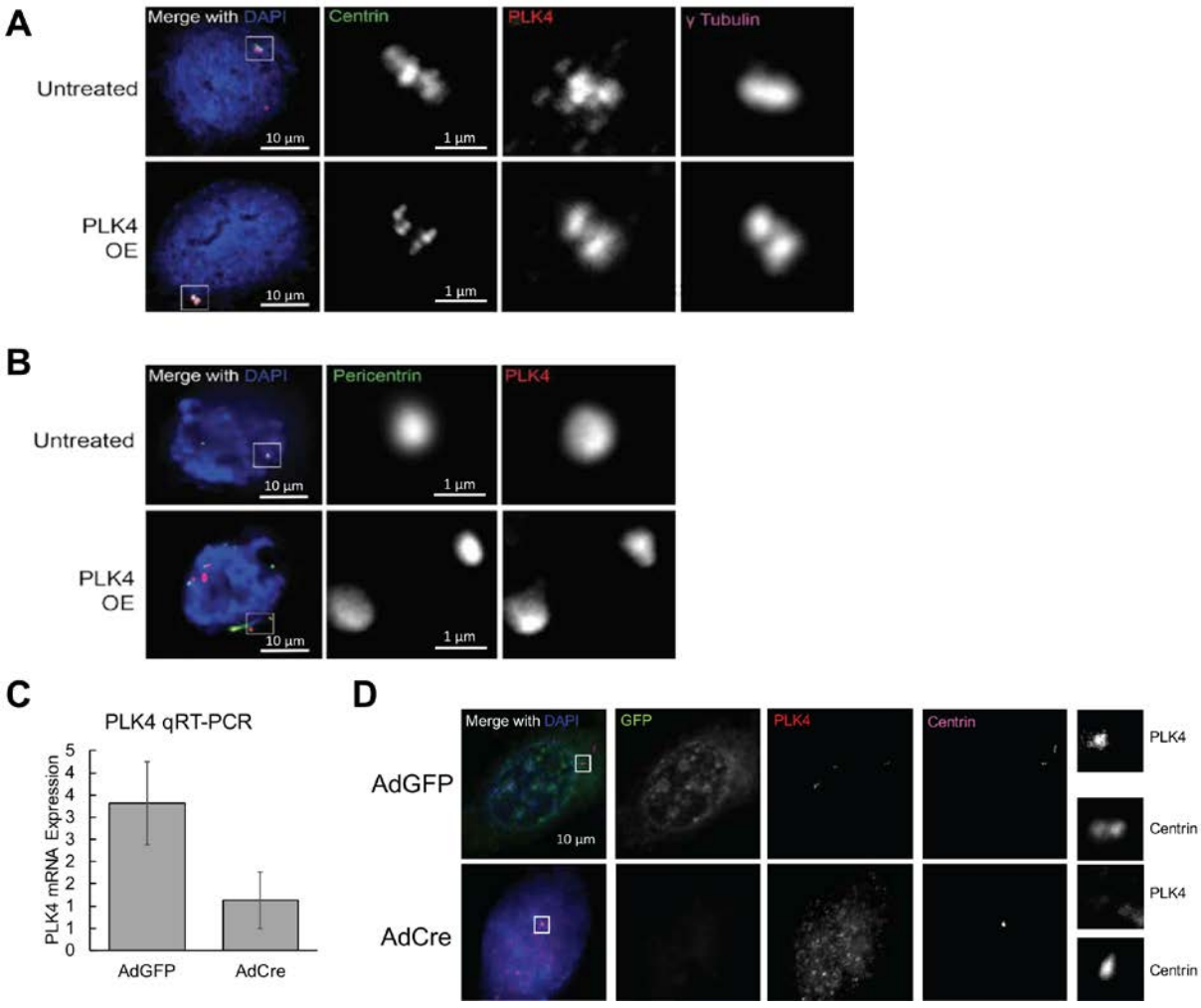
A
Merge with DAPI
Centrin
PLK4
γ Tubulin
Untreated
PLK4 OE
10 μm
1 μm
B
Merge with DAPI
Pericentrin
PLK4
Untreated
PLK4 OE
10 μm
1 μm
C
PLK4 qRT-PCR
PLK4 mRNA Expression
0
1
2
3
4
5
AdGFP
AdCre
D
Merge with DAPI
GFP
PLK4
Centrin
AdGFP
AdCre
10 μm

Supplemental Figure 3-5

Melanoma patient survival based on PLK4 expression.

(A) Dot plot demonstrating PLK4 mRNA Z score in the TCGA melanoma cohort. **(B)** Overall survival (OS) and **(C)** disease-free survival (DFS) were analyzed based on PLK4 mRNA expression from 401 melanoma patients with available survival data from TCGA. cBioPortal [196] was used to query the data. Patients were divided into groups based on Z score. There were 52 patients with Z scores < -1, 184 with -1 < Z < 0, 121 with 0 < Z < 1, and 44 with Z > 1. P values from log rank tests are indicated on the plots. **(D-E)** CA20 was calculated as described by Ogden et al [180]. Patients were stratified into 2 groups using the median CA20 score. (F-I) Centrosome index (CI) was calculated as described by Chng et al. [178,179]. Patients were stratified into 2 groups using either the median CI score **(F-G),** or a CI score of 4.5 **(H-I),** as Chng et al. had reported [179]. P values shown on the survival curves were determined by log-rank tests. **(J-L)** Scatterplots demonstrating the correlations between CA20, CI, and PLK4 (mRNA Z scores were utilized). Pearson's r and P values are shown on the plots. **(M)** Demonstration of p53 and PLK4 alterations in the melanoma TCGA cohort. The diagram only shows the patients that had p53 or PLK4 alterations, and others are not shown.

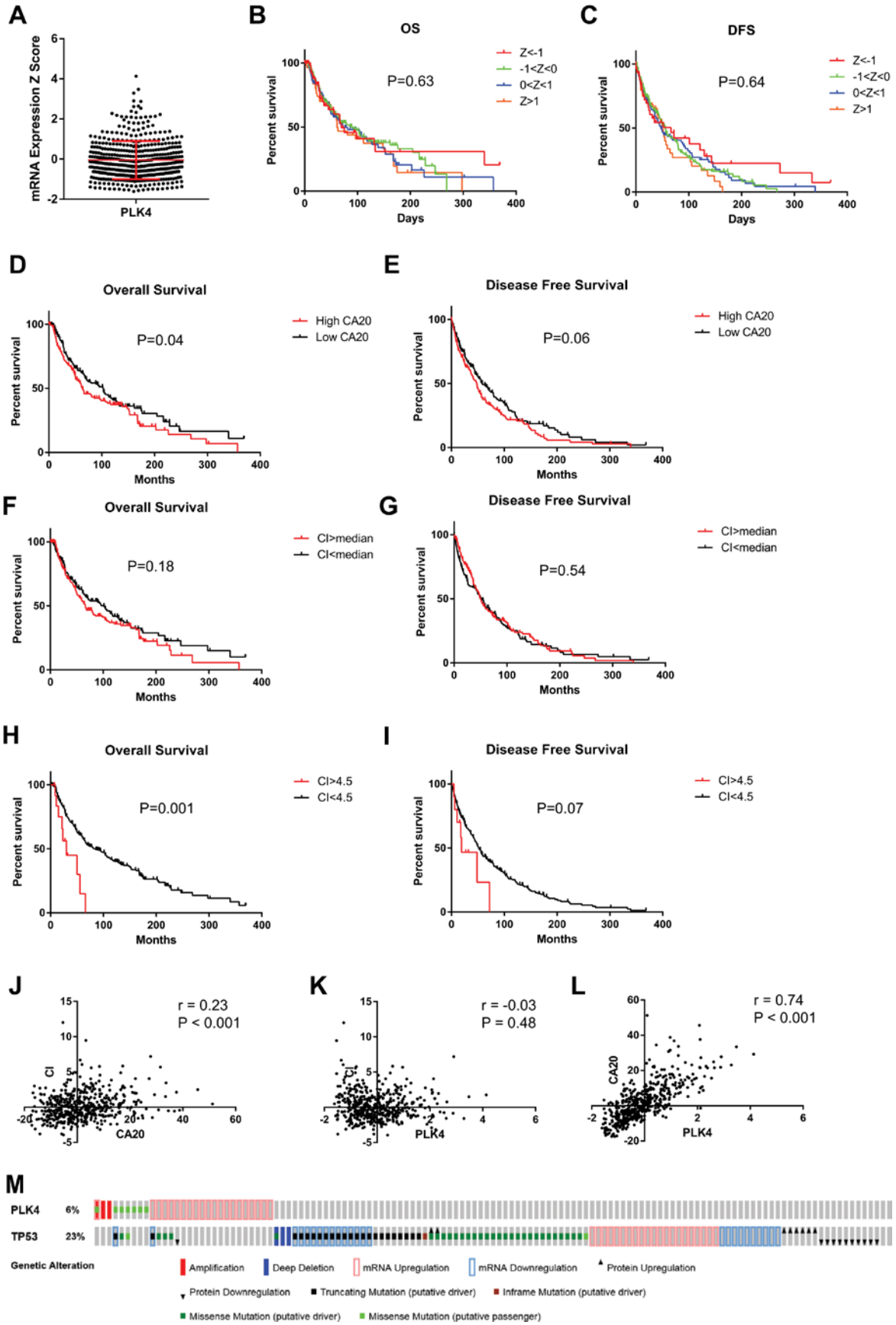
A
mRNA Expression Z Score
PLK4
B
OS
P=0.63
Z<-1
-1<Z<0
0<Z<1
Z>1
Percent survival
Days
C
DFS
P=0.64
D
Overall Survival
P=0.04
High CA20
Low CA20
Months
E
Disease Free Survival
P=0.06
F
Overall Survival
P=0.18
CI>median
CI<median
G
Disease Free Survival
P=0.54
H
Overall Survival
P=0.001
CI>4.5
CI<4.5
I
Disease Free Survival
P=0.07
J
r = 0.23
P < 0.001
CI
CA20
K
r = -0.03
P = 0.48
PLK4
L
r = 0.74
P < 0.001
M
PLK4 6%
TP53 23%
Genetic Alteration
Amplification
Deep Deletion
mRNA Upregulation
mRNA Downregulation
Protein Upregulation
Protein Downregulation
Truncating Mutation (putative driver)
Inframe Mutation (putative driver)
Missense Mutation (putative driver)
Missense Mutation (putative passenger)

Supplemental Figure 3-6

Effects of centrinone B on melanoma cell lines are dependent on PLK4 inhibition.

To demonstrate that the observed effects of centrinone B on the melanoma cell lines was due to inhibition of PLK4, we overexpressed a FLAG-tagged PLK4 with G95L mutation, which is resistant to centrinone B inhibition. Hs294T **(A)** and A375 **(B)** cells were transfected with FLAG-PLK4^{G95L} or empty vector (FLAG), selected with G418, then used for proliferation assays. Proliferation values were normalized to the untreated cells within each condition. Bars represent means ± SD and asterisks represent P value < 0.05 comparing each treated condition to its respective untreated control.

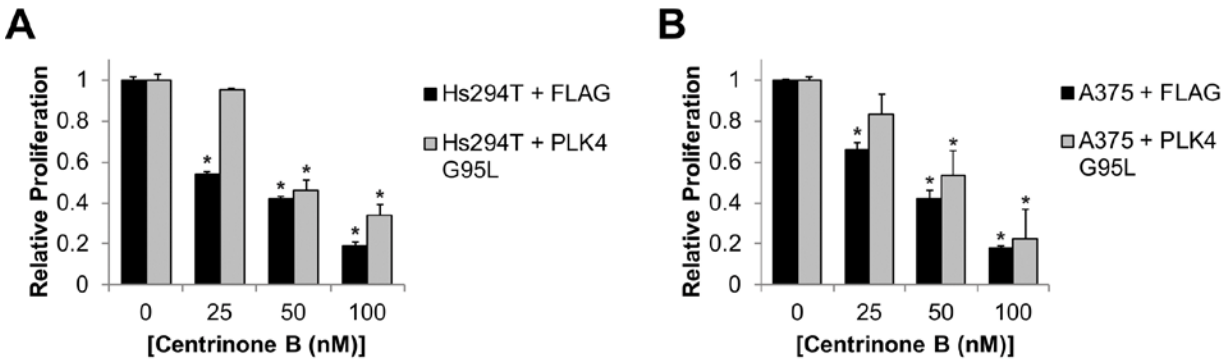

Supplemental Figure 3-7

Centrosome amplification does not sensitize to centrinone B.

(A) Schema of the doxycycline-inducible transgenes utilized in the experiments shown in this figure. Overexpression of PLK4 608 transgene (amino acids 1-608) lacks a crucial C-terminal localization domain, so PLK4 fails to localize to the centrosome and drive centriole overduplication. **(B)** Representative images demonstrating doxycycline-inducible PLK4 system to induce centrosome amplification. **(C)** Quantification of the percent of cells with CA, as defined by >4 centrioles (centrin foci). **(D)** To assess sensitivity to centrinone B, cells were plated at a density of 1000 cells/well on day 1. Doxycycline was added on day 2. Centrinone B was added at the indicated concentrations on day 3. Cell viability was assessed on day 6 by Vita Orange (CCK-8) staining. **(E)** Crystal violet staining was also performed to assess sensitivity to centrinone B in the same cell lines. The same timeline and procedure were used as in panel B, except that 5000 cells/well were plated in 24-well plates on day 1.

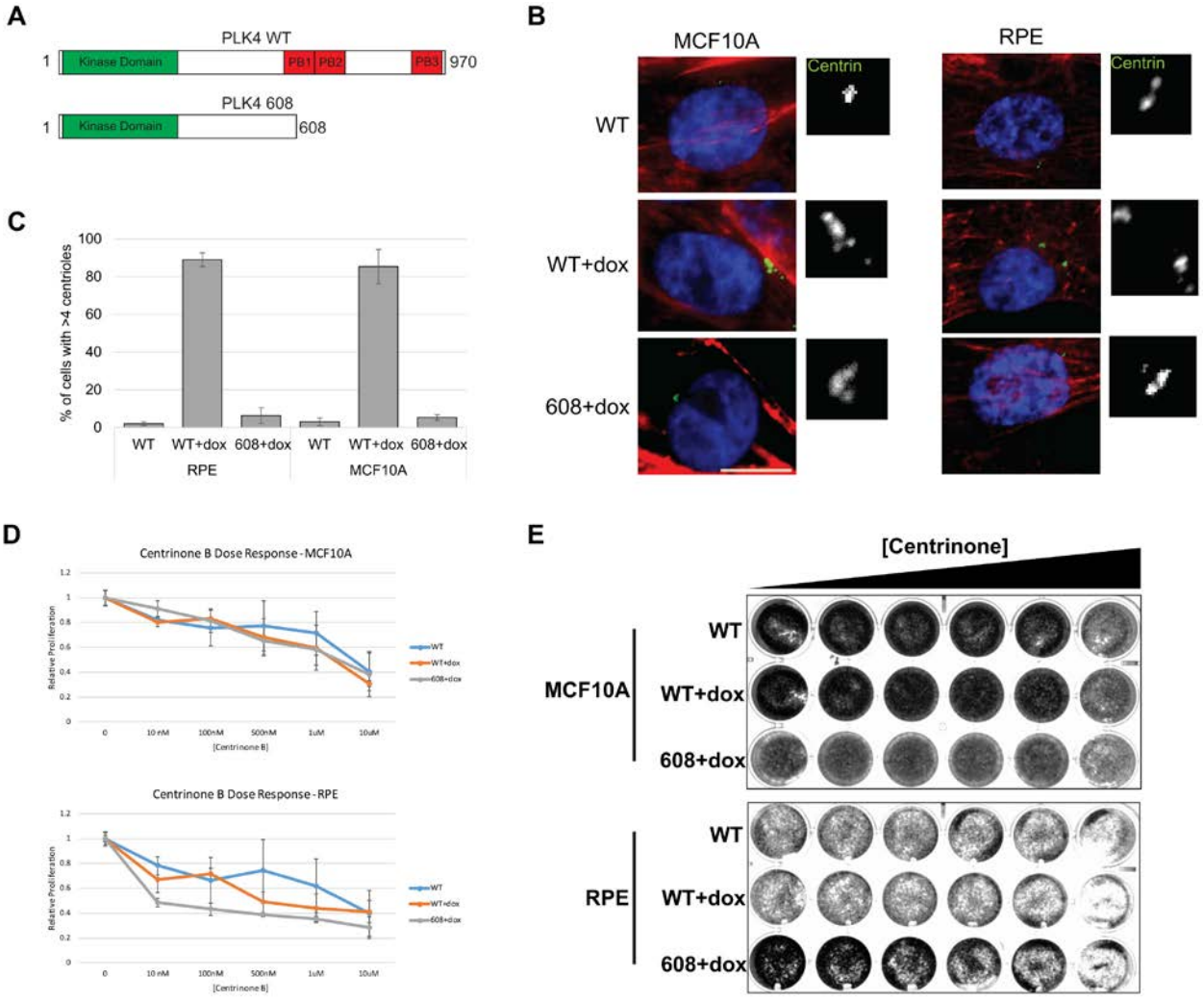
A
PLK4 WT
1
Kinase Domain
PB1
PB2
PB3
970
PLK4 608
1
Kinase Domain
608
B
MCF10A
RPE
Centrin
Centrin
WT
WT+dox
608+dox
C
% of cells with >4 centrioles
100
80
60
40
20
0
WT
WT+dox
608+dox
WT
WT+dox
608+dox
RPE
MCF10A
D
Centrinone B Dose Response - MCF10A
Relative Proliferation
[Centrinone B]
WT
WT+dox
608+dox
Centrinone B Dose Response - RPE
Relative Proliferation
[Centrinone B]
WT
WT+dox
608+dox
E
[Centrinone]
MCF10A
WT
WT+dox
608+dox
RPE
WT
WT+dox
608+dox

Acknowledgements

Research reported in this chapter was supported by the National Institutes of Health grants R01AR059130, R01CA176748, F30CA203271, T32GM008692, UL1TR000427 and TL1TR000429 and the Department of Veterans Affairs (VA Merit Review Award number 1I01BX00100). Also, we acknowledge the core facilities supported by the Skin Diseases Research Center (SDRC) Core Grant P30AR066524 from the National Institute of Arthritis and Musculoskeletal and Skin Diseases (NIAMS). The authors thank the University of Wisconsin Carbone Cancer Center's Experimental Pathology Lab, supported by University of Wisconsin Carbone Cancer Center Cancer Center Support Grant P30 CA014520. Lastly, the authors thank Karla Esbona and Sally Drew for help with imaging and analysis. The content is the responsibility of the authors and does not necessarily represent the views of the NIH.

CHAPTER 4: Analysis of the "centrosome-ome" reveals that MCPH1 genomic deletion is a common cause of centrosome amplification in human cancer

Work in this chapter is in preparation for submission:

Analysis of the "centrosome-ome" reveals that MCPH1 genomic deletion is a common cause of centrosome amplification in human cancer

Ryan A. Denu, Mark E. Burkard

Abstract

The centrosome is the microtubule organizing center of human cells and facilitates a myriad of cellular functions including organization of the mitotic spindle to ensure faithful chromosome segregation during mitosis, cell polarization and migration, and primary cilia formation. A numerical increase in centrosomes, or centrosome amplification (CA), is common in cancer and correlates with more aggressive clinical features and worse patient outcomes. However, the causes of CA in human cancer are unclear. Many previous studies have identified mechanisms of CA *in cellulo*, such as overexpression of PLK4, but the clinical relevance of these mechanisms is unclear and has not been demonstrated. To address this question, we analyzed genomic and transcriptomic data in the 367 proteins reported to localize to the centrosome using TCGA data. We identified a list of candidate centrosome proteins that are most frequently altered in cancer. Furthermore, given that cells with CA arrest unless other compensatory alterations are made, such as loss of p53, we considered the fold enrichment in p53 mutant versus p53 wild type tumors. We identified the following candidates: gain of function of CEP19, CEP72, CTNNB1, PTK2, NDRG1, SPATC1, TBCCD1; and loss of function of CEP76, MCPH1, NEURL4, NPM1. *In cellulo* analysis of these candidates reveals that loss of MCPH1/microcephalin causes the most robust increase in centriole number. MCPH1 gene deletions are seen in 5-15% of human cancers, depending on the anatomic site of the tumor. We conclude that a myriad of different alterations in centrosome genes can give rise to CA in human cancer, and that loss of MCPH1 is a common and penetrant cause of CA in human cancer.

Introduction

The centrosome is the microtubule organizing center of human cells. A numerical increase in centrosomes, or centrosome amplification (CA), is common in cancer and correlates with more aggressive clinical features and worse patient outcomes.[107-109] Many previous studies have investigated the consequences of CA. CA increases mitotic errors, including multipolar spindles and chromosome missegregation,[134,197] often resulting in aneuploidy. Furthermore, CA increases microtubule nucleation,[117,124] cellular invasiveness.[126]

Many previous studies have identified *in cellulo* mechanisms of CA, such as overexpression of pericentrin,[185] PLK4[126], SASS6[183], CEP57[198], PIM1[199], CEP70[200], gamma tubulin, CEP152[201], MPS1[202,203], cyclin A[204], SIRT2[205], MOB1A/B[206], STIL[184], Aurora A[207], Aurora B[207], PLK1,[207] among others.[114] Despite these findings, the actual mechanisms driving CA in human cancer have not been determined.

CA is thought to arise by two major mechanisms: (1) centriole overduplication and (2) cell doubling events. We previously determined that the former, centriole overduplication, is primarily responsible for CA in human melanoma.[208] Additional evidence comes from centriole analysis of human cancer cell lines, demonstrating that only a subpopulation of cell liens with CA have an increase in ploidy, suggesting different origins of ploidy and CA.[209] We therefore sought to identify the predominant molecular mechanisms leading to centriole overduplication in human cancer. To address this question, we analyzed genomic and transcriptomic alterations in 367 centrosome proteins using TCGA data from 9555 patients representing 21 of the most common tumor sites. We identified a list of hits of centrosome proteins that are most frequently altered in cancer, then tested them *in cellulo* to determine the predominant causes of centriole overduplication in cancer.

Results

Survey of Centrosome Gene Alterations in Human Cancer

The goal of this project was to determine the causes of CA in human cancer. We began by testing the hypothesis that CA is due to genetic alterations in centrosome genes. To systematically examine the "centrosome-ome" in human cancer, we interrogated publicly-available genomic, transcriptomic, and proteomic datasets. We analyzed the 367 proteins that localize to the centrosome. This list was put together by searching for "centrosome" on Uniprot and supplementing with proteins discovered at the centrosome identified by previously proteomic analysis of isolated centrosomes and validation by immunofluorescence.[210] We used TCGA datasets to assess mutations in these 367 genes in all human cancers. This preliminary analysis revealed the most commonly genomically altered centrosome genes in human cancer: NPM1, CTNNB1, STIL, AKAP9, PKHD1, HERC2, BIRC6, BRCA2, PCNT, FRY, PDE4DIP, KIF2B, TACC2, TRIOBP, CHD4, CEP350, and ZFYVE26.

The most common single point mutation was found in nucleophosmin/NPM1, which is found exclusively in acute myeloid leukemia (AML). It causes a frameshift mutation at the C-terminus. Patients with this mutation have worse outcomes (Supplemental Figure 4-1). The effects of this mutation on centrosome/centriole number have not been reported. We generated the mutant cDNA that would be produced with this frameshift mutation and overexpressed it in HeLa cells. We compared the centriole number in these cells compared to HeLa cells in which we overexpressed WT NPM1. We observe no significant changes in centriole number (Supplemental Figure 4-1). Further evidence for this NPM1 mutation not driving CA is found by lack of compensatory changes to allow cells to proliferate with extra centrioles, as these cells typically arrest. TP53, p21, and the PIDDosome genes (PIDD1, CRADD, and CASP2) have been

shown to mediate this arrest, so we examined their status in NPM1 mutated cases of AML. We find a lack of coincidence of NPM1 mutations with these other genes (Supplemental Figure 1); further, there is a significant mutual exclusivity of NPM1 mutations and TP53 alterations (Bonferroni corrected p value < 0.001). We conclude that NPM1 mutations do not drive CA in AML.

The next most common single point mutations were found in AKAP9, PLK2, and STIL. We also looked at outcomes in patients with AKAP9, PLK2, and STIL mutations. Patients with AKAP9, PLK2, or STIL mutations do not have significant differences in survival (Supplemental Figure 4-2); however, one caveat to this analysis is that these analyses are underpowered because the mutations are so rare.

We also looked in more detail at the list of centrosome genes that have been shown to be required for centriole duplication: PLK4, STIL, CEP152, CEP192, TUBE1, CETN2, CPAP, SAS6, and CEP135. CEP152 and CEP192 recruit PLK4, then PLK4 binds STIL, which activates PLK4 activity. PLK4 then phosphorylates STIL, allowing STIL to bind SAS6. CEP120, CPAP/CENP-J, and SPICE-1 are then recruited, followed by CEP135, POC1A, POC1B, POC5, CNTROB, and CP110. These all allow for elongation. Interestingly, there is a relative dearth of alterations in these genes, perhaps suggesting that centriole duplication is crucial to the vitality of cancer cells. It has been hypothesized that CP110 is a tumor suppressor, as it is important for restraining the length of the centrioles, and recent evidence has demonstrated that some cancer cell lines have over-elongated centrioles, and that this can promote CA.[209] We hypothesized that CP110 loss-of-function may drive CA, mutation could increase the length of centrioles, which has been shown to increase the amount of microtubule nucleation; however, mutations or genomic deletions are not commonly seen in CP110. Similarly, CPAP is important for centriole

elongation, so we hypothesized that CPAP gain of function may drive CA; however, gain-of-function mutations or genomic amplifications are rarely seen. Interestingly, we observed 9 reported cases of STIL S76L missense mutations and decided to follow up on this. This mutation occurs in a domain that has no clear or previously reported function. STIL was recently reported to be a substrate of SCF-βTrCP-mediated degradation of STIL occurs throughout interphase and mutations in the DSG (394-399).[211] However, we rarely see mutations in this DSG motif in human cancer. As PLK4 is the master regulator of centriole duplication, we delved further into changes in PLK4 and its regulators in human cancer. We also looked at potential alterations in PLK4, and largely found a lack of common alterations. Mutations in the phosphodegron of PLK4 cause centriole amplification, most notably S285 and T289 play the biggest roles in βTrCP binding.[67] However, we rarely see mutations in these sites (Supplemental Figure 4-3). We also looked at previously reported genes known to regulate PLK4 levels and activity. PP1 has been shown to dephosphorylate PLK4.[212] PLK4 autophosphorylates in *trans*, triggering ubiquitination by the SCF (SKP1-CUL1-F box protein) E3 ubiquitin ligase. The F-box proteins in human cells is βTrCP (BTRC). We examined potential alterations in these three genes, but again find a relative dearth of modifications (Supplemental Figure 4-3). Gene amplifications and deletions were not commonly seen. We conclude that genomic alterations in the core centriole duplication machinery, including PLK4, are not common drivers of CA in human cancer, but that PLK4 activity is likely required for CA.

We also hypothesized that epigenetic and transcriptional deregulation of centrosome genes could give rise to CA. To assess this, we looked at the gene expression levels of these centrosome genes in the TCGA datasets. We found the following genes to be the most commonly overexpressed (Z scores >2): PTK2, MAPRE1, TBCCD1, CCT5, ARFGEF2,

CEP250, TOPBP1, AURKA, MPLKIP. Further, we found the following genes to be the most commonly under-expressed (Z scores <2): MCPH1, PAFAH1B1, PCM1, TTC19, CTDP1, NEURL4, KIAA0753 (moonraker), IST1, CNTROB, ACTR1A. Next, we used KM Plotter[213] to assess the impact of the expression of genes on survival in breast, ovarian, lung, and gastric cancers. We analyzed survival differences based on expression level. Found that of the 367 centrosome proteins, there were 70 where overexpression was associated with worse outcomes versus 182 where under-expression was associated with worse outcomes. There were 35 genes where under-expression correlated with worse PFS in all 4 cancer types assessed compared to 11 genes where overexpression correlated with worse PFS. 4 genes where under-expression significantly correlated with worse outcome in all 4 cancer types: PDC6IP, NUBP1, ERCC6L2, POC1B. 0 genes met these criteria for overexpressed genes. 35 genes where under-expression correlated with worse outcome in all 4 cancer types (not necessarily all significant, just the above are). Interestingly, MCPH1 also made this list. 11 genes where overexpression correlated with worse outcome in all 4 cancer types (not necessarily all significant, just the above are): RUVBL1, CCDC124, TUBG1, DTL, MLLT11, CEP89, MAD1L1, DCTN2, CUL7, CDK6, DYNC1H1. We found 35 centrosome genes to correlate with worse outcomes when under-expressed in both overall survival and disease-free survival in all four patient sets.

Next, we combined our analyses of mutations, copy number alterations, and gene expression changes to compile a list of the most commonly altered centrosome genes. More weight was given to genes with a known role in centriole duplication or in controlling centriole/centrosome numbers. Furthermore, given that cells with CA arrest unless other compensatory alterations are made, such as loss of p53, we ranked alterations in centrosome genes by the fold enrichment in p53 mutant versus p53 wild type tumors (Supplemental Table 6).

Lastly, since the PIDDosome has also been shown to be important for cell cycle arrest in the presence of CA,[214] and assuming that tumor cells with CA would only be able to proliferate in the presence of one of these compensating events, we looked at which centrosome genes are most commonly altered in tumors with mutant PIDDosome proteins. This study identified caspase 2, PIDD1, RAIDD, p53, p21 as important for PIDDosome-mediated cell cycle arrest in the presence of CA. Therefore, we assessed enrichment in alterations in centrosome genes with PIDD1, RAIDD (CRADD), p53, or p21 (CDKN1A) mutations. Lastly, we compared our list to the list of genes found to be significantly mutated in cancer from a previous study, which incorporated high mutational burden relative to background expectation, clustering of mutations within a gene, enrichment of mutations in evolutionarily conserved sites.[215] This list of commonly mutated cancer genes contained 3 centrosome genes: CEP76, NPM1, and CTNNB1. All 3 of these were included in our analysis.

Taking all these data sources into account, we identified the following candidates for causing CA in human cancer: gain of function of CEP19, CEP72, CTNNB1, PTK2, NDRG1, SPATC1, TBCCD1; and loss of function of CEP76, MCPH1, NEURL4, NPM1. The rationale for each of these selections is described in Table 4-1. Detailed genomic alteration analysis by cancer site is shown in Supplemental Figure 4-4. Interestingly, there is a strong co-occurrence of genomic amplifications of NDRG1, PTK2, and SPATC1; all three of these genes are on chromosome 8q. Gain of chromosome 8q is associated with poorer prognosis in clear cell renal cell carcinoma [216], gastric cancer [217], prostate cancer[218-220], hepatoblastoma[221], uveal melanoma[222], and pancreatic adenocarcinoma[223]. Gain of 8q has also been associated with resistance to taxanes in node-positive breast cancer.[224] The proto-oncogene C-MYC is also on this chromosome, and is thought to be responsible for this phenotype.[216,225]

Loss of MCPH1 is a common and penetrant cause of CA

To test these hypotheses, we cloned and overexpressed mNeonGreen-tagged constructs of CEP19, CEP72, PTK2, NDRG1, SPATC1, and TBCCD1, and utilized shRNA to deplete CEP76, CTNNB1, MCPH1, NEURL4, and NPM1 (Figure 4-1). We quantified the centrioles in these cells. We find that loss of MCPH1 causes the most robust increase in centriole number (Figure 4-1A-C). MCPH1 mutations are known to give rise to microcephaly and CA.[226] MCPH1 gene deletions are seen in 5-15% of human cancers, depending on the anatomic site of the tumor. Furthermore, MCPH1 deletion significantly co-occurs with TP53 alterations (Bonferroni-adjusted p value < 0.001), PIDD1 alteration (p value < 0.001), and CASP2 alterations (p value = 0.007. We conclude that a myriad of different alterations in centrosome genes can give rise to CA in human cancer, and that loss of MCPH1 is a common and penetrant cause of CA in human cancer.

MCPH1 (aliases BRIT1 and microcephalin) has been reported to be a tumor suppressor gene.[227-230] MCPH1 localizes to the centrosome in both mitosis and interphase,[231] independent of ATM, BRCA1, CHK1, cell cycle stage, IR.[232] It also localizes to sites of DNA damage.[232] MCPH1 levels decrease in late M and early G1 phases due to degradation by APC/C.[233] Inherited MCPH1 mutations cause microcephaly.[234] Furthermore, there is a previously reported link between MCPH1 and CA. CA has been reported in MCPH1-knockdown U2OS cells,[235] Mcph1(-/-)p53(-/-) MEFs, and Mcph1$^{-/-}$ DT40 cells, especially in response to IR.[236] In addition, MCPH1 depletion makes cells more likely to have CA and PCM expansion in response to DNA damage/IR.[237] In addition, levels of MCPH1 inversely correlate with CA, defective mitosis and cancer metastasis in human breast cancer.[235] In addition, MCPH1 alterations associated with

poor response to DNA-damaging drugs and radiation.[238] Lastly, mutating MCPH1 in Drosophila causes CA.[239] MCPH1 promoter methylation is also a mechanism seen in human breast cancers that can lead to downregulation of MCPH1, and in one study this was seen in 56 of 122 (47%) of breast cancers. Therefore, there is strong evidence suggesting that deletion of MPCH1 could be driving CA in human cancer.

We looked at the clinical consequences of loss of MCPH1 in 6 of the cancers that had the most cases of MCPH1 loss: bladder, breast, colorectal, lung adenocarcinoma, ovarian, and prostate. We analyzed both overall survival (OS) and disease-free survival (DFS). We find that patients whose tumors demonstrate loss of MCPH1 demonstrated worse DFS in bladder ($P<0.001$), colorectal ($P = 0.025$), and prostate ($P = 0.038$) cancers (Figure 4-2).

MCPH1 depletion causes centriole overduplication

To further investigate the mechanism by which MCPH1 deletion leads to CA, we engineered a doxycycline -inducible MCPH1 shRNA HeLa cell line. Treatment with doxycycline reduces MCPH1 gene expression (Figure 4-3A) and causes CA (Figure 4-3B-C). CA can arise by two major mechanisms: (1) centriole overduplication, or (2) cell doubling (e.g. cytokinesis failure or cell-cell fusion). To determine the relative contributions of these two mechanisms, we employed a previously described technique (Chapter 3 and Ref [177,208,240]) to assess mother/mature centrioles, as the defining protein markers of mother centrioles are loaded in late G2. If centriole overduplication is the predominant mechanism, one would expect a relative dearth of mother centrioles. In contrast, if cell doubling is the predominant mechanism, one would expect to see most of the extra centrosomes containing a mother centriole. We assessed mother centrioles by staining for CEP164 and observe a smaller percentage of mother

centrioles in the MCPH1-depleted cells (Figure 4-3D-F). We conclude that MCPH1 deletion causes centriole overduplication.

We sought to further probe the mechanism underlying CA in the presence of MCPH1 depletion. Firstly, we asked whether PLK4 is required for CA induced by MCPH1 depletion. We treated our doxycycline-inducible MCPH1 shRNA cells with doxycycline and centrinone B, a chemical inhibitor of PLK4.[157] Indeed, PLK4 activity is required for CA in the context of MCPH1 depletion (Figure 4-4A-C).

Centrosomal CHK1 signal, which is required for DNA damage-induced CA,[241,242] is downregulated through MCPH1.[237] Therefore, we tested the hypothesis that CA caused by MCPH1 depletion is dependent on CHK1 activity. We treated our doxycycline-inducible MCPH1 shRNA cells with doxycycline and a chemical inhibitor of CHK1. This CHK1 inhibitor does not significantly reduce CA in the presence of MCPH1 depletion (Figure 4-4A-C). We conclude that CA induced by MCPH1 depletion does not depend on CHK1. This is consistent with previous findings that CHK1 is specifically involved in CA in response to DNA damage.[241]

MCPH1-depleted cells demonstrate increased CDK2 levels and CDK2 T160 activating phosphorylation after ionizing radiation.[236] Furthermore, CDK2 is known to be required for centriole duplication,[243-248] and CDK2 activity protects STIL, a crucial regulator of centriole duplication, from SCF-βTrCP-mediated degradation.[211] At the same time, $Cdk2^{-/-}$ DT40 cells show robust CA after IR,[242] so CDK2 does not appear to be absolutely required for CA. In addition, CDK2 inactivates the APC/C-CDH1 complex toward the end of G1, and APC/C-CDH1 normally targets several crucial centriole duplication mediators for degradation by the 26S proteasome, including SAS6, STIL, and CPAP.[73,249,250] To test the hypothesis that MCPH1 depletion requires CDK2 to drive CA, we treated our doxycycline-inducible MCPH1 shRNA

cells with doxycycline and a chemical inhibitor of CDK2. We find that CDK2 inhibition reduces CA in the context of MCPH1 depletion (Figure 4-4A-C). Furthermore, we utilized a genetic inhibition approach by overexpressing p27, a CDK2 inhibitor. Consistently, we find that p27 overexpression reduces CA in the context of MCPH1 depletion (Figure 4-4D-E). We conclude that CA induced by MCPH1 depletion depends on PLK4 and CDK2.

Given that CDK2 protects STIL from SCF-βTrCP-mediated degradation,[211] we hypothesized that MCPH1 depletion increases levels of STIL at the centrosome. By quantitative immunofluorescence, we observe that STIL levels are increased upon MCPH1 depletion in asynchronous cells (Figure 4-4F-G). Given that STIL levels at the centrosome change during the cell cycle, we assessed STIL levels at the centrosome during different phases of the cell cycle. We observe that cells arrested in S phase with thymidine (Figure 4-4H) and G2 with the CDK1 inhibitor RO-3306 (Figure 4-4I) display greater levels of STIL at the centrosome. We conclude that MCPH1 depletion causes CA by increasing CDK2 activity, which results in greater levels of STIL at the centrosome, resulting in centriole overduplication.

Loss of MCPH1 causes chromosomal instability

Next we looked at the effects of MCPH1 depletion on mitosis. Previous reports have demonstrated that loss of MCPH1 causes premature chromosome condensation, increased mitotic index, slowed mitosis dynamics, delayed chromosome alignment, and multipolar spindles.[235,239,251-257] We examined the effect of MCPH1 depletion on mitosis. Depletion of MCPH1 caused an increase in the incidence of multipolar metaphases and an increased incidence in lagging chromosomes and/or chromosome bridges in anaphase (Figure 4-5). We conclude that MCPH1 deletion causes chromosomal instability.

Summary of causes of centrosome amplification in human cancer

Figure 4-6 summarizes the causes of CA in human cancer. Our previous work has demonstrated that approximately 35% of breast cancers exhibit CA, defined as an average centrosome number greater than two.[109] Of this 35%, our previous work has estimated that approximately 80% of CA is due to centriole overduplication, while 20% is due to cell doubling events; this is based on the observation that 80% of melanomas exhibited a decrease in the percentage of centrosomes containing mother/mature centrioles.[208] Of this 80%, we estimate that 30% is due to viral causes of CA. This is based on the fact that 3% of cancers are caused by viruses and the observations that these viruses, including HBV,[258-261] HPV,[262,263] HTLV,[264] EBV,[265] and KSHV/HHV8,[266-269] have been shown to cause CA. Therefore, our estimated 30% of centriole overduplication being due to viruses is based on the assumption that all viral-induced cancers have CA. Additionally, cyclin E (CCNE1) amplification occurs in about 5% of the cancers analyzed in this study has been shown to cause CA (Supplemental Figure 4-5).[270,271] Cyclin D amplification occurs in about 8% of cancers (Supplemental Figure 4-5) and may cause CA.[272] Cyclin A (CCNA2) is also important for centriole duplication,[204,246,273] but amplification occurs in <1% of cancers (Supplemental Figure 4-5). Furthermore, the mechanism of MCPH1 depletion-mediated CA depends on increased CDK2 activity,[236] and CDK2 protects STIL from βTrCP-mediated degradation.[211] βTrCP is also known to ubiquitinate PLK4.[68] Reduced βTrCP activity is hypothesized to increase PLK4 and STIL at the centrosome, thereby driving centriole overduplication.

Discussion

CA is common in human cancer, but the causes of CA have been unclear. Herein, we investigated alterations in all 366 known centrosome genes. In general, we identified a relative dearth of genomic alterations in the centrosome genes, particularly the genes required for centriole duplication. This is consistent across most genes involved in mitosis,[274] suggesting these genes are so fundamental to the survival and proliferation of tumors. This is further corroborated by our findings that downregulation of many crucial centrosome proteins results in worse patient outcomes. This is rather surprising, given the reports of CA being common in cancer and our hypothesis that CA would arise from overexpression of centrosome components. However, this is in line with some reports of downregulation of centrosome components resulting in loss of centrioles and increased mitotic infidelity, such as depletion or inhibition of PLK4.[62,157,275] In addition, $PLK4^{+/-}$ mice are more likely to get liver tumors.[276,277]

Our study revealed MCPH1 deletion to be the most common and penetrant cause of CA in human cancer. MCPH1 was first identified as a determinant of human brain size, and inherited mutations in MCPH1 give rise to microcephaly.[226,234] MCPH1 is a *bona fide* tumor suppressor,[227] and many previous studies have demonstrated aberrant expression in diverse cancer types.[228,278-281] Further, reduced expression of MCPH1 has been linked to higher grade and stage tumors and worse outcomes.[227,282] In addition, MCPH1 localizes to the centrosome,[232,235] and previous studies have linked depletion of MCPH1 to CA.[226,235] However, one study demonstrated that $Mcph1^{-/-}$ DT40 cells have normal centrosome structure and number;[236] we speculate this may be because this study counted γ-tubulin foci instead of centrioles.

This study also reveals MCPH1 deletion as a cause of chromosomal instability in human cancer. This is consistent with previous reports that MCPH1 knockout MEFs exhibit more

metaphase aberrations in response to ionizing radiation compared to MCPH1 WT MEFs.[283] *Prima facie*, this finding conflicts with two previous reports of MCPH1 depletion in U2OS cells;[255,284] however, U2OS cells are p53 competent, and it is possible that loss of p53 is permissive of CIN in the context of MCPH1 deletion. There is precedent for this, as previous work has demonstrated that loss of p53 is permissive of more mitotic errors induced by depletion of various mitosis genes.[285] We conclude that loss of p53 is required for CIN in the setting of MCPH1 deletion.

MCPH1 is on chromosome 8p, a region that is commonly deleted in human cancer, [286,287] is occasionally associated with gains of chromosome 8q,[218] and portends worse outcomes.[218] This is likely to be an initiating event, as it is detected at early stages of breast cancer.[288,289] Interestingly, it does not appear that deletion of a single gene on 8p is responsible, but likely that suppression of multiple genes contributes to the observed phenotype in 8p-deleted cancers.[290,291] Herein we provide evidence that one mediator of the phenotype of observed in 8p-deleted cancers is MCPH1 deletion, which likely causes CA and chromosomal instability in 8p-deleted tumors. Furthermore, monosomy 8p is a rare congenital disorder characterized by growth deficiency, mental retardation, malformations of the skull, cardiac abnormalities, genital defects, and microcephaly.[292] As microcephaly is seen with inherited mutation of MCPH1 and other key drivers of centriole duplication, is likely that the microcephaly and mental retardation seen is conferred by loss of MCPH1. Neural progenitor cells are particularly sensitive to alterations in centrosome/centriole number and integrity.

Proliferation in the presence of CA requires additional adaptive alterations, such as loss/mutation of p53,[67] p21,[293,294] or the PIDDosome genes (CRADD, PIDD1, CASP2).[214] Some evidence suggests that loss of p53 is sufficient for CA,[295,296] and one potential mechanism

underlying this is that p53 negatively regulates PLK4 mRNA recruiting HDAC repressors to the PLK4 promoter.[297] However, other evidence suggests that loss of p53 itself does not appear to drive CA, as the analysis of brains of $p53^{-/-}$ mice revealed that these animals have normal centrosome number,[298] and many cancer cell lines with mutant p53 show no increase in centriole number.[209] In tumors with MCPH1 deletion, we observed that approximately 55% also had one of the above compensatory alterations compared to approximately 40% of tumors without MCPH1 deletion that have a mutation in p53, p21, CRADD, PIDD1, or CASP2. Therefore, there are likely other potential compensatory alterations that are permissive of cellular proliferation in the context of CA.

Our study focused mostly on causes of numerical CA. However, structural centrosome abnormalities have also been reported, such as increased centriole length. Increased centriole length has been demonstrated to be caused by CPAP/CENPJ/Sas4 overexpression[71-73,209] or CP110 depletion,[72] but according to our analyses, neither genomic amplification nor mRNA overexpression are commonly seen in human cancer. Increased centrosome size can be caused by overexpression of NLP/NINL[299] and other mediators of microtubule nucleation, but our analyses demonstrate that neither genomic amplification nor mRNA overexpression are commonly seen in human cancer. Increased centrosome size can also be caused by increased centriole number of length,[209] and the relative contribution of all these mechanisms to centrosome size remain unclear. Our study only focused on genes with reported localization to the centrosome; however, we know that other extra-centrosomal genes, such as transcriptional regulators or post-translational modifiers, can alter the levels of centrosome proteins and could drive CA. Additionally, inhibition of cell cycle progression can lead to CA. For example, G2 arrest, which

can be induced by DNA damage, leads to PLK1 activation and premature centriole reduplication.[300]

This study provides additional insight into the clinically-relevant causes of CA in human cancer, revealing MCPH1 deletion as a common and penetrant drive of CA. Additional drivers of CA were likely missed and warrant future investigation.

Materials and Methods

Bioinformatic Analysis of Centrosome Genes

A list of all 367 centrosome genes was compiled by searching for "centrosome" on Uniprot and supplementing with proteins discovered at the centrosome in previous proteomic analysis of isolated centrosomes and validation by immunofluorescence.[210] Data were extracted from the following 22 TCGA datasets using cBioPortal,[196,301] selected based on their size and availability of associated clinical data: acute myeloid leukemia (AML), 200 patients; breast carcinoma, 1105 patients; melanoma, 478 patients; colorectal carcinoma, 633 patients; glioblastoma, 607 patients; low grade glioma, 532 patients; ovarian serous adenocarcinoma, 607 patients; lung adenocarcinoma, 522 patients; lung squamous cell carcinoma, 504 patients; prostate adenocarcinoma, 499 patients; head and neck squamous cell carcinoma, 530 patients; renal clear cell carcinoma, 538 patients; stomach adenocarcinoma, 478 patients; bladder urothelial carcinoma, 413 patients; hepatocellular carcinoma, 442 patients; cervical carcinoma, 309 patients; endometrial carcinoma, 373 patients; esophageal adenocarcinoma, 186 patients; pancreatic adenocarcinoma, 186 patients; pheochromocytoma and paraganglioma, 184 patients; sarcoma, 365 patients; and thyroid carcinoma, 516 patients. This yielded a total of 10,087 patients/tumors. We analyzed the percent of tumors with mutations, copy number variations, and altered gene expression (mRNA Z score < 2 or > 2) for each of the 367 centrosome genes. Each data set was weighted equally during analyses in order to be able to detect certain tissue-specific alterations that may give rise to CA. Data were not available for the following centrosome genes: BOD1L2, PTPN20, ROSSF10, STARD9, TSSK2, WASH1.

For assessing centrosome gene alterations more common in p53 mutated/deleted cancers, we excluded the tumors associated with viruses that have been shown to inhibit p53 function:

(head and neck, liver, and cervical). We then calculated the fold enrichment of alterations in each centrosome gene in TP53 mutated/deleted cancers versus TP53 wild type cancers.

Cell Culture

All cell lines were propagated at 37 °C in 5% CO_2. HeLa, Phoenix, and 293T cell lines (ATCC) were grown in high glucose DMEM supplemented with 2.5 mm l-glutamine, with 10% fetal bovine serum and 100 units/mL penicillin-streptomycin.

Lentivirus encoding shRNAs were produced by transfecting a T25 of 293T cells with 2µg pLKO.1 vector, 1µg pVSV-G, and 1µg psPAX2, and Fugene (Promega). For stable retroviral transduction, a T25 of Phoenix cells was transfected with 2µg pSuperior.retro.puro construct and 1µg pVSV-G into Phoenix cells. For both lentivirus and retrovirus, fresh medium was applied at 24 hours post-transfection, harvested 24 hours later, clarified by centrifugation and filtration through a 0.45 µm membrane to remove cell debris, and diluted 1:1 with complete medium containing 10 µg/mL polybrene. Target cells (HeLa) were infected at 40-60% confluence for 24 hours. For stable doxycycline-inducible MCPH1 shRNA HeLa cells, polyclonal transductants were subcloned by limiting dilution to obtain individual clones and screened by qRT-PCR before and after doxycycline treatment.

To overexpress cDNAs of centrosome candidate genes, HeLa cells were plated in 6-well plates, grown to 80% confluency, and transfected with 2 µg cDNA in pcDNA5 using Fugene (Promega). Cells were given fresh media 12 hours after the transfection. 24 hours after the transfection, cells were either transferred to coverslips for fixation and immunofluorescence or harvested for qRT-PCR to assess transfection efficiency.

Chemicals used in this study include aphidicolin (5 µM, Sigma), 3-MB-PP1 (10 µM, Toronto Research Chemicals), doxycycline (2 µg/mL, Fisher), puromycin (1 µg/mL for HeLa cells, Thermo), CHIR-124 (100nM, MedChemExpress), milciclib (100nM, PHA-848125, MedChemExpress), and centrinone B (500nM, Tocris).

Molecular Biology

The following cDNAs were acquired: NPM1 was cloned from HeLa cDNA library, STIL was obtained from transOMIC (BC16223), PTK2 was a kind gift from Michael Davidson (Addgene plasmid #55122), NDRG1 was a kind gift from Ben Park (Johns Hopkins), CTNNB1 wild type and S33Y were kind gifts from Eric Fearon (Addgene plasmids #16828 and #19286), and CEP19 (GE MHS6278-202828648), SPATC1 (GE MHS6278-202802271), and TBCCD1 (GE MHS6278-202801247) were obtained from GE Healthcare. These cDNAs were cloned into pCDNA5/FRT/TO with C-terminal mNeonGreen tag (vector provided by Jun Wan and Beth Weaver, University of Wisconsin). Sequencing was performed to verify cloning fidelity (Protein CT, Quintara Biosciences). All constructs were full-length cDNAs unless otherwise noted.

Mutant NPM1 (W288Cfs*12 insertional frameshift mutation, which is predicted to mutate the remaining C-terminal amino acids of the protein and increase the length of the protein by 10 amino acids) were cloned from a HeLa cDNA library using the following primers: forward 5’CCCCGGATCCATGGAAGATTCGATGGACATGG, reverse: CCCCGAATTCCTATTTTCTTAAAGAGACTTCCTCCACTGCCAGACAGAGATCTTGAA TAGCCTCTTGGT.

To make shRNA vectors, shRNAs targeting sequences were cloned into pLKO.1-TRC, a kind gift from David Root (Addgene plasmid #10878). The following sequences were used for

initial screening: CEP76, ACGACTTTAGTAGCATCATAT; MCPH1, AGGAAGTTGGAAGGATCCA; NEURL4, CCATCATGCAAGACGGTAATT; NPM1, TTACGAAGGCAGTCCAATTAA; non-targeting control, CCGCAGGTATGCACGCGT (kind gift from David Root, Addgene plasmid #10879). Lentivirus was produced as described above. Efficiency of gene depletion was assessed by qRT-PCR. Primers are available in Supplemental Table 7.

To make doxycycline-inducible shRNA cell lines, the MCPH1 targeting sequences were cloned into pSuperior.retro.puro following the manufacturer's protocol (OligoEngine). Two different shRNAs were used for MCPH1: AGGAAGTTGGAAGGATCCA and CTCTCTGTGTGAAGCACCT. Retrovirus was made and used to transduce HeLa cells stably expressing TetR (kind gift from Jun Wan and Beth Weaver, University of Wisconsin), as described above.

CRISPR/Cas9

The CRISPR/Cas9 system was used to create knockout and edited cell lines in HeLa cells. pSpCas9(BB)-2A-Puro (PX459) V2.0 was a gift from Feng Zhang (Addgene plasmid # 62988).[302] The MCPH1 guides used included: TAAAGCTCGTTTCGGTGCT and GAGAGGCGTAAAGCTCGTT. Both target an exonic region near the N terminus. Cutting efficiency of each guide was assessed by surveyor assay (IDT, 706025) following PCR of 600bp fragments from genomic DNA encompassing the guide RNA locus. PX459 vectors were transfected into HeLa cells using Fugene (Promega). Prior to transfection, media was replaced with serum- and antibiotic-free media. 24 hours after transfection, cells were selected with puromycin (1µg/mL) for 72 hours, then allowed to recover for 24 hours in fresh media and

subcloned by limiting dilution. Colonies were selected and screened by PCR of the region flanking the cut site and subsequent sequencing. Verification of knockout lines was performed with MCPH1 sequencing.

Immunofluorescence (IF) and Microscopy

IF and imaging were carried out as previously described [194,195]. Cells were seeded on glass coverslips in 24-well plates and fixed with 100% ice-cold methanol for 30 minutes. Fixed cells were then blocked for 30 minutes in 3% bovine serum albumin (BSA) and 0.1% triton X-100 in PBS (PBSTx + BSA). Primary antibodies were incubated in PBSTx + BSA for 1 hour at room temperature and washed three times in PBSTx, followed by secondary antibody incubation in PBSTx + BSA for 30 minutes at room temperature and two washes with PBSTx. Cells were counterstained with DAPI and mounted on glass slides with Prolong Gold antifade medium (Invitrogen). Image acquisition was performed on a Nikon Eclipse Ti inverted microscope equipped with 10x, 20x, 40x, 60x, and 100x objectives; a temperature-controlled motorized stage with 5% CO_2 support (In Vivo Scientific); and Hamamatsu ORCA Flash 4.0 camera. For images displayed in the figures, optical sections were taken at 0.2-μm intervals and deconvolved using Nikon Elements. Where appropriate, the observer was blinded to treatment condition during image acquisition and analysis. Images were processed and analyzed using Nikon Elements.

Primary antibodies used were: centrin (Millipore, 04-1624), γ-tubulin (Abcam, ab27074), pericentrin (Abcam, ab4448), β-actin (DSHB, JLA20, deposited by Lin, J.J.-C.), and β-tubulin (DSHB, 12G10, deposited by Frankel, J./Nelsen, E.M.). Alexa fluor-conjugated secondary antibodies were used (Invitrogen, 1:350).

Quantitative Reverse Transcriptase Polymerase Chain Reaction (qRT-PCR)

RNA was isolated from cells using TRI Reagent (Molecular Research Center). DNase treatment was used to remove DNA contamination. RNA was then converted to cDNA using the Quantitect Reverse Transcription Kit (Qiagen). A StepOne Plus (Applied Biosystems) real-time PCR thermal cycler was used for amplification. The average C_T value of three housekeeping genes (*RRN18S, GAPDH and ACTB*) was subtracted from each experimental C_T, then 2^-C_T values were normalized and compared. Additionally, the $\Delta\Delta C_T$ method was employed to calculate the fold change in gene expression.

Survival Analysis with KM Plotter

Kaplan Meier (KM) Plotter[213] was queried to assess the impact of gene expression of the 367 centrosome genes on survival. We assessed both overall survival (OS) and progression-free survival (PFS) in breast, ovarian, lung, and gastric cancers. Number of patients included in each analysis are as follows: breast PFS, n= 3554; ovarian PFS, n = 484; lung FP, n=982; gastric, FP, n= 646. Data were not available for the following 5 centrosome genes: AGBL4, PPP1R42, WASH1, WASH2P, and WASH3P.

Statistics

Statistical evaluations were performed using Prism (Graphpad Software) or Microsoft Excel (Microsoft Office). Two-tailed t-tests and one-way ANOVA were used for comparisons. For multiple comparisons, Tukey's correction was made. Survival analysis was performed using the Kaplan Meier method. P-values < 0.05 were considered significant for all tests, and designations are made in the figures for statistical significance.

Table 4-1

Top hits for drivers of centrosome amplification in human cancer

Centrosome Gene	Known Functions (Especially Centrosome-Related)	Hypothesis
CEP19	Ciliation; microtubule anchoring to the centrosome; inactivation results in morbid obesity.[303]	Gain of function causes CA
CEP72	Centriolar satellite component; recruit key centrosomal proteins to centrosome; microtubule nucleation; BRCA1 interactor; overexpression increases CIN, aneuploidy, lagging chromosomes.[304]	Gain of function causes CA
CEP76	Limits centriole duplication; depletion drives aberrant amplification of centrioles.[305]	Loss of function causes CA
CTNNB1	Wnt signaling pathway; negative regulator of centrosome cohesion; overexpression of stabilized mutant increases centrosomes.[306-309]	Gain of function causes CA
MCPH1	Neurogenesis; chromosome condensation; DNA damage response; restrains DNA damage-induced CA; germline mutations cause microcephaly.	Loss of function causes CA
NEURL4	Interacts with CP110 (important for limiting centriole elongation).[310]	Loss of function causes CA
NDRG1	Cell trafficking; regulates centrosome number.[311]	Gain of function causes CA
NPM1	Depleting NPM1 resulted in CA.[312]	Loss of function causes CA
PTK2	Cell migration, adhesion, spreading, actin reorganization, focal adhesion formation, proliferation, apoptosis.	Gain of function causes CA
SPATC1	Proximal centriole marker[313]	Gain of function causes CA
TBCCD1	TBCCD1 localizes to a region sub-proximal to centrioles[314]; mutant cells have variable numbers of centrioles and centriole positioning defects required for mother-daughter centriole linkage and mitotic spindle orientation[315]; migration.	Gain of function causes CA

Figure 4-1

Screening of lead candidates for drivers of centrosome amplification in human cancer.

(A) Representatives images of cells overexpressing mNeonGreen-tagged cDNAs corresponding to genes for which gain of function is hypothesized to cause CA, as well as shRNA-mediated depletion of genes for which loss of function is hypothesized to cause CA. Scale bars = 10 μm. **(B)** qRT-PCR was performed to assess the amount of overexpression of the mNeonGreen-tagged genes. **(C)** qRT-PCR was performed to assess depletion by shRNA. **(D)** Quantification of centrioles (centrin foci) in the indicated conditions. Each dot represents one cell. **(E)** Quantification of the percentage of cells with CA, defined as greater than 4 centrioles (centrin foci). Bars represent means ±SD. ***P value < 0.001.

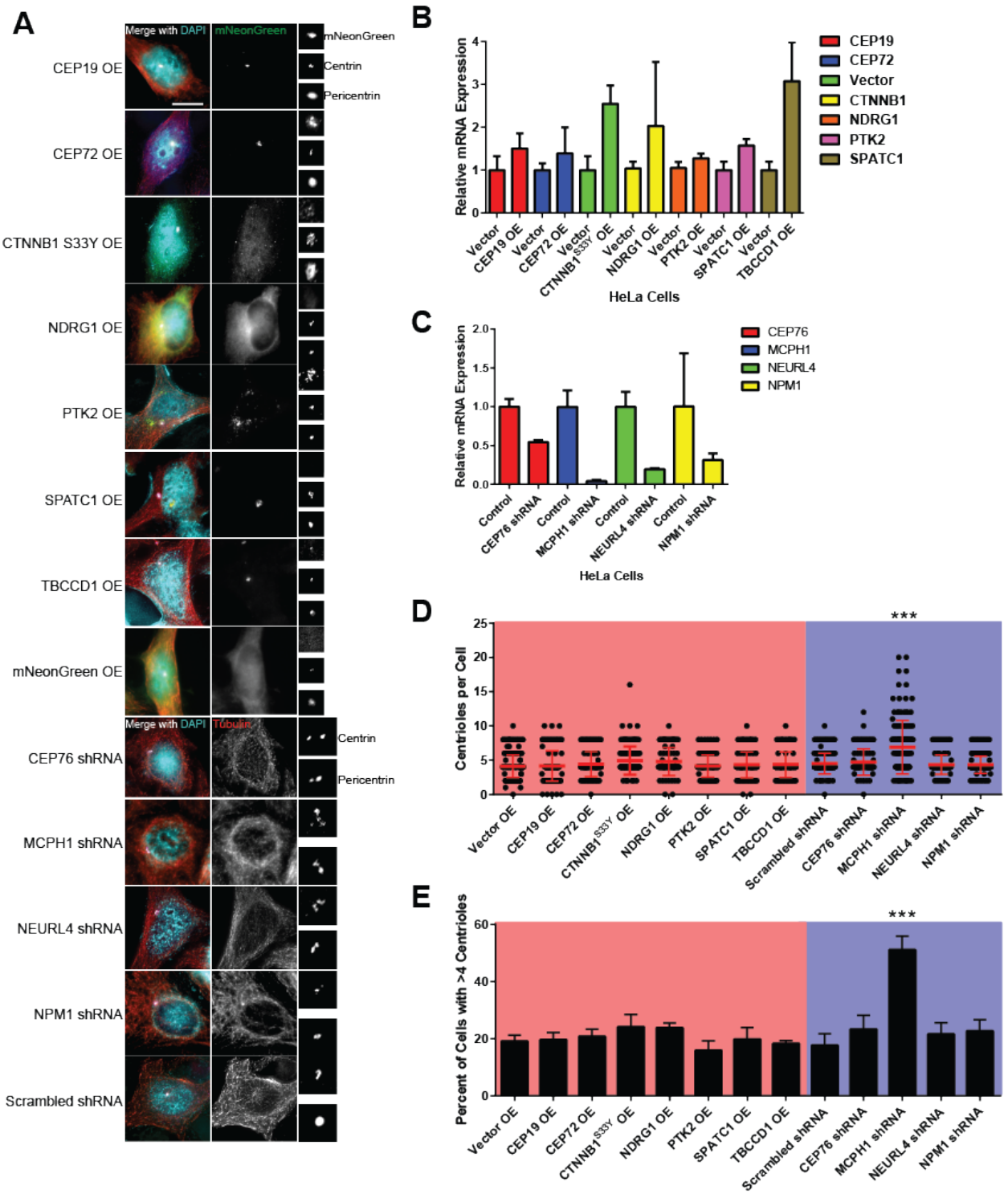
A
Merge with DAPI
mNeonGreen
Centrin
Pericentrin
CEP19 OE
CEP72 OE
CTNNB1 S33Y OE
NDRG1 OE
PTK2 OE
SPATC1 OE
TBCCD1 OE
mNeonGreen OE
Merge with DAPI
Tubulin
Centrin
Pericentrin
CEP76 shRNA
MCPH1 shRNA
NEURL4 shRNA
NPM1 shRNA
Scrambled shRNA
B
Relative mRNA Expression
CEP19
CEP72
Vector
CTNNB1
NDRG1
PTK2
SPATC1
Vector
CEP19 OE
Vector
CEP72 OE
Vector
CTNNB1S33Y OE
Vector
NDRG1 OE
Vector
PTK2 OE
Vector
SPATC1 OE
Vector
TBCCD1 OE
HeLa Cells
C
Relative mRNA Expression
CEP76
MCPH1
NEURL4
NPM1
Control
CEP76 shRNA
Control
MCPH1 shRNA
Control
NEURL4 shRNA
Control
NPM1 shRNA
HeLa Cells
D
Centrioles per Cell
***
Vector OE
CEP19 OE
CEP72 OE
CTNNB1S33Y OE
NDRG1 OE
PTK2 OE
SPATC1 OE
TBCCD1 OE
Scrambled shRNA
CEP76 shRNA
MCPH1 shRNA
NEURL4 shRNA
NPM1 shRNA
E
Percent of Cells with >4 Centrioles
***
Vector OE
CEP19 OE
CEP72 OE
CTNNB1S33Y OE
NDRG1 OE
PTK2 OE
SPATC1 OE
TBCCD1 OE
Scrambled shRNA
CEP76 shRNA
MCPH1 shRNA
NEURL4 shRNA
NPM1 shRNA

Figure 4-2

MCPH1 deletion is common in human cancer and correlates with worse outcomes.

(A) Graphical demonstration of the percent of tumors within each tumor site that harbor deletions (blue), amplifications (red), or mutations (green). **(B)** Kaplan Meier curves demonstrating overall survival (OS) or disease-free survival (DFS) in bladder, breast, colorectal, ovarian, and prostate cancers (some of the tumor sites where MCPH1 deletion is most common and where patient number is high).

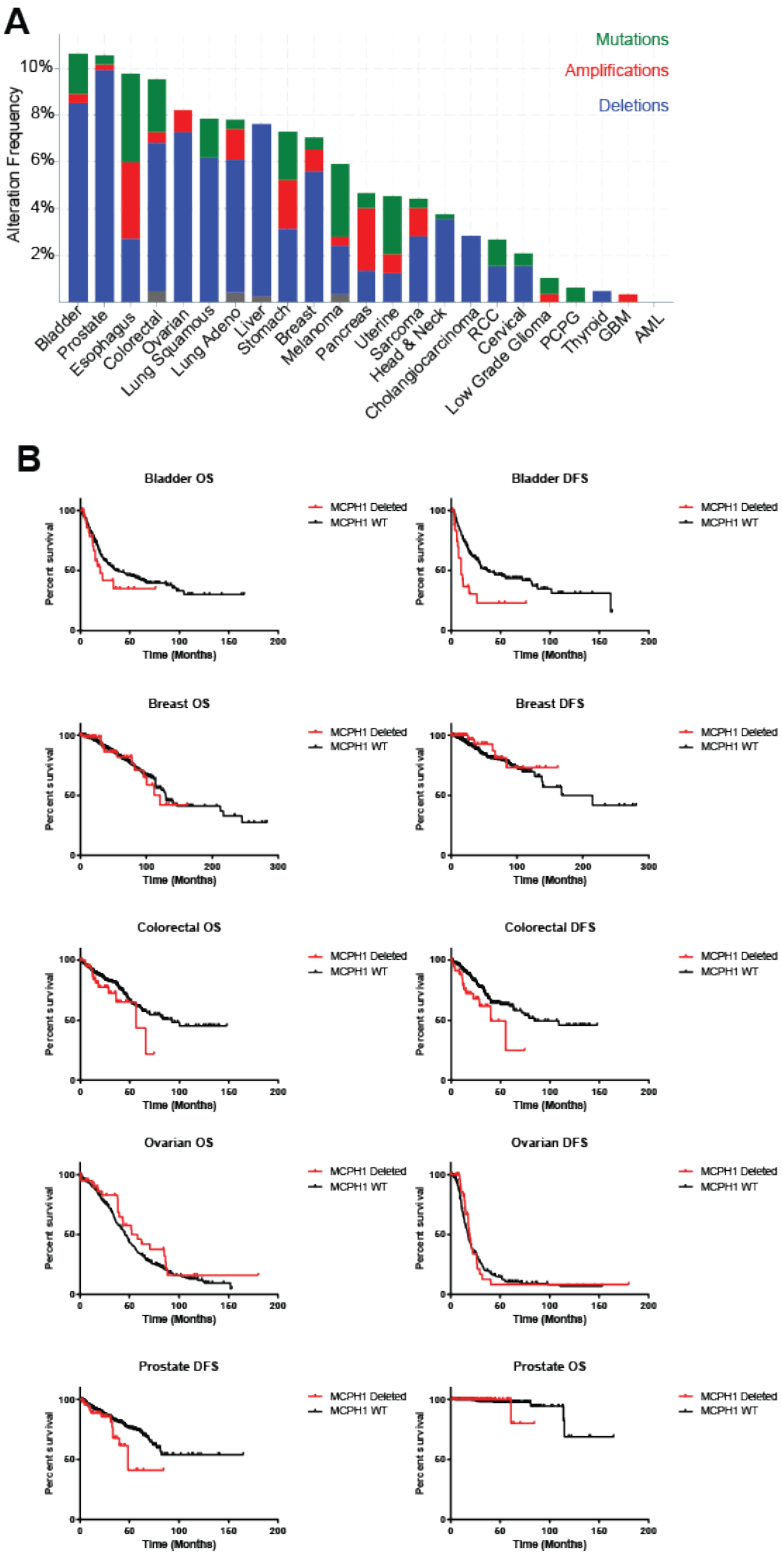
A
Mutations
Amplifications
Deletions
Alteration Frequency
10%
8%
6%
4%
2%
Bladder
Prostate
Esophagus
Colorectal
Ovarian
Lung Squamous
Lung Adeno
Liver
Stomach
Breast
Melanoma
Pancreas
Uterine
Sarcoma
Head & Neck
Cholangiocarcinoma
RCC
Cervical
Low Grade Glioma
PCPG
Thyroid
GBM
AML
B
Bladder OS
Bladder DFS
Breast OS
Breast DFS
Colorectal OS
Colorectal DFS
Ovarian OS
Ovarian DFS
Prostate DFS
Prostate OS
MCPH1 Deleted
MCPH1 WT
Percent survival
Time (Months)

Figure 4-3

MCPH1 depletion causes centriole overduplication.

(A) MCPH1 qRT-PCR to assess the fidelity of knockdown in our tetracycline-inducible system. Relative mRNA was computed by taking 2^-ΔCt and normalizing to HeLa TetR. HeLa TetR is the parental cell line from which the HeLa MCPH1 shRNA cell line was made. Doxycycline was added to the indicated conditions for 24 hours. **(B)** Representatives image of centrioles in the indicated conditions. **(C)** Quantification of centrioles (centrin foci) in the indicated conditions. **(D)** Representative images of CEP164 staining to mark the mother centrioles. PLK4 overexpression was used as a positive control for centriole overduplication (should see lower percentage of centrioles with CEP164), and cytochalasin B induces cytokinesis failure and was used as a positive control for cell doubling (should see higher percentage of centrioles with CEP164). **(E)** Quantification of the percentage centrioles. **(F)** Quantification of the percentage of centrioles with CEP164 only in the cells with centrosome amplification (greater than 4 centrioles).

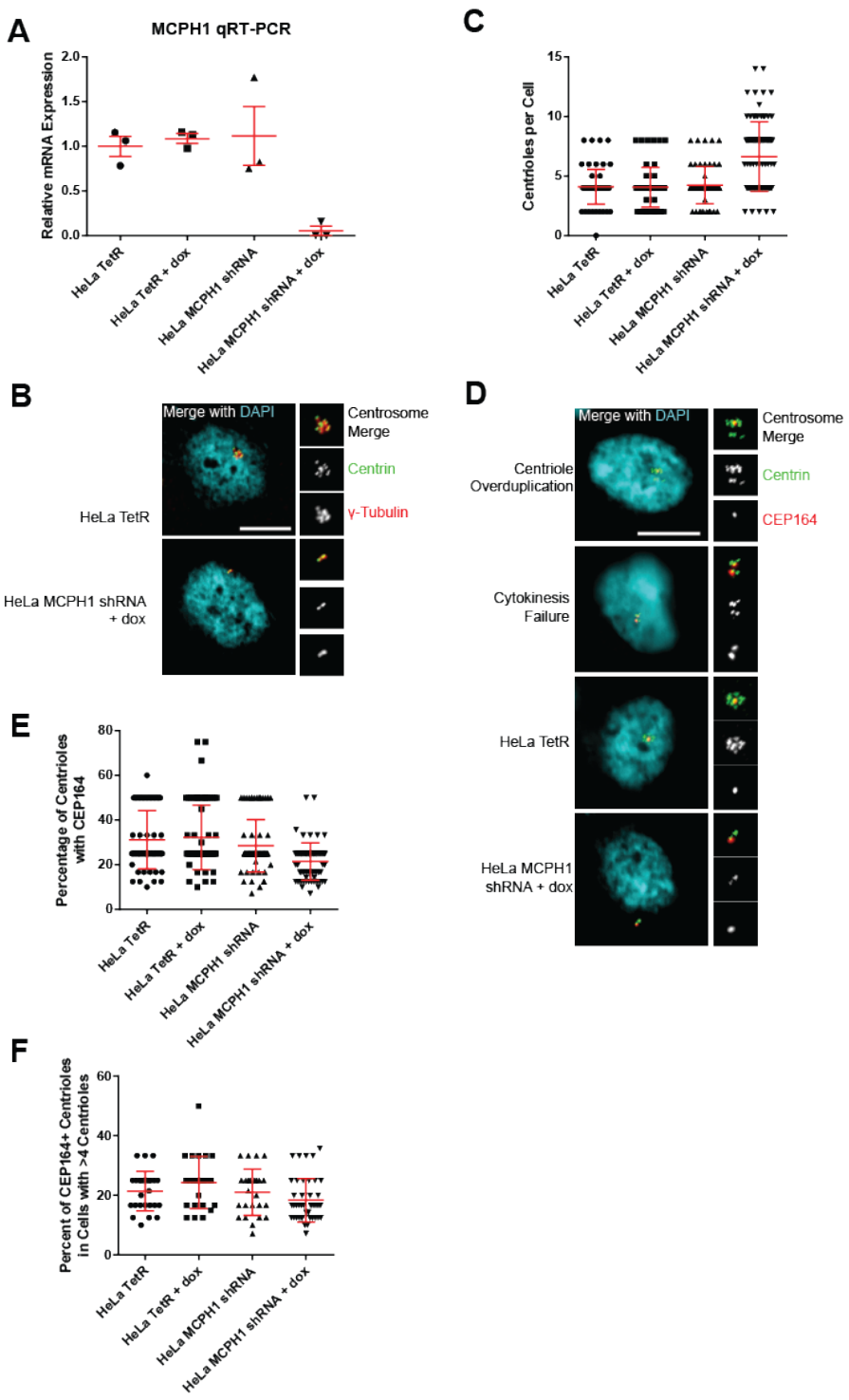
A
MCPH1 qRT-PCR
Relative mRNA Expression
2.0
1.5
1.0
0.5
0.0
HeLa TetR
HeLa TetR + dox
HeLa MCPH1 shRNA
HeLa MCPH1 shRNA + dox
C
Centrioles per Cell
15
10
5
0
HeLa TetR
HeLa TetR + dox
HeLa MCPH1 shRNA
HeLa MCPH1 shRNA + dox
B
Merge with DAPI
Centrosome
Merge
Centrin
γ-Tubulin
HeLa TetR
HeLa MCPH1 shRNA
+ dox
D
Merge with DAPI
Centrosome
Merge
Centrin
CEP164
Centriole
Overduplication
Cytokinesis
Failure
HeLa TetR
HeLa MCPH1
shRNA + dox
E
Percentage of Centrioles
with CEP164
80
60
40
20
0
HeLa TetR
HeLa TetR + dox
HeLa MCPH1 shRNA
HeLa MCPH1 shRNA + dox
F
Percent of CEP164+ Centrioles
in Cells with >4 Centrioles
60
40
20
0
HeLa TetR
HeLa TetR + dox
HeLa MCPH1 shRNA
HeLa MCPH1 shRNA + dox

Figure 4-4

Centrosome amplification caused by MCPH1 depletion is dependent on PLK4 and CDK2 activities.

(A) Representative images of MCPH1-depleted cells treated with centrinone (a PLK4 inhibitor), CHIR-124 (a CHK1 inhibitor), or milciclib (a CDK2 inhibitor). Cells were treated with these drugs for 24 hours, then fixed and stained. The adjacent images of the centrosome merge, centrin, and γ-tubulin are enlargements of the centrosome. **(B)** Quantification of centrioles (centrin foci) in the indicated conditions. **(C)** Quantification of the percent of cells with centrosome amplification, defined as the presence of >4 centrioles. **(D)** Representative images of cells overexpressing p27, a CDK2 inhibitor. **(E)** Quantification of centrioles in the indicated conditions. **(F)** Representative images of STIL staining at the centrosome. **(G-I)** Quantification of STIL levels at the centrosome in asynchronous cells **(G)**, cells synchronized in S phase with thymidine **(H)**, and cells synchronized in G2 phase with the CDK1 inhibitor RO-3306.

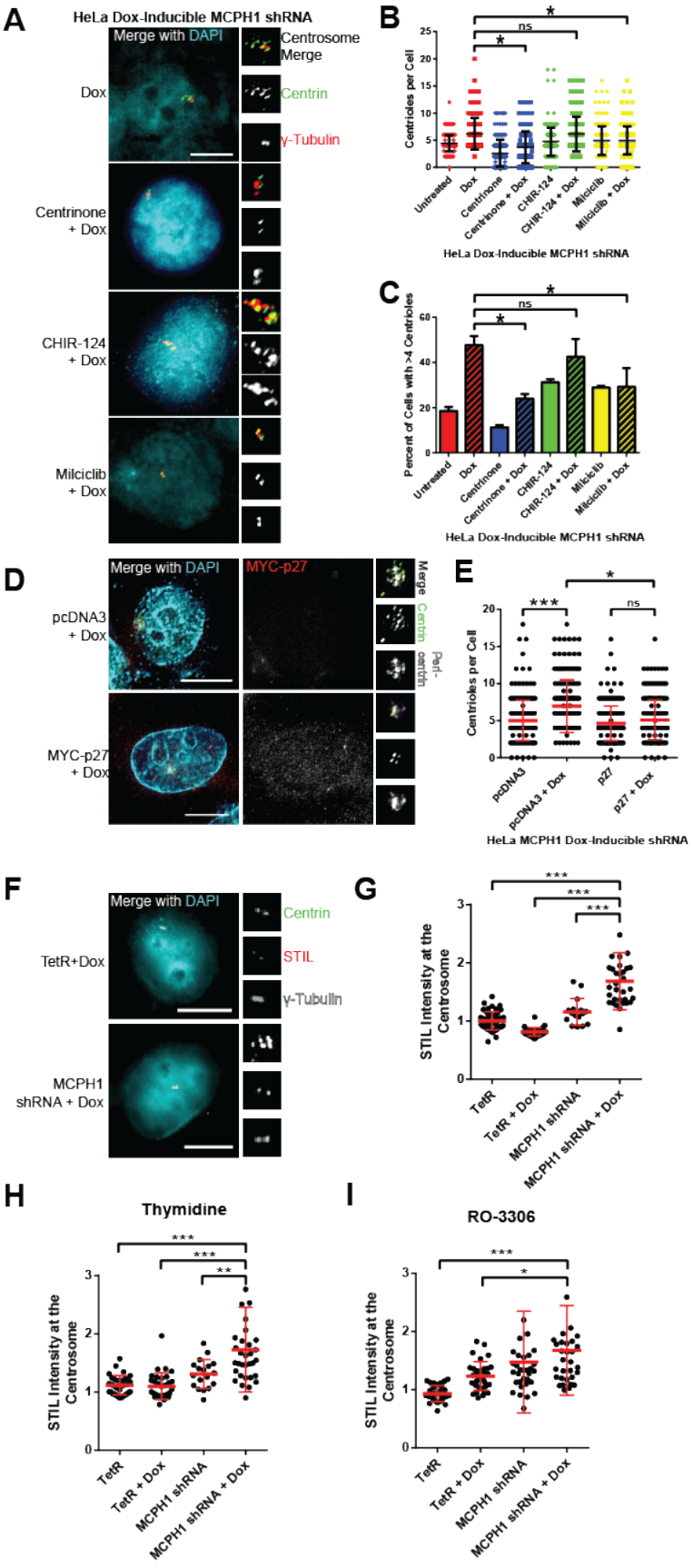
A
HeLa Dox-Inducible MCPH1 shRNA
Merge with DAPI
Centrosome Merge
Centrin
γ-Tubulin
Dox
Centrinone + Dox
CHIR-124 + Dox
Milciclib + Dox
B
Centrioles per Cell
Untreated
Dox
Centrinone
Centrinone + Dox
CHIR-124
CHIR-124 + Dox
Milciclib
Milciclib + Dox
HeLa Dox-Inducible MCPH1 shRNA
C
Percent of Cells with >4 Centrioles
HeLa Dox-Inducible MCPH1 shRNA
D
Merge with DAPI
MYC-p27
Merge
Centrin
γ-Tubulin
pcDNA3 + Dox
MYC-p27 + Dox
E
Centrioles per Cell
pcDNA3
pcDNA3 + Dox
p27
p27 + Dox
HeLa MCPH1 Dox-Inducible shRNA
F
Merge with DAPI
Centrin
STIL
γ-Tubulin
TetR+Dox
MCPH1 shRNA + Dox
G
STIL Intensity at the Centrosome
TetR
TetR + Dox
MCPH1 shRNA
MCPH1 shRNA + Dox
H
Thymidine
STIL Intensity at the Centrosome
TetR
TetR + Dox
MCPH1 shRNA
MCPH1 shRNA + Dox
I
RO-3306
STIL Intensity at the Centrosome
TetR
TetR + Dox
MCPH1 shRNA
MCPH1 shRNA + Dox

Figure 4-5

MCPH1 depletion causes genomic instability.

(A) Representative images of the mitotic phenotypes assessed in metaphase and anaphase cells. **(B)** Quantification of metaphase and anaphase cells as either normal bipolar, multipolar, monopolar, or misaligned (includes polar chromosomes). *P value < 0.05 for 2-way ANOVA interaction.

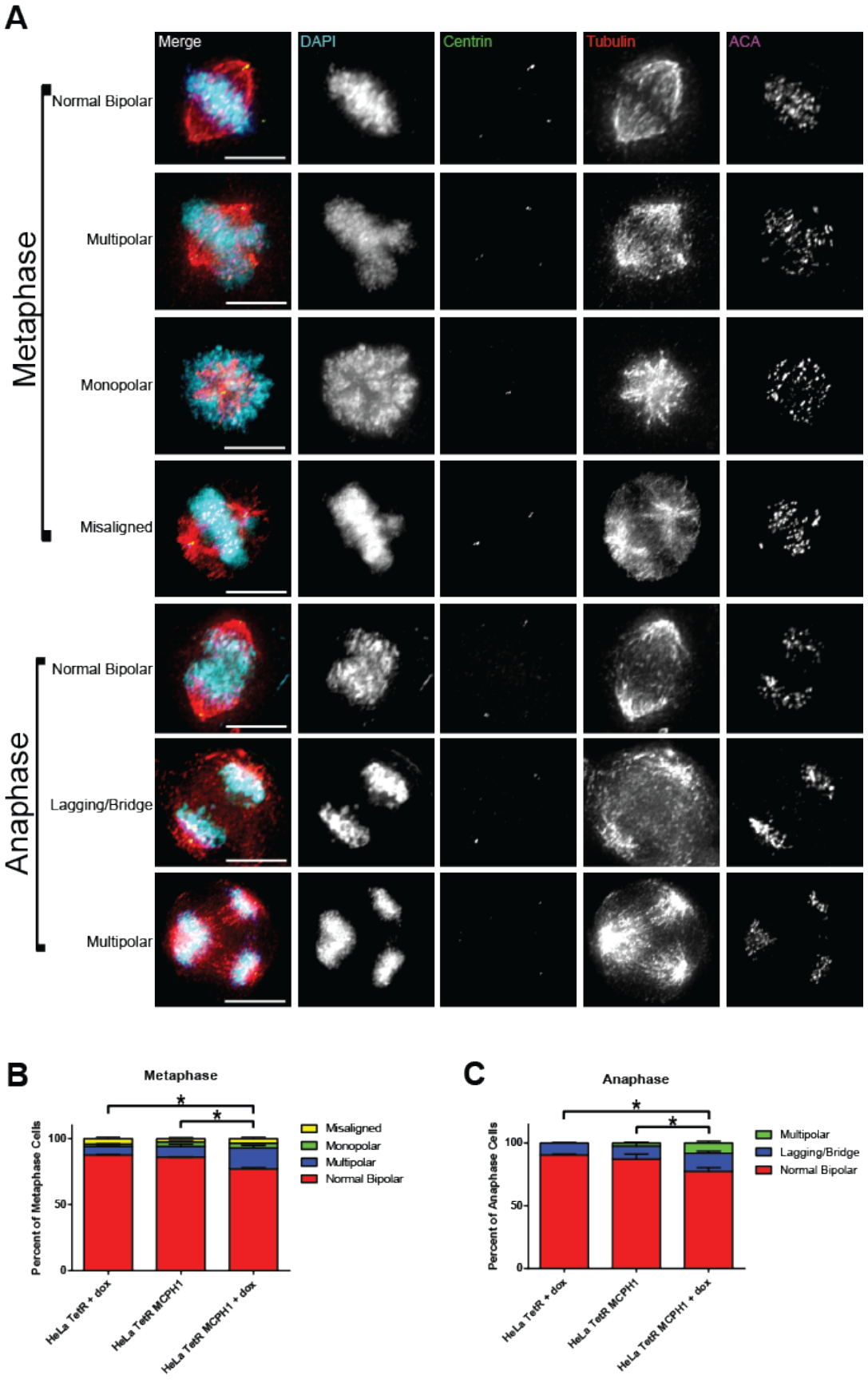
A
Merge
DAPI
Centrin
Tubulin
ACA
Metaphase
Normal Bipolar
Multipolar
Monopolar
Misaligned
Anaphase
Normal Bipolar
Lagging/Bridge
Multipolar
B
Metaphase
Percent of Metaphase Cells
100
50
0
Misaligned
Monopolar
Multipolar
Normal Bipolar
HeLa TetR + dox
HeLa TetR MCPH1
HeLa TetR MCPH1 + dox
C
Anaphase
Percent of Anaphase Cells
100
50
0
Multipolar
Lagging/Bridge
Normal Bipolar
HeLa TetR + dox
HeLa TetR MCPH1
HeLa TetR MCPH1 + dox

Figure 4-6

Summary of the major causes of centrosome amplification in human cancer.

Based on previous work (Chapter 2), approximately 35% of tumors are centrosome amplified (average centrosome number per cell is greater than 2). Of these 35% of tumors, previous work has demonstrated that approximately 80% of centrosome amplification is due to centriole overduplication and 20% is due to cell doubling (Chapter 3). Of these cases of centriole overduplication, 30% are caused by MCPH1 deletion, 15% are caused by cyclin E amplification, 10% are caused by viruses (e.g. EBV, HPV, HBV, HCV), and about 45% are caused by other mechanisms. MCPH1 deletion gives rise to centriole overduplication by decreasing CDK2 activity at the centrosome, thereby reducing βTrCP activity, which increases centrosomal PLK4 and STIL levels, thereby driving centriole overduplication.

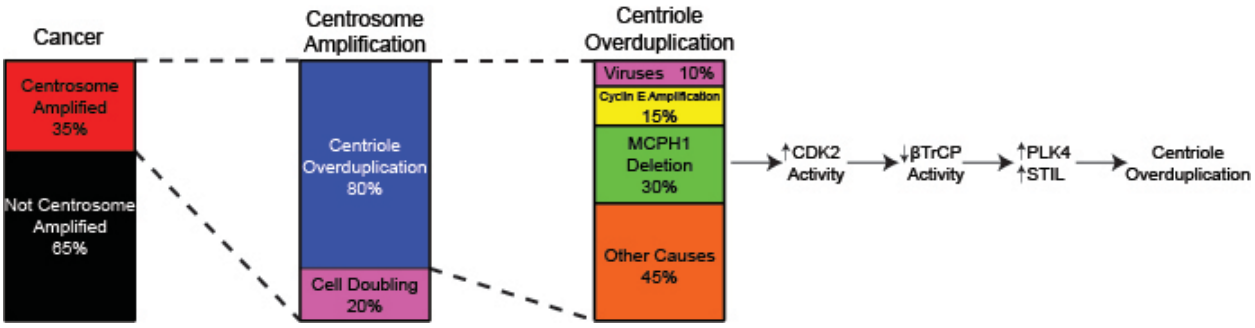

Supplemental Figure 4-1

NPM1 mutations seen in AML do not cause centrosome amplification.

(A) Diagram of NPM1 mutations in TCGA datasets. The most common alterations involves a frameshift at the C terminus. **(B)** Kaplan Meier curve demonstrating overall survival in AML patients with mutant NPM1 versus wild type NPM1. **(C)** Kaplan Meier curve demonstrating disease-free survival in AML patients with mutant NPM1 versus wild type NPM1. **(D)** Oncoprint of NPM1 alterations along with genes whose loss is permissive of proliferation in the setting of centrosome amplification (TP53, CDKN1A, PIDD1, CRADD, and CASP2). There is a lack of coincidence of NPM1 mutation with loss of these other genes. **(E)** Representative images of HeLa cells transfected with either wild type or mutant NPM1. Scale bar = 5μm. **(F)** Quantification of centrioles (centrin foci) per cell in the indicated conditions. **(G)** Quantification of the percentage of cells with centrosome amplification, defined as greater than 4 centrioles (centrin foci).

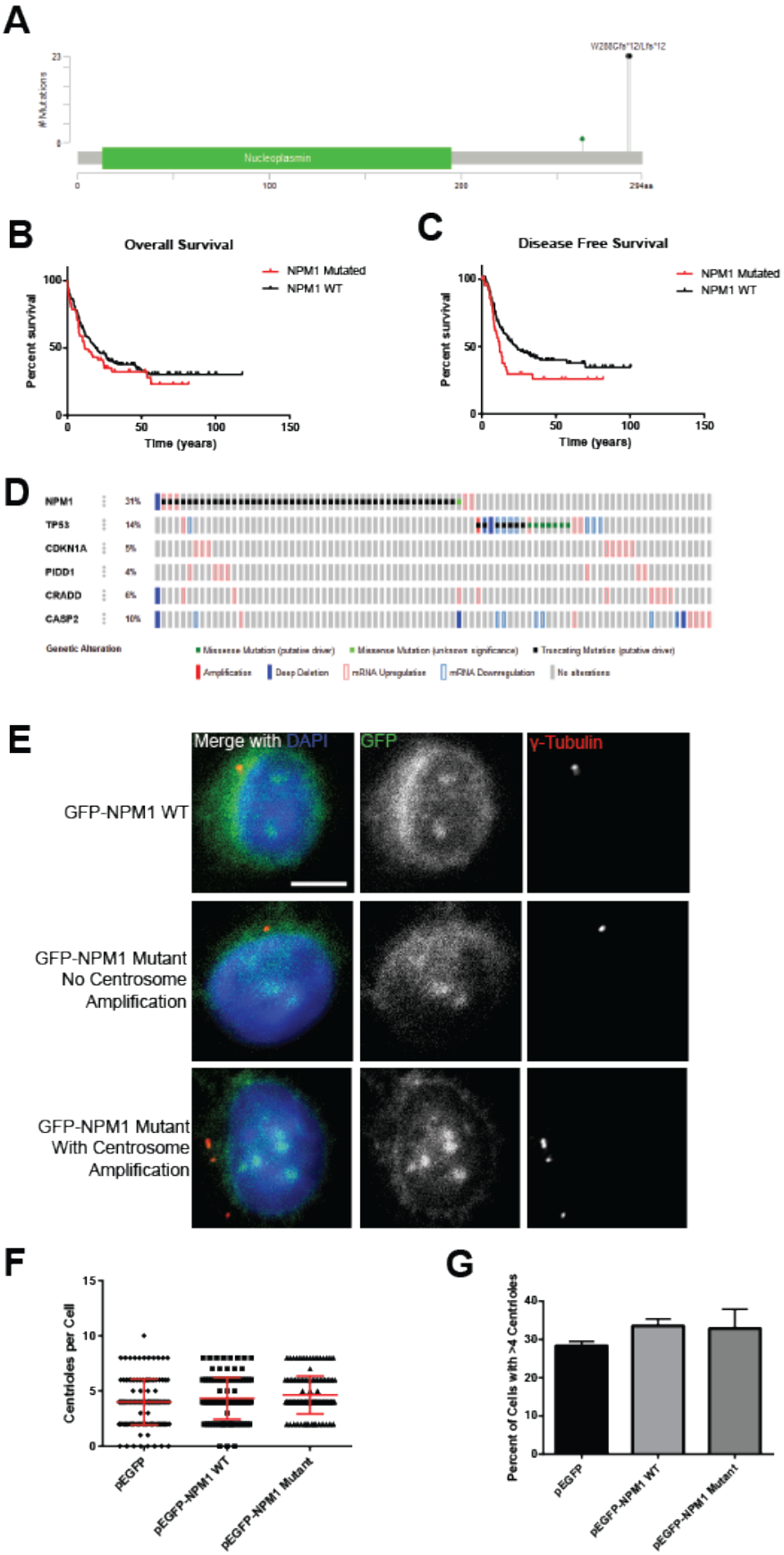
A
W288Cfs*12/Ufs*12
#Mutations
Nucleoplasmin
294aa
B
Overall Survival
NPM1 Mutated
NPM1 WT
Percent survival
Time (years)
C
Disease Free Survival
NPM1 Mutated
NPM1 WT
Percent survival
Time (years)
D
NPM1
TP53
CDKN1A
PIDD1
CRADD
CASP2
Genetic Alteration
Missense Mutation (putative driver)
Missense Mutation (unknown significance)
Truncating Mutation (putative driver)
Amplification
Deep Deletion
mRNA Upregulation
mRNA Downregulation
No alterations
E
Merge with DAPI
GFP
γ-Tubulin
GFP-NPM1 WT
GFP-NPM1 Mutant No Centrosome Amplification
GFP-NPM1 Mutant With Centrosome Amplification
F
Centrioles per Cell
pEGFP
pEGFP-NPM1 WT
pEGFP-NPM1 Mutant
G
Percent of Cells with >4 Centrioles
pEGFP
pEGFP-NPM1 WT
pEGFP-NPM1 Mutant

Supplemental Figure 4-2

AKAP9 and PLK2 mutations do not correlate with worse outcomes.

(A) Oncoprint of AKAP9 alterations along with genes whose loss is permissive of proliferation in the setting of centrosome amplification (TP53, CDKN1A, PIDD1, CRADD, and CASP2). There is a lack of coincidence of AKAP9 mutation with loss of these other genes. (B) Kaplan Meier curves demonstrating overall survival and disease-free survival in stomach and uterine cancer patients (the tumor types with highest prevalence of AKAP9 mutations) with mutant AKAP9 versus wild type AKAP9. **(C)** Oncoprint of PLK2 alterations along with genes whose loss is permissive of proliferation in the setting of centrosome amplification (TP53, CDKN1A, PIDD1, CRADD, and CASP2). There is a lack of coincidence of AKAP9 mutation with loss of these other genes. **(D)** Kaplan Meier curves demonstrating overall survival and disease-free survival in stomach and renal clear cell carcinoma patients (the tumor types with highest prevalence of PLK2 mutations) with mutant PLK2 versus wild type PLK2.

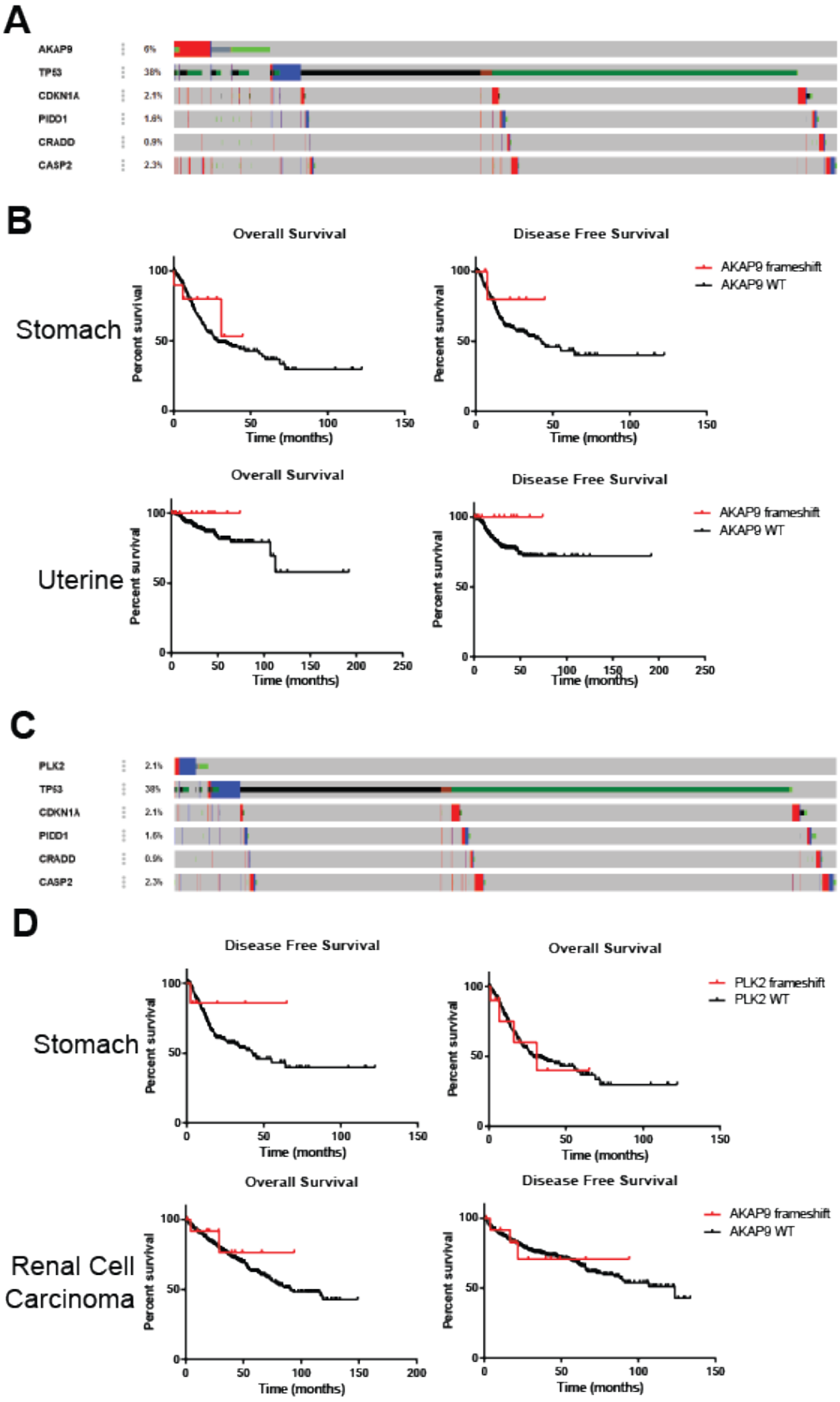
A
AKAP9
TP53
CDKN1A
PIDD1
CRADD
CASP2
B
Overall Survival
Disease Free Survival
Stomach
Uterine
Percent survival
Time (months)
AKAP9 frameshift
AKAP9 WT
C
PLK2
TP53
CDKN1A
PIDD1
CRADD
CASP2
D
Disease Free Survival
Overall Survival
Stomach
Renal Cell Carcinoma
Percent survival
Time (months)
PLK2 frameshift
PLK2 WT
AKAP9 frameshift
AKAP9 WT

Supplemental Figure 4-3

Investigation of alterations in PLK4 and its regulators.

(A) Mutation diagram and prevalence of genomic alterations in PLK4, the master regulator of centriole duplication. **(B)** Mutation diagram and prevalence of genomic alterations in SKP1, which helps degrade autophosphorylated PLK4. **(C)** Mutation diagram and prevalence of genomic alterations in CUL1, which helps degrade autophosphorylated PLK4. **(D)** Mutation diagram and prevalence of genomic alterations in BTRC, which helps degrade autophosphorylated PLK4. Green = mutations; red = amplifications; blue = deletions.

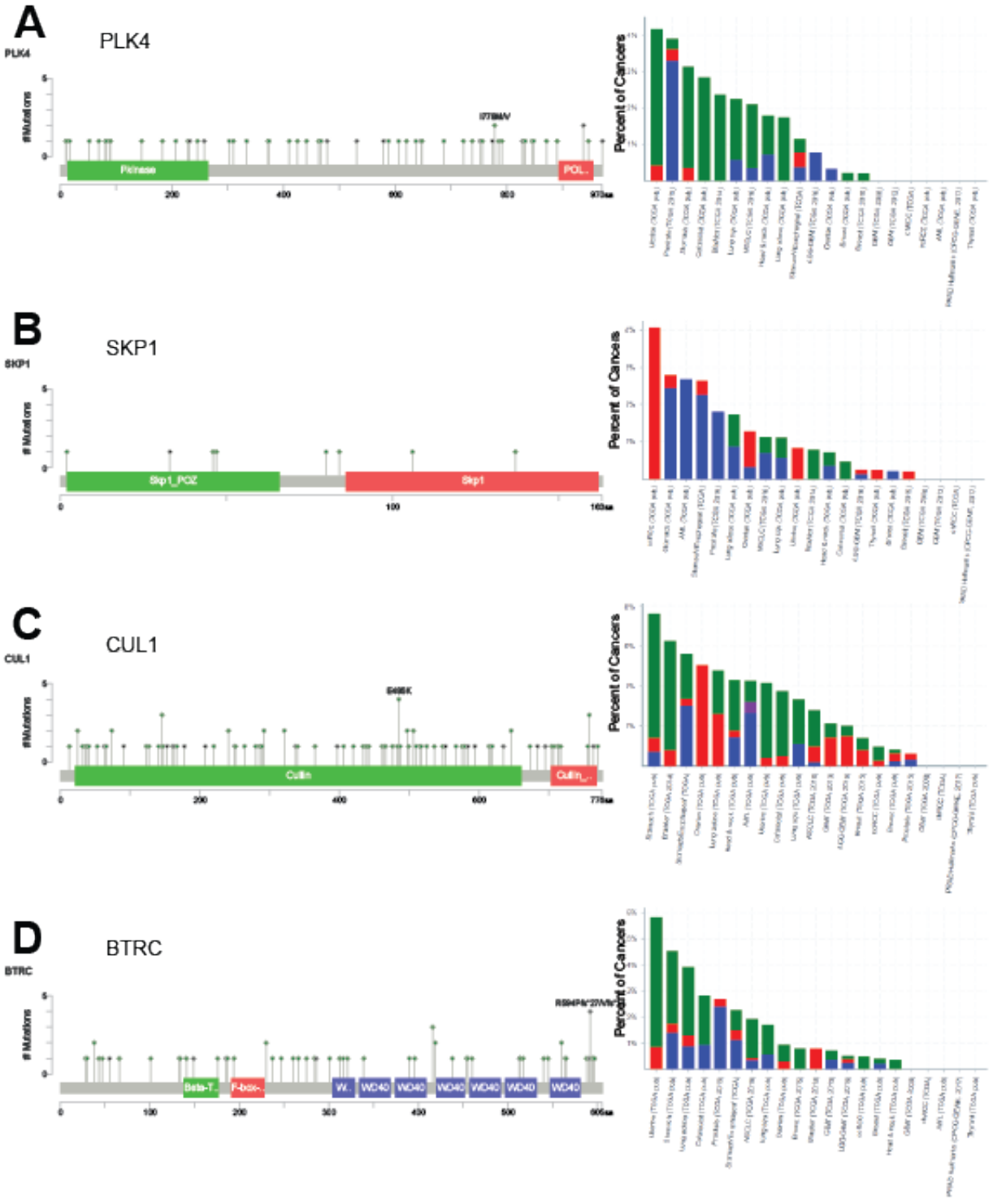
A
PLK4
PLK4
#Mutations
I778MV
Pkinase
POL...
Percent of Cancers
B
SKP1
SKP1
Mutations
Skp1_POZ
Skp1
Percent of Cancers
C
CUL1
CUL1
#Mutations
E466K
Cullin
Cullin_...
Percent of Cancers
D
BTRC
BTRC
Mutations
Beta-T...
F-box-...
W...
WD40
WD40
WD40
WD40
WD40
WD40
Percent of Cancers

Supplemental Figure 4-4

Prevalence of alterations in the top hypothesized drivers of centrosome amplification in human cancer.

Diagrammatic representations of the percent of tumors within each tumor site that harbor deletions (blue), amplifications (red), or mutations (green) in the indicated centrosome genes.

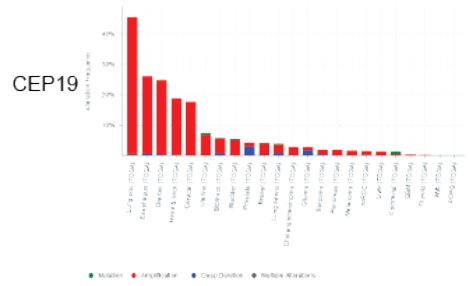
CEP19

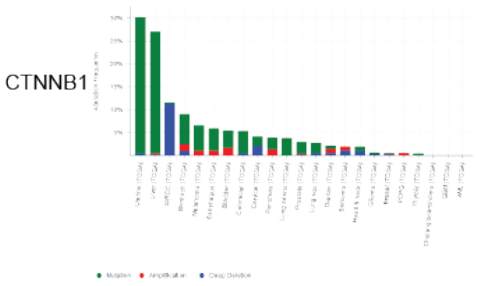
CTNNB1

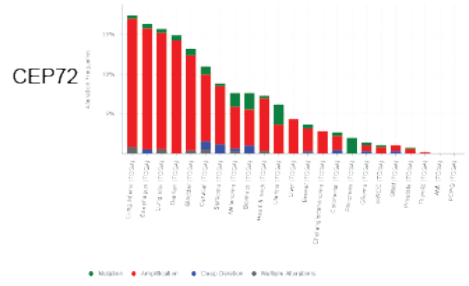
CEP72

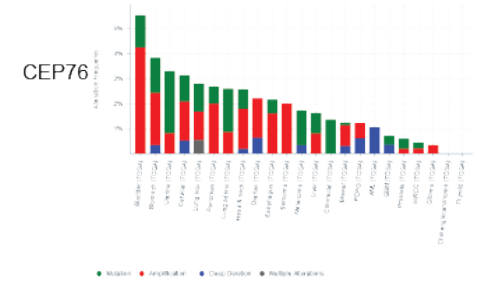
CEP76

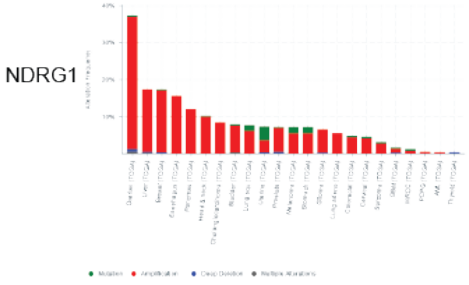
NDRG1

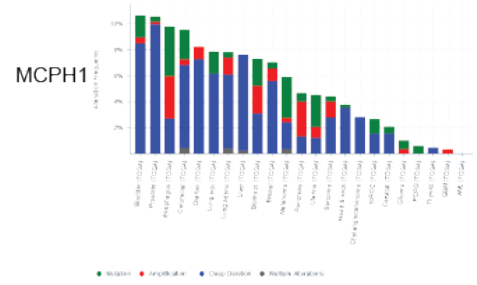
MCPH1

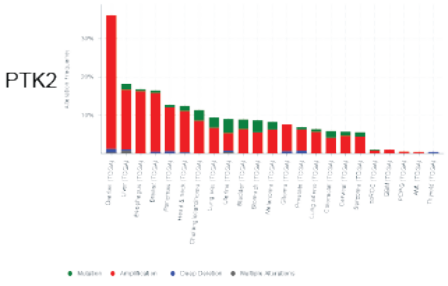
PTK2

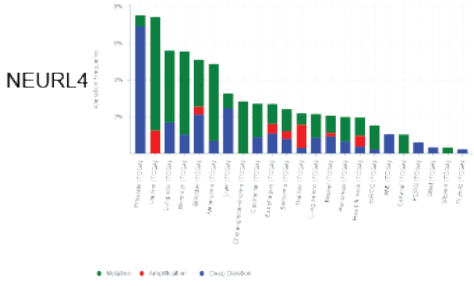
NEURL4

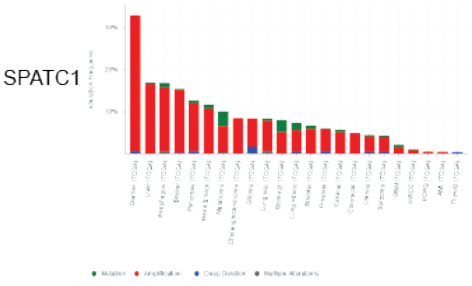
SPATC1

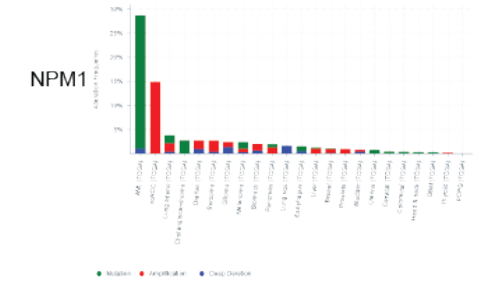
NPM1

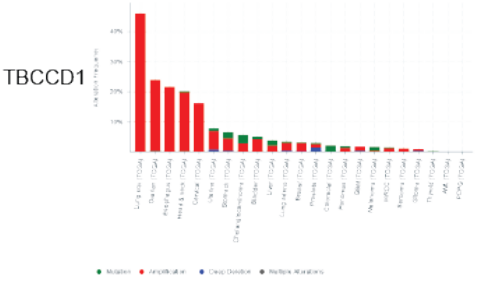
TBCCD1

Supplemental Figure 4-5

Coincidence of MCPH1 deletion with chromosome 8p deletions.

(A) Mutation diagram and prevalence of genomic alterations in cyclin D (CCND1). (**B)** Mutation diagram and prevalence of genomic alterations in cyclin E (CCNE1). **(C)** Mutation diagram and prevalence of genomic alterations in cyclin A (CCNA2).

A

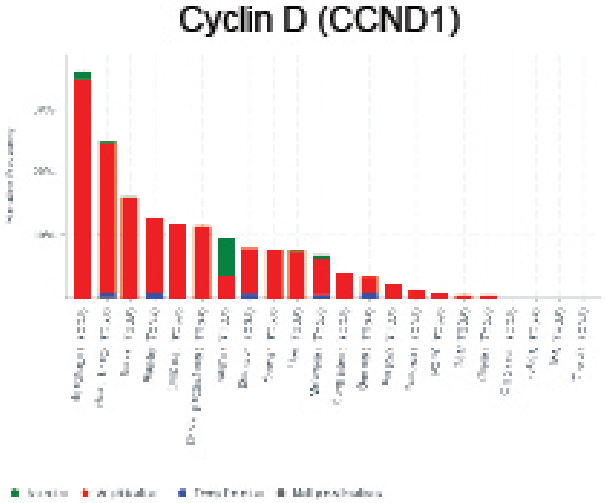

B

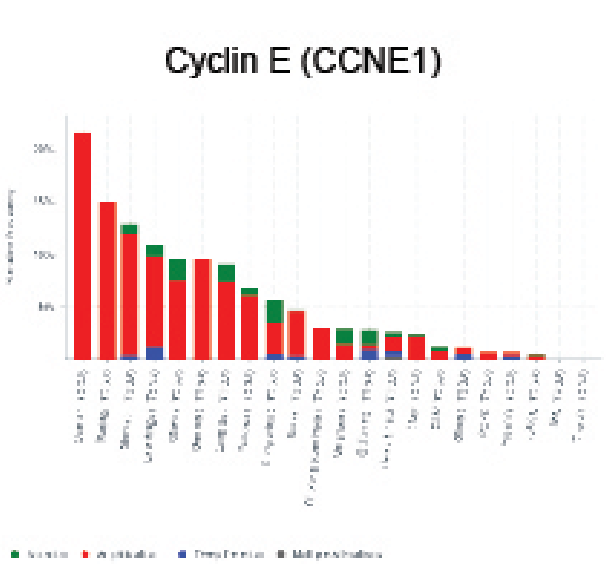

C

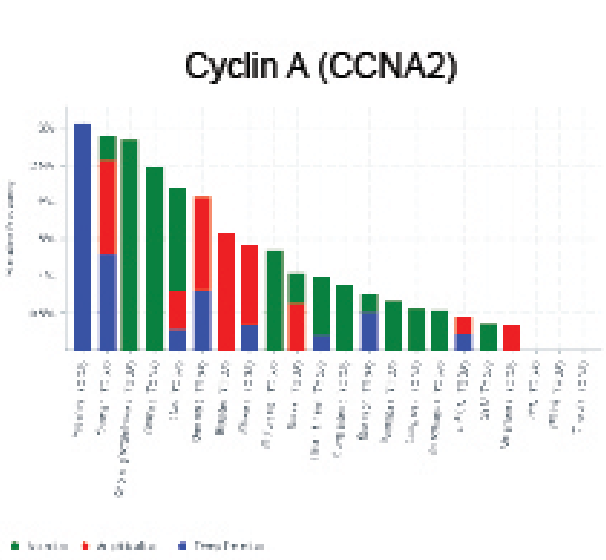

Acknowledgements

The authors thank Justin Jagodinsky (University of Wisconsin) for technical assistance; Jun Wan (University of Wisconsin), Beth Weaver (University of Wisconsin), Ben Park (Johns Hopkins University), Phoebus Lin and Hui Dai (MD Anderson) for reagents. Research reported in this publication was supported by the following NIH awards: F30CA203271, GM097245, T32GM008692, UL1TR000427, and TL1TR000429. The content is the responsibility of the authors and does not necessarily represent the views of the NIH.

CHAPTER 5: Consequences of centrosome abnormalities in human cancer

Work in this chapter is in preparation for submission:

An optimal number of centrosomes is required for diverse cellular functions

Ryan A. Denu, Stephanie M. Olson, Mark E. Burkard

Abstract

Centrosome amplification is a hallmark of cancer cells and correlates with poor outcomes**.** Despite this, downstream cellular signaling consequences of centrosome amplification are still widely unexplored; better understanding of these effects of centrosome amplification may reveal novel methods to selectively target cancer cells with centrosome amplification. Herein, through bioinformatic assessment of genomic alterations in human cancer, we posit that some cancer cells may lose centrioles, such as by deletion of SAS6. We therefore assessed the effects of both gain and loss of centrosomes on mitosis, migration, polarization, centriolar satellites, and nuclear structure. To model gain of centrosomes, we overexpressed polo-like kinase 4 (PLK4), an enzyme required for centriole duplication. To model loss of centrosomes, we utilized a chemical genetic approach to specifically inhibit PLK4. Using these cell models, we determined that both gain and loss of centrosomes reduce the efficiency of mitosis, migration, polarization, centriolar satellite organization, and maintenance of nuclear structure. These results suggest that there is an optimal number of centrosomes that enable the cell to carry out these processes.

Introduction

Centriole duplication is regulated by the conserved serine/threonine protein kinase Polo-like kinase 4 (PLK4), and PLK4 inhibition may represent a strategy for treating cancer [155-157]. Centrioles duplicate once per cell cycle due to autophosphorylation and subsequent degradation of PLK4. Loss of PLK4 causes loss of centrioles,[62,63] while overexpression of PLK4 causes centrosome amplification [126]. PLK4 knockout mice are lethal,[277,316] and inhibition of PLK4 results in cell cycle arrest.[157,275]

Centrosome amplification (CA) is a hallmark of cancer cells and increases chromosomal instability, high-grade phenotypes, and cellular invasiveness.[109,126,134,179,197] Centrosomes are the major microtubule organizing centers (MTOCs) in human cells and are involved in organizing the mitotic spindle and cytoskeleton, determining cell polarity, forming primary cilia formation, and migration. The centrosome consists of two orthogonally positioned centrioles surrounded by the pericentriolar material (PCM) protein complex. In dividing cells, centrioles duplicate once per cell cycle adjacent to preexisting centrioles. Errors in this process lead to the production of an abnormal centrosome number that can promote errors in spindle formation and subsequent chromosome missegregation and aneuploidy.[108,123,124,134,165,197] Understanding the causes and consequences of CA can help us identify therapeutic strategies.

There is also evidence that some cancers may lose centrioles. For example, some studies have demonstrated decreased PLK4 expression or loss of PLK4 alleles in certain cancers.[276,317-319] Furthermore, some tumor cells have pericentrin foci that lack centrioles;[108,109] however, it is possible that the centrioles were missed due to tissue sectioning artifact or problems with immunostaining. Therefore, it remains to be shown that some cancer cells lack centrioles.

Herein we manipulate PLK4 to be able to study cells with centrosome number ranging from 0 to many. We utilize a chemical genetic system to reversibly turn off PLK4 function in non-transformed human cells. Combining this chemical genetic system with a well-established model of centrosome amplification,[126] we studied the role of centrosomes, from zero to many, on mitosis and numerous microtubule-dependent signaling pathways. We find that an optimal number of centrosomes is required for maximum efficiency of many microtubule-dependent signaling pathways, such as migration, polarization, and nuclear integrity, and that gain or loss of centrosomes impedes these processes.

Results

Both gain and loss of centrioles occurs in human cancer

Centriole amplification is common in all types of human cancer.[107,109,208] Our previous analysis of centrosomes in nearly 400 primary human breast cancer specimens demonstrated that a greater percentage of centrosomes lacked centrioles in a subset of these cancers compared to benign breast specimens.[109] Therefore, we hypothesized that loss of centrioles also occurs in human cancer.

To assess potential genomic mechanisms leading to loss of centrioles in human cancer, we examined The Cancer Genome Atlas (TCGA) for the genes known to be required for centriole duplication in human cells. By and large, there is a relative dearth of mutations and alterations in the core components of the centriole duplication machinery, suggesting that cancer cells rely exquisitely on proper centriole duplication. However, we did observe a subset of patients with SAS6 deletions and frameshift mutations, which would be predicted to deplete centrioles, as SAS6 is a key structural component of the centriole and depletion/deletion decreases centriole number.[54,56,294] As it is known that cells without centrioles arrest unless they have lost p53, p21 (CDKN1A), 53BP1, or USP28,[294,320] we examined whether deletion or loss of function mutation of SAS6 coincided with loss of function of p53, p21, 53BP1, or USP28. We find that SAS6 mutation significantly co-occurs with TP53 (Bonferroni adjusted p value = 0.003) and TP53BP1 (Bonferroni adjusted p value = 0.027). This finding begs the question: why would losing centrioles be advantageous for cancer cells? Previous evidence suggests that loss of centrioles increases mitotic errors.[48] Therefore, we hypothesize that loss of centrioles generates CIN and aneuploidy, which we are common features of cancers and may enhance tumor

evolution.[321-323] We set out to validate this and find other potential advantages and/or vulnerabilities conferred by loss of centrioles.

Subsequently, we sought to use cell models of both gain and loss of centrioles to see how multiple centrosome- and microtubule-independent pathways are affected by gain and loss of centrioles. To model loss of centrioles, we engineered an analog sensitive (AS) cell line in immortalized, non-transformed RPE-1 cells (See Chapter 7 for more details and validation). This cell line possesses a point mutation at a conserved gatekeeper residue (L89G) that enlarges the ATP-binding pocket and allows the kinase to be selectively inhibited by the bulky ATP analogue 3-MB-PP1.[68] Exons 3-4 are deleted in the other genomic locus of PLK4, so the genotype of this cell line is *PLK4*$^{AS/\Delta}$. Treatment with 3-MB-PP1 causes loss of centrioles with multiple rounds of cell division (Supplemental Figure 5-1).

To model centriole amplification, we utilized RPE-1 and MCF10A cell lines with doxycycline-inducible PLK4; doxycycline treatment results in CA (Supplemental Figure 1), which has been reported in many human cancers and causes error-prone mitotic cell divisions, high-grade cellular phenotypes, and invasive properties.[126] Interestingly, cells with CA also demonstrated a proliferative defect (Supplemental Figure 5-1), which has been previously reported.[67,126]

Loss and amplification of centrosomes cause defects in mitotic spindle and chromosome segregation

Centrosomes organize the mitotic spindle apparatus to allow for proper chromosome segregation. However, it is unclear whether the presence of centrioles is required for proper mitosis, as entire organisms can thrive without centrioles.[36] Laser microablation of centrosomes

during prophase can still result in bipolar spindle formation, suggesting that cells can still form functional mitotic spindles without centrosomes;[324] however, another study using microsurgery to create acentriolar cells demonstrated that loss of centrioles impairs the fidelity of bipolar spindle assembly.[325] Furthermore, laser microablation of centrosomes during spindle formation has been shown to result in loss of astral microtubules.[326] Regarding CA, the presence of extra centrosomes increases the frequency of multipolar spindles and merotelic kinetochore attachments, both of which can cause chromosome missegregation and aneuploidy.[134,197]

To further probe the necessity of centrioles for proper mitosis, we analyzed spindle formation based on centriole number in the PLK4 AS cell line treated with 3-MB-PP1 versus DMSO. Only cells in metaphase and anaphase were assessed. In the DMSO control, nearly 80 percent of cells in metaphase or anaphase exhibited bipolar spindles with 2 centrioles at each pole (Figure 5-2A-B). In contrast, the cells treated with 3-MB-PP1 exhibited significant differences. Most notably, there was an increase in monopolar spindles (Figure 5-2A). Furthermore, there were many cells that formed bipolar spindles with 1 centriole at each pole. In addition, we assessed chromosome segregation defects. Cells with more or less than 2 centrioles at each pole demonstrated an increase in lagging chromosomes and chromosome bridges (Figure 5-2C). We also assessed astral microtubule formation in both metaphase and anaphase cells; astral microtubules are thought to be important for spindle pole and cleavage furrow positioning, and therefore whether or not a division will be symmetric or asymmetric.[327] There were no significant differences in astral microtubule formation in metaphase; however, spindle poles with more or less than 2 centrioles were less likely to form astral microtubules in anaphase (Figure 5-2D).

Centrosome loss and centrosome amplification inhibit polarity and migration

Centrosomes are thought to play a major role in establishing cell polarity, in part by controlling the organization of the microtubules that will determine cell shape and motility.[328] During cell polarization and migration, the Golgi and the centrosome orient toward the leading edge.[329] We assessed polarity in cells by staining for the Golgi at 3-hour intervals for a total of 9 hours after scratching a near-confluent layer of cells. Cells without centrosomes and cells with supernumerary centrosomes demonstrated a delay in polarization, as they showed less recovery at earlier time points compared to controls (Figure 5-3A-B). This suggests that an optimal number of centrosomes is required for maximum polarization efficiency.

A similar scratch assay was performed to assess migration. Cells without centrosomes migrated more slowly compared to controls (Figure 5-3C). Additionally, cells with CA also migrated more slowly (Figure 5-3C).

Loss of centrioles results in PCM fragmentation and disrupts centriole satellite integrity

Interestingly, we noticed that a large fraction of cells without centrioles displayed scattered pericentrin, suggesting PCM fragmentation (Supplemental Figure 5-2A-B). This is similar to the PCM fragmentation that has been reported in cancer as a potential mechanism of CA.[109,131,140] Previous studies have also demonstrated that some spindle poles in cancer cell lines lack centrioles, assessed by both immunofluorescence and electron microscopy.[140] This suggests that PCM fragmentation is caused by loss of centrioles or PLK4 activity. More broadly, we propose that errors in duplicating centrosomes, whether genetic or stochastic, are responsible for PCM fragmentation. This is further supported by past findings that loss of centrioles by treatment with anti-polyglutamylation antibody results in PCM scattering.[330]

We next asked whether this observed PCM scattering corresponded with centriolar satellite formation. Centriolar satellites are electron-dense regions outside the centrosome that regulate microtubule organization, ciliogenesis, Previous reports have suggested that centriole splitting caused by loss of the centrosomal linker c-Nap1 reduced centriolar satellite density.[331] Interestingly, both loss and gain of centrosomes resulted in centriolar satellite dispersion, as assessed by PCM1 staining (Figure 5-4). We conclude that properly regulated centriole number is important for the integrity and organization of centriolar satellites.

Centrosome loss and centrosome amplification disrupt nuclear structure

In many non-polarized cells, such as interphase fibroblasts, the centrosome is located near the cell center and is physically linked to the nucleus, with microtubules radiating out to the cell cortex.[328] It has previously been observed that loss of PLK4 can result in multi-lobed and other pleomorphic nuclei, presumably due to error-prone mitotic cell divisions.[275] Here we observed an increase in the number of pleomorphic nuclei in interphase cells with loss of centrosomes. This was quantified in two different ways: nuclear circularity (Figure 5-5B) and pleomorphic index (Figure 5-5C). Further, we find a trend toward the coincidence in time of centriole disappearance and pleomorphic nuclei appearance (Figure 5-5D).

Next we sought to identify the mechanism by which gain and loss of centrioles leads to pleomorphic nuclei. We tested the following hypotheses: (1) gain and loss of centrioles disrupts interactions between the nuclear lamina and the cytoplasmic microtubule cytoskeleton; (2) aberrant mitosis in cells with gain or loss of centrioles results in pleomorphic nuclei. To test the first hypothesis, we further examined the interaction between lamins and the cytoplasmic microtubule cytoskeleton. Lamins attach to SUN proteins on the inner nuclear membrane, which

interact with KASH proteins on the outer nuclear membrane, which in turn connect to the actin and tubulin cytoskeletons in the cytoplasm.[332] Lamins position nuclear pores and centrosomes, and depletion of lamins disrupts nuclear pore complex organization.[333] We hypothesized that loss or gain of centrosomes would have similar effects on nuclear pore organization. We assessed nuclear pores by Mab414 staining and classification into asymmetric, clustered, or even (Figure 5-5E). Interestingly, we observed altered nuclear pore organization with both gain and loss of centrosomes (Figure 5-5F). Next, we asked whether the lamins are altered with gain and loss of centrioles. By lamin immunofluorescence, we observe altered lamin structure, similar to that seen in cells from progeria patients (Figure 5-5G); progeria is caused by a mutation in lamin A/C. However, we do not see changes in lamin splicing, as seen in progeria cells (Figure 5-5J).

To test the second hypothesis (pleomorphic nuclei depend on aberrant mitosis), we assessed nuclear circularity after arrest in G1 using aphidicolin (Figure 5-5H). We observe no significant decrease in pleomorphic nuclei with aphidicolin treatment (Figure 5-5I), suggesting that the pleomorphic nuclei are not entirely dependent on aberrant mitosis.

Lastly, to assess whether or not the pleomorphic nuclei depend on disrupted microtubule organizations seen with loss or gain of centrioles, we treated cells with nocodazole and taxol to depolymerize or stabilize microtubules, respectively (Figure 5-5K), and quantified nucleus circularity. In cells with normal numbers of centrosomes (i.e. 1-2), we observe a significant decrease in nucleus circularity with nocodazole and taxol; however, cells with loss or gain of centrioles do not demonstrate a significant decrease (Figure 5-5L-M). We conclude that loss and gain of centrioles disrupts microtubule networks, which disrupts the physical connections between the microtubule cytoskeleton and nuclear lamina, leading to impaired lamin architecture.

Discussion

Herein, we posit that both gain (CA) and loss of centrioles occurs in human cancer. Using a combination of chemical genetics and inducible overexpression models, we determined the effects of gain and loss of centrioles on numerous signaling pathways. Our results support the conclusion that an optimal number of centrosomes (i.e. 1-2) is required for optimal efficiency of many cellular processes, such as mitosis, migration, polarization, centriolar satellite organization, and nuclear structure. A number of studies have cast doubt on the necessity of centrosomes with centrioles for numerous cellular functions, which has been well reviewed.[37] Regarding mitosis, it appears that centrioles are not universally required. Several cell types divide without centrioles, with the classic examples being those of higher plants and oocytes,[38] the planarian flatworm *Schmidtea mediterranea,*[39] and *Myxozoa.*[40] Additionally, genetically engineered *Drosophila* lines without centrioles are able to develop with near normal timing into morphologically normal adults,[36,41] and the first few divisions of a mouse embryo use MTOCs that lack centrioles.[42] However, other cells depend on centrioles for accurate cell division, such as embryos, neural progenitor cells, and spermatocytes from a variety of species.[38,43,44] In humans, inherited mutations in several centrosome proteins cause microcephaly,[45,46] suggesting that neural progenitor cell divisions are particularly dependent on centrioles.[47] Further evidence from human cells suggest that loss of centrioles causes chromosomal instability and aneuploidy.[48] Our data confirm this finding and demonstrate that both gain and loss of centrioles. We propose that loss of centrioles, such as by SAS6 mutation or deletion, may be advantageous to some tumors, as it may increase CIN and drive tumor evolution and resistance to therapy. Further evidence will be required to ascertain the claim that some cancers exist without centrioles.

With regard to other cellular processes, centrosomes are not entirely dispensable, as they have been shown to be important for primary cilia formation and neural development.[33-35] The aforementioned *Drosophila* without centrioles cannot make cilia or flagella and die shortly after birth because their sensory neurons lack cilia.[36] There are also defects in cilia formation with amplification of centrosomes, as some have shown that CA prevents cilia formation,[334] while others have shown that supernumerary centrosomes nucleate extra cilia and compromise primary cilium signaling.[35,125]

Human cells without centrioles exhibit a cell cycle arrest, as many have shown using diverse methods, such as microsurgical removal,[335] laser ablation,[326,336] auxin-inducible degradation of PLK4,[275] inhibition of a genetically-engineered analog-sensitive PLK4,[64] and treatment with a PLK4-specific inhibitor.[157] This arrest is mediated by p53, the p53-binding protein 53BP1, the deubiquitinase USP28, and the ubiquitin ligase TRIM37.[294,320,337]

PCM fragmentation seen with loss of centrioles is similar to what we see in human cancer [109]. This suggests one mechanism of PCM fragmentation is failed centriole duplication. This is consistent with previous reports that centrioles help recruit PCM.[275,330,338,339] There is other evidence to support these claims. For example, injection of HeLa cells with anti-polyglutamylation antibody (GT335) resulted in centrosome fragmentation,[330,340] suggesting that centrioles help to resist forces applied to the centrosome.[328] Furthermore, there are reports of abnormal centrioles in human cancer cells due to insufficient PLK4, and the expression of exogenous PLK4 eliminates these abnormal centrioles.[341] Additional studies have demonstrated decreased PLK4 expression or loss of PLK4 alleles in certain cancers,[276,317-319] and some tumor cells have pericentrin foci that lack centrioles.[108]

Cell migration is an immensely complex cellular process. To migrate directionally, cells need to coordinate signaling pathways to control polarity and cytoskeleton rearrangements to generate forces required for directional movement. There have been conflicting reports of the role of centrosomes and PLK4 on migration. $Plk4^{+/-}$ MEFs demonstrated impaired motility, and overexpressing Plk4 in these cells caused more protrusions and spreading.[342] Similarly, depleting PLK4 in the MDA-MB-231 breast cancer line suppressed invasion.[342] Another study of laser ablation of centrosomes revealed that loss of centrosomes impaired cell polarization.[343] However, another study demonstrated that laser ablation of centrosomes did not affect directional cell migration, but did affect migration and protrusion formation after nocodazole washout.[344] Our data support the conclusion that centrosomes are required for efficient cell migration.

With regard to the effects of CA on migration, there have been contradictory reports. Some evidence suggests that CA makes cells more migratory and invasive; CA caused by PLK4 overexpression increased invasiveness and migration in MCF10A cells, and inhibiting Rac reversed this effect.[121,126] However, some reports have suggested the opposite, reporting that CA in tumor-derived endothelial cells and overexpression of PLK4 or Cdc14B knockdown in HUVECs decreased migration.[345] Perhaps CA is associated with increased dynamic centrosome movements during interphase, and that these movements may prevent normal directional migration.[345] Furthermore, ablation of supernumerary centrosomes restored centrosome dynamics and endothelial cell migration. Our data supports the latter conclusion: CA inhibits migration. Similarly, we found that CA inhibits cell polarization. Disruption of cell polarity is a hallmark of cancer, and CA may represent one mechanism leading to disrupted cell polarity in human cancer.

Pathologists have long used nuclear shape as a diagnostic tool to distinguish a normal cell from a cancer cell, and we use this on the Papanicolaou test. Many studies have hinted at the role of centrosomes in maintaining nuclear integrity. Interactions between SUN and KASH proteins on the nuclear membranes link the nucleus to cytoskeleton.[332] We demonstrate that both gain and loss of centrosomes result in pleomorphic nuclei, suggesting that centrosome-mediated microtubule nucleation and organization and required for proper nuclear structure. This is consistent with reports that paclitaxel treatment results in pleomorphic nuclei.[346] Further work will be necessary to determine the functional consequence of pleomorphic nuclei in the setting of gain and loss of centrosomes. An intact nuclear lamina is important for DNA replication, regulation of transcription, and conferring stiffness to the nucleus. Future work will assess the effects of gain and loss of centrioles on these three functions. Since CA has been shown to cause increased cellular invasiveness, it is tempting to speculate that CA-induced pleomorphic nuclei allow greater nuclear and cellular flexibility as cells migrate through tight spaces. Therefore, CA-induced pleomorphic nuclei could be a mechanism explaining the potentially increased invasiveness of cells with CA.

In conclusion, our results indicate that an optimal number of centrosomes is required for maximum efficiency of a diverse collection of cellular signaling pathways, and that gain or loss of centrosomes decreases the efficiency of these pathways.

Materials and Methods

Cell Culture

PLK4 analog sensitive (AS) cells were generated as previously described. Gene editing was performed using adeno-associated virus (AAV) in RPE-1 (ATCC, Manassas, VA) an immortalized, non-transformed human epithelial cell line. A targeting vector was made by inserting a neo cassette surrounded by FRT sites in the intron upstream of exons 3-4 of PLK4, all flanked by loxP sites. To generate adenovirus producing this targeting vector, HEK293 cells were transfected with pRC and pHelper. RPE-1 cells were infected with adenovirus collected from the supernatant and subcloned in the presence of G418 (0.4 μg/mL). Clones were screened by PCR, transfected with pFLIPe to remove the neo cassette, and subcloned. Clones were screened for sensitivity to G418 to isolate a WT^{flox}/WT cell line. This cell line was targeted in two ways: (1) to make a conditional knockout cell line; and (2) to make an analog sensitive cell line. To make the conditional knockout cell line, one copy of PLK4 was deleted by treating with Cre, then cells were re-targeted with the same initial vector (neo cassette, exons 3-4, all flanked by loxP sites), resulting in a WT^{flox}/Δ cell line. To make the analog sensitive cell line, cells were targeted with a vector derived from the same initial targeting vector, but the gatekeeper residue was mutated to a glycine (L89G) to enlarge the ATP binding pocket and genetically encode chemical sensitivity to the bulky ATP analog 3-MB-PP1.[68] The resulting AS^{flox}/WT^{flox} cell lines were treated with Cre and subcloned in the presence G418. Clones were screened by PCR with primers both inside and outside the neo cassette. Procedures for preparation of infectious AAV particles, transduction of RPE-1 cells, and isolation of properly targeted clones was performed as described previously.[347,348]

All cell lines were propagated at 37 °C in 5% CO_2. RPE-1-derived cell lines were grown in a 1:1 mixture of DMEM and Ham's F-12 medium supplemented with 2.5 mm l-glutamine, with 10% fetal bovine serum and 100 units/mL penicillin-streptomycin. MCF10A-derived cell lines (ATCC) were grown in 1:1 DMEM and Ham's F-12 medium supplemented with 2.5 mm l-glutamine, 5% horse serum, EGF, hydrocortisone, and cholera toxin. HeLa cells were grown in high glucose DMEM with 10% fetal bovine serum and 100 units/mL penicillin-streptomycin. Human primary dermal fibroblast cell lines were obtained from The Progeria Research Foundation (PRF) Cell and Tissue Bank. The HGPS cell lines were HGADFN167; the control lines were HGADFN168.

For stable retroviral transduction, constructs were co-transfected with the pVSV-G envelope plasmid into Phoenix cells. Fresh medium was applied at 24 hours post-transfection, harvested 24 hours later, clarified by centrifugation and filtration through a 0.45 μm membrane to remove cell debris, and diluted 1:1 with complete medium containing 10 μg/mL polybrene. Target cells were infected at 40-60% confluence for 24 hours. Polyclonal transductants were further subcloned by limiting dilution to obtain individual clones.

Chemicals used in this study include aphidicolin (5 μM, Sigma), monastrol (100 μM; Tocris), nocodazole (0.2 mg/mL; EMD Biosciences), 3-MB-PP1 (10 μM, Toronto Research Chemicals), doxycycline (2 μg/mL, Fisher), and centrinone B (300nM, Tocris).

Immunofluorescence (IF) and Microscopy

IF and imaging were carried out as previously described.[194,195] Cells were seeded on glass coverslips in 24-well plates and fixed with 100% ice-cold methanol for 30 minutes, 4% paraformaldehyde in PBS for 15 minutes, or 10% trichloroacetic acid (TCA) for 15 minutes.

Fixed cells were then blocked for 30 minutes in 3% bovine serum albumin (BSA) and 0.1% triton X-100 in PBS (PBSTx + BSA). Primary antibodies were incubated in PBSTx + BSA for 1 hour at room temperature and washed three times in PBSTx, followed by secondary antibody incubation in PBSTx + BSA for 30 minutes at room temperature and two washes with PBSTx. Cells were counterstained with DAPI and mounted on glass slides with Prolong Gold antifade medium (Invitrogen).

Primary antibodies used were: alpha tubulin (Abcam, ab4074, 1:5000), pericentrin (Abcam, ab4448, 1:1000), polyglutamylated tubulin (Adipogen, AG-20B-0020, 1:500), GM130 (BD Biosciences, 610822, kindly provided by Dr. Beth Weaver, 1:1000), centrin (Millipore, 04-1624, 1:500), γ-tubulin (Abcam, ab27074, 1:500), β-actin (Abcam, ab6276, 1:5000), Mab414 (Kindly provided by Dr. Beth Weaver, 1:1000). Alexa Fluor-conjugated secondary antibodies were used at 1:350 (Invitrogen).

Image acquisition was performed on a Nikon Eclipse Ti inverted microscope equipped with 10x, 20x, 40x, and 100x objectives; a temperature-controlled motorized stage with 5% CO_2 support (In Vivo Scientific); and CoolSNAP HQ2 charge-coupled device camera (Photometrics). Optical sections were taken at 0.2-μm intervals and deconvolved using Nikon Elements. Where appropriate, the observer was blinded to treatment condition during image acquisition and analysis. Images were processed and analyzed using Nikon Elements.

Immunoblotting

Cells were incubated for 30 minutes on ice in lysis buffer (50 mm HEPES, pH 7.5, 100 mm NaCl, 0.5% Nonidet P-40, 10% glycerol) containing phosphatase inhibitors (10 mm sodium pyrophosphate, 5 mm β-glycerol phosphate, 50 mm NaF, 0.3 mm Na_3VO_4), 1 mm PMSF, 1X

protease inhibitor mixture (Thermo Scientific), and 1 mm dithiothreitol. Proteins were separated by SDS-PAGE, transferred to Immobilon PVDF membrane (Millipore), and blocked for 30 minutes in 4% milk in tris-buffered saline, pH 7.4. Membranes were incubated 1 hour at room temperature with primary antibodies diluted in TBST + 5% milk, washed three times with TBST, and incubated for 1 hour at room temperature in secondary antibodies conjugated to horseradish peroxidase (Jackson) in TBST + 5% milk. Membranes were washed and developed with luminol/peroxide (Millipore) and visualized with film. Primary antibodies used in this study include: lamin A/C (MANLAC1/4A7, deposited to the DSHB by Morris, G.E.), actin (JLA20, deposited to the DSHB by Lin, J. J.-C.).

Migration and polarization

Cells were grown to confluency and scratched with a 200 μL pipette tip. For migration assessment, wound width was assessed at various time points. For polarization assessment, cells were fixed at various time points after the scratch. Polarization was assessed based on the location of Golgi (determined by GM130 staining) relative to the wound. A cell was deemed “polarized” if more than half of the Golgi was located in the radial third of the cell facing the wound. Cells were fixed at 3-hour intervals post-wound (0–9 hours) and probed for GM130, pericentrin, tubulin, and co-stained with DAPI.

Flow cytometry

Cell pellets were fixed in cold 70% EtOH for at least 24 hours, washed once in PBS, and resuspended in PBS with 0.5 mg/mL RNase A and 50 mg/mL propidium iodide. Samples were incubated at 4° C overnight and analyzed on a flow cytometer (FACSCalibur; BD).

Statistics

Statistical evaluations were performed using Graphpad Prism (Graphpad Software, San Diego, CA) or Microsoft Excel (Office 2011, Microsoft). Two-tailed t-tests and one-way ANOVA were used for comparisons. P-values <0.05 were considered significant for all tests, and designations are made in the figures for statistical significance.

Figure 5-1

Loss of centrioles occurs in human cancer.

(A) Diagram of the most frequent alterations in SAS6 in human cancer using the TCGA data sets and cBioPortal to query the data. **(B)** The top diagram of the mutations in SAS6 occuring in the TCGA data sets. The bottom diagram shows just the SAS6 frameshift mutations. **(C)** Coincidence of SAS6 alterations with alterations required for the cell to proliferate without centrioles (loss of TP53, CDKN1A, TP53BP1, or USP28).

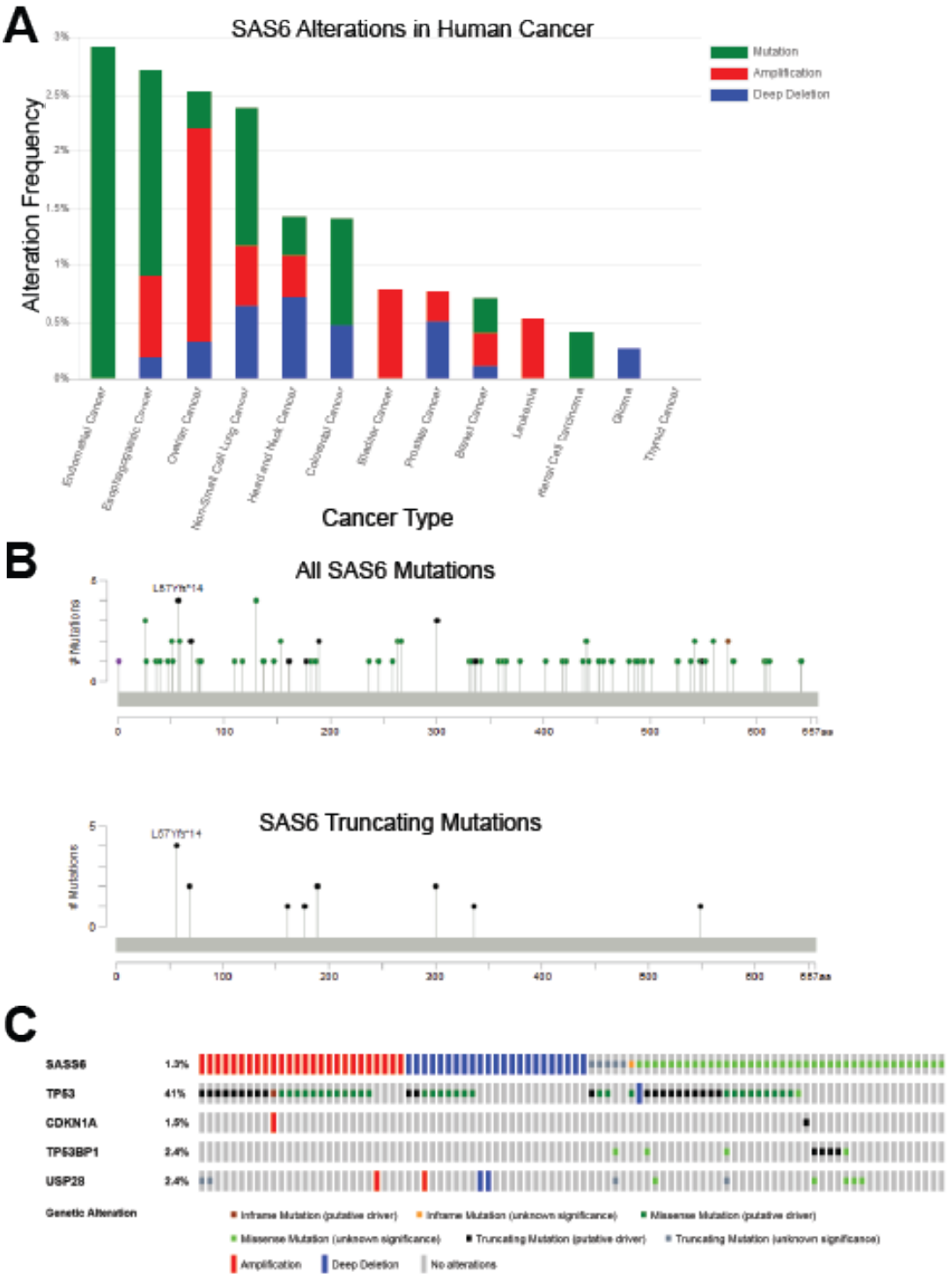
A
SAS6 Alterations in Human Cancer
Mutation
Amplification
Deep Deletion
Alteration Frequency
3%
2.5%
2%
1.5%
1%
0.5%
0%
Endometrial Cancer
Esophagogastric Cancer
Ovarian Cancer
Non-Small Cell Lung Cancer
Head and Neck Cancer
Colorectal Cancer
Bladder Cancer
Prostate Cancer
Breast Cancer
Leukemia
Renal Cell Carcinoma
Glioma
Thyroid Cancer
Cancer Type
B
All SAS6 Mutations
L67Yfs*14
Mutations
0
100
200
300
400
500
600
657aa
SAS6 Truncating Mutations
L67Yfs*14
Mutations
5
0
100
200
300
400
500
600
657aa
C
SASS6
1.3%
TP53
41%
CDKN1A
1.5%
TP53BP1
2.4%
USP28
2.4%
Genetic Alteration
Inframe Mutation (putative driver)
Inframe Mutation (unknown significance)
Missense Mutation (putative driver)
Missense Mutation (unknown significance)
Truncating Mutation (putative driver)
Truncating Mutation (unknown significance)
Amplification
Deep Deletion
No alterations

Figure 5-2

Loss and gain of centrioles impair mitosis.

(A) Cells were treated with 10 μM 3-MB-PP1 for 5 days and fixed, probed for alpha-tubulin, pericentrin, and centrin. The spindles of mitotic cells were assessed and categorized as either monopolar, bipolar, or multipolar. For bipolar cells, we further assessed how many centrioles were found in each pole. **(B)** Representative images from the cells described in A. **(C)** Lagging chromosomes and chromosome bridges were assessed in cells in anaphase. Only cells with bipolar or pseudo-bipolar spindles were included. Bars represent the average of at least 25 cells in each of 3 independent experiments ± SEM. Representative images of lagging chromosomes and chromosome bridges are shown on the right. Scale bar = 5 μm. **(D)** Astral microtubule formation was assessed in cells in both metaphase and anaphase. Representative images are shown on the right, demonstrating a robust aster at the pole with centrioles but minimal aster at the pole without centrioles. Scale bar = 5 μm. **(E)** To assess for the dependence of PLK4 activity on cytokinesis, cells were arrested in mitosis with nocodazole, then a mitotic shake off was performed. Cells were washed, then with new media containing either DMSO or 3-MB-PP1. Cells were fixed 12 hours later, probed for actin (red) and stained with DAPI (blue), and the percent of binucleate cells was assessed. Representative images of uninucleate versus binucleate cells are shown adjacent to the graph. Blue = DNA, red = actin, scale bar = 5 μm. **(F)** The effects of PLK4 activity on cytokinesis were also assessed by staining or RhoA following fixation with TCA. The bar graph demonstrates the percent of cells in cytokinesis (determined by anillin localization at the cleavage furrow) that demonstrate RhoA localization to the cleavage furrow. Representative images are shown to the right of the bar graph. Blue = DAPI, green = anillin, red = RhoA, scale bars = 5 μm.

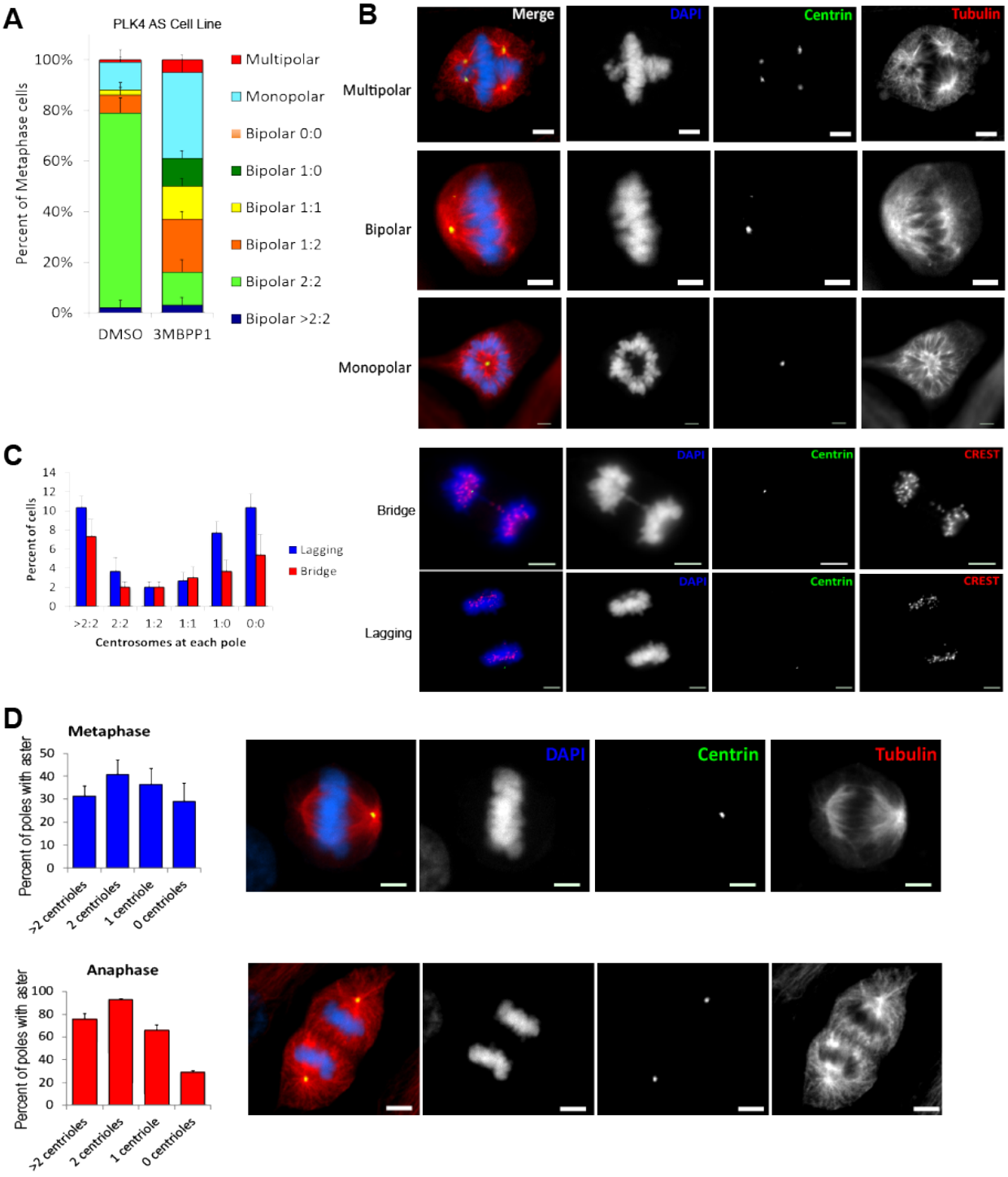
A
PLK4 AS Cell Line
Percent of Metaphase cells
100%
80%
60%
40%
20%
0%
DMSO
3MBPP1
Multipolar
Monopolar
Bipolar 0:0
Bipolar 1:0
Bipolar 1:1
Bipolar 1:2
Bipolar 2:2
Bipolar >2:2
B
Merge
DAPI
Centrin
Tubulin
Multipolar
Bipolar
Monopolar
C
Percent of cells
Centrosomes at each pole
>2:2
2:2
1:2
1:1
1:0
0:0
Lagging
Bridge
CREST
D
Metaphase
Percent of poles with aster
>2 centrioles
2 centrioles
1 centriole
0 centrioles
Anaphase

Figure 5-3

Loss and gain of centrioles impair migration and polarization.

(A) To assess for polarity, cells were grown to near confluency in 24-well plates, scratched, and fixed at different time points after the scratch. Cells were fixed and probed for pericentrin (green) and GM130 (red), a cis-Golgi marker whose orientation can be used to assess the polarity of the cell. **(B)** Quantification of polarized cells based on centrosome number. Dots represent averages ± SEM for 3 independent experiments. **(C)** For assessing migration, cells were grown to near confluency in 24-well plates, scratched, and wound length was assessed in at least 3 areas of 3 wells for each condition. Representative brightfield images of the scratch assay are shown. Scale bars = 100 µm. Quantification of wound length at the indicated time points is shown in the graphs on the right. Dots represent averages ± SEM for 3 independent experiments.

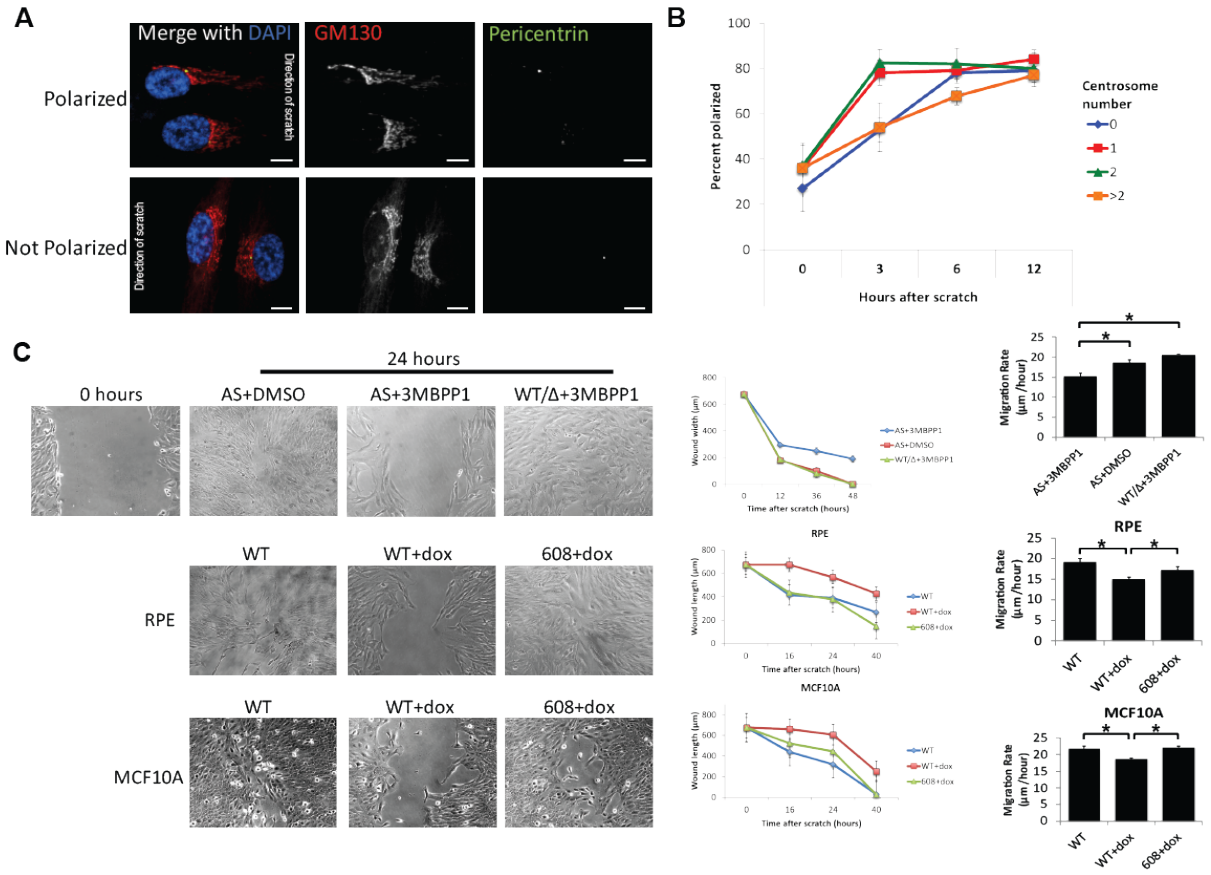

Figure 5-4

Loss and gain of centrioles disrupts centriolar satellite organization.

(A) Representative micrographs of centriolar satellites (PCM1, red) in cells with the indicated numbers of centrosomes. **(B)** Quantification of centriolar satellite dispersal by calculating the percentage of PCM intensity within a 2.5 radius of the center of the centrosome. Bars represent means ±SD.

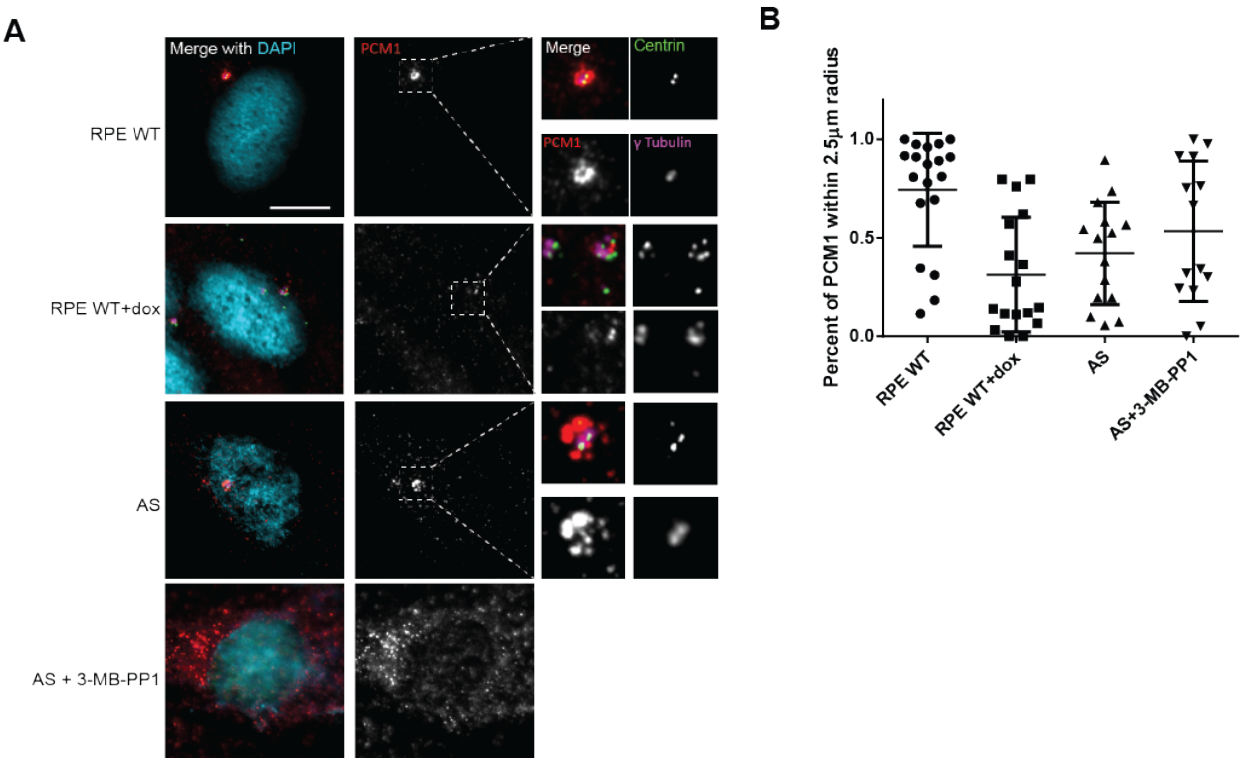

Figure 5-5

Loss and gain of centrioles causes nuclear pleomorphisms.

(A) Representative images of pleomorphic nuclei seen in cells with gain and loss of centrosomes. Scale bars = 5 μm. The bar graph on the right shows the percentage of cells with pleomorphic nuclei based on centrosome number. **(B)** Pleomorphic index was calculated by drawing a regular circle/oval around the perimeter of the nucleus (green circle on micrographs), drawing the actual shape of the nucleus (red circle on micrographs), and calculating the percentage of the nucleus that falls inside the (area of red divided by area of green). Higher values indicate a greater degree of pleomorphism. **(C)** Loss of centrosomes coincides with the appearance of pleomorphic nuclei in the AS cell line. **(D)** To assess whether the appearance of pleomorphic nuclei in the CA cell lines is due to aberrant mitoses, cells were first arrested for 16 hours with aphidicolin, then 2 μg/mL doxycycline was added. The percent of cells with pleomorphic nuclei was analyzed 24 hours later. **(E)** To further probe nuclear structure, nuclear pores were analyzed by staining with Mab414 and classification into 3 categories: symmetric, asymmetric, and clustered. Representative images of these 3 categories are shown. **(F)** Quantification of the 3 categories based on centrosome number. **(G)** Representative images of nuclear pleomorphisms by lamin staining. Fibroblast derived from a progeria patient are shown as a control, as progeria is caused by a mutation in lamin A/C; a fibroblast from the patient's healthy parent is shown as a control. **(H)** Cells were arrested in G1 using aphidicolin. Representative histograms from propidium iodide-stained cells are shown. **(I)** Quantification of nucleus circularity before and after aphidicolin. **(J)** Lamin A/C immunoblotting to assess for altered lamin splicing, as is seen in progeria. **(K)** Representative micrographs of RPE cells treated with nocodazole and taxol to depolymerize or stabilize microtubules, respectively. **(L)** Quantification of nucleus circularity

with and without nocodazole treatment. **(M)** Quantification of nucleus circularity with and without taxol treatment. Bars represent averages of 3 independent experiments of at least 100 cells each ± SEM.

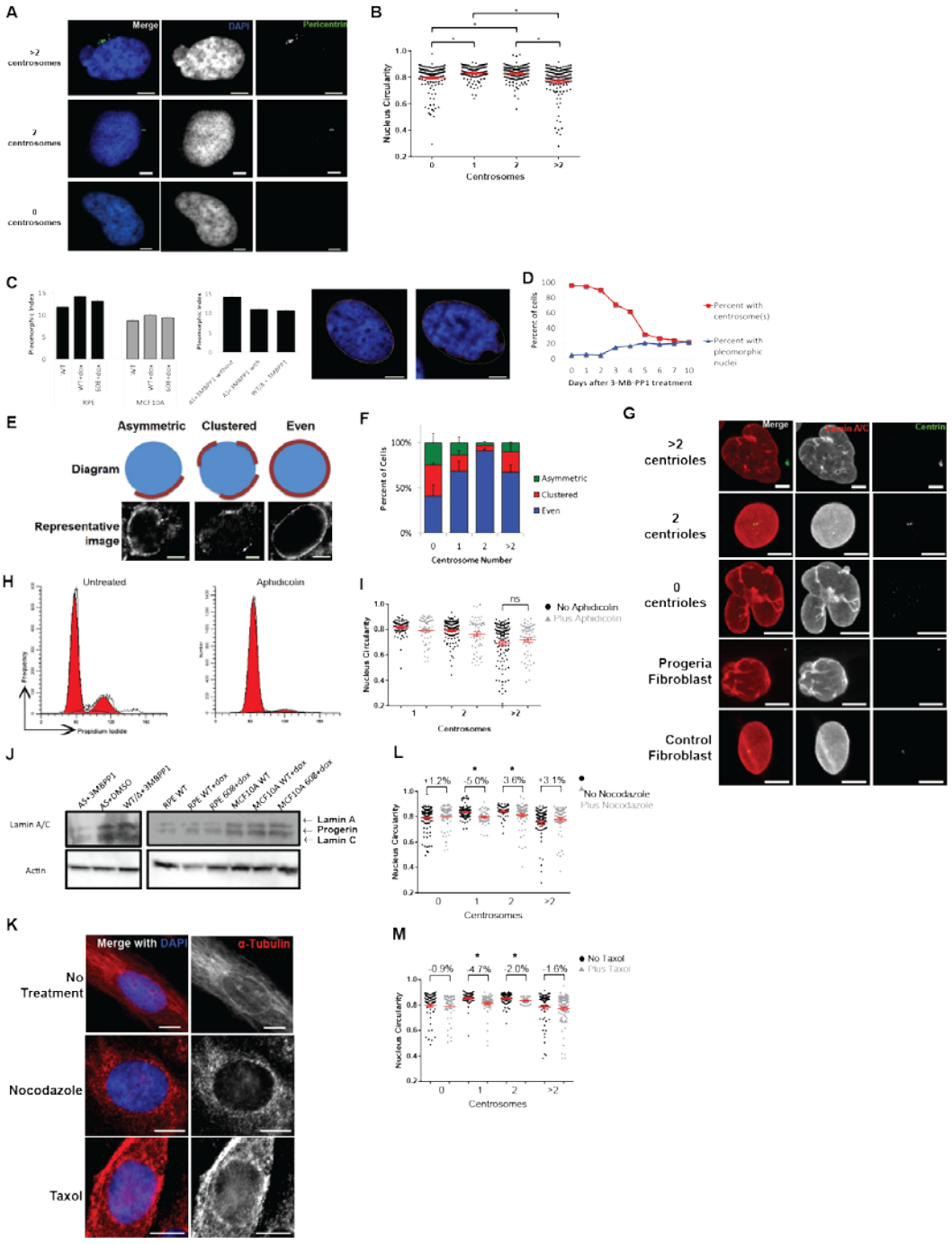

Supplemental Figure 5-1

Validation of RPE1 and MCF10A doxycycline-inducible PLK4 cell lines to model centrosome amplification.

(A) Representative images of centrosome amplification in RPE and MCF10A cell lines. Blue=DNA/DAPI, green=pericentrin, scale bar = 5 μm. **(B)** Quantification of centrosome number after 48 hours of treatment with 2 μg/mL doxycycline. **(C)** Proliferation was assessed by counting cells at the indicated time points. 1000 cells were plated per well in a 6-well plate (day -2), and 2 μg/mL doxycycline was added on day 0. Cells were counted every 2 days. Each point represents the average of 3 technical replicates ± SEM.

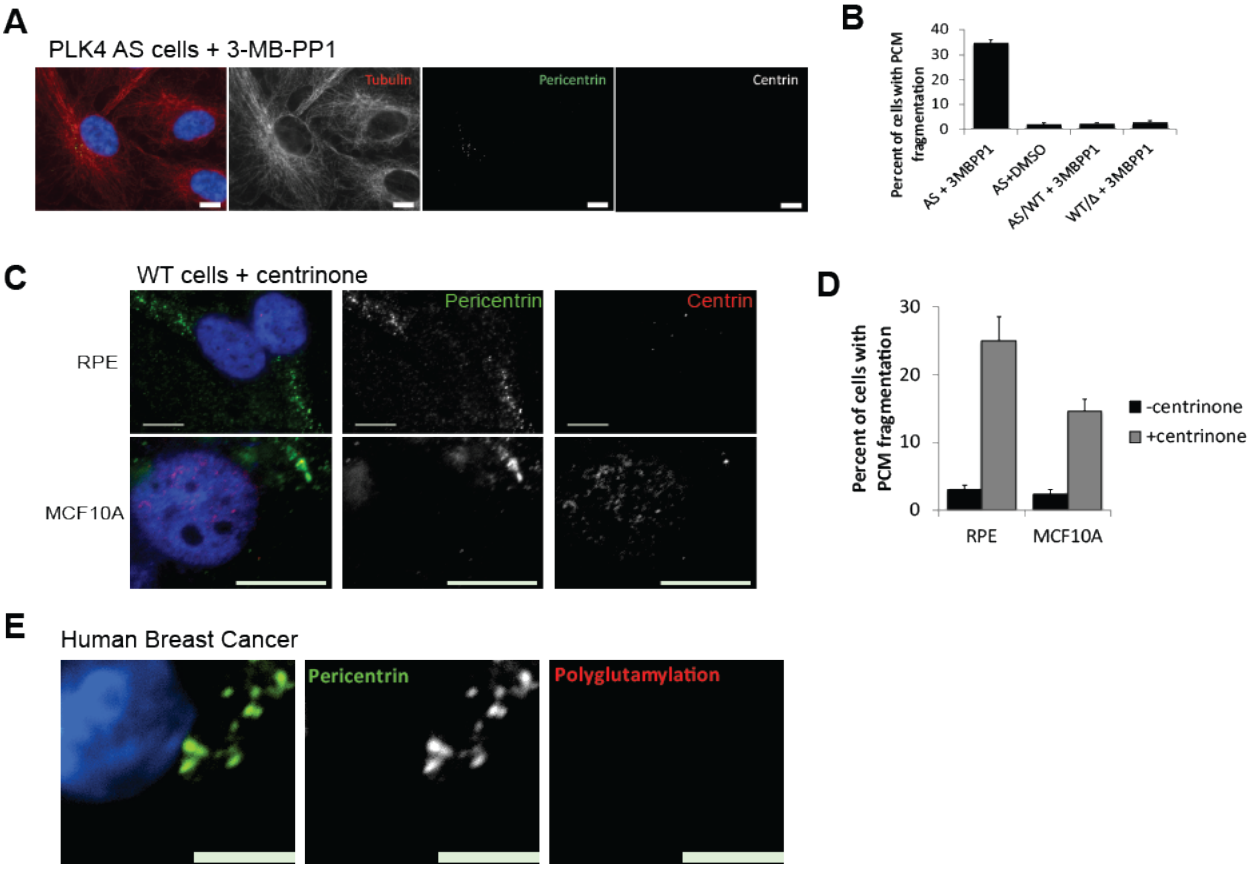

Supplemental Figure 5-2

Loss of centrioles results in PCM fragmentation.

(A) Representative immunofluorescent images of PCM fragmentation. PLK4 AS cells were treated with 10 µM 3-MB-PP1 for 5 days. Green = pericentrin, red = alpha tubulin, white = centrin, blue = DNA. **(B)** Quantification of the percentage of cells with PCM fragmentation. Bars represent the average of 3 biological replicates of 100 cells each ± SEM. **(C)** Representative images of PCM fragmentation in RPE and MCF10A cells treated with 300 nM centrinone B for 4 days. Green = pericentrin, red = centrin, blue = DNA, scale bar = 10 µm. **(D)** Quantification of the experiment described in C. **(E)** An image of PCM fragmentation from a formalin-fixed, paraffin-embedded breast tumor. Green = pericentrin (PCM marker), red = polyglutamylated tubulin (centriole marker), blue = DNA. Scale bar = 5 µm.

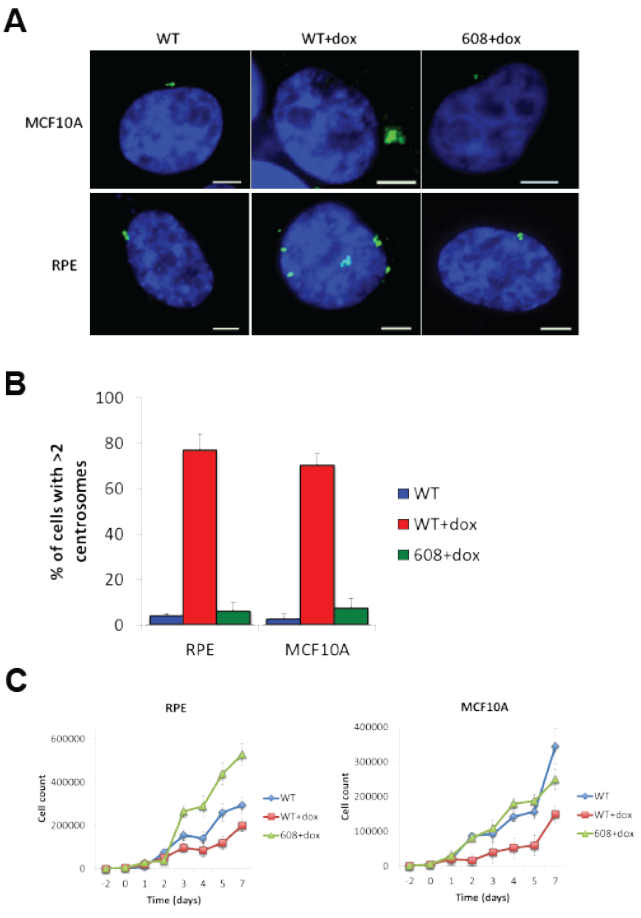

Acknowledgements

The authors thank: David Pellman for cell lines; Jun Wan and Beth Weaver for reagents; Alka Choudhary for technical assistance; Rob Lera for critical review of this chapter; the University of Wisconsin Translational Initiatives in Pathology (TRIP) Laboratory; the University of Wisconsin Small Molecule Screening and Synthesis Facility; the University of Wisconsin Carbone Cancer Center Flow Cytometry Laboratory. Research reported in this chapter was supported by the following NIH awards: F30CA203271 to RAD, R01 GM097245 to MEB, University of Wisconsin Carbone Cancer Center Support Grant P30 CA014520. RAD has also been supported by the University of Wisconsin Medical Scientist Training Program (T32GM008692) and University of Wisconsin ICTR TL1 training program (supported under NIH awards UL1TR000427 and TL1TR000429). The content is the responsibility of the authors and does not necessarily represent the views of the NIH.

CHAPTER 6: Centrosome amplification disrupts autophagy and sensitizes to chloroquine

Work in this chapter is in preparation for submission:

Centrosome amplification in cancer disrupts autophagy and sensitizes to autophagy inhibition

Ryan A. Denu, Gulpreet Kaur, Aparna Lakkaraju, Mark E. Burkard

Abstract

Autophagy is a catabolic process whereby autophagosomes engulf damaged organelles and proteins and deliver these contents to the lysosome for degradation and subsequent recycling. Proper autophagosome fusion with lysosomes depends on movement along intact microtubules, which are organized by centrosomes in human cells. Centrosome amplification (CA), or a numerical increase in centrosomes, is common in human cancers, particularly high-risk cancers. Using cell models of CA, we have discovered that autophagy is disrupted by CA. Cells with CA demonstrated elevated levels of LC3 and p62 by immunoblotting and immunofluorescence. Further, using LC3 reporter assays and autophagosome tracking experiments, we demonstrate that CA causes an accumulation of autophagosomes. The following three hypotheses were tested to explain the mechanism by which CA disrupts autophagy: (1) increased lysosome hubs around the increased number of centrosomes; (2) chromosome missegregation leading to altered protein complex stoichiometry; and (3) disrupted microtubule networks. We find that CA inhibits autophagy via both chromosome missegregation and disruption of microtubule networks. Lastly, we tested autophagy inhibitors in our cell models of CA. Our results show that cells with CA are sensitized to the autophagy inhibitor chloroquine. Taken together, our results suggest that autophagy is disrupted by CA and sensitizes cells to inhibition of autophagy. These findings suggest a novel precision medicine strategy, whereby CA increases reliance on autophagy and serves as a biomarker for autophagy inhibitors in high-risk cancers.

Introduction

Autophagy, or macroautophagy, is a catabolic process whereby autophagosomes engulf damaged organelles and protein aggregates and deliver these contents to the lysosome for degradation.[349,350] Autophagy is activated under various cellular stress conditions such as starvation and oxidative stress. In cancer, autophagy has been reported to be both a tumor suppressor and promoter; the prevailing view is that autophagy is a tumor suppressive pathway and inhibits tumor initiation, but once the tumor has developed, autophagy provides nutrients for the growing tumor and is pro-tumorigenic.[351] As such, there are a number of ongoing trials evaluating autophagy inhibitors, such as hydroxychloroquine, in advanced and drug-resistant cancers.[352]

Autophagy is a complex, multi-step process during which the following major events happen in sequence: (1) sequestering of cytoplasmic contents by an isolation membrane or phagophore; (2) closure of the isolation membrane to form a double-membrane autophagosome; (3) fusion of the autophagosome with the lysosome to create the autolysosome; and (4) degradation of autophagic cargo by lysosomal enzymes.[353-355] The cytoskeleton, particularly the microtubule cytoskeleton, is crucial for autophagy.[356] Movement of endolysosomal organelles depends on coupling to microtubule motors and actin, with long-range transport mostly dependent on microtubule motors (e.g. dynein, kinesins) and short-range transport mostly dependent on actin and myosin.[357] Further, autophagosome movements depends on intact microtubules to bring them into the proximity of lysosomes, which tend to be clustered near the centrosome, the major microtubule organizing center in animal cells.[355,358-360] Concordantly, disrupting microtubules with the depolymerizing drugs nocodazole and vinblastine results in an

accumulation of autophagosomes.[361-365] The contributions of the centrosome and centrosome-mediated microtubule nucleation and organization to autophagy have not been determined.

Centrosome amplification (CA), or a numerical increase in centrosomes, has been reported in virtually all human cancer sites.[107,109,208] CA promotes error-prone mitoses with multipolar spindles and merotelic microtubule-kinetochore attachments [114], high-grade phenotypes,[109] invasiveness,[121,126] and ultimately worse outcomes.[109] Given that CA is very specific to cancer cells, it represents a potential therapeutic target for cancer therapy. Heretofore, the roles of the centrosome and centrosome-mediated microtubule nucleation in autophagy have not been elucidated. Herein, we provide evidence that centrosomes are required for efficient autophagy. Further, CA inhibits autophagy by disrupting microtubules and promoting chromosome missegregation, and cells with CA are sensitized to autophagy inhibition. This suggests that CA may be a potential biomarker for autophagy inhibition in cancer.

Results

Centrosome amplification disrupts autophagy

CA is very specific to cancer cells and represents an attractive therapeutic target [114]. Based on findings that microtubule disruption and loss of microtubules are required for proper autophagy, we hypothesized that CA disrupts autophagy. We utilized two cell line models of CA, which mimic the biology of cancer cells. These RPE-1 and MCF10A cell lines utilize a tetracycline-inducible PLK4 transgene (labeled PLK4 WT). As a control for tetracycline treatment and for increased kinase activity in the cell, we utilized a tetracycline-inducible truncated construct (amino acids 1-608 of PLK4), which lacks a crucial C-terminal localization domain (labeled ΔC) and does not result in CA when overexpressed (Supplemental Figure 6-1).[66,126]

To assess autophagy in these models of CA, we used the reported consensus guidelines.[349,366] Firstly, we assessed the autophagy markers p62 and LC3B by immunofluorescence. CA increased the expression of both p62 and LC3B (Figure 1A-E), suggesting that there is a block in the autophagy pathway resulting in buildup of autophagosomes and autophagic cargo. Chloroquine, which is known to inhibit lysosome acidification and results in autophagosome accumulation, was used as a positive control.

For autophagosome formation, the cytosolic form of LC3, or LC3-I, is cleaved and conjugated to phosphatidylethanolamine to create the LC3-II form mediated by the ATG5-ATG12 conjugate,[367,368] which is incorporated into autophagosome membranes.[366,369,370] Therefore, LC3-II serves as a good reporter of autophagosome formation. Both RPE and MCF10A cell lines with CA demonstrated increased LC3-II:LC3-I ratios (Figure 6-1F-G, Supplemental Figure 6-2), indicating a change in the autophagy status of these cells. To

determine whether this relative increase in LC3-II resulted from activation of autophagy or a block in autophagic degradation, we assessed LC3-II levels in the same conditions after treatment with an inhibitor of lysosomal degradation, bafilomycin A1. The increase in LC3-II levels between uninhibited and bafilomycin A1-treated cells will be greater than controls if CA induces autophagy or lesser than controls if CA inhibits autophagy. After bafilomycin A1 treatment, the relative increase in LC3-II was greater in the non-CA conditions compared to CA conditions (Figure 6-1H, Supplemental Figure 6-2), indicating that CA blocks autophagy.

In addition, we assessed the expression of autophagy-related genes by qRT-PCR. Cells with CA exhibited greater expression of the autophagy related genes ATG5, BECN1/Beclin-1, and p62/SQSTM1 (Figure 6-1I). These data suggest a compensatory increase in autophagy to counteract an autophagy defect in cells with CA.

To demonstrate that these effects are not simply due to increasing PLK4 expression or activity in the cell, we also induced CA by overexpressing STIL. Similarly, we found that STIL overexpression-induced CA disrupts autophagy, as assessed by p62 and LC3B quantitative immunofluorescence (Supplemental Figure 6-3). Further, we assessed autophagy in tetraploid cells generated by cytokinesis failure by treatment with cytochalasin D, which also typically have extra centrosomes. Concordantly, tetraploid cells with CA demonstrated an increase in p62 and LC3B expression.

Loss of centrosomes impairs autophagy

Because intact microtubules are required for autophagy and because we found that gain of centrosomes impairs autophagy, we hypothesized that centrosomes are required for proper autophagy and that loss of centrosomes would disrupt autophagy. To test this, we utilized an

analog-sensitive PLK4 cell line to model loss of centrosomes. This analog sensitive allele is made by mutating the gatekeeper residue of PLK4 (L89G) in order to genetically encode chemical sensitivity to a bulky ATP analog, 3-MB-PP1. Upon treatment with 3-MB-PP1, these cells lose centrioles after multiple rounds of cell division (Supplemental Figure 6-4A). Interestingly, cells without centrioles demonstrated an increase in autophagosomes, as assessed by p62 and LC3B immunofluorescence (Supplemental Figure 6-4B-F). We conclude that centrosomes are required for efficient autophagy.

Centrosome amplification causes autophagosome accumulation

To determine which part of the autophagy pathway is disrupted by CA, we utilized an LC3B reporter construct, in which LC3B is fused with both mCherry and GFP, whose fluorescent properties change as a result of changes in pH (Figure 6-2A). This reporter enables simultaneous estimation of both the induction of autophagy and flux through autophagic compartments. The GFP signal is quenched by the acidic and/or proteolytic conditions of the lysosome lumen, whereas mCherry is more stable with changes in pH.[371,372] Therefore, colocalization of both GFP and mCherry fluorescence (yellow foci) indicates a compartment that has not fused with a lysosome, such as the phagophore or an autophagosome. In contrast, mCherry signal without GFP (red foci) corresponds to an autolysosome. Therefore ratios of GFP to mCherry are a measure of autophagic flux. We quantified the Pearson correlation of GFP and mCherry channels as well as the number of GFP+ mCherry+ foci and GFP- mCherry+ foci. Autophagic flux is increased when both yellow and red puncta are increased, while autophagic flux is blocked when only yellow puncta are increased without an accompanying increase of red puncta in cells.[373] Chloroquine, which inhibits lysosomal acidification, was used as a control in

these experiments; as expected chloroquine increased the Pearson correlation and the number of yellow puncta without a significant increase in red puncta (Figure 6-2C). CA (PLK4 WT+dox conditions) resulted in a similar increase in the Pearson correlation (Figure 6-2B) and the number of yellow puncta without a significant increase in red puncta compared to controls (Figure 6-2C). We conclude that CA results in an accumulation of autophagosomes.

Centrosome amplification correlates with p62 expression in panel of breast cancer cell lines

To assess whether our findings were consistent in different models and in a more cancer-relevant system, we utilized a syngeneic cell line panel, consisting of MCF10A (non-transformed, immortalized human epithelial cell line) and two derivative cell lines, DCIS (mimics the biology of breast ductal carcinoma *in situ*) and Ca1d (mimics the biology of invasive breast carcinoma). We assessed centrioles and autophagy by immunofluorescent staining of centrin and p62, respectively (Figure 6-3A). We find an increase in centrioles in DCIS compared to MCF10A and an even greater increase in centrioles in Ca1d compared to the two other cell lines (Figure 6-3B). A similar trend was observed in p62 expression (Figure 6-3C). Further, centrioles and p62 expression were significantly correlated with combining the data from all 3 cell lines together (Figure 6-3D). We conclude that CA correlates with autophagy in an independent breast cancer cell line panel.

Centrosome amplification-induced autophagy inhibition is dependent on progression through mitosis

To assess the mechanism by which CA disrupts autophagy, we tested three alternate but non-mutually exclusive hypotheses: (1) CA disrupts microtubule networks, thereby preventing

efficient transport of autophagic vesicles along microtubules; (2) CA increases the number of lysosome hubs, as lysosomes are known to cluster around centrosomes; and (3) CA causes chromosome missegregation resulting in aneuploidy and altered stoichiometry of protein complexes, resulting in an autophagic stress response[374] (Figure 6-4A).

First, we tested the hypothesis that CA inhibits autophagy via microtubule disruption. Movement autophagosomes to lysosomes is dependent on microtubules,[361-365] and microtubule disruption with nocodazole and paclitaxel inhibit autophagy, as evaluated by increased p62 and LC3B expression, increased LC3B-II/I ratios, and autophagosome accumulation (Supplemental Figure 6-5); Further, CA disrupts microtubules and cause increased microtubule nucleation.[124] To test our hypothesis, we measured autophagosome trafficking by live-cell imaging. Cells were plated in glass-bottom chambers, treated with doxycycline, and transduced with baculovirus-expressing LC3B-mCherry. Following each experiment, we fixed the cells and stained *in situ* to confirm CA in the PLK4 WT+doxycycline condition (Figure 6-4B). Consistent with our previous findings, CA caused an increase in the number of autophagosomes (Figure 6-4C). However, there was no statistically significant effect of CA on autophagosome trafficking parameters, including track displacement as a function of track length (Figure 6-4D-G), average autophagosome speed (Figure 6-4H), autophagosome track displacement (Figure 6-4I), or autophagosome track length (Figure 6-4J). Based on these data, we conclude that CA increases autophagosome numbers without disrupting trafficking, which is inconsistent with hypothesis 1. Although the trafficking parameters are not disrupted, it remains possible that this trafficking is occurring on distinct, separate hubs (hypothesis 2).

To test the second hypothesis that CA increases the number of number of lysosome hubs, as lysosomes tend to cluster around centrosomes, we analyzed lysosomes by

immunofluorescence using the lysosome marker LAMP1. We observed no significant differences in LAMP1 expression in cells with CA compared to controls (Supplemental Figure 6-6). Furthermore, cells with CA cluster their centrioles,[375] so it is unlikely that additional lysosome hubs form.

Lastly, we tested the third hypothesis that CA-mediated autophagy disruption depends on chromosome missegregation. Previously, aneuploidy and chromosome missegregation induced by inhibition of the mitotic checkpoint kinase MPS1 have been shown to disrupt autophagy.[374] This is thought to be due to an aneuploidy-induced gene imbalance, causing altered protein complex stoichiometry, increased proteotoxic stress, and accumulation of autophagic products in lysosomes.[376,377] CA is known to cause chromosome missegregation via multipolar spindles, merotelic kinetochore attachments, and lagging chromosomes.[134] To determine if our observed effect of CA on autophagy is dependent on mitosis and chromosome missegregation events, we arrested cells at the G1/S transition with aphidicolin (Figure 6-5A), then treated with doxycycline for 24 hours to induce CA; aphidicolin arrested cells are still able to duplicate and amplify centrosomes (Figure 6-5B and ref [378]). We compared the change in p62 or LC3B expression between aphidicolin-arrested and non-arrested conditions. We observe a partial reduction in p62 and LC3B with aphidicolin in cells with CA (Figure 6-5C-D). Additionally, the statistically significant difference in p62 and LC3B seen between CA (WT+dox) and non-CA controls (WT or ΔC+dox conditions) is lost with aphidicolin treatment (Figure 6-5C-D). We conclude that the CA-induced autophagy disruption may partially be explained by mitosis or chromosome missegregation but largely cannot be explained by an increase in the number of lysosomal hubs or disruption of microtubule networks.

Centrosome amplification sensitizes to inhibition of autophagy

The role of autophagy in cancer has been somewhat unclear and controversial. Most data support the conclusion that autophagy is a tumor-suppressive pathway, but that after a tumor has initiated, autophagy helps the tumor progress. As such, chloroquine and its derivative hydroxychloroquine, FDA-approved drugs for non-oncologic indications, are currently being investigated for cancer treatment. Therefore, the effect of CA on autophagy could have clinical implications. Because cells with CA display an accumulation of autophagosomes, we hypothesized that they are more dependent on autophagy for survival and are more sensitive to inhibition of autophagy. We assessed cell viability in the RPE-1 and MCF10A models of CA treated with chloroquine. We also screened a panel of other drugs in these cell lines, finding that cells with CA appear more resistant to anti-mitotic drugs, such as PLK1 inhibitors and vinca alkaloids (data not shown); this finding is likely due to the slower proliferative rate of cells with CA[67] and is consistent with previous reports.[379] In both cell lines, cells with CA were more sensitive to chloroquine, as assessed by Cell Titer Glo viability assays (Figure 6-6A-B), crystal violet staining (Figure 6-6C), and cell counts (Figure 6-6D). We then assessed the mechanism of reduced viability by testing the hypotheses that chloroquine increases either apoptosis or senescence to a greater extent in cells with CA versus controls. Our data demonstrate a significantly greater rate of both apoptosis (Figure 6-6E) and senescence (Figure 6-6F) in cells with CA (PLK4 WT+dox conditions) versus controls (PLK4 WT and ΔC+dox). We conclude that cells with CA are more sensitive to autophagy inhibition, and that the mechanism of reduced viability with chloroquine treatment involves both apoptosis and senescence.

Discussion

CA is common in cancer, particularly in higher risk cancers, and has a number of effects on cell physiology, such as chromosome missegregation, increased microtubule nucleation, and formation of invasive acini.[109,114,121,126] As CA is very specific to cancer cells, it represents a potentially good therapeutic target. Therefore, it is important to continue to study the consequences of CA with the goal of learning how to target CA to treat cancer. Herein we have reported a novel precision medicine strategy, whereby cells with CA demonstrate disrupted autophagy and are more susceptible to inhibition of autophagy. This may indicate that CA is a potential biomarker for autophagy inhibition in cancer. We demonstrate that the mechanism of CA-induced autophagy disruption is dependent on cell division.

Our study demonstrates that CA-induced autophagy disruption is dependent on cell divisions. Cells with CA are more likely to undergo chromosome missegregation,[134] often resulting in aneuploid progeny. In eukaryotic cells, changes in gene copy number largely lead to a proportional change in the amount of protein produced.[380-382] As a result, aneuploid cells have more imbalances in protein complex stoichiometry and generate more misfolded and aggregated proteins.[383,384] Further, aneuploidy has been shown to activate an autophagic stress response, characterized by accumulation of autophagosomes and upregulation of TFEB-responsive genes, presumably in response to the aneuploidy-induced proteotoxic stress.[374,385] We similarly found that CA causes an accumulation of autophagosomes and increased expression of autophagy genes, suggesting a similar mechanism is at play. Previous work demonstrates that the accumulated autophagosomal proteins are not efficiently cleared within lysosomes, but that lysosomal functions in aneuploidy cells remain intact.[374] Further work will be necessary to determine why autophagosomal proteins are not efficiently cleared in aneuploidy cells.

Recent work has connected the centrosome with autophagy.[386] First, one study demonstrated that the centrosome may regulate autophagosome formation by facilitating transport of GABARAP, another ATG8 family member similar to LC3, to the forming autophagosome membrane. Additional work has suggested that autophagy plays a role in maintaining the proper number of centrosomes via degradation of CEP63.[387] Our work adds to this growing body of knowledge suggesting that the centrosome contributes to the autophagy pathway.

The role of autophagy in cancer has been rather controversial, but the prevailing view had been that autophagy acts as a tumor suppressor initially but helps the tumor progress once it has already developed.[388] Autophagy was thought to be a tumor suppressor because mice with allelic loss of *Becn1* develop tumors.[389,390] However, it was later determined that *BECN1* is adjacent to *BRCA1,* and *BECN1* loss is not found independently of co-deletion with *BRCA1* suggesting that loss of *BRCA1* was driving tumorigenesis in these mice.[391] As the tumor progresses it becomes dependent on autophagy for survival, so autophagy is pro-tumorigenic in later stages of cancer [388,392,393]. This is confirmed by observations that loss of function of core autophagy genes is uncommon in cancer, whereas mutations that activate autophagy been identified.[394,395] Immunohistochemical analyses demonstrate that more aggressive tumors express lower levels of p62 and LC3B, consistent with increased autophagy.[396] There are several ongoing clinical trials of chloroquine in advanced cancer. In addition, more specific inhibitors of the autophagic machinery (e.g. ULK1 and ATG7 inhibitors) are in preclinical development for potential use in cancer clinical trials. Our work suggests that the use of CA as a biomarker for autophagy inhibitors could increase the success of this therapeutic strategy.

There are some limitations to this body of work. First, most of our experiments were performed with one model of CA (i.e. PLK4 overexpression). While this model certainly causes CA, it is unclear if this model accurately reflects the mechanism(s) of CA that occur(s) in human cancer. Next, we have not demonstrated the correlation between CA and autophagy in human cancer samples. A potential problem with using CA as a biomarker is that analysis of centrosomes in human cancer patients may not realistically translate well to clinical practice, as this method is time- and labor-intensive. Another potential challenge relates to the potential use of CA as a therapeutic target. While CA is specific to cancer cells, it is usually only present in a fraction of the cells in a tumor and may be a transient phenotype; for example, we previously reported that an average of 23% of breast cancer cells have CA.[109] However, data suggesting that only a fraction of cancer cells have CA is based on immunohistochemical staining of tissue sections, which may underestimate the number of centrosomes via sectioning artifact. Lastly, we have not demonstrated that CA sensitizes to autophagy inhibition using *in vivo* models, which will be crucial before moving forward.

In conclusion, we have presented evidence that CA causes an autophagic defect that is dependent on both cell division (presumably with chromosome missegregation) and disruption of microtubules. Further, CA confers a vulnerability and renders cells more susceptible to autophagy inhibition. These results suggest a rationale for precisely targeting autophagy in high-risk cancers with CA.

Materials and Methods

Cell culture

All cell lines were propagated at 37 °C in 5% CO_2. All cell lines were authenticated by STR analysis using the Promega PowerPlex 16 HS System Kit (DC2101) at the University of Wisconsin Translational Research Initiatives in Pathology (TRIP) laboratory. RPE1 (ATCC) cells were grown in a 1:1 mixture of DMEM and Ham's F-12 medium supplemented with 2.5 mm l-glutamine, with 10% fetal bovine serum and 100 units/ml penicillin-streptomycin. MCF10A (non-transformed breast line, ATCC), DCIS (breast ductal carcinoma *in situ* line derived from MCF10A, provided by Dr. Patricia Keely), and Ca1d (invasive breast cancer line derived from MCF10A, provided by Dr. Patricia Keely) cells were grown in 1:1 DMEM and Ham's F-12 supplemented with 2.5 mm l-glutamine, horse serum, EGF, hydrocortisone, cholera toxin, and 100 units/mL penicillin-streptomycin. Doxycycline-inducible PLK4 cell lines (RPE-1 and MCF10A) were kindly provided by David Pellman (Harvard). Doxycycline was added to achieve a final concentration of 2 μg/mL. HeLa and Phoenix cells (ATCC) were cultured in DMEM high glucose medium with 10% fetal bovine serum and 100 units/ml penicillin-streptomycin. DLD1 cells (ATCC) were cultured in RPMI 1640 medium with 10% fetal bovine serum and 100 units/ml penicillin-streptomycin. Tetraploid DLD1 cells were generated as previously described [397]. Briefly DLD1 cells were treated with blebbistatin to induce cytokinesis failure, subcloning by limiting dilution, and screening of clones using propidium iodide staining and flow cytometric detection.

For the LC3B autophagic flux reporter assay, we utilized pBABE-puro-mCherry-EGFP-LC3B, a gift from Jay Debnath (Addgene plasmid # 22418).[398] Retrovirus was generated by transfecting a T25 of Phoenix cells with 2 μg of the retroviral vector and 1 μg pVSV-G pantropic

envelope vector using Fugene transfection reagent (Promega). Phoenix cells were given fresh media 24 hours after transfection, and this supernatant was collected 48 hours after transfection and used to transduce RPE and MCF10A cells. Polybrene was added to a concentration of 10 μg/mL. Cells were selected with puromycin for 5 days, and monoclonal cell lines were isolated and propagated.

Cellular senescence was assayed using a pH-dependent β-galactosidase staining kit (Cell Signaling Technology) according to the manufacturer's instructions.

Chemicals used in this study include chloroquine (Fisher, ICN19391910, 100 μm), aphidicolin (Fisher, BP615, 5 μM), doxycycline (Fisher, BP26531, 2 μg/mL), nocodazole (Sigma, M1404, 0.2 μg/ml), 3-MB-PP1 (Toronto Research Chemicals, 10 μM), bafilomycin A1 (Fisher, NC9686929, 100nM), puromycin (Invivogen, 10 μg/mL), polybrene (Millipore, TR-1003-G, 10 μg/mL), blebbistatin (Tocris, 176010R), doxorubicin (Fisher, 15910101), paclitaxel (Fisher, P3456), vincristine (Acros, 203440050), thapsigargin (Fisher, AC328570010), tunicamycin (MP Biomedicals, ICN15002801), BI-2536 (Selleck Chemicals, S1109), BI-6727 (Selleck Chemicals, S2235).

Immunofluorescence

Cells were seeded on sterilized glass coverslips in 24-well plates and fixed with 4% paraformaldehyde or 100% ice-cold methanol for 15 minutes. Methanol was always used when analyzing centrioles. Fixed cells were then blocked for 30 minutes in 3% bovine serum albumin (BSA) and 0.1% Triton X-100 in PBS (PBSTx + BSA). Primary antibodies were incubated in PBSTx + BSA for at least 1 hour at room temperature in a humidified chamber and washed three times in PBSTx, followed by secondary antibody (Alexa fluor-conjugated, Invitrogen, 1:350)

incubation in PBSTx + BSA for 30 minutes at room temperature and one wash with PBSTx. Cells were counterstained with DAPI and mounted on glass slides with Prolong Gold antifade medium (Invitrogen). Image acquisition was performed on a Nikon Eclipse Ti inverted microscope equipped with: 10x, 20x, 40x, 60x, and 100x objectives; a temperature-controlled motorized stage with 5% CO_2 support (In Vivo Scientific); and Hamamatsu ORCA Flash 4.0 camera. For images displayed in the figures, optical sections were taken at 0.2-μm intervals and deconvolved using Nikon Elements. Where appropriate, the observer was blinded to treatment condition during image acquisition and analysis. Images were processed and analyzed using Nikon Elements.

Antibodies utilized for immunofluorescence include: p62/SQSTM1 (Santa Cruz, SC-28359, 1:1000), alpha tubulin (Abcam ab4074, 1:5000), lysosomal-associated membrane protein-1 (LAMP-1; H4A3, deposited to the DSHB by August, J.T. / Hildreth, J.E.K.; 1:500), LAMP-2 (H4B4, deposited to the DSHB by August, J.T. / Hildreth, J.E.K.; 1:500), LC3B (Cell Signaling Technology, 2775, 1:500), pericentrin (Abcam, ab4448, 1:1000), centrin (Millipore, 04-1624, 1:500), and gamma tubulin (Abcam, ab27074, 1:1000). Alexa fluor-conjugated secondary antibodies were used (Invitrogen, 1:350).

Flow cytometry

For cell cycle and DNA content analyses, cells were harvested, washed with PBS, fixed in cold 70% EtOH for at least 24 hours, washed once in PBS, and resuspended in PBS with 0.5 mg/mL RNase A and 50 mg/mL propidium iodide. Samples were incubated at 4° C overnight and analyzed on a flow cytometer (FACSCalibur, BD Biosciences).

For apoptosis staining, cells were collected, centrifuged, resuspended in Annexin V

binding buffer, and stained with FITC Annexin V and propidium iodide, per manufacturer's protocol (BD Biosciences). Cells positive for both Annexin V and propidium iodide were considered apoptotic.

Quantitative reverse transcriptase polymerase chain reaction (qRT-PCR)

RNA was isolated from cells using the RNeasy Micro Kit (Qiagen, Valencia, CA), and converted to cDNA using the Quantitect Reverse Transcription Kit (Qiagen). Primer sequences are shown in Supplemental Table 1 [399-401]. Primers were used at a final concentration of 0.67 μM each, and 25ng cDNA was used per reaction. A StepOne Plus (Applied Biosystems) real-time PCR thermal cycler was used for amplification with iQ SYBR Green Supermix (Biorad) per manufacturer's protocol. Quantification of CEP131 mRNA was normalized to three housekeeping genes (*RRN18S, GAPDH and ACTB*). The $\Delta\Delta C_T$ method was employed to calculate the fold change in expression.[164]

Immunoblotting

Cells were lysed in buffer (50 mM HEPES, pH 7.5, 100 mM NaCl, 0.5% NP-40, 10% glycerol) containing phosphatase inhibitors (10 mm sodium pyrophosphate, 5 mM β-glycerol phosphate, 50 mm NaF, 0.3 mm Na_3VO_4), 1 mM PMSF, protease inhibitor cocktail (Thermo Scientific), and 1 mm dithiothreitol. Samples were sonicated and heated in SDS buffer. Proteins were separated by SDS-PAGE (12% acrylamide gels), transferred to PVDF membrane (Millipore), and blocked for at least 30 minutes in 5% milk and 0.1% Tween 20 in Tris-buffered saline, pH 7.4 (TBST + milk). Membranes were incubated 1 hour at room temperature with primary antibodies diluted in TBST + 5% milk, washed three times with TBST, and incubated

for 1 hour at room temperature in secondary antibodies conjugated to horseradish peroxidase in TBST + 5% milk. Membranes were washed and developed with luminol/peroxide (Millipore) and visualized with film. The iBind device (Thermo Fisher) was utilized for LC3B western blots in lieu of incubations with antibodies diluted in milk.

LC3-I is more labile and more sensitive to freezing-thawing and to degradation in SDS sample buffer than LC3-II,[349] so fresh samples were used and not subjected to repeated freeze-thaw cycles.

Antibodies utilized for immunoblotting include: LC3B (CST, 2775, 1:1000), p62/SQSTM1 (Santa Cruz, SC-28359, 1:1000), and actin (DSHB, JLA20, 1:1000). HRP-conjugated secondary antibodies were used (Jackson). Relative intensities of bands were calculated using ImageJ from scanned images and normalized to their respective β-actin intensity.

Cell Proliferation Assays

Doxycycline-inducible cell lines were pre-treated with doxycycline for 24 hours to induce CA, then harvested for drug screening. 1000 cells in 150 μL media were plated per well in 96 well plates. Cells were allowed to attach overnight, then chloroquine was added the next morning in 50 μL. After 5 days of incubation, 50μL of Cell Titer Glo (Promega) was added to each well, incubated for 15 minutes at room temperature, and luminescence was analyzed using an Enspire Plate Reader (Perkin Elmer) at the UW Small Molecule Screening and Synthesis Facility. From each experimental luminescence value, we subtracted the luminescence value of wells with media plus Cell Titer Glo (indicating background luminescence without cells) and normalized to the luminescence value of untreated cells within each condition. This screen was

replicated using Vita-Orange Cell Viability Reagent (Biotool) in 96-well plates (same protocol as above), as well as crystal violet staining in 24-well plates. For crystal violet staining, cells were pre-treated with doxycycline for 24 hours, then harvested and plated in 24-well plates at a density of 5000 cells/well. Chloroquine was added the next day, and cells were incubated for 5 days before staining with crystal violet.

Autophagosome Tracking

RPE PLK4 WT and ΔC cells were grown on the cover slip of 35mm dishes (MatTek), treated with 2 µg/mL doxycycline the next day (if indicated), and transduced the following day with BacMam LC3-GFP or LC3-RFP (Thermo-Fisher P36235, P36236) for 16-24 hours. Live imaging of autophagosome traffic and autophagic flux was performed as previously described [402]. Live, transduced cells were rapidly imaged (2000ms per Z-stack, 50 times) using: the Revolution XD spinning-disk microscopy system equipped with Yokogawa CSU-X1 confocal spinning disk head; Nikon Eclipse Ti inverted microscope surrounded by an Okolab cage incubator; iXon x3 897 EM-CCD camera; Andor laser combiner with four solid-state lasers at 405, 488, 561 and 640 nm and corresponding band-pass filter sets (Sutter); and ASI motorized stage with piezo-Z for rapid Z-stack acquisition. Andor IQ2 software was used for image acquisition and Imaris X64 (Bitplane) for image analysis. Spots module was used to obtain speed, track displacement, track straightness and total track length of autophagosomes.

Statistics

Statistical evaluations were performed using Prism software (GraphPad). Two-tailed t-tests were used for comparing two groups, and one-way ANOVA and Tukey multiple

comparison tests were used for comparing more than two groups. P-values <0.05 were considered significant for all tests, and designations are made in the figures for statistical significance. Unless otherwise stated, data are presented as means ± SEM of three or more independent experiments, with at least three replicates per condition per experiment.

Figure 6-1

Centrosome amplification disrupts autophagy.

(A) Micrographs of fixed cells probed for autophagososomes (p62/SQSTM1, red) and centrioles (centrin, green) in a doxycycline-inducible PLK4 overexpression system. The PLK4 WT cell line overexpresses full length PLK4 when treated with doxycycline, while the ΔC cell line overexpresses a truncated form of PLK4 (the first 608 amino acids, lacking the C-terminal localization domain) and does not result in centrosome amplification. Insets show enlargements of the centrioles (centrin staining). Blue = DNA/DAPI, green = centrin, red = p62. Scale bar = 5 μm. **(B)** Quantification of p62 immunofluorescence. Chloroquine, an autophagy inhibitor, was used as a positive control. **(C)** Quantification of p62 foci exceeding a predefined threshold in the indicated cell lines pictured in panel A. **(D)** Representative images of LC3B immunofluorescence. Insets show enlargements of the centrioles (centrin staining). **(E)** Quantification of LC3B immunofluorescence. **(F)** Western blotting for an autophagosome marker, LC3B, which is cleaved and lipidated when autophagy is activated, visualized by a shift from a 16 kDa (LC3B-I) to 14 kDa product (LC3B-II). All conditions were also treated with bafilomycin A1, an inhibitor of autophagy, to determine how centrosome amplification affects autophagic flux. Replicate blots are shown in Supplemental Figure 2. **(G)** To assess a potential change in autophagic flux, we quantified the fold increase in LC3-II/I ratio after treatment with bafilomycin A1. **(H)** The expression of autophagy genes was analyzed by qRT-PCR. Fold change was calculated using the 2^-ΔΔCt method after normalization to 3 housekeeping genes (*RRN18S, GAPDH and ACTB*). **(I)** RPE PLK4 WT cells were treated with doxycycline and fixed after 3, 6, 12, 24, 36, and 48 hours. Centrioles (centrin foci), p62 expression, and LC3B expression were quantified. Dots represent at least 30 cells with bars indicating SD. In panels B,

C, and E, dots represent individual cells. Bars represent means ± SEM from at least 3 independent experiments unless otherwise indicated. *P value < 0.05 with correction for multiple comparisons.

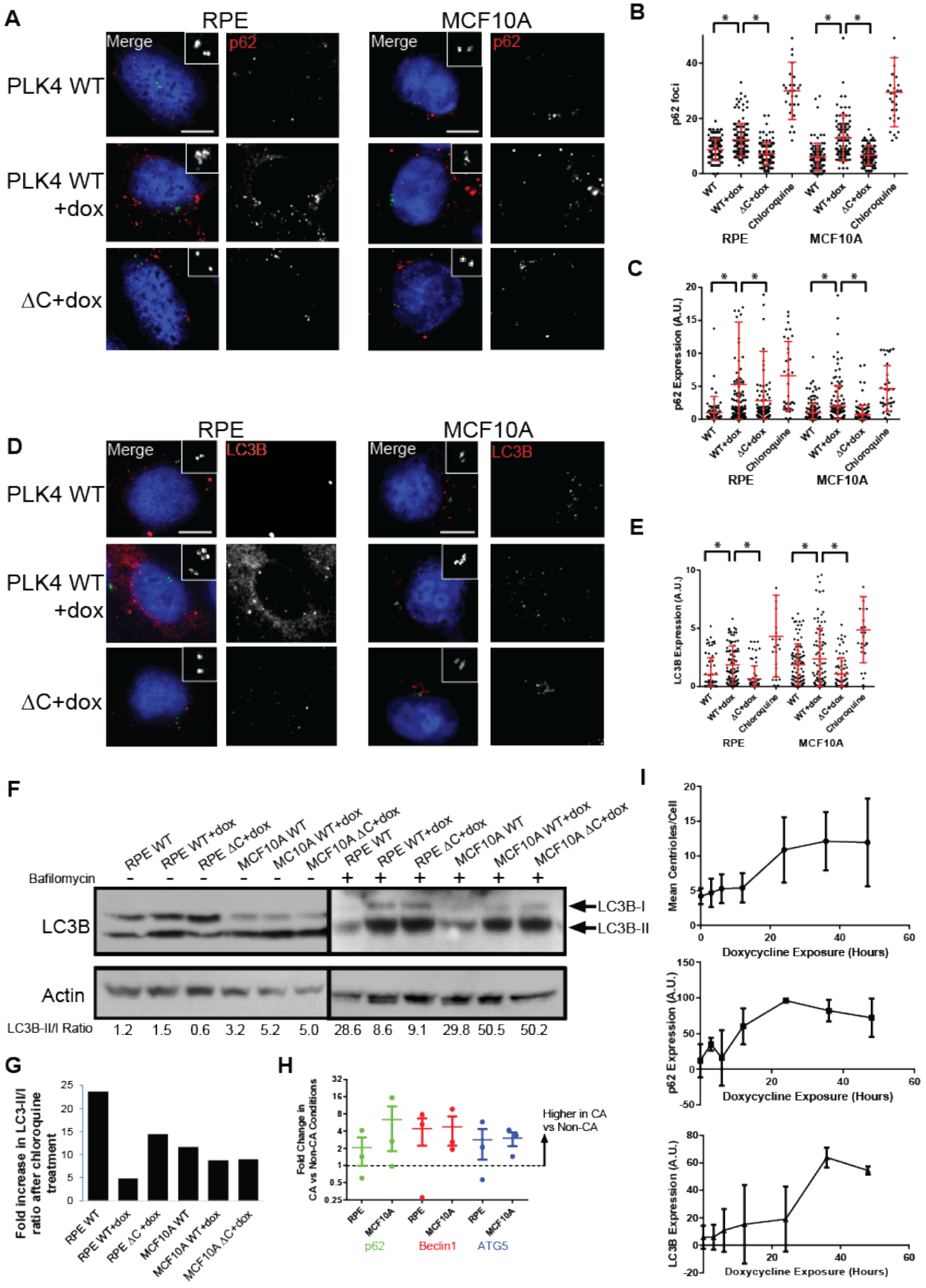
A
RPE
MCF10A
Merge
p62
PLK4 WT
PLK4 WT +dox
ΔC+dox
B
p62 foci
WT
WT+dox
ΔC+dox
Chloroquine
RPE
MCF10A
C
p62 Expression (A.U.)
D
LC3B
E
LC3B Expression (A.U.)
F
RPE WT
RPE WT+dox
RPE ΔC+dox
MCF10A WT
MC10A WT+dox
MCF10A ΔC+dox
Bafilomycin
LC3B
LC3B-I
LC3B-II
Actin
LC3B-II/I Ratio
1.2 1.5 0.6 3.2 5.2 5.0 28.6 8.6 9.1 29.8 50.5 50.2
G
Fold increase in LC3-II/I ratio after chloroquine treatment
H
Fold Change in CA vs Non-CA Conditions
Higher in CA vs Non-CA
p62
Beclin1
ATG5
I
Mean Centrioles/Cell
Doxycycline Exposure (Hours)
p62 Expression (A.U.)
LC3B Expression (A.U.)

Figure 6-2

Centrosome amplification causes an accumulation of autophagosomes.

(A) Representative immunofluorescent micrographs of cells expressing an LC3B reporter, in which LC3B is fused to both GFP and mCherry. In acidic environments (i.e. the lysosome), the GFP signal is quenched. Scale bar = 5 μm. **(B)** Quantification of Pearson correlations between GFP and mCherry expression. Higher values indicate more GFP-mCherry overlap, indicating more autophagosomes. **(C)** Quantification of yellow and red foci in RPE cells. Yellow foci represent autophagosomes, while red foci represent autolysosomes. Dots represent individual cells. Bars represent means ± SEM. *P value < 0.05.

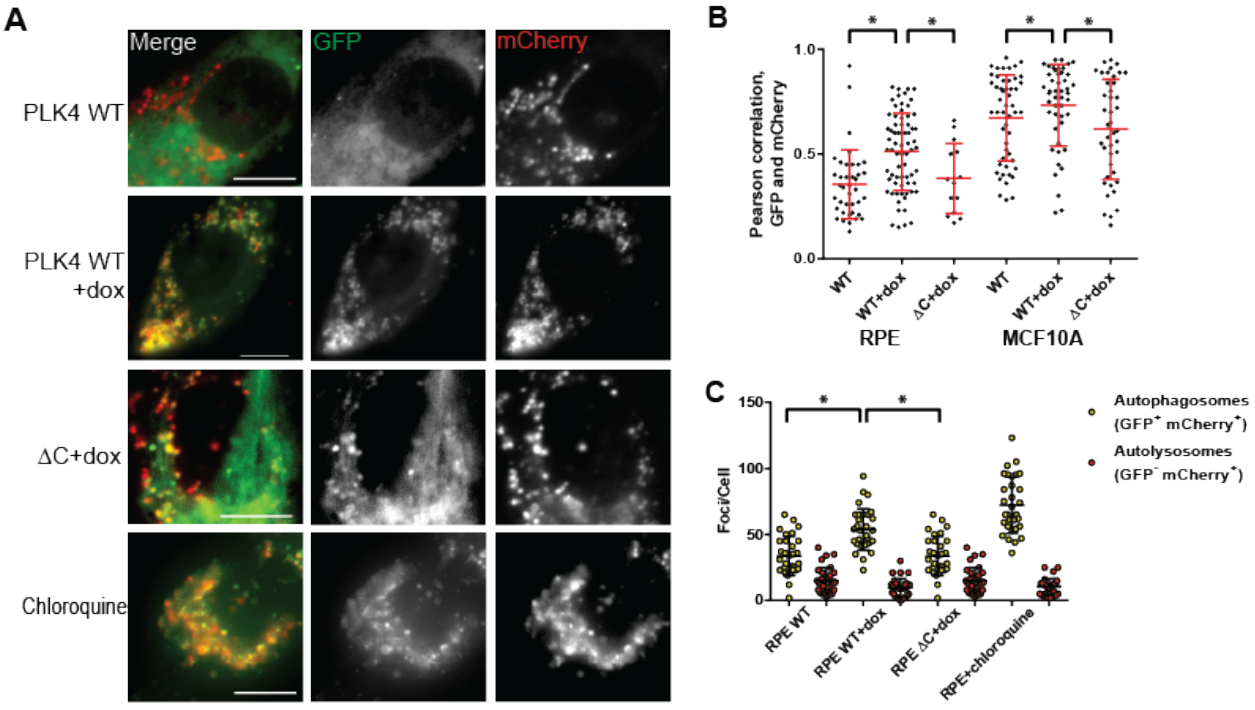

Figure 6-3

Centrosome amplification correlates with p62 in breast cancer models.

(A) Representative images of MCF10A, DCIS, and Ca1d cell lines, representing benign breast epithelium, ductal carcinoma in situ, and invasive ductal carcinoma, respectively. Insets show enlargements of the centrioles (centrin staining). Blue = DNA/DAPI, green = centrin, red = p62. Scale bar = 10 μm. **(B)** Correlation of centrioles with p62 expression, quantified from immunofluorescence images. Pearson r = 0.281, P value < 0.001. Data are combined from all 3 cell lines shown in panel A. **(C)** Quantification of centrioles in each of the 3 cell lines. **(D)** Quantification of p62 expression in each of the 3 cell lines. ANOVA P value = 0.013, Tukey's multiple comparisons test demonstrated significant difference between MCF10A and Ca1d (P < 0.015). Dots represent individual cells. Bars represent means ± SD. *P value < 0.05, ***P< 0.001.

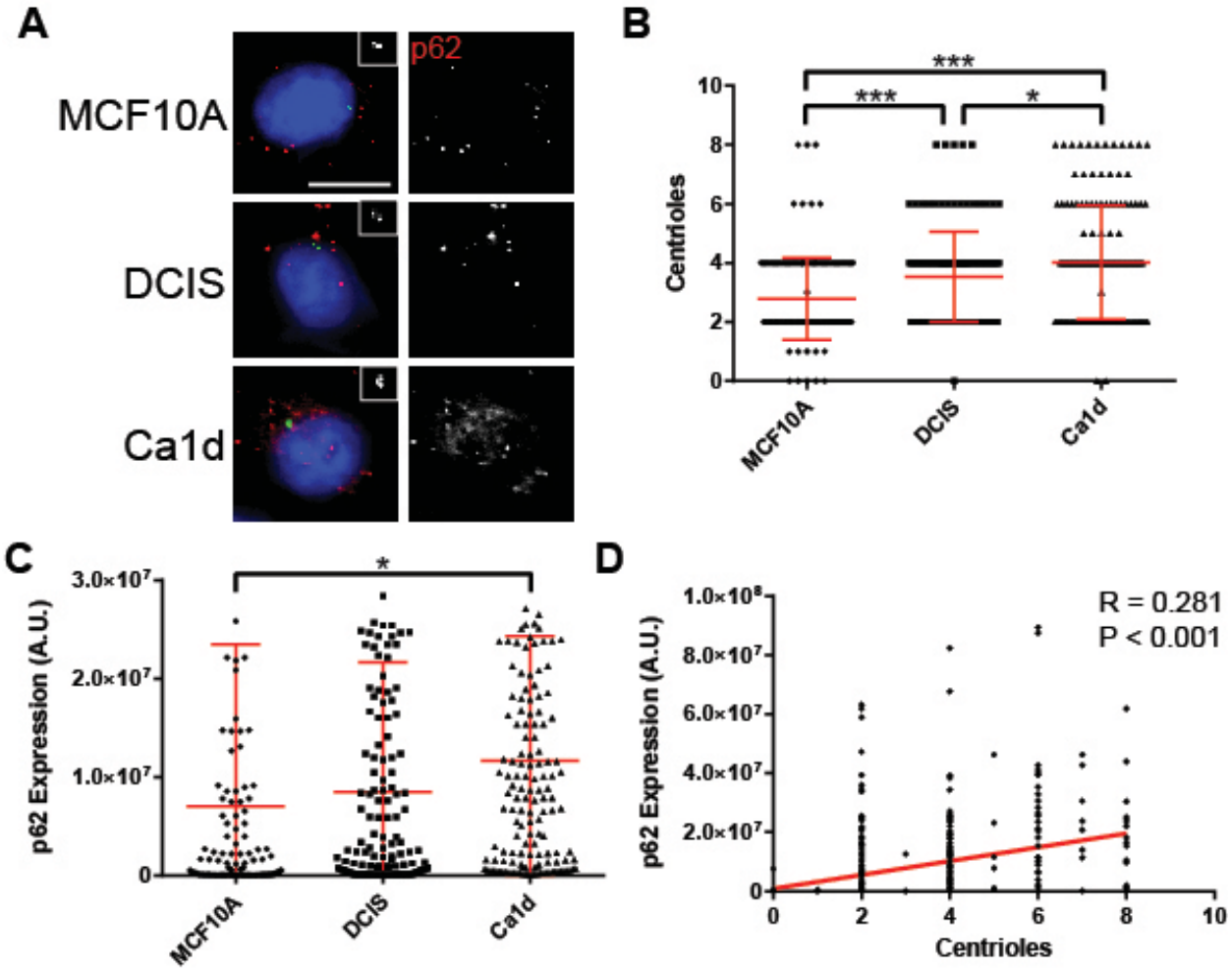
A
MCF10A
DCIS
Ca1d
p62
B
***
***
*
Centrioles
0
2
4
6
8
10
MCF10A
DCIS
Ca1d
C
*
p62 Expression (A.U.)
0
1.0×10⁷
2.0×10⁷
3.0×10⁷
MCF10A
DCIS
Ca1d
D
R = 0.281
P < 0.001
p62 Expression (A.U.)
0
2.0×10⁷
4.0×10⁷
6.0×10⁷
8.0×10⁷
1.0×10⁸
0
2
4
6
8
10
Centrioles

Figure 6-4

Centrosome amplification does not alter autophagosome trafficking.

(A) Diagrammatic representation of three potential hypotheses for disrupted autophagy in cells with centrosome amplification. In the first scenario, an increase in centrosomes generates an increase in lysosomes hubs, as lysosomes tend to cluster around centrosomes. In the second scenario, centrosome amplification causes chromosome missegregation, resulting in aneuploidy and therefore altered stoichiometry of protein complexes, increasing the cell's dependence on autophagy. In the third scenario, centrosome amplification results to a disordered array of microtubules, thereby decreasing the efficiency of transportation of autophagic vesicles in the cell. **(B)** Cells were plated in glass-bottom chamber slides, treated with doxycycline (if indicated), and transduced with baculovirus encoding LC3-RFP to label autophagosomes. Timelapse imaging was used to measure autophagosome trafficking. Following imaging, cells were fixed and stained to assess CA, which is quantified in this panel. **(C)** Quantification of the number of autophagosomes (LC3B punctae) per cell. **(D-F)** Plots of track displacement of LC3-labeled autophagosomes versus total track length and adjacent representative images of autophagosome tracks in RPE WT (D), WT+dox (E), and ΔC+dox (F). **(G)** Table summarizing the percent of cells autophagosomes. **(H)** Quantification of autophagosome track speed. **(I)** Quantification of average track displacement. **(J)** Quantification of average track speed. Dots represent individual cells. Bars represent means ± SD. *P value < 0.05, ***P < 0.001. NS = not significant. ANOVA and t test with Tukey's correction for multiple comparisons were utilized.

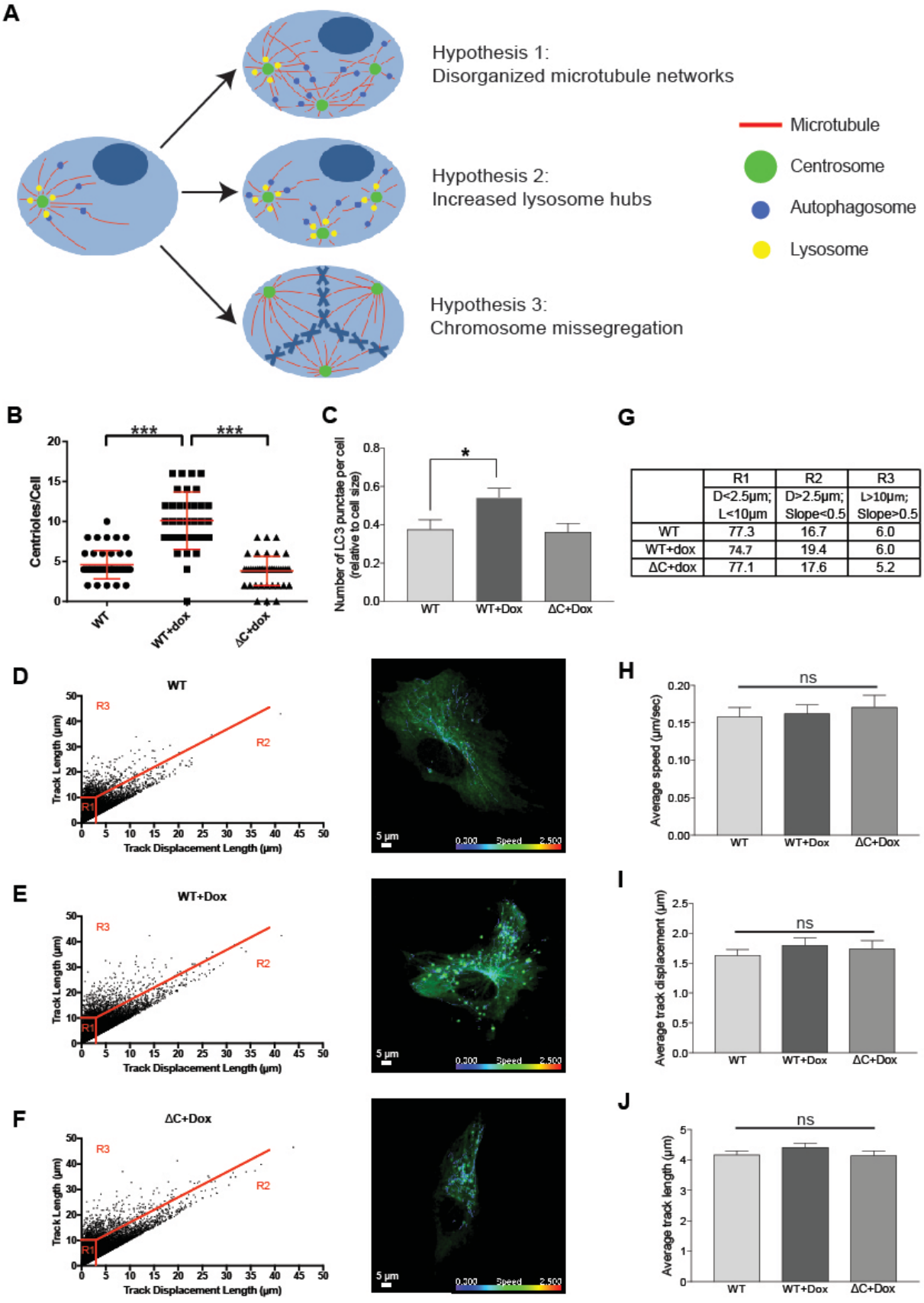
A
Hypothesis 1:
Disorganized microtubule networks
Hypothesis 2:
Increased lysosome hubs
Hypothesis 3:
Chromosome missegregation
Microtubule
Centrosome
Autophagosome
Lysosome
B
Centrioles/Cell
WT
WT+dox
ΔC+dox
C
Number of LC3 punctae per cell (relative to cell size)
WT
WT+Dox
ΔC+Dox
G
R1 D<2.5μm; L<10μm
R2 D>2.5μm; Slope<0.5
R3 L>10μm; Slope>0.5
WT 77.3 16.7 6.0
WT+dox 74.7 19.4 6.0
ΔC+dox 77.1 17.6 5.2
D
WT
E
WT+Dox
F
ΔC+Dox
Track Length (μm)
Track Displacement Length (μm)
R1
R2
R3
5 μm
H
Average speed (μm/sec)
I
Average track displacement (μm)
J
Average track length (μm)
ns

Figure 6-5

Centrosome amplification-mediated autophagy disruption depends on mitosis and disorganized microtubules.

(A) Cells were arrested at the G1/S transition with aphidicolin for 14 hours, then doxycycline was added to overexpress PLK4 and therefore amplify centrosomes. Cell cycle arrest was assessed by staining with propidium iodide and analyzing by flow cytometry. **(B)** Validation by immunofluorescent staining that aphidicolin-arrested cells can still amplify centrosomes when treated with doxycycline. Blue = DNA/DAPI, green = pericentrin. Scale bar = 5 μm. **(C-D)** Dotplots quantifying p62 expression (C) and LC3B expression (D) in RPE and MCF10A cells with or without arrest with aphidicolin. Black dots indicate no aphidicolin treatment, and gray triangles indicate aphidicolin-treated conditions. Dots represent individual cells. Bars represent means ± SD. *P value < 0.05 and NS = not significant when comparing WT+dox to WT and ΔC+dox. Aphidicolin-treated conditions were compared, and non-aphidicolin-treated conditions were compared.

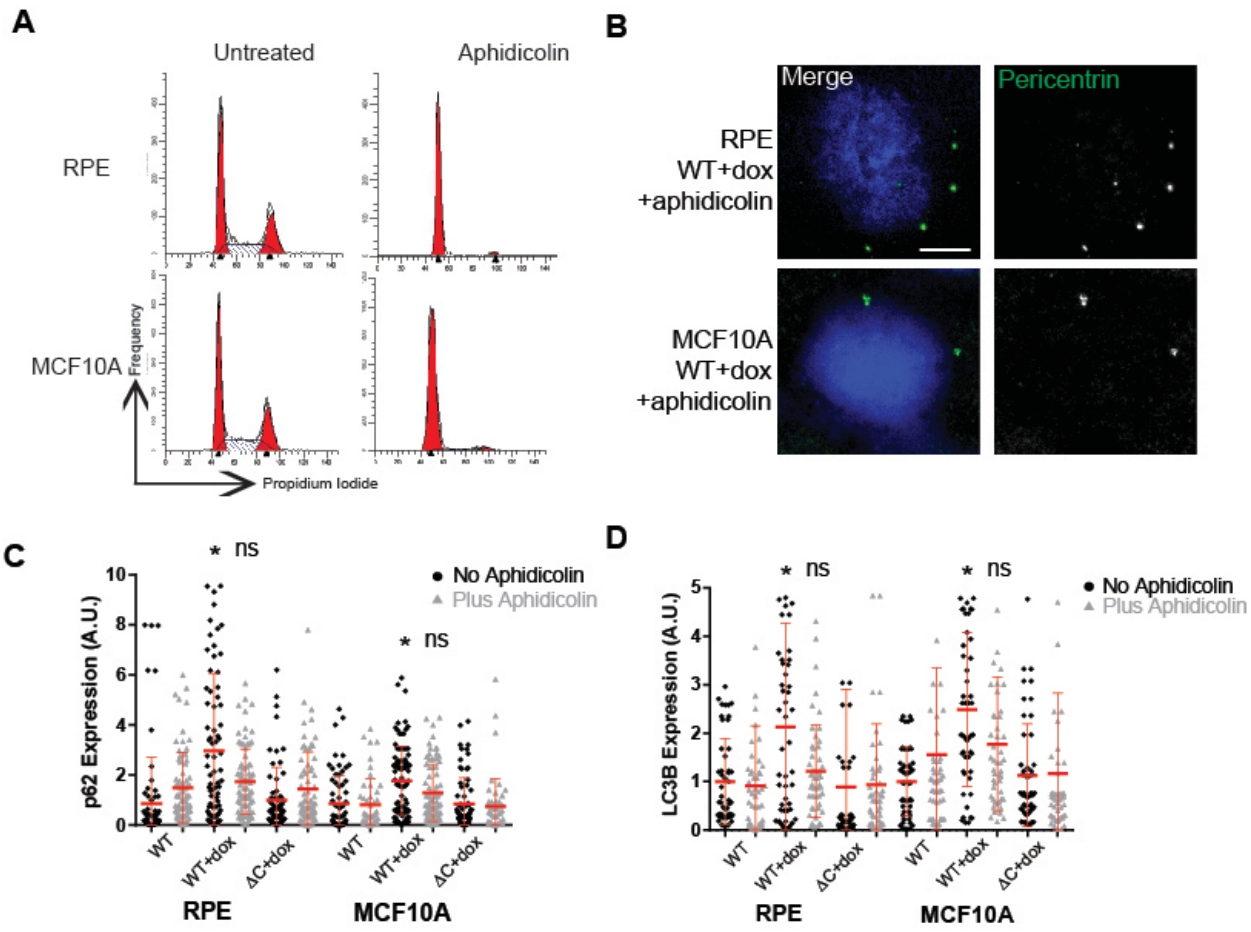
A
Untreated
Aphidicolin
RPE
MCF10A
Frequency
Propidium Iodide
B
Merge
Pericentrin
RPE
WT+dox
+aphidicolin
MCF10A
WT+dox
+aphidicolin
C
p62 Expression (A.U.)
No Aphidicolin
Plus Aphidicolin
* ns
* ns
WT
WT+dox
ΔC+dox
WT
WT+dox
ΔC+dox
RPE
MCF10A
D
LC3B Expression (A.U.)
No Aphidicolin
Plus Aphidicolin
* ns
* ns
WT
WT+dox
ΔC+dox
WT
WT+dox
ΔC+dox
RPE
MCF10A

Figure 6-6

Centrosome amplification sensitizes cells to chloroquine.

(A-B) Cells were pre-treated with doxycycline for 24 hours to induce centrosome amplification, then 1000 cells per well were plated in 96 well plates. Chloroquine was added the next day at the indicated concentrations, then proliferation was assessed 3 days later. **(C)** 5000 cells per well were plated in 24 well plates. Doxycycline was added the next day, followed by chloroquine at the indicated concentration the following day. The plates were stained with crystal violet 5 days after the addition of chloroquine. **(D)** Cell counts were performed using cells treated with 10 μM chloroquine for the indicated time points. **(E)** Apoptosis assays were performed by staining cells with propidium iodide and anti-Annexin V-FITC after 5 days of treatment with 10 μM chloroquine. Cells staining positive for both propidium iodide and Annexin V were considered to be apoptotic. **(F)** Senescence assays were performed by assessing β-galactosidase activity after 5 days of treatment with 10 μM chloroquine. Bars represent means ± SEM. *P value < 0.05.

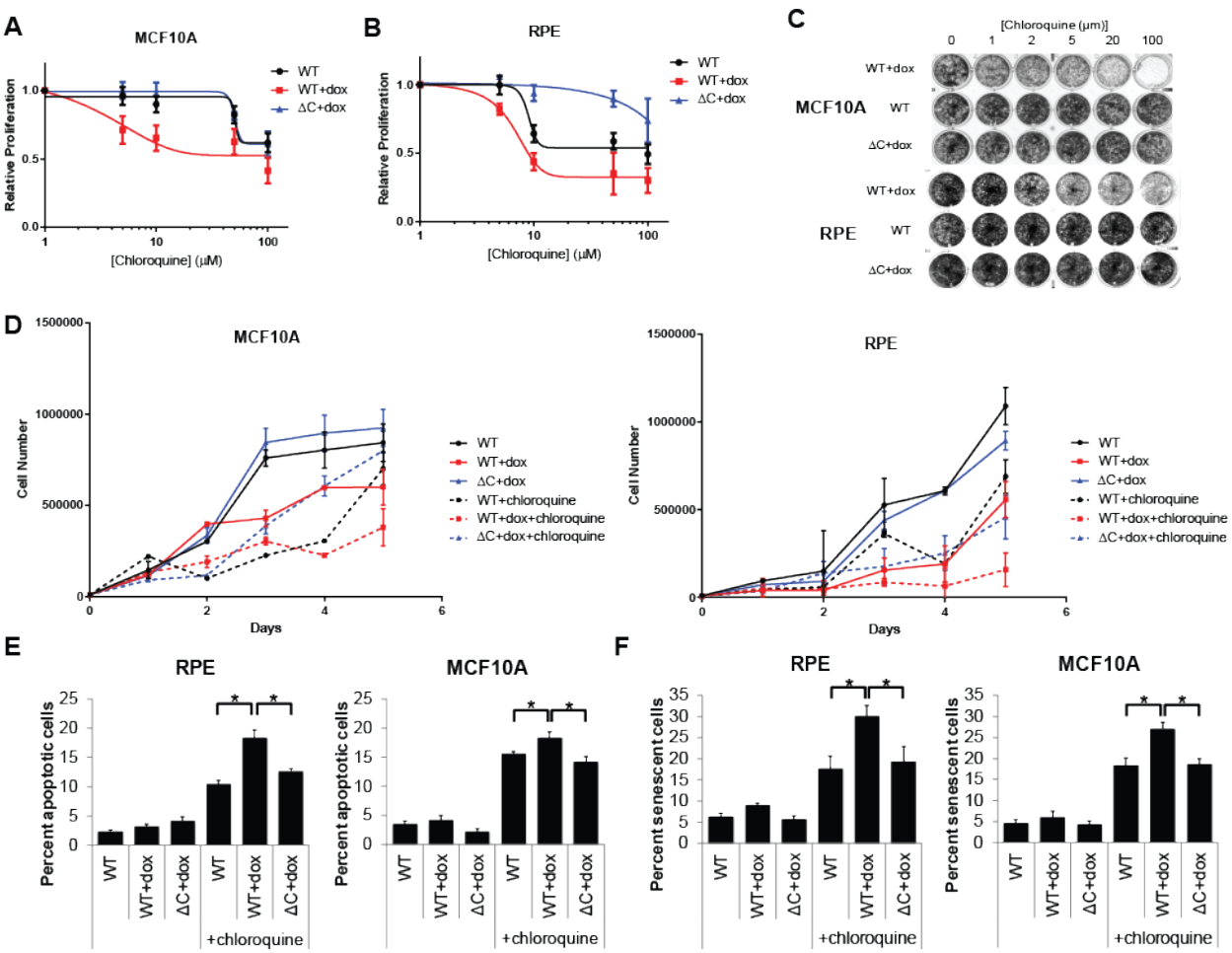
A
MCF10A
Relative Proliferation
[Chloroquine] (μM)
WT
WT+dox
ΔC+dox
B
RPE
Relative Proliferation
[Chloroquine] (μM)
WT
WT+dox
ΔC+dox
C
[Chloroquine (μm)]
0
1
2
5
20
100
WT+dox
MCF10A
WT
ΔC+dox
WT+dox
RPE
WT
ΔC+dox
D
MCF10A
Cell Number
Days
WT
WT+dox
ΔC+dox
WT+chloroquine
WT+dox+chloroquine
ΔC+dox+chloroquine
RPE
Cell Number
Days
WT
WT+dox
ΔC+dox
WT+chloroquine
WT+dox+chloroquine
ΔC+dox+chloroquine
E
RPE
Percent apoptotic cells
WT
WT+dox
ΔC+dox
WT
WT+dox
ΔC+dox
+chloroquine
MCF10A
Percent apoptotic cells
WT
WT+dox
ΔC+dox
WT
WT+dox
ΔC+dox
+chloroquine
F
RPE
Percent senescent cells
WT
WT+dox
ΔC+dox
WT
WT+dox
ΔC+dox
+chloroquine
MCF10A
Percent senescent cells
WT
WT+dox
ΔC+dox
WT
WT+dox
ΔC+dox
+chloroquine

Supplemental Figure 6-1

Validation of centrosome amplification cell models.

(A) Representative images of RPE and MCF10A doxycycline-inducible PLK4 overexpression. Blue = DNA/DAPI, green = centrin. Scale bar = 5 μm. Insets show enlargements of the centrioles (centrin staining). **(B)** Quantification of the percentage of cells with >4 centrioles, assessed by centrin staining. ***P < 0.001.

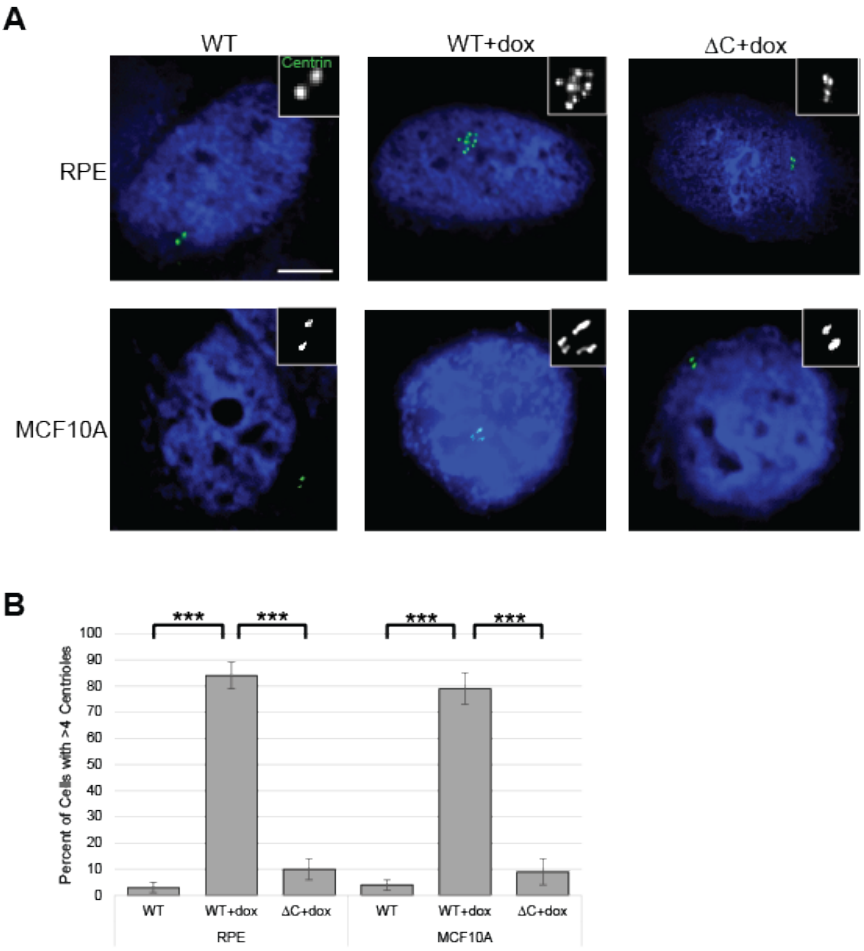

Supplemental Figure 6-2

Centrosome amplification inhibits autophagy. Additional LC3B blots that were used for quantification shown in Figure 1F. Cells were treated with doxycycline (2µg/mL) for 48 hours. To assess autophagic flux, 10 µM chloroquine was added to the cells for 4 hours before harvesting for lysis and blotting. The LC3B-II/I ratio is quantified and displayed below each sample lane. Bands were quantified using ImageJ. The adjacent bar graphs show the percent increase in LC3B-II/LC3B-I ratio after chloroquine treatment for each condition.

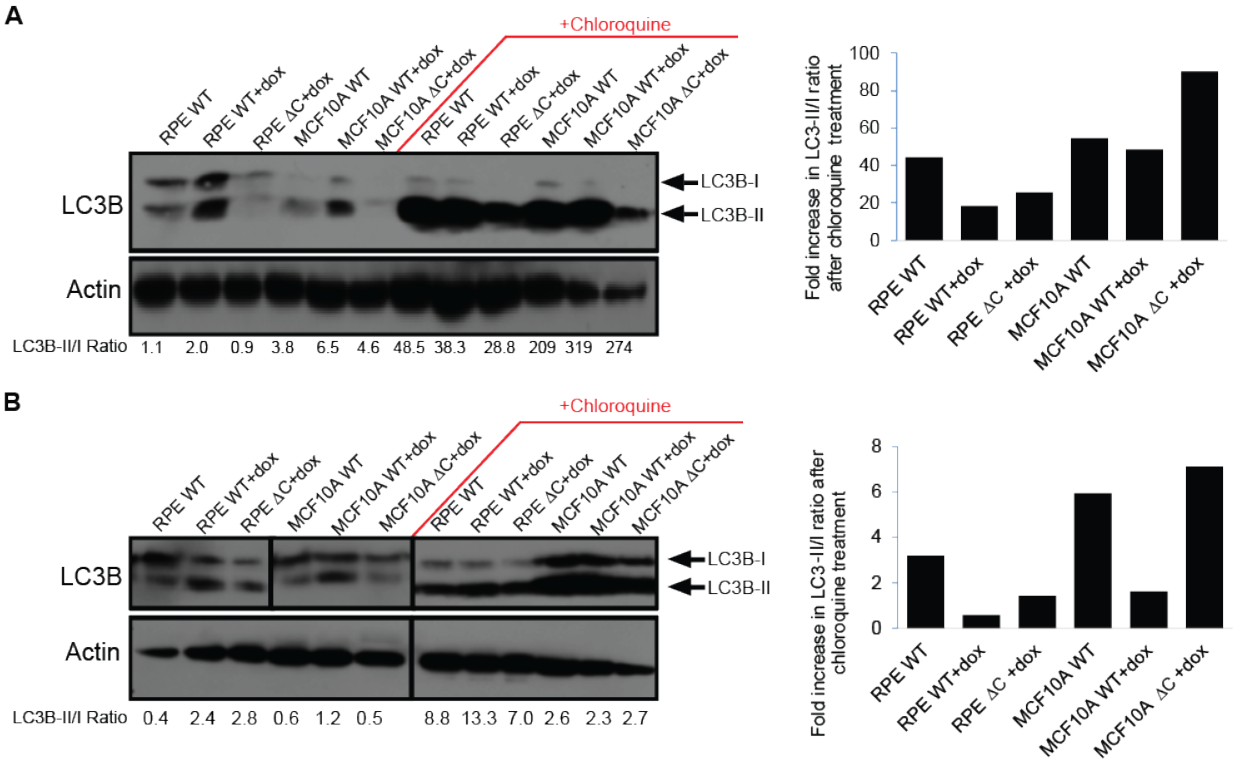

Supplemental Figure 6-3

Centrosome amplification induced by cytokinesis failure and STIL overexpression also inhibits autophagy.

(A) Immunofluorescent images of diploid and tetraploid RPE and MCF10A cells. Blue = DNA/DAPI, green = centrin, red = p62, purple = LC3B. Scale bar = 10 μm. Insets show enlargements of the centrioles (centrin staining). **(B)** Correlation of centriole number with p62 expression. Pearson r = 0.193, P value = 0.127. **(C)** Correlation of centriole number with LC3B expression. Pearson r = 0.240, P value = 0.056. **(D)** Flow cytometry histograms of propidium iodide staining demonstrating diploid and tetraploid MCF10A and RPE cells. Correlation of centriole number with LC3B expression. **(E)** Immunofluorescent images demonstrating STIL overexpression increases centrioles in HeLa cells. As a control, cells were transfected with empty vector. **(F)** Correlation of centriole number with p62 expression. Pearson r = 0.308, P value = 0.002. **(G)** Correlation of centriole number with LC3B expression. Pearson r = 0.216, P value = 0.047.

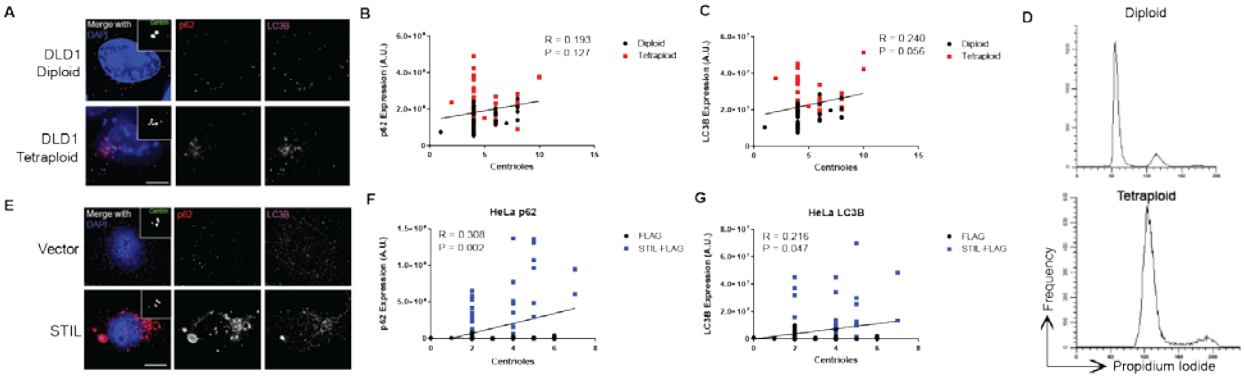

Supplemental Figure 6-4

Centrosomes are important for efficient autophagy.

(A) A PLK4 analog sensitive cell line was employed to demonstrate the importance of the centrosome for autophagy. Treatment of this cell line with 3-MB-PP1 causes loss of centrioles with multiple rounds of cell division. Immunofluorescent images demonstrate the loss of centrosomes with 3-MB-PP1 treatment. AS+DMSO serves as a control for AS cell-line specific effects, and WT/Δ+3-MB-PP1 serves as a control for off-target effects of 3-MB-PP1 and for potential PLK4 haploinsufficiency. Blue = DNA/DAPI, white = pericentrin, green = centrin. Scale bar = 5 μm. **(B)** Quantification of centriole numbers in the analog sensitive cell line compared to a haploid control. Dots represent means ± SEM. **(C)** Quantification of p62 foci (exceeding a predefined threshold) and p62 expression. For p62 expression quantification, we distinguished cells in the AS+3-MB-PP1 condition based on whether centrin and pericentrin staining demonstrated the cell had centrosomes with centrioles. ANOVA P value < 0.001 (not including chloroquine positive control). **(D)** Quantification of p62 expression. ANOVA P value < 0.001 (not including chloroquine positive control). **(E)** Quantification of LC3B expression. ANOVA P value < 0.001 (not including chloroquine positive control). In panels C-E, bars represent means ± SD, and indications are made for statistical significance from Tukey's multiple comparisons tests with the following levels of significance: *P value < 0.05, **P value < 0.01, ***P value < 0.001.

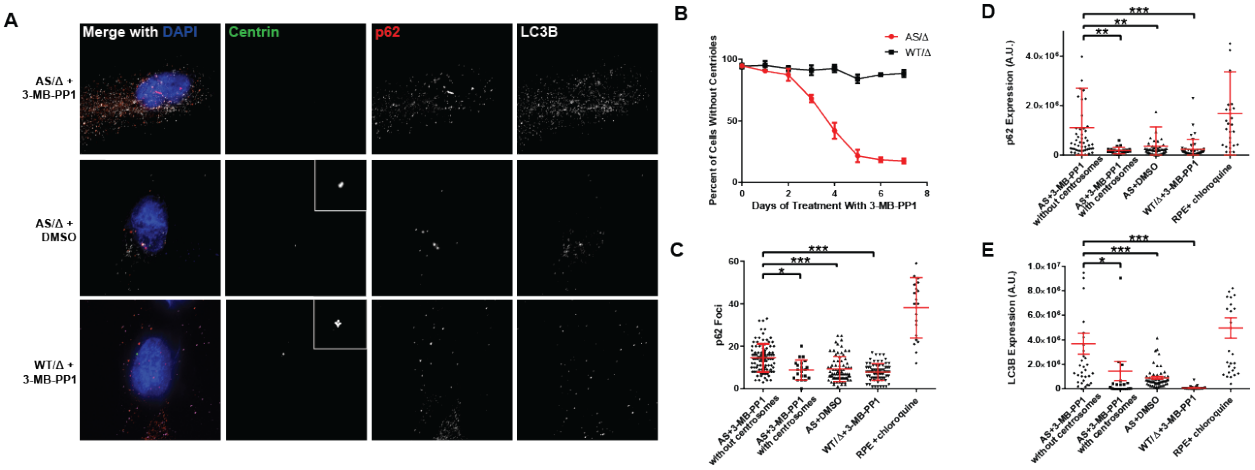
A
Merge with DAPI
Centrin
p62
LC3B
AS/Δ + 3-MB-PP1
AS/Δ + DMSO
WT/Δ + 3-MB-PP1
B
AS/Δ
WT/Δ
Percent of Cells Without Centrioles
Days of Treatment With 3-MB-PP1
C
p62 Foci
AS+3-MB-PP1 without centrosomes
AS+3-MB-PP1 with centrosomes
AS+DMSO
WT/Δ+3-MB-PP1
RPE+ chloroquine
D
p62 Expression (A.U.)
E
LC3B Expression (A.U.)

Supplemental Figure 6-5

Microtubule disruption inhibits autophagy.

(A) Immunofluorescent images demonstrating nocodazole-induced microtubule depolymerization and paclitaxel-induced microtubule stabilization. Cells were treated with 0.2 μg/mL nocodazole or 1μM paclitaxel for 2 hours before fixation. **(B)** Quantification of p62 and LC3B in RPE and MCF10A cells treated with nocodazole and taxol. **(C)** Quantification of p62 and LC3B in RPE and MCF10A cells treated with nocodazole and taxol. **(D)** The LC3B reporter assay was used to assess the effects of nocodazole and taxol on autophagic flux. Representative images are shown. **(E)** Quantification of yellow and red foci in RPE and MCF10A cells treated with nocodazole and taxol. Yellow foci represent autophagosomes, and red foci represent autolysosomes. **(F)** Western blotting for p62 and LC3B in RPE and MCF10A cells treated with nocodazole and taxol. **(G)** Quantification of LC3B-II/LC3B-I values from panel F. Bars represent means ± SD. *P value < 0.05, **P value < 0.01, ***P value < 0.001.

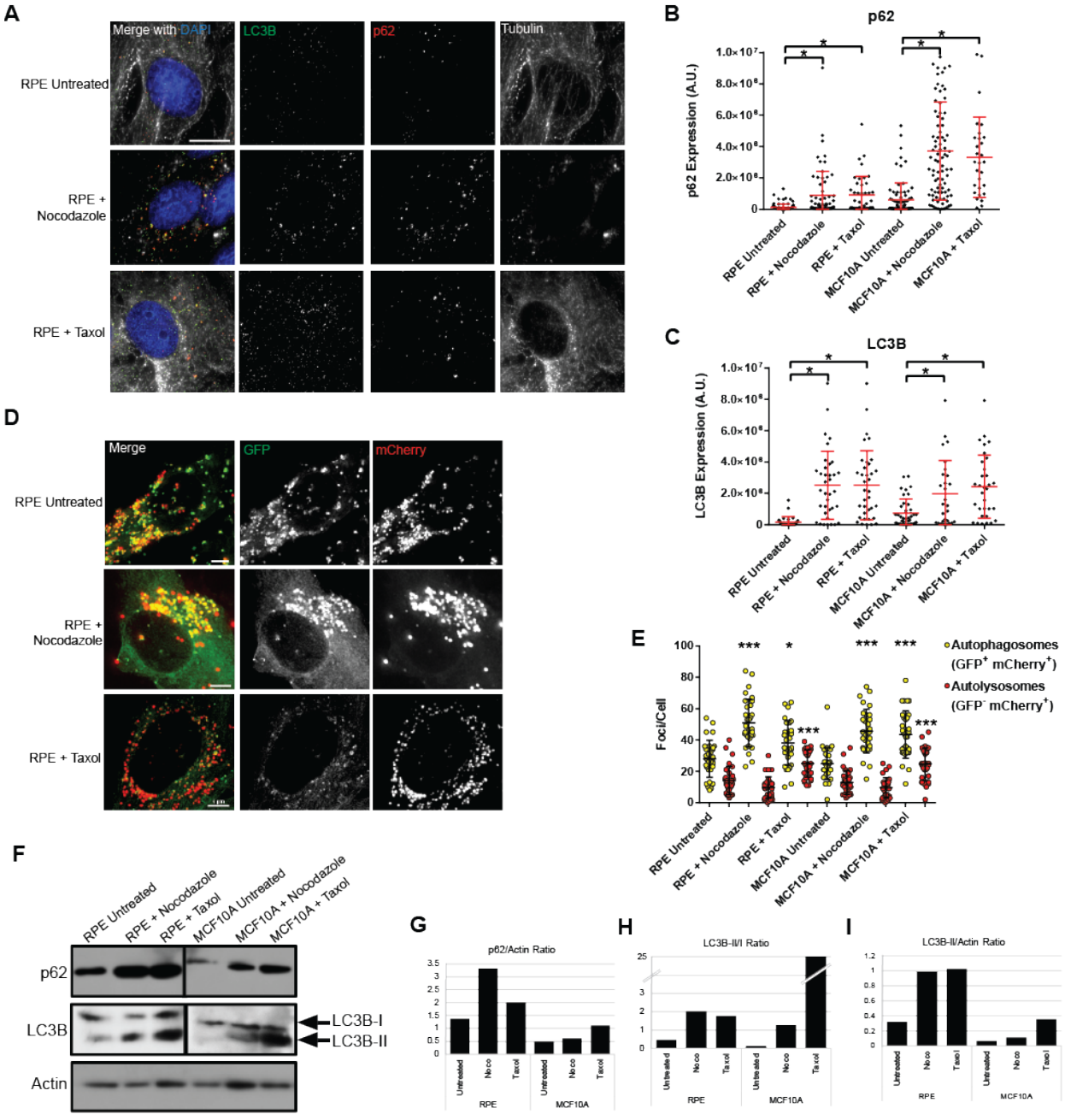
A
Merge with DAPI
LC3B
p62
Tubulin
RPE Untreated
RPE + Nocodazole
RPE + Taxol
B
p62
p62 Expression (A.U.)
RPE Untreated
RPE + Nocodazole
RPE + Taxol
MCF10A Untreated
MCF10A + Nocodazole
MCF10A + Taxol
C
LC3B
LC3B Expression (A.U.)
D
Merge
GFP
mCherry
E
Foci/Cell
Autophagosomes (GFP+ mCherry+)
Autolysosomes (GFP- mCherry+)
F
p62
LC3B
LC3B-I
LC3B-II
Actin
G
p62/Actin Ratio
H
LC3B-II/I Ratio
I
LC3B-II/Actin Ratio
RPE
MCF10A

Supplemental Figure 6-6

Centrosome amplification does not increase lysosomal hubs around the centrosomes.

(A) Representative images of lysosome staining (LAMP1, red) in RPE cells. Centrosomes are labeled in green, and DAPI/DNA in blue. **(B)** Quantification of LAMP1 expression. Each dot indicates one cell. Bars represent means ± SD.

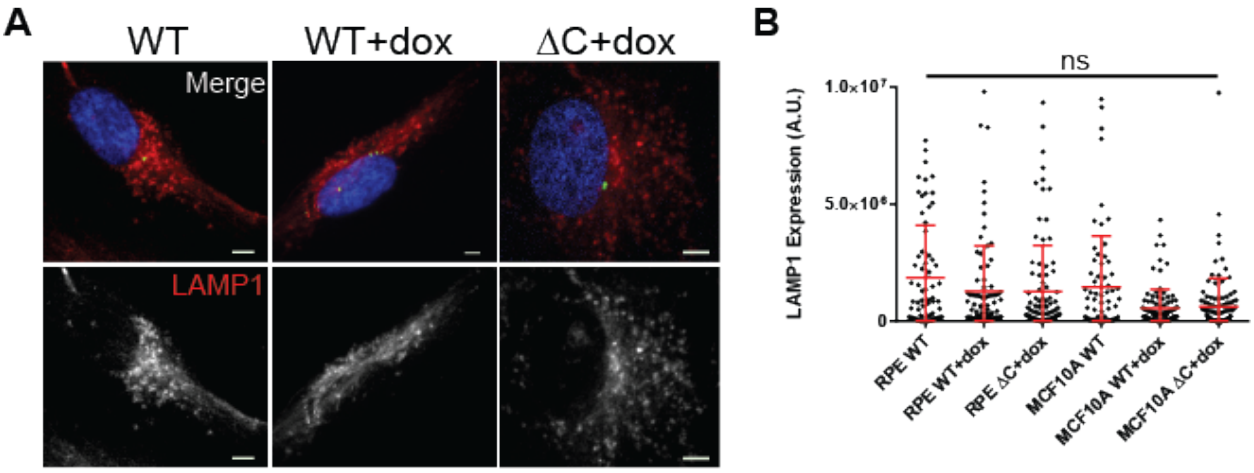

Supplemental Table 6-1

Primer sequences for qRT-PCR.

Gene	Forward Primer (5'-3')	Reverse Primer (5'-3')	Reference
BECN1	CTTACCACAGCCCAGGCGAAAC	GCCAGAGCATGGAGCAGCAA	[399]
ATG5	AACTGAAAGGGAAGCAGAACCA	CCATTTCAGTGGTGTGCCTTC	[399]
SQSTM1	TGAAACACGGACACTTCG	TTCGGATTCTGGCATCTG	[400]
RRN18S	GTAACCCGTTGAACCCCATT	CCATCCAATCGGTAGTAGCG	[109]
GAPDH	GGAGCGAGATCCCTCCAAAAT	GGCTGTTGTCATACTTCTCATGG	[109]
ACTB	CATGTACGTTGCTATCCAGGC	CTCCTTAATGTCACGCACGAT	Harvard Primer Bank ID 4501885a1

Acknowledgements

The authors thank: David Pellman, Jun Wan, Beth Weaver, Patricia Keely, and Peiman Hematti for reagents and use of equipment; Alka Choudhary for technical assistance; the University of Wisconsin Translational Initiatives in Pathology (TRIP) Laboratory; the University of Wisconsin Small Molecule Screening and Synthesis Facility; the University of Wisconsin Carbone Cancer Center Flow Cytometry Laboratory. Research reported in this chapter was supported by the following NIH awards: F30CA203271 to RAD, R01 GM097245 to MEB, University of Wisconsin Carbone Cancer Center Support Grant P30 CA014520. RAD has also been supported by the University of Wisconsin Medical Scientist Training Program (T32GM008692) and University of Wisconsin ICTR TL1 training program (supported under NIH awards UL1TR000427 and TL1TR000429). The content is the responsibility of the authors and does not necessarily represent the views of the NIH.

CHAPTER 7: PLK4 phosphoproteomics identifies CEP131 as a substrate important for centriolar satellite organization

Work in this chapter is in preparation for submission:

Polo-like kinase 4 phosphorylates CEP131 to maintain centriolar satellite integrity

Ryan A. Denu, Madilyn M. Sass, James M. Johnson, Gregory K. Potts, Alka Choudhary, Joshua J. Coon, Mark E. Burkard

Abstract

Polo-like kinase 4 (PLK4) is the master regulator of centriole duplication, but may play additional roles in centrosome function. To identify novel effectors of PLK4 activity, we performed an unbiased multiplex phosphoproteomic screen using an analog sensitive PLK4 RPE-1 human cell line. Using this system, we identified 11,501 phosphopeptides, corresponding to 3711 proteins, of which 2401 were sensitive to PLK4 inhibition. Importantly, our screen identified previously reported PLK4 substrates (CEP152 and PCM1) as well as novel putative centrosome substrates. Several of these new substrates were validated as direct PLK4 substrates through *in vitro* kinase assays. Among them, we identified CEP131/AZI1 S78 as a confirmed direct target of PLK4. CEP131 localizes to centrioles and centriolar satellites and is required for the recruitment of key regulators of centriole duplication, organization of centriolar satellites, and ciliogenesis. Although PLK4 phosphorylation of S78 is dispensable for CEP131 localization, ciliogenesis, and centriole duplication, it is crucial to maintain integrity of centriolar satellites. These satellites are dispersed with impaired phosphorylation of S78 through inhibition of PLK4 or through a non-phosphorylatable mutant of CEP131. Moreover, replacement of endogenous CEP131 with S78D phospho-mimetic mutant promoted aggregation of centriolar satellites. We conclude that PLK4 phosphorylates CEP131 at the S78 residue to help to maintain the integrity of centriolar satellites, which may promote recruitment of key centrosome proteins.

Introduction

The centrosome is the major microtubule organizing center of animal cells and consists of two orthogonal centrioles, which are cylindrical, ninefold symmetric arrays of microtubules that help to organize microtubule nucleation. The presence of centrioles is important for accurate chromosome segregation,[48] primary cilia formation and neural development.[33-35] Centrosomes are associated with centriolar satellites, which are small, dynamic structures surrounding the centrosome. Centriolar satellites are important for the recruitment of proteins involved in microtubule organization,[25], ciliogenesis,[28] and centriole duplication.[26]

Polo-like kinase 4 (PLK4) is required for duplication of centrioles.[62,403] Depletion of PLK4 results in a loss of centrioles due to impaired duplication, whereas overexpression causes overduplication with increased centriole number.[109,126,403] On a molecular level, the formation of a new (daughter) centriole in proximity to the preexisting (maternal) centriole is initiated by CEP152- and CEP192-mediated recruitment[404,405] of PLK4 at the G1/S transition and involves the interactions of several additional centrosomal proteins including SASS6, STIL, CPAP, CEP135, and CP110.[406] After initiation of procentriole formation by PLK4 recruitment, cartwheel formation is initiated. The ninefold symmetric structure of the cartwheel is derived from the intrinsic ninefold symmetry of SAS6 oligomers that form the cartwheel.[14] The next step is elongation. Lastly, the plus end of the centriole is capped by CP110 and associated proteins.[72]

In addition to its well-known role in duplicating centrioles, PLK4 is implicated in other critical roles in centrosome biology independent of its role in centriole duplication, such as ciliogenesis[101,102] and centriolar satellite maintenance.[103] Regarding the latter, PLK4 phosphorylates PCM1 which partly regulates the integrity of centriolar satellite integrity.[103]

These data support a role for PLK4 in other centrosome functions, but a comprehensive list of substrates or functions is not available.

A number of centrosomal PLK4 substrates relevant to highly regulated centriole duplication are known (Table 1). Most notably, PLK4 autophosphorylation results in ubiquitination and subsequent proteasomal degradation,[66,67,70,100] which is critical for limiting PLK4-mediated centriole duplication to once per cell cycle. Effectors such as STIL/Ana2,[64,91,92] SAS6,[93] FBXW5,[94], GCP6,[95] CEP135,[96] CPAP,[97] and CP110[98] are important for centriole duplication. Phosphorylation of the following identified substrates have other roles not related to centriole duplication: PCM1,[103] ARP2,[168] ECT2,[319] and HAND1.[407] Additionally, CEP152,[91,408] CDC25C,[409] CHK2,[410] have been identified as PLK4 substrates, but the role of these phosphorylation events is not well understood. Three previous studies have reported mass spectrometry (MS)-based screens to identify PLK4 substrates and/or interactors. One study purified Plx4 from *Xenopus* egg extracts by affinity chromatography and analyzed its associated binding partners by MS,[408] the second study performed PLK4 BioID to identify proximity interactions,[411] and the third study immunoprecipitated tagged PLK4 from HeLa cells and examined binding partners by MS.[91] To our knowledge, there has not been reported an unbiased MS-based analysis of PLK4 phosphorylation targets. Here, we sought to use a chemical genetic system to perform an unbiased MS-based analysis of PLK4 phosphorylation targets in non-transformed human cells to discover novel substrates of PLK4. We identify CEP131 as a novel substrate of PLK4, and that PLK4 phosphorylation of CEP131 is an important contributor to maintaining centriolar satellite integrity.

Results

Generation of PLK4 analog sensitive cell line

PLK4 is the master regulator of centriole duplication,[62,403] and plays additional roles, but few substrates have been identified. In order to identify new substrates, we engineered a PLK4 conditional knockout cell line and a PLK4 analog sensitive cell line. First, adeno-associated virus (AAV) was used to insert loxP sites around (flox) exons 3 and 4 of one endogenous PLK4 locus. The other genomic locus of PLK4 was deleted, so the genotype of this cell line is $PLK4^{WT/\Delta}$. Two clones were identified and validated by PCR (Supplemental Figure 7-1A-B) and by examining the disappearance of centrosome components by immunofluorescence after treatment with adenoviral Cre (AdCre; Supplemental Figure 7-1C-D). The efficiency of centrosome loss is similar to a previous report of 39% of cells losing centrosomes 2 days after treatment with PLK4 siRNA.[403] As expected in p53 wildtype cells,[157,275] loss of PLK4 significantly reduced colony formation (Supplemental Figure 7-1E).

Next, we used AAV to engineer an analog sensitive (AS) cell line in immortalized, non-transformed RPE-1 cells. We targeted exons 3-4 to generate a point mutation at the conserved gatekeeper residue (L89G), enlarging the ATP-binding pocket for selective inhibition by the bulky ATP analog 3-MB-PP1.[68] We deleted exons 3-4 in the PLK4 locus of PLK4 and screened for edited colonies suing PCR (Supplemental Figure 7-1F-G). The genotype of this cell line is $PLK4^{AS/\Delta}$, which will henceforth be labeled “AS” in the text and figures.

PLK4 inhibition is expected to prevent new centriole assembly without disassembling preexisting centrioles. Consistent with this, inhibition of AS with 3-MB-PP1 for 5 days yields about 65% of cells with fewer than 2 centrioles (Figure 7-1A-B), consistent with previous reports.[157,275]

Loss of centrioles causes cell cycle arrest and subsequent senescence

Coincident with the loss of centrioles, we noted a proliferation defect in the PLK4 AS cells after 5 days incubation in 10 □M 3-MB-PP1 (Figure 7-1C-E). Importantly, the effect was specific to AS cells, as PLK4 WT cells had normal cloning efficiency and proliferated well in the presence of 3-MB-PP1 (Figure 7-1C-E). Further characterization of the proliferation defect revealed cell cycle arrest, but not cell death, as evidenced by negative trypan blue and annexin V staining (Figure 7-1F) and positive β-galactosidase staining (Figure 7-1G). These findings are consistent with previous reports indicating cells lacking centrioles undergo cell cycle arrest, but not apoptosis.[157,275] To summarize, we have generated a PLK4 AS cell line that is specifically inhibited by 3-MB-PP1, resulting in loss of centrioles and cell cycle arrest.

CEP131 is a substrate of PLK4

Next, we utilized our analog sensitive PLK4 model to identify novel substrates of PLK4 to further interrogate PLK4's role in centriole duplication and uncover additional PLK4 functions. To accomplish this, we employed quantitative high resolution mass spectrometry for phosphoproteome analysis of PLK4 AS cells arrested at the G1/S boundary (Figure 7-2A) with or without 3-MB-PP1 challenge for six hours. Isobaric labeling with six-plex TMT tags allowed us to run three replicates each of AS cells with and without 3-MB-PP1 in a single MS experiment.[412-415] We analyzed cells arrested at the G1/S boundary (Figure 7-2A) because centriole duplication occurs at this phase of the cell cycle.[76,406] We identified a total of 11,501 phosphopeptides, corresponding to 3711 proteins, of which 2401 were downregulated by PLK4 inhibition. The most regulated

proteins included proteins such as RUNX1, PTPN12, IL6ST, TRIM3, and SCRIB. Given that none of these proteins are known to localize to the centrosome or play any role in centrosome or microtubule biology, we conclude these are likely indirect hits. We then focused on proteins known to localize to the centrosome, as these are most likely to be direct substrates rather than phosphorylation events controlled indirectly (Figure 2B, Table 2). We considered proteins to be centrosomal if their Uniprot entry mentioned localization to the centrosome, centriole, or minus ends of microtubules or if the protein was identified in a phosphoproteomic screen of purified centrosomes[210] (Figure 7-2C). Many of these peptides had only modest changes, possibly due to the moderating effect of feedback regulation of PLK4 catalytic activity.[68] Two centrosome proteins identified in our screen, CEP152 and PCM1, were previously identified as PLK4 substrates (Table 1), providing credence that this screening approach is valuable for identifying new substrates. From the remaining list, we selected the proteins known to be associated with centriole duplication: CEP131,[26,416] CEP215/CDK5RAP2,[417] CEP350.[418] None of these proteins have been previously identified as PLK4 substrates. Among the potential phosphorylation sites, we identified residues that are evolutionarily conserved: S78 and S89 on CEP131, S1238 on CEP215, and S1648 on CEP350 (Figure 7-2C). To evaluate these as potential phosphorylation sites, we next constructed GST-tagged 13-mer peptide fragments with the serine of interest located centrally (sequences listed in Supplemental Table 2). STIL (S1108 ± 6 amino acids) was used as a positive control.[64] Of the potential fragments identified, only CEP131 S78 produced a positive signal when incubated with WT PLK4 (Figure 7-2E). Importantly, phosphorylation is dramatically reduced when the PLK4 inhibitor, centrinone B,[157] is added to the reaction and abolished when the

fragment is incubated with the kinase-dead PLK4 (K41M) mutant. Moreover, a CEP131 fragment containing the S78A mutation is not phosphorylated (Figure 7-2F). We conclude that CEP131 S78 is directly phosphorylated by PLK4 *in vitro*.

CEP131 S78 phosphorylation is required for centriolar satellite integrity but is dispensable for centriole duplication and ciliogenesis

CEP131 is a component of the centrosome and centriolar satellites and was previously identified as a PLK4 interactor in BioID experiments.[411] CEP131 is known to have three major functions in the cell: centriole duplication, ciliogenesis, and centriolar satellite formation. Moreover, PLK4 activity is implicated in each of these activities.[62,103,403] Therefore, we tested whether PLK4 phosphorylation of CEP131 is required for these functions. To do this, we inhibited PLK4 in RPE-1 AS cells with 3-MB-PP1 and in HeLa cells using centrinone B. As expected, inhibition of PLK4 blocked centriole duplication (Supplemental Figure 2A-B), ciliogenesis (Supplemental Figure 7-2C-D), and centriolar satellite organization (Supplemental Figure 2E-F).

To test if CEP131 S78 phosphorylation is important for any of these three functions, we expressed siRNA-resistant, EGFP-tagged, non-phosphorylatable (S78A) or phospho-mimetic (S78D) CEP131 mutants in HeLa cells. These mutants properly localize to centrioles and centriolar satellites (Figure 7-3A), suggesting that this phosphorylation event is not required for CEP131 localization. Next, we depleted endogenous CEP131 with siRNA (Figure 7-3B). Knockdown-addback efficiency was also assessed by qRT-PCR (Figure 7-3C).

We next analyzed the ability of these cells to duplicate centrioles and nucleate primary cilia. We did not observe defects in centriole numbers among all conditions (Figure 7-3D-E).

With regard to primary cilia formation, CEP131 depleted cells exhibited a reduction in primary cilia formation, consistent with previous reports.[240,419] However, we did not observe defects in primary cilia formation in either the non-phosophorylatable (S78A) or phosphomimetic (S78D) mutant cell lines (Figure 7-3F-G). Combined, these data suggest that PLK4 phosphorylation of CEP131 S78 is dispensable for centriole duplication and primary cilia formation.

PCM1 comprises a structural platform for centriolar satellites[24] and PLK4 phosphorylation of PCM1 is required for proper organization of centriolar satellites.[103] To test if CEP131 S78 phosphorylation is also important for centriolar satellite integrity, we quantified PCM1 as either normal, dispersed, or aggregated, as has been previously reported.[103,420] Nocodazole served as positive control for dispersion.[421] We find that depletion of CEP131 increases the dispersion of centriolar satellites (Figure 7-3H-I). Additionally, addback of WT and S78D CEP131 rescues this phenotype, but addback of the S78A non-phosphorylatable mutant does not rescue this phenotype. Furthermore, we devised a more objective method of quantifying centriolar satellite organization by computing the percentage of PCM1 intensity found within 2.5μm of the center of the centrosome (Figure 7-3J). Similarly, we find that addback of the S78A non-phosphorylatable mutant does not rescue centriolar satellite dispersion (Figure 7-3L). Additionally, addback of the S78D phosphomimetic mutant causes increased aggregation of centriolar satellites (Figure 7-3K). These data support a model where phosphorylation of S78 by PLK4 helps restrain dispersion of centriolar satellites.

CEP131 S78 was previously reported to be phosphorylated in response to ultraviolet (UV) irradiation by mitogen-activated protein kinase-activated protein kinase 2 (known as MK2 or MAPKAP2).[422] In the presence of UV and other cellular stresses, centriolar satellites disperse in a manner dependent on p38-mediated MK2 phosphorylation of CEP131 at both S47 and S78,

thereby allowing 14-3-3 proteins to bind and sequester CEP131 to the cytoplasm. Given our findings, we tested whether PLK4 is important for this stress-induced remodeling. Indeed, p38 is required for this remodeling in response to UV, but PLK4 activity is dispensable (Supplemental Figure 3). This suggests that PLK4 may also regulate centriolar satellite integrity via CEP131 phosphorylation in a similar manner to MK2, albeit under different conditions.

CEP131 is known to enhance CEP152 recruitment to the centrosome. CEP152 then recruits WDR62 and CEP63 and promotes the centrosomal localization of CDK2.[26] We therefore tested whether CEP131 S78 phosphorylation alters the recruitment of CEP152 to the centrosome by quantitative immunofluorescence in our knockdown-depletion experiment. However, we did not observe any differences in CEP152 localization to the centrosome (Supplemental Figure 7-4A).

CEP131 knockout cell lines exhibit reduced centriolar satellite organization and increased sensitivity to nutrient stresses

To assess the effects of chronic loss of endogenous CEP131, we engineered CEP131 knockout cell lines using CRISPR/Cas9 editing. CEP131 is not a lethal gene,[423] and we were able to recover monoclonal CEP131 knockout cell lines. We utilized two different knockout clones for our experiments, denoted KO4E and KO9. We confirmed the knockout cell lines by CEP131 Western blotting (Figure 7-4A) and immunofluorescence (Figure 4B). As expected, these knockout cells had dispersed centriolar satellites, as visualized by PCM1 (Figure 7-4C-D), a decrease in CEP152 expression at the centrosome (Supplemental Figure 7-4B), and an increase in mitotic errors and multinuclei (Figure 7-4E-H), consistent with previous reports.[26,416]

However, no differences were seen in centriole number (Figure 7-4I) or formation of primary cilia (Figure 7-4J-K).

Next, we assessed whether our CEP131 knockout cell lines demonstrated a proliferative defect. Indeed, both knockout cell lines demonstrate slightly reduced proliferation (Figure 7-4L), which has been shown previously by RNAi knockdown of CEP131.[416]

Centriolar satellites are thought to be important for response to cellular stresses.[24,422,424] Therefore, we tested whether our knockout cell lines were more sensitive to nutrient stresses. Indeed, we find that both knockout cell lines are more sensitive to both serum-free media (Figure 7-4M) and 1% serum media (Figure 7-4N), as the CEP131 knockout cell lines demonstrated a greater decrease in cell proliferation in response to these treatments.

Next, we expressed GFP-tagged WT, S78A, and S78D CEP131 constructs in the CEP131 knockout cell lines to assess whether they could rescue centriolar satellite integrity. Only cells with visible GFP signal were analyzed. Consistent with our knockdown-addback experiments, we find that addback of WT and S78D rescues the dispersed satellite phenotype, while addback of the S78A mutant does not rescue centriolar satellite dispersion (Figure 7-4O-Q). Additionally, there is an increase in centriolar satellite aggregation in the S78D addback. To confirm that this effect observed using PCM1 as a centriolar satellite marker is indeed a disruption in centriolar satellite integrity versus other causes (e.g. disruption in CEP131 interaction with PCM1), we assessed centriolar satellites in these same conditions using a different marker of centriolar satellites: CEP72. Similarly, we find that CEP72 is dispersed in CEP131 knockout cells and is rescued by addback of WT or S78D transgenes but not S78A (Figure 7-5).

Next, we assessed whether this aggregation defect observed in S78D mutants is dependent on dynein. Previous reports have demonstrated that PCM1[25,421,425] and CEP131[416]

localization to centriolar satellites is dynein-dependent. We expressed WT CEP131 and CEP131 S78D phospho-mimetic mutant in CEP131 knockout cells and treated with the dynein inhibitor ciliobrevin D. We find that ciliobrevin D causes dispersion of PCM1 and/or accumulation of PCM1 aggregates outside of the centrosome (Supplemental Figure 7-5A-B). Further, treatment with ciliobrevin D in CEP131 knockout cells expressing the S78D mutant significantly reduced the aggregation of PCM1 at the centrosome (Supplemental Figure 7-5C-D). These findings suggest that aggregation of satellites by PLK4 phosphorylation of CEP131 is dynein-dependent.

To demonstrate that these observed effects of CEP131 S78 mutants depend on PLK4 activity, we overexpressed WT, S78A, or S78D constructs and GFP control in WT HeLa cells (Figure 7-6A), treated with the PLK4 inhibitor centrinone B, and observed the effects on centriolar satellite organization by PCM1 immunofluorescence (Figure 7-6B). Consistent with previous findings, we observe that PLK4 inhibition increases dispersion of centriolar satellites, and that the S78D phospho-mimetic mutant is able to rescue the dispersion of centriolar satellites in the presence of PLK4 inhibition (Figure 7-6C-D).

Additive effects of PLK4 phosphorylation of PCM1 and CEP131 on centriolar satellite organization

The effect of PLK4 phosphorylation of CEP131 on centriolar satellite organization is reminiscent of the previously reported effect of PLK4 phosphorylation of PCM1.[103] Therefore, we tested whether these two phosphorylation events cooperate to control centriolar satellite integrity. We overexpressed both phosphomimetic versions of FLAG-CEP131 (S78D) and GFP-PCM1 (S372D) in WT HeLa cells (Figure 7-7A) and treated with centrinone B. We observe an increase in centriolar satellite aggregation in cells co-expressing both CEP131 S78D and PCM1

S372D phospho-mimetic constructs compared to cells expressing just one of these phospho-mimetic constructs (Figure 7-7B-C), suggesting that phosphorylations of both CEP131 and PCM1 by PLK4 are important for centriolar satellite integrity. In summary, PLK4 phosphorylates CEP131 and PCM1 to maintain the integrity of centriolar satellites in interphase (Figure 7-7D).

Discussion

Herein, we have coupled a chemical genetic system of selective PLK4 inhibition and an unbiased, multiplex phosphoproteomic screen to identify novel substrates of PLK4. We identify CEP131 S78 as a substrate of PLK4 and find that PLK4 phosphorylation of this site is important for maintaining the integrity of centriolar satellites in interphase. We speculate that a cellular phosphatase reverses these phosphorylation events prior to the onset of mitosis, and future work will be needed to explore this regulation. Additionally, our phosphoproteomic screen has uncovered many other potential substrates that could be explored.

This is the first study to characterize knockout of PLK4. Previous studies have knocked down PLK4 with RNAi,[62] auxin-inducible degradation,[275] or inhibited PLK4 catalytic activity.[64,157] Consistent with knockdown studies, we find that knockout of PLK4

PLK4 regulates other centrosomal activities independent of centriole duplication, including phosphorylation of PCM1 to maintain centriolar satellite integrity and primary cilia formation,[103] and phosphorylation of CEP135 to regulate its interaction with CEP152 and influence the radial positioning of CEP152 on centrioles.[96] Herein we have contributed to our understanding of one such non-canonical role of PLK4: the organization of centriolar satellites. Centriolar satellites are structures located around the centrosome and are important for proper microtubule nucleation, centrosome assembly, and primary cilia formation.[24,25,421] Our data suggest that PLK4 phosphorylation of both PCM1 and CEP131 is required to maintain centriolar satellite organization and/or integrity. However, PLK4 phosphorylation of CEP131 is dispensable for centriole duplication and primary cilia formation. Given the previously reported findings that intact, functional centriolar satellites and/or their components are important for centriole duplication[26,416] and ciliogenesis,[103,426] it is likely that different methods of centriolar

satellite perturbations affect these pathways differently. It will be important to determine whether it is centriolar satellites or the individual components themselves that are important for these processes.

A number of centriolar satellite components are important for accurate mitosis. For example, we and others[416] have demonstrated that depletion of CEP131 increases multipolar spindles and chromosome missegregation. Given this increase in chromosomal instability with loss of CEP131, it might be suspected that CEP131 is a tumor suppressor. However, data from The Cancer Genome Atlas (TCGA) indicates that genomic deletion of CEP131 or decreased CEP131 gene expression are extremely rare events in cancer and are likely not drivers of chromosomal instability in cancer. Furthermore, increased CEP131 expression has been reported in hepatocellular carcinoma and correlates with worse outcomes.[427] The specific mechanism by which centriolar satellites regulate proper chromosome segregation remains to be elucidated. As the cell enters mitosis, centriolar satellites disperse, and upon completion of mitosis and entry into G1, the satellites reorganize around the centrosome.[27] PLK4 phosphorylation of PCM1 and CEP131 may help regulate the reorganization of centriolar satellites in G1 in preparation for centriole duplication. Previous evidence has suggested that centriolar satellites are required for recruiting many key regulators of centriole duplication to the centrosome. Other possible mechanisms explaining centriolar satellite dispersion at the onset of mitosis include NEK2A kinase-dependent loss of C-NAP1 from the centrosome leading to reduced centriolar satellite density.[331] There may be additional mechanisms of centriolar satellite dispersion in mitosis and reorganization in G1 that remain to be elucidated, and this is an important area of future research. One additional question is why and how do some centriolar satellite proteins remain at the centrosome when centriolar satellites are dispersed in mitosis and with microtubule

depolymerization (e.g. OFD1 and CEP290), while others (e.g. BBS4 and PCM1) do not remain at the centrosome under these conditions.[28] Further work is required to elucidate this mechanism of centriolar satellite dispersion and aggregation during the cell cycle and its functional significance.

Centriolar satellites are also important for response to stresses,[24] such as UV, heat stock, proteotoxic reagents, and nutrient deprivation. In response to serum starvation, MIB1 E3 ubiquitin ligase activity is reduced, which decreases PCM1 and CEP131 ubiquitination.[424] Furthermore, loss of centriolar satellites by depletion of PCM1 sensitizes glioblastoma cells to temozolomide,[428] a DNA alkylating agent commonly used to treat glioblastoma. Further work will be needed to further elucidate these molecular mechanisms regarding centriolar satellites and response to cellular stresses. For example, since PLK4 inhibition causes centriolar satellite dispersion, does PLK4 inhibition also sensitize glioblastoma and other cancer types to temozolomide and other stress-inducing agents? As PLK4 inhibition is a potential strategy to treat cancer,[155,157,208,429] this is an important area of future research. Another stressor, UV light, induces restructuring of centriolar satellites, including the displacement of PCM1, CEP131, CEP290 from satellites.[422,424] Phosphorylation of CEP131 at the S47 and S78 residues by the p38 effector kinase MK2 reduces centriolar satellite dispersion and dissociation of CEP131 from PCM1 in response to UV light.[422] Additionally, this report found that the expression of the both non-phosphorylatable and phospho-mimetic CEP131 transgenes prevented dispersion in response to UV light. Prima facie, this finding that phosphorylation of CEP131 by MK2 allows for centriolar satellite dispersion contradicts with our finding that the S78A non-phosphorylatable mutant causes centriolar satellite dispersion. However, there are several potential explanations for this. The cell lines (U2OS versus HeLa), conditions (UV light versus

PLK4 inhibition), and methods of quantification are different and could explain the reported differences.

CEP131 is thought to be involved in centriole duplication or, at least, controlling centriole numbers. However, one report demonstrated that CEP131 depletion increases centriole numbers,[416] while another report demonstrated that CEP131 depletion decreases centriole numbers.[26] Additional evidence from Cep131-mutant MEFs found no differences in centrin foci or centrosome amplification (percent of cells with >2 gamma tubulin foci).[419] Furthermore, USP9X is a deubiquitinase that was shown to stabilize CEP131. This report also found that USP9X is required for centriole duplication, providing some indirect evidence that CEP131 may be required for centriole duplication.[430] However, herein we demonstrate neither acute nor chronic and neither complete nor incomplete depletion of CEP131 significantly alters centriole numbers.

A limitation of our experiments is that PLK4 has low abundance with rare phosphorylation events, making it particularly challenging to detect lowly abundant substrates. For example, our analysis did not identify some of the previously identified PLK4 substrates, such as STIL and GCP6. Despite this limitation, we detected other known substrates including CEP152 and PCM1, as well as CEP131 which is validated as a direct substrate in biochemical assays. Another limitation of our work is that we narrowly focused our potential substrates (e.g., evolutionary conservation, role in centriole duplication), and these criteria may have been too strict to uncover novel PLK4 functions and substrates.

In summary, we developed a chemical genetic method to interrogate PLK4 signaling and utilized multiplex phosphoproteomics to discover novel substrates of PLK4. We identified CEP131 as a novel substrate of PLK4 and find that PLK4 phosphorylation of CEP131 S78 is

important for proper organization and integrity of centriolar satellites and may help explain the changes seen in centriolar satellite organization during the cell cycle.

Materials and Methods

Generation of PLK4 Conditional Knockout and Analog Sensitive Cell Lines

Gene editing was performed using adeno-associated virus (AAV) in RPE-1 (ATCC, Manassas, VA) an immortalized, non-transformed human epithelial cell line. Procedures for preparation of infectious AAV particles, transduction of RPE-1 cells, and isolation of properly targeted clones was performed as described previously [347,348]. Briefly, a targeting vector was made by inserting a neo cassette surrounded by FRT sites in the intron upstream of exons 3-4 of PLK4, all flanked by loxP sites (Supplemental Figure 1). To generate adenovirus producing this targeting vector, HEK293 cells were transfected with pRC and pHelper. RPE-1 cells were infected with adenovirus collected from the supernatant and subcloned in the presence of G418 (0.4 μg/mL) and screened/verified. This cell line was targeted in two ways: (1) to make a conditional knockout cell line; and (2) to make an analog sensitive cell line. To make the conditional knockout cell line, one copy of PLK4 was deleted by treating with Cre, then cells were re-targeted with the same initial vector (neo cassette, exons 3-4, all flanked by loxP sites). To make the analog sensitive cell line, cells were transfected with pFLIPe to remove the neo cassette, subcloned and re-targeted with the initial targeting vector in which the gatekeeper residue was mutated to a glycine (L89G) to enlarge the ATP binding pocket and genetically encode chemical sensitivity to the bulky ATP analog 3-MB-PP1 [68] (Supplemental Figure 2). The resulting ASflox/WTflox cell lines were treated with Cre and subcloned in the presence G418. Clones were screened by PCR with primers both inside and outside the neo cassette (Supplemental Figure 2). In addition, RNA was isolated from the AS cells, converted to cDNA, exon 3 was PCR-amplified and sequenced to confirm the presence of only the mutant (L89G).

Cell Culture and Assays

All cell lines were propagated at 37 °C in 5% CO_2. RPE-1-derived cell lines were grown in a 1:1 mixture of DMEM and Ham's F-12 medium supplemented with 2.5 mm l-glutamine, with 10% fetal bovine serum and 100 units/mL penicillin-streptomycin. HeLa cells (ATCC) were grown in high glucose DMEM supplemented with 2.5 mm l-glutamine, with 10% fetal bovine serum and 100 units/mL penicillin-streptomycin. For stable retroviral transduction, constructs were co-transfected with a VSV-G envelope plasmid into Phoenix cells. Fresh medium was applied at 24 hours post-transfection, harvested 24 hours later, clarified by centrifugation and filtration through a 0.45 μm membrane to remove cell debris, and diluted 1:1 with complete medium containing 10 μg/mL polybrene. Target cells were infected at 40-60% confluence for 24 hours. Polyclonal transductants were further purified by limiting dilution to obtain individual clones.

To test for a proliferative defect, sub-cloning was performed in presence of 10 μM 3-MB-PP1. Poisson correction was used to determine cloning efficiency. Cellular senescence was assayed using a pH-dependent β-galactosidase staining kit (Cell Signaling Technology) according to the manufacturer's instructions.

Chemicals used in this study include aphidicolin (Sigma), 3-MB-PP1 (Toronto Research Chemicals), doxycycline (Fisher), puromycin (Thermo), SB203580 (p38 inhibitor, MedChem Express), etoposide (obtained from UW Oncology Pharmacy), doxorubicin (Fisher), paclitaxel (Fisher), vincristine (Fisher), thapsigargin (Fisher), tunicamycin (Fisher), chloroquine (Fisher), and bafilomycin A1 (Fisher).

siRNA directed against CEP131 (5′-AGGCCCTCAAGGCCAACAA-3′) was purchased from GE Healthcare, and control siRNA (Universal Negative Control #1) was purchased from Thermo Scientific.

For CEP131 knockdown-addback experiments, HeLa cells were grown to 80-90% confluence in 6-well plates. 2 µg CEP131 cDNA plasmid and 4 µL of 20 µM siRNA were co-transfected simultaneously using lipofectamine 2000 according to the manufacturer's instructions. Cells were given fresh media 4 hours after the transfection. 24 hours after the transfection, cells were either transferred to coverslips for fixation and immunofluorescence or harvested for Western blotting and qRT-PCR.

CRISPR/Cas9

The CRISPR/Cas9 system was used to create CEP131 knockout cell lines in HeLa cells. Four gRNAs targeting CEP131 were cloned into lentiCRISPRv2[431,432] from Feng Zhang (Addgene plasmid #52961). The four guides used were: GCGCTCCGGGACGCTGCCGA, CCGGGACGCTGCCGATGGCC, TTGACTCACCAGCGGGCCCG, GGCACTGGAACTCCGGGCAT. Cutting efficiency of each guide was assessed by surveyor assay (IDT, 706025) following PCR of 600bp fragments from genomic DNA encompassing the guide RNA locus. lentiCRISPRv2 vectors were transfected into HeLa cells using Fugene (Promega). Prior to transfection, media was replaced with serum- and antibiotic-free media. 24 hours after transfection, cells were selected with puromycin (1µg/mL) for 72 hours, then allowed to recover for 24 hours in fresh media. The guide RNA yielding the greatest cutting by surveyor assay (TTGACTCACCAGCGGGCCCG) was transfected again into HeLa cells, which were then subcloned by limiting dilution. Colonies were selected and screened by PCR of the region

flanking the cut site and sequencing. Verification of knockout lines was performed with CEP131 Western blotting and immunofluorescence.

Immunofluorescence (IF) and Microscopy

IF and imaging were carried out as previously described [194,195]. Cells were seeded on glass coverslips in 24-well plates and fixed with 100% ice-cold methanol for 30 minutes. Fixed cells were then blocked for 30 minutes in 3% bovine serum albumin (BSA) and 0.1% triton X-100 in PBS (PBSTx + BSA). Primary antibodies were incubated in PBSTx + BSA for 1 hour at room temperature and washed three times in PBSTx, followed by secondary antibody incubation in PBSTx + BSA for 30 minutes at room temperature and two washes with PBSTx. Cells were counterstained with DAPI and mounted on glass slides with Prolong Gold antifade medium (Invitrogen). Image acquisition was performed on a Nikon Eclipse Ti inverted microscope and Hamamatsu ORCA Flash 4.0 camera. Where indicated in the figure legends, optical sections were taken at 0.2-μm intervals and deconvolved using Nikon Elements. Where appropriate, the observer was blinded to treatment condition during image acquisition and analysis. Images were processed and analyzed using Nikon Elements.

Qualitative analysis of centriolar satellites was performed by categorizing cells as either normal, dispersed, or aggregated, as previously described [103]. Further, quantitative analysis of centriolar satellites was performed by taking Z stack images, deconvolving, and quantifying the percentage of PCM1 or CEP72 intensity within a 2.5 μm radius of the center of the centrosome (identified by gamma tubulin).

Primary antibodies used were: CEP131 (Thermo, PA5-38978, 1:500), CEP72 (Proteintech, 19928-1-AP, 1:500), CEP152 (Bethyl, A302-480A, 1:500), alpha tubulin (Abcam,

ab4074, 1:5000), acetylated tubulin (Santa Cruz, sc-23950, 1:1000), pericentrin (Abcam, ab4448, 1:1000), polyglutamylated tubulin (Adipogen, AG-20B-0020, 1:500), PCM1 (Cell Signaling, 5259, 1:500), centrin (Millipore, 04-1624, 1:500), gamma tubulin (Abcam, ab27074, 1:1000), beta actin (Abcam, ab6276, 1:5000), FLAG (Sigma, F1804, 1:1000), GFP (Invitrogen, A-11120, 1:1000). Alexa Fluor-conjugated secondary antibodies were used at 1:350 (Invitrogen).

Western Blotting

Cells were lysed in buffer (50 mM HEPES, pH 7.5, 100 mM NaCl, 0.5% NP-40, 10% glycerol) containing phosphatase inhibitors (10 mm sodium pyrophosphate, 5 mM β-glycerol phosphate, 50 mm NaF, 0.3 mm Na_3VO_4), 1 mM PMSF, protease inhibitor cocktail (Thermo Scientific), and 1 mm dithiothreitol. Samples were sonicated and heated in SDS buffer. Proteins were separated by SDS-PAGE, transferred to PVDF membrane (Millipore), and blocked for at least 30 minutes in 5% milk and 0.1% Tween 20 in Tris-buffered saline, pH 7.4 (TBST + milk). Membranes were incubated 1 hour at room temperature or overnight at 4° C with primary antibodies diluted in TBST + 5% milk, washed three times with TBST, and incubated for 1 hour at room temperature in secondary antibodies conjugated to horseradish peroxidase in TBST + 5% milk. Membranes were washed and developed with luminol/peroxide (Millipore) and visualized with film.

Antibodies utilized for immunoblotting include: actin (DSHB, JLA20, 1:1000), CEP131 (Thermo, PA5-38978, 1:1000), FLAG (Sigma, F1804, 1:5000), GFP (Invitrogen, A-11120, 1:1000), and alpha tubulin (DSHB, 12G10, 1:1000). HRP-conjugated secondary antibodies were used (Jackson, 1:5000). Relative intensities of bands were calculated using ImageJ from scanned images and normalized to their respective loading control intensity.

Preparation of Samples for Mass Spectrometry

PLK4 AS cells were cultured in T175 plates. At 75% confluence, cells were synchronized at the G1-S phase with aphidicolin (5 μM) for 24 hours. To assess cell cycle, a fraction of cells from MS sample preps were taken for flow cytometry. Cell pellets were fixed in cold 70% EtOH for at least 24 hours, washed once in PBS, and resuspended in PBS with 0.5 mg/mL RNase A and 50 mg/mL propidium iodide. Samples were incubated at 4° C overnight and analyzed on a flow cytometer (FACSCalibur, BD). 3-MB-PP1 (10 μM) was added for the last 6 hours to half of the plates. 3 independent replicates were utilized for each of the 2 conditions. Cells were collected, pelleted, snap frozen in liquid nitrogen and stored at -80°C until ready for lysis. Cell pellets were then lysed in buffer (8 M urea, 50 mM Tris pH 8.0, 100 mM $CaCl_2$) containing dissolved protease and phosphatase inhibitor tablets (Roche) and then sonicated for 20 minutes. Protein concentrations were determined using a BCA kit (Thermo Pierce). Cell lysates were then reduced by addition of dithiothreitol (final concentration of 5 mM), incubated at 37°C for 45 minutes, and alkylated by adding iodoacetamide (15 mM final concentration). Next, lysates were incubated for 45 minutes in the dark at room temperature, and remaining iodoacetamide was quenched by bringing each lysate back to a final 5 mM dithiothreitol concentration. Lysates were diluted to a 1.5 M urea concentration using a 50 mM Tris and 100 mM $CaCl_2$ solution. Trypsin was added to each lysate in a 50:1 (protein: enzyme) ratio and digested overnight at ambient temperature. The six samples were desalted using 100 mg C18 Sep-Paks (Waters) and dried down using a vacuum centrifuge to obtain tryptically digested peptides. 1 mg of peptides for each of the six samples was incubated with 6-plex tandem mass tags (TMT) reagents (Thermo Scientific) for three hours at room temperature. An

aliquot of each sample was mixed in a 1:1 ratio and run on an Orbitrap Elite mass spectrometer (Thermo Scientific) to ensure complete TMT peptide labeling. The 6 samples were mixed in a final 1:1 ratio across all 6 TMT channels and desalted using a 500 mg C18 Sep-Pak (Waters) to produce a single pooled sample containing chemically labeled peptides from all 6 samples. The pooled sample was fractionated using Strong Cation Exchange (SCX) chromatography to produce 12 total peptide fractions, which were subsequently lyophilized and desalted. The resultant 12 peptide fractions were each enriched using Immobilized Metal Affinity Chromatography (IMAC) Ni-NTA magnetic agarose beads (Qiagen), leading to 12 final SCX fractionated enriched phosphopeptide and unenriched peptide fractions. Each fraction was dried down using a vacuum centrifuge and resuspended in 0.2% formic acid for MS analyses.

LC-MS/MS

Each sample was introduced to an Orbitrap Fusion mass spectrometer (Thermo Scientific) during a 90 minute nano-liquid chromatography separation using a nanoAcquity UPLC (Waters). A “Top N” Fusion method was used to analyze eluting peptides, using a 15,000 resolving power survey scan followed by MS/MS scans collected at 15,000 resolving power. Peptides were fragmented using higher-energy collisional dissociation (HCD) at a normalized collision energy of 35%. Phosphopeptide fractions were analyzed with 200 msec maximum injections times for MS scans and 120 msec maximum injection times for MS/MS scans, while unenriched fractions were analyzed with 100 msec maximum injections times for MS scans and 75 msec maximum injection times for MS/MS scans. Only peptides with charge states from +2 to +8 were selected for MS/MS with an exclusion duration of 30 seconds. The 12 phosphopeptide samples were run in duplicate.

MS Data Analysis

Data was searched using Proteome Discoverer 1.4.1.14 (Thermo Fisher) with the Sequest search algorithm. Thermo RAW files were searched against a Homo sapiens target-decoy database (UniProt, downloaded 11/06/2014). Peptide and phosphopeptide datasets were searched using a 50 ppm precursor mass tolerance and 0.02 Da fragment tolerance for b- and y-type ions produced by HCD fragmentation. All fractions were searched with static carbadimomethyl of cysteine residues, static TMT 6-plex modifications of peptide N-termini and lysines, dynamic methionine oxidation, and dynamic TMT 6-plex modification of tyrosine residues. Phosphopeptide fractions were searched with additional dynamic phosphorylation modifications of serine, threonine, and tyrosine residues. Resulting peptide identifications were filtered to 1% false discovery rate (FDR) and exported to tab-delimited text files compatible with the COMPASS software suite.[433] COMPASS calculated the six-plex TMT protein and phosphopeptide quantitation for all the 12 peptide fractions and 12 phosphopeptide fractions. Peptides were mapped back to their parent proteins using COMPASS, and Phospho RS [434] was used to localize phosphorylation to amino acid residues with a fragment tolerance of 0.02 Da automatically considering neutral loss peaks for HCD and considering a maximum of 200 maximum position isoforms per phosphopeptide. The raw 6-plex reporter ion intensities of localized phosphopeptide isoforms were $\log_2$ transformed and normalized against inhibited PLK4 (+3-MB-PP1) to obtain the relative phosphopeptide and protein quantitation for each cell line and condition.

Kinase Assays

The PLK4 kinase domain (amino acids 1–390) of human PLK4 was cloned into pGEX-6P-1 vector (GE Healthcare). The catalytically inactive mutant, K41M, was generated using Phusion site-directed Quikchange mutagenesis. 15-amino acid fragments of the identified potential PLK4 substrates (putative phosphosite ±7 amino acids) were also cloned into pGEX-6P-1. Sequences of these peptides can be found in Supplemental Table 2. Protein was expressed in Rosetta DE3 bacteria, extracted with Glutathione Sepharose 4B (GE Healthcare, 17-0756-01), and eluted by addition of glutathione for the production of the intact GST fusion proteins.

All kinase assay reactions were incubated at 30°C for 30 minutes in buffer (50mM Tris-HCl, pH 7.5, 10mM $MgCl_2$, 0.1mM NaF, 10μM Na_3VO_4) with 1mM DTT, 1μM cold ATP, 2μCi [γ-^{32}P] ATP, 5μg substrate, and 100ng PLK4. Reactions were resolved by SDS-PAGE. Dried gels were exposed to a storage phosphor screen (GE Healthcare), and γ-^{32}P incorporation was visualized by Typhoon TRIO imager (GE Healthcare).

To confirm that CEP131 S78 is a substrate of PLK4, S78A mutant (15 amino acid fragment, as above) was generated using Phusion site-directed mutagenesis, purified, and utilized in kinase assays, as described above.

Molecular Biology

CEP131 cDNA was obtained as a kind gift from Drs. Spencer Collis and Katie Myers (corresponds to Uniprot isoform 2, Q9UPN4-2). Phusion site-directed mutagenesis was used to generate S78A and S78D mutants and to make CEP131 siRNA-resistant (mutated AGGCCCTCAAGGCCAACAA to AAGCATTGAAAGCAAATA).

Quantitative Reverse Transcriptase Polymerase Chain Reaction (qRT-PCR)

RNA was isolated from cells using TRI Reagent (Molecular Research Center) per manufacturer's protocol. DNase treatment was used to remove DNA contamination (Promega). RNA was then converted to cDNA using the Applied Biosystems High Capacity cDNA Reverse Transcription Kit and manufacturer's protocol. Primer sequences are provided in Supplemental Table 7-2. Primers were used at a final concentration of 0.67 μM each, and 25ng cDNA was used per reaction. A StepOne Plus (Applied Biosystems) real-time PCR thermal cycler was used for amplification with iQ SYBR Green Supermix (Bioard) per manufacturer's protocol. Quantification of CEP131 mRNA was normalized to three housekeeping genes (*RRN18S, GAPDH and ACTB*). The $\Delta\Delta C_T$ method was employed to calculate the fold change in expression.[164]

Drug Screening

To assess the sensitivity of CEP131 knockout cell lines to chemicals, 1000 cells/well were plated in 96-well plates and allowed to adhere for 24 hours. Chemicals were added the next day. Four days later, media was removed and cell viability was determined using Vita-Orange Cell Viability Reagent (Biotool) according to the manufacturer's instructions. The Vita-Orange reagent detects metabolically active cells, which linearly correlates with the number of viable cells. Relative proliferation was determined by subtracting absorbance values of wells containing only Vita-Orange reagent from the experimental wells and then normalizing them to untreated control wells for each cell line.

Statistics

Statistical evaluations were performed using Prism software (GraphPad). Two-tailed t-tests and one-way ANOVA were used for comparisons. P-values <0.05 were considered significant for all tests, and designations are made in the figures for statistical significance.

Table 7-1

Previously identified substrates of PLK4.

Gene	Uniprot ID	Other Names and Orthologs	Residue(s)	Protein function	Effect of phosphorylation	Reference
PLK4	O00444	Sak, STK18, ZYG-1, Plx4	T170, S293, T297, S305	Coordinates centriole duplication	Results in ubiquitination and degradation, limiting centriole duplication to once per cell cycle	66-68,70,100,435
FBXW5	Q969U6	F-box/WD repeat-containing protein 5, FBW5,PP3971	S151	Substrate recognition component of both SCF (SKP1-CUL1-F-box protein) and DCX (DDB1-CUL4-X-box) E3 ubiquitin-protein ligase complexes	Prevents its ability to phosphorylate SAS6, keeping SAS6 at the centrosome and enabling centriole duplication	94
TUBGCP6	Q96RT7	GCP6, KIAA1669	Undetermined	Microtubule nucleation	Required for centriole duplication	95
SAS6	Q6UVJ0	SASS6, HsSAS-6, MCPH14	S123 (in C. elegans); phosphorylation has not been determined in mammalian cells	Centriole cartwheel formation	Allows maintenance of SAS6 and emerging centriole	93
HAND1	O96004	BHLHA27, EHAND	T107, S109	Transcription factor that plays an essential role in both trophoblast-giant cells differentiation and in cardiac morphogenesis	Frees HAND1 from the nucleolus, allowing for cell differentiation	407

ECT2	Q9H8V3	Epithelial Cell Transforming 2, ARHGEF31	Undetermined	Guanine nucleotide exchange factor (GEF), facilitates myosin contractile ring formation during cytokinesis	Undetermined	[319]
STIL	Q15468	SCL/TAL1-interrupting locus, SIL, MCPH7, Ana2, SAS5	S1108 and S1116 in human STIL; S318, S365, S370, S373 in Drosophila Ana2	Recruits SAS6, allowing for proper centriole duplication	Allows for SAS6 recruitment	[91,92]
CEP110	O43303	CCP110, CP110, KIAA0419	S98	Centriole duplication, caps mother centriole	Promotes centriole duplication, may stabilize SAS6	[98]
CEP152	O94986	KIAA0912 , MCPH9, SCKL5, MCPH4, asterless, Asl	Undetermined	Scaffold for recruitment of PLK4 and CENPJ	Undetermined	[408]
CDC25C	P30307		Undetermined	Tyrosine protein phosphatase required for progression of the cell cycle	Undetermined	[409]
CHK2	O96017	Checkpoint kinase 2, CHEK2, CDS1, RAD53	Undetermined	DNA damage response and cell-cycle arrest	Undetermined	[410]
PCM1	Q15154	Pericentriolar material 1, PTC4	S372	Centrosome assembly, ciliogenesis, forms centriolar satellites	Required for centriolar satellite formation and ciliogenesis	[103]

CPAP	Q9HC77	Centromere protein J, CENPJ, LAP, LIP1	S595	Recruits centrosome components, inhibits microtubule nucleation from centrosome	Allows for procentriole assembly and centriole elongation	[97]
CEP135	Q66GS9	CEP4, KIAA0635	Undetermined	Centriole duplication, recruitment of centriolar satellite proteins	Allows for recruitment of asterless to centrioles	[96]
ARP2	P61160	ACTR2	T237, T238	Actin organization	Enhances cell motility	[168]
CDC6	Q99741	CDC18L	S30, T527	DNA replication, inhibits centriole duplication	Disrupts CDC6 binding to SAS6, allowing SAS6 to bind STIL	[99]

Table 7-2

Potential centrosome targets of PLK4.

This table displays all the proteins identified in our MS screen that have been shown to localize to the centrosome. The reported phosphosites refer to isoform 1 on Uniprot for each protein.

Centrosome genes	Aliases/ Homologs	Phosphosites Identified in Screen	Previously identified PLK4 substrate?	Involved in centriole duplication?	Ref for centriole duplication involvement (if applicable)	Function
CAMSAP2	CAMSAP1L1, KIAA1078	S970	No	No		Regulates the organization of non-centrosomal microtubules
CEP110	CCP110, CP110, KIAA0419	S366, S372	Yes	Yes	[63,76,436-438]	Negative regulator of centriole length; negative regulator of ciliogenesis in collaboration with CEP97 by capping the mother centriole thereby preventing cilia formation
CEP131	AZI1, KIAA1118, dilatory, DILA	S78, S89, S381	No	Yes	[26,416]	Centriolar satellites, genomic stability, ciliogenesis
CEP152	KIAA0912	S1461	Yes	Yes	[26,201,439]	Scaffold for centriole duplication components (facilitating the interaction of PLK4 and CENPJ)
CEP170	FAM68A, KAB, KIAA0470	S381, S446, S466, S630, S1012, S1019, T1023, S1160, S1165, S1239, S1241, S1522, S1529	No	No		Microtubule organization, centriole elongation, mother centriole marker
CEP170B	FAM68C, KIAA0284	S360, S492, S565, S569, S655, S711	No	No		Microtubule elongation
CEP215	CDK5RAP2, KIAA1633	S1238	No	Yes	[417]	Regulates centrosomal maturation by recruitment of a gamma-tubulin ring complex onto centrosomes. Negative regulator of centriole disengagement (licensing) which maintains centriole engagement and cohesion
CEP250	CEP2, CNAP1	S2322	No	No		Centrosome cohesion

CEP350	CAP350, KIAA0480, GM133	S1648	No	Yes	[440]	Plays an essential role in centriole growth by stabilizing a procentriolar seed composed of at least, SAS S6 and CENPJ. Required for anchoring microtubules to the centrosomes and for the integrity of the microtubule network
CEP41	TSGA14	S99, S333	No	No		Required during ciliogenesis for tubulin glutamylation in cilium
CEP89	CCDC123	S44	No	No		Ciliogenesis, mitochondrial metabolism
CROCC	Rootletin	S483, S488, T492, S494	No	No		Centriole cohesion
MAPRE1		S155, S165	No	No		Involved in spindle function by stabilizing microtubules and anchoring them at centrosomes
MPLKIP	C7orf11, TTDN1	S115, S124	No	No		maintenance of cell cycle integrity
MZT2A	FAM128A, MOZART2A	S152, T141, S139	No	No		Unknown
MZT2B	FAM128B, MOZART2B	S152	No	No		Unknown
NUMA1	NMP22, NUMA	S77, S1225, S1757	No	No		Required for maintenance and establishment of the mitotic spindle poles during symmetric cell divisions, functioning as a tether linking bulk microtubules of the spindle to centrosomes; positioning spindle pole during asymmetric cell division
PCM1		S110, S116, S119, S428, S872, S1287, S1290, S1304	Yes	Yes	[25,103]	Essential for the correct localization of several centrosomal proteins including CEP250, CETN3, PCNT and NEK2. Required to anchor microtubules to the centrosome; ciliogenesis
TTBK2	KIAA0847	T402, S407, S1182	No	No		Ciliogenesis; binding to the distal end of the basal body and promoting the removal of CCP110, which caps the mother centriole, leading to the recruitment of IFT proteins, which build the ciliary axoneme

Figure 7-1

Validation of PLK4 chemical genetic system.

(A) Representative images of cells treated with 10 μM 3-MB-PP1 for 5 days. Individual cells are outlined with dotted lines in the centrin image, and the arrow points to the one cell in the image with centrioles. Scale bar = 5 μm. **(B)** Centrosomes were quantified after treatment with 3-MB-PP1 for the indicated time points. Bars represent the average of 3 biological replicates of 100 cells each ± SEM. **(C)** *PLK4*$^{AS/\Delta}$ and *PLK4*$^{WT/\Delta}$ were subcloned by limiting dilution, and cloning efficiency was assessed using a Poisson correction. **(D)** Proliferation was assessed by culturing cells in the indicated concentration of 3-MB-PP1 for 7 days, then staining with crystal violet. **(E)** 1000 cells were plated per well in a 6-well plate (day -2), and 3-MB-PP1 was added on day 0. Cells were counted every 2 days. Each point represents the average of 3 technical replicates ± SEM. **(F)** Cells were cultured for 7 days with DMSO or 3-MB-PP1, and apoptosis was assessed by both trypan blue exclusion assay and staining with propidium iodide and anti-annexin V followed by flow cytometric detection. The percentage of cells staining negative for both propidium iodide and annexin V are plotted. **(G)** Senescence was assessed by β-galactosidase staining after 14 days of culture with 3-MB-PP1. The micrographs are representative images of the staining, and the bar graphs quantifies the percentage of senescent cells.

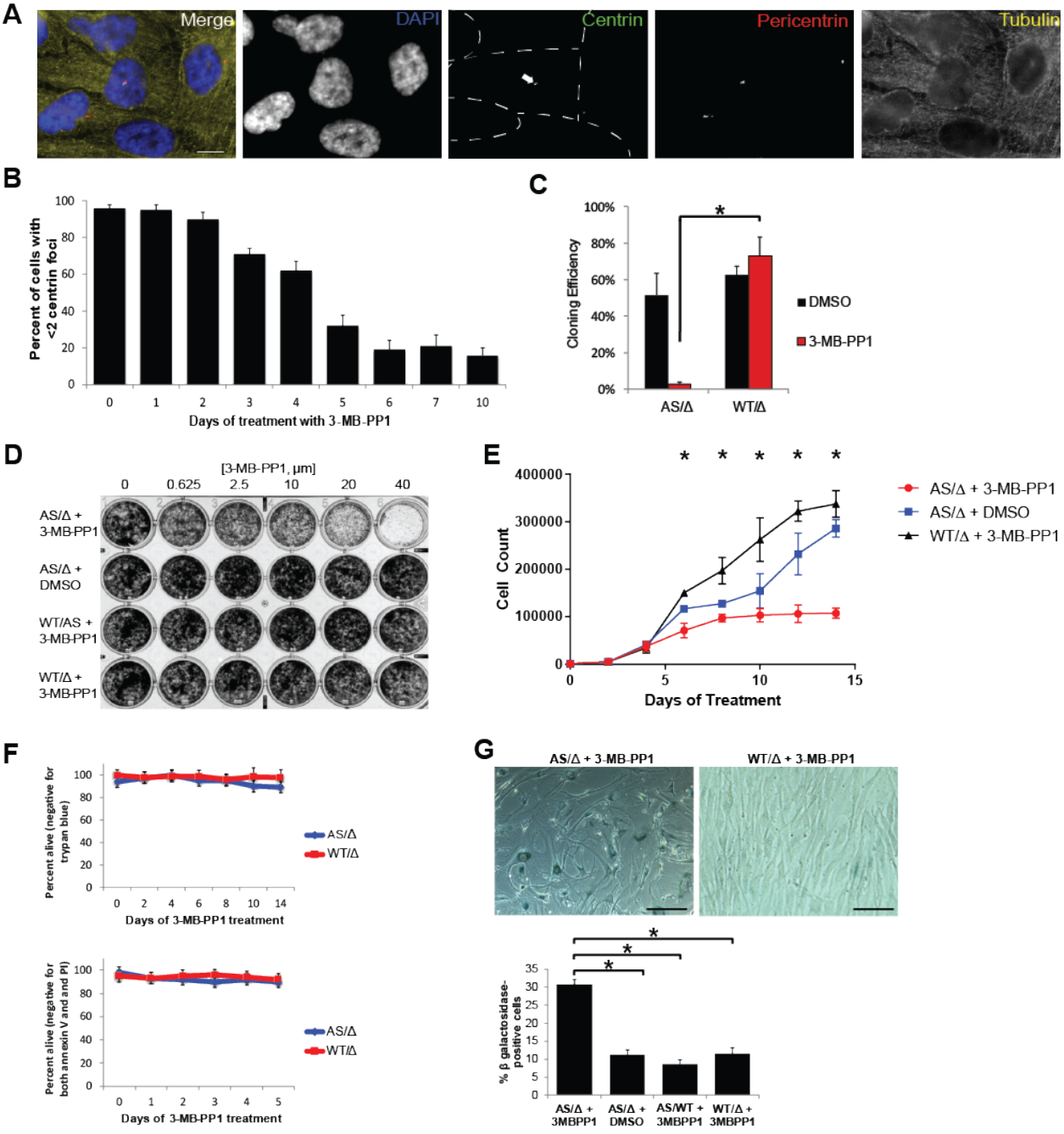
A
Merge
DAPI
Centrin
Pericentrin
Tubulin
B
Percent of cells with <2 centrin foci
Days of treatment with 3-MB-PP1
C
Cloning Efficiency
DMSO
3-MB-PP1
AS/Δ
WT/Δ
D
[3-MB-PP1, μm]
0
0.625
2.5
10
20
40
AS/Δ + 3-MB-PP1
AS/Δ + DMSO
WT/AS + 3-MB-PP1
WT/Δ + 3-MB-PP1
E
Cell Count
Days of Treatment
AS/Δ + 3-MB-PP1
AS/Δ + DMSO
WT/Δ + 3-MB-PP1
F
Percent alive (negative for trypan blue)
Days of 3-MB-PP1 treatment
AS/Δ
WT/Δ
Percent alive (negative for both annexin V and and PI)
Days of 3-MB-PP1 treatment
G
AS/Δ + 3-MB-PP1
WT/Δ + 3-MB-PP1
% β galactosidase-positive cells
AS/Δ + 3MBPP1
AS/Δ + DMSO
AS/WT + 3MBPP1
WT/Δ + 3MBPP1

Figure 7-2

PLK4 phosphorylates CEP131 S78.

(A) Cell cycle profile of cells arrested with aphidicolin to enrich cells in the G1/S transition, which is when centriole duplication occurs and therefore when PLK4 is active. These cells were utilized for mass spectrometry. **(B)** Volcano plot of –log10(p value) versus log2(fold change) for the centrosome components (red dots) that were identified in the MS screen. **(C)** Diagram of the centrosome showing where each of these proteins are thought to localize. Adapted from [441]. **(D)** Alignment of each of the 3 main centrosome hits for which abundance was significantly reduced in 3-MB-PP1 treated cells compared to untreated cells. **(E)** GST-tagged peptides and PLK4 kinase domain were purified from E. coli and utilized for *in vitro* kinase assays. GST serves as a negative control and STIL serves as a positive control. Centrinone B is a PLK4 inhibitor. **(F)** An S78A mutation was created in the CEP131 peptide and purified for *in vitro* kinase assay to confirm that PLK4 phosphorylates CEP131 S78.

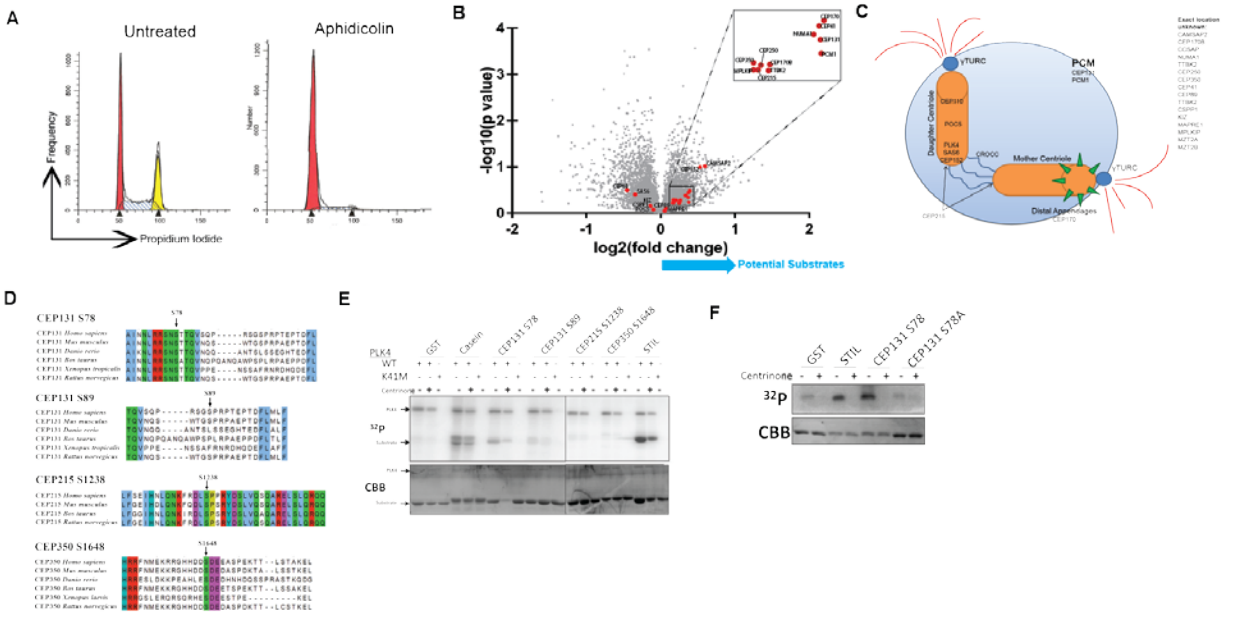

Figure 7-3

PLK4 phosphorylation of CEP131 maintains centriolar satellite integrity.

(A) Localization of WT CEP131, S78A and S78D mutants. The dotted white box is enlarged. Scale bar sizes are indicated on the images. **(B)** Knockdown addback experiment timeline. **(C)** Quantitative RT-PCR experiment demonstrating the efficiency of knockdown and addback of CEP131. **(D-E)** Images and quantification of centriole duplication. Each dot represents one cell, and bars represent means ±SD of at least 100 cells per condition. **(F-G)** Images and quantification of ciliogenesis. Cilia were marked by staining for acetylated tubulin. At least 300 total cells were analyzed per condition. **(H-I)** Images and quantification of centriolar satellites. At least 300 total cells were analyzed per condition. **(J)** Schema of a more quantitative approach to assess centriolar satellites. The yellow circle measures the PCM1 intensity within a 2.5 radius of the center of the centrosome, while the blue circle measures the PCM1 intensity in the entire cell. **(K)** Quantification of centriolar satellites using the schema described in panel J. Nocodazole is used as a positive control for centriolar satellite dispersion. Bars represent means ±SEM from 3 independent experiments. Scale bars = 10μm. *P value < 0.05. NS = not significant.

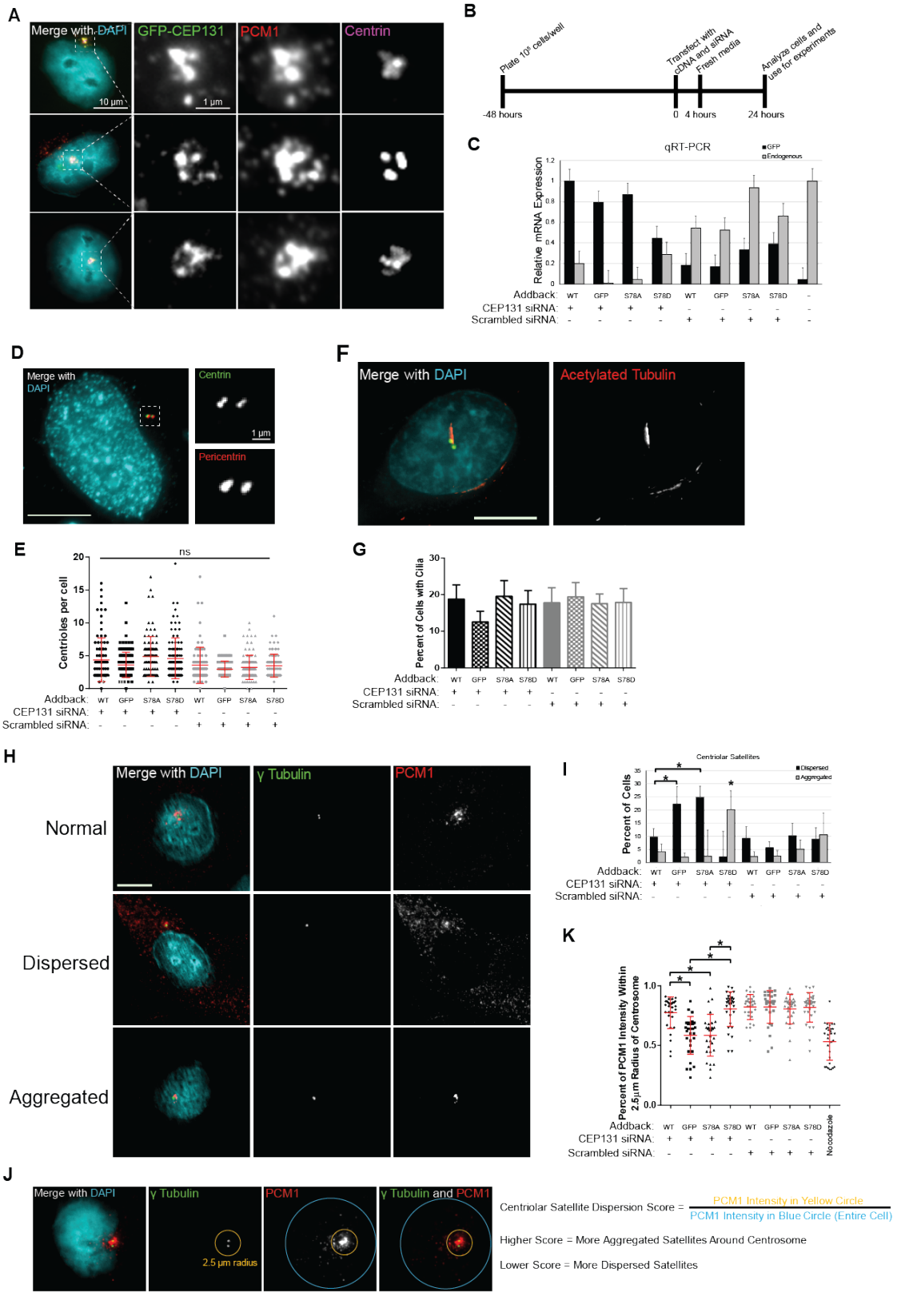
A
Merge with DAPI
GFP-CEP131
PCM1
Centrin
10 µm
1 µm
B
Plate 10⁵ cells/well
Transfect with cDNA and siRNA
Fresh media
Analyze cells and use for experiments
-48 hours
0
4 hours
24 hours
C
qRT-PCR
GFP
Endogenous
Relative mRNA Expression
Addback:
CEP131 siRNA:
Scrambled siRNA:
D
Merge with DAPI
Centrin
Pericentrin
1 µm
E
ns
Centrioles per cell
F
Merge with DAPI
Acetylated Tubulin
G
Percent of Cells with Cilia
H
Merge with DAPI
γ Tubulin
PCM1
Normal
Dispersed
Aggregated
I
Centriolar Satellites
Dispersed
Aggregated
Percent of Cells
K
Percent of PCM1 Intensity Within 2.5µm Radius of Centrosome
Nocodazole
J
Merge with DAPI
γ Tubulin
PCM1
γ Tubulin and PCM1
2.5 µm radius
Centriolar Satellite Dispersion Score = PCM1 Intensity in Yellow Circle / PCM1 Intensity in Blue Circle (Entire Cell)
Higher Score = More Aggregated Satellites Around Centrosome
Lower Score = More Dispersed Satellites

Figure 7-4

Chronic CEP131 depletion causes dispersion of centriolar satellites and is rescued by CEP131 phosphorylation.

(A) CEP131 Western blot in WT HeLa cells compared to two CEP131 knockout cell lines, KO4E and KO9. **(B)** Immunofluorescent images showing loss of CEP131 in the knockout cell lines. **(C)** Immunofluorescent imaging of centrioles and centriolar satellites in the knockout cell lines. **(D)** Quantification of centriolar satellites in WT HeLa cells and the two CEP131 knockout lines. **(E)** HeLa cell lines (WT and CEP131 knockout cell lines KO9) were fixed with methanol, stained, and analyzed. The images depict representatives of the different mitotic phenotypes that were assessed. **(F)** Quantification of metaphase cells as either normal bipolar, multipolar, monopolar, or misaligned (includes polar chromosomes). **P value < 0.01 for 2-way ANOVA interaction. **(G)** Quantification of anaphase cells as either normal bipolar, lagging or bridge chromosomes, or multipolar. **(H)** Quantification of micronuclei and multinucleated cells. *P < 0.05 for 2-way ANOVA with Sidak's multiple comparison test. **(I)** Quantification of centrioles (centrin foci) in WT and CEP131 knockout HeLa lines. **(J)** Representative images of primary cilia in WT and CEP131 knockout HeLa lines. **(K)** Quantification of primary cilia in WT HeLa cells and the two CEP131 knockout lines. Scale bars = 10μm. **(L)** Cell counts over 12 days in WT HeLa cells compared to two CEP131 knockout cell lines. **(M-N)** Proliferation in cells treated with serum-free media **(M)** or with 1% serum **(N).** Proliferation was normalized to untreated cells within each cell line. **(O)** Representative images of centriolar satellites (marked by PCM1) in CEP131 knockout cells transfected with either WT, S78A, or S78D CEP131 transgenes. **(P)** Quantification of the percent of cells with dispersed and aggregated PCM1. **(Q)** Quantification of the percent of PCM1 intensity within a 2.5 μm radius of the center of the

centrosome. Nocodazole is used as a positive control for centriolar satellite dispersion. Bars represent means ±SEM. Scale bars = 10µm. *P value < 0.05, ns = not significant.

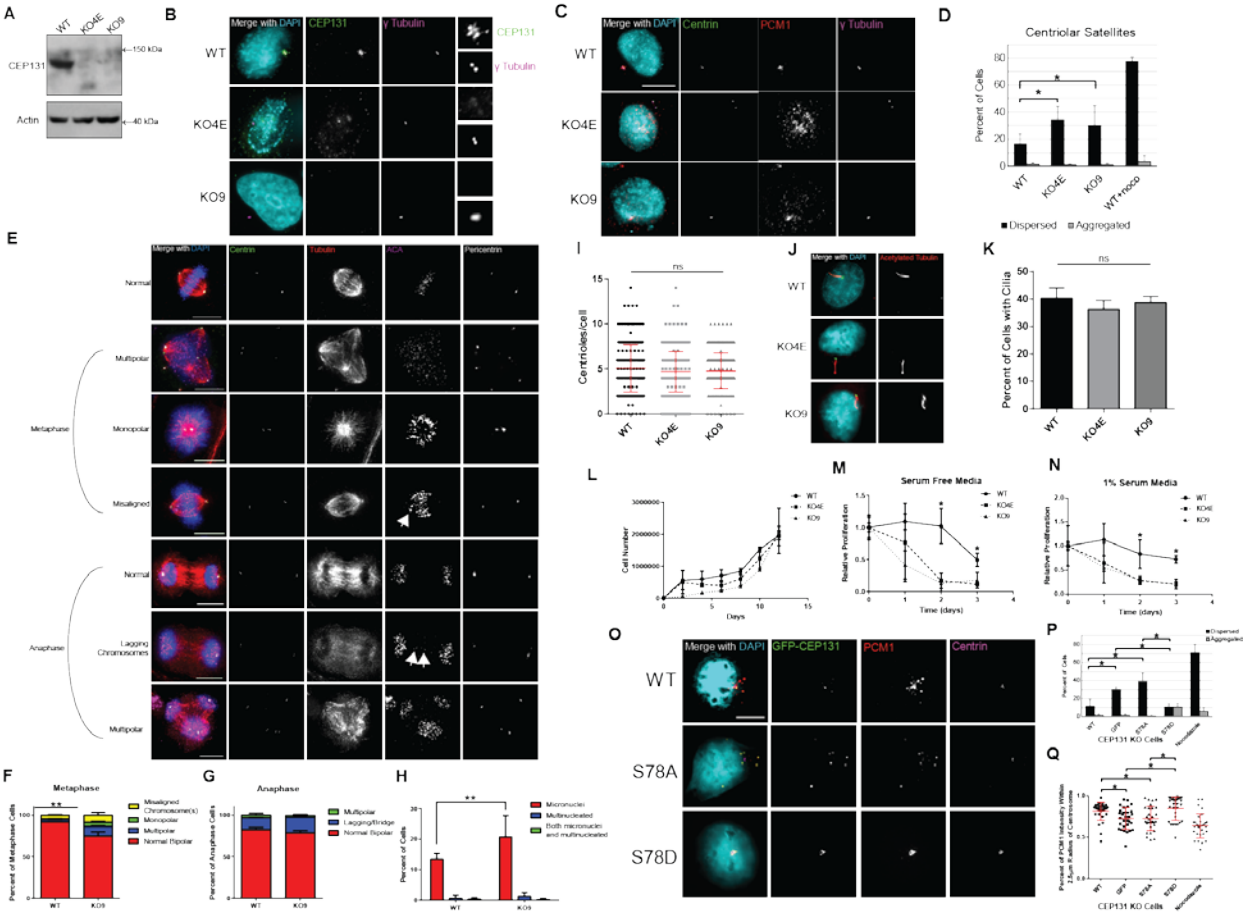

Figure 7-5

CEP72 staining recapitulates regulation of centriolar satellite integrity by CEP131 S78 phosphorylation status.

(A) To ensure that our results regarding PLK4 phosphorylation of CEP131 regulating centriolar satellite integrity were not specific to PCM1, we also analyzed another marker of centriolar satellites, CEP72. Wild type (WT) or CEP131 knockout (KO) HeLa cell lines were transfected with GFP-tagged CEP131 constructs (WT, S78A, S78D) versus GFP-only control. Nocodazole treatment served as a positive control for satellite dispersion. Representative images are shown. **(B)** CEP72 was assessed as either dispersed or aggregated, just as done for PCM1 staining of centriolar satellites in other figures. Bars represent means ±SD from three replicates. Scale bars = 10μm. At least 300 cells were analyzed for each condition. *P value < 0.05.

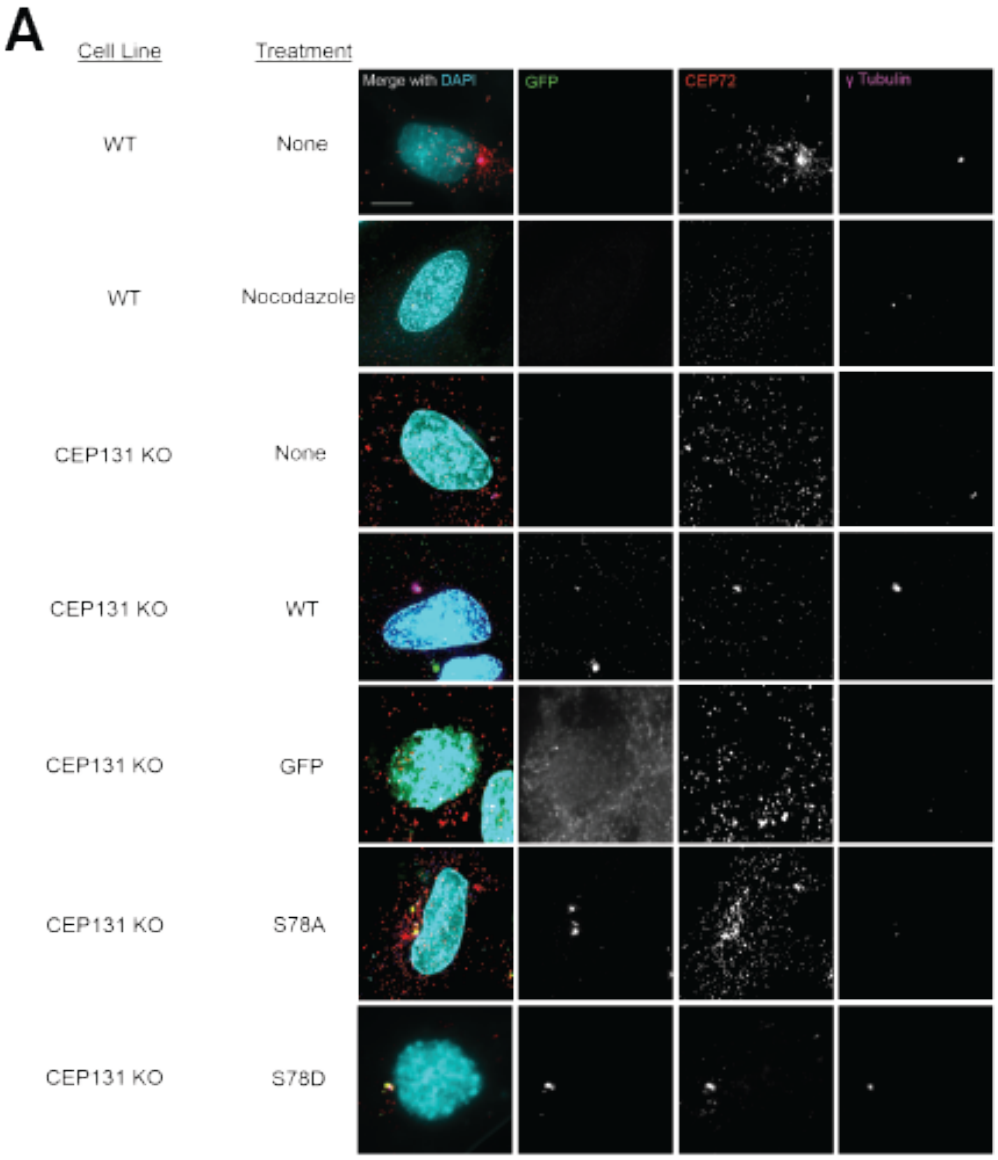
A
Cell Line
Treatment
Merge with DAPI
GFP
CEP72
γ Tubulin
WT
None
WT
Nocodazole
CEP131 KO
None
CEP131 KO
WT
CEP131 KO
GFP
CEP131 KO
S78A
CEP131 KO
S78D

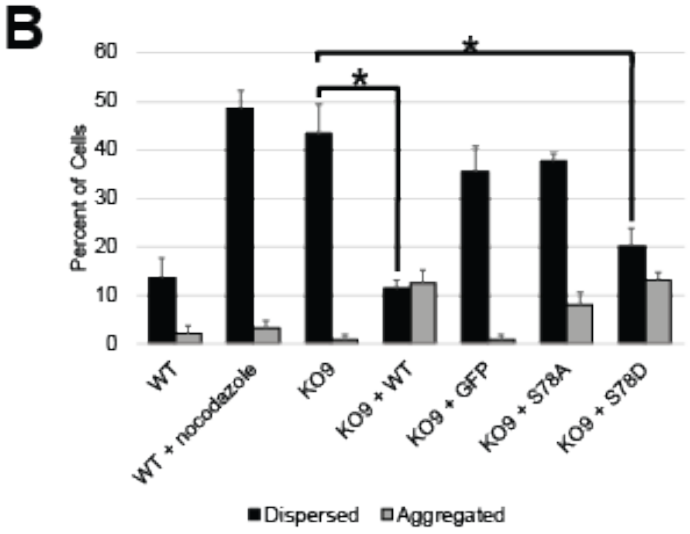
B
Percent of Cells
60
50
40
30
20
10
0
*
*
WT
WT + nocodazole
KO9
KO9 + WT
KO9 + GFP
KO9 + S78A
KO9 + S78D
Dispersed
Aggregated

Figure 7-6

PLK4 phosphorylation of CEP131 at S78 is critical for proper centriolar satellite integrity.

(A) WT HeLa cells were transfected with GFP or GFP-tagged WT CEP131, S78A or S78D mutants. Western blot demonstrating transfection efficiency. **(B)** Images of centriolar satellites in these transfected cells before and after treatment with the PLK4 inhibitor centrinone B. Scale bar = 10µm. **(C)** Qualitative assessment of centriolar satellites as either dispersed or aggregated. **(D)** Quantitative assessment of centriolar satellite dispersion/aggregation. Bars represent means ±SEM. Scale bars = 10µm. *P value < 0.05; **P value < 0.01; *** P value < 0.0001; ns = not significant.

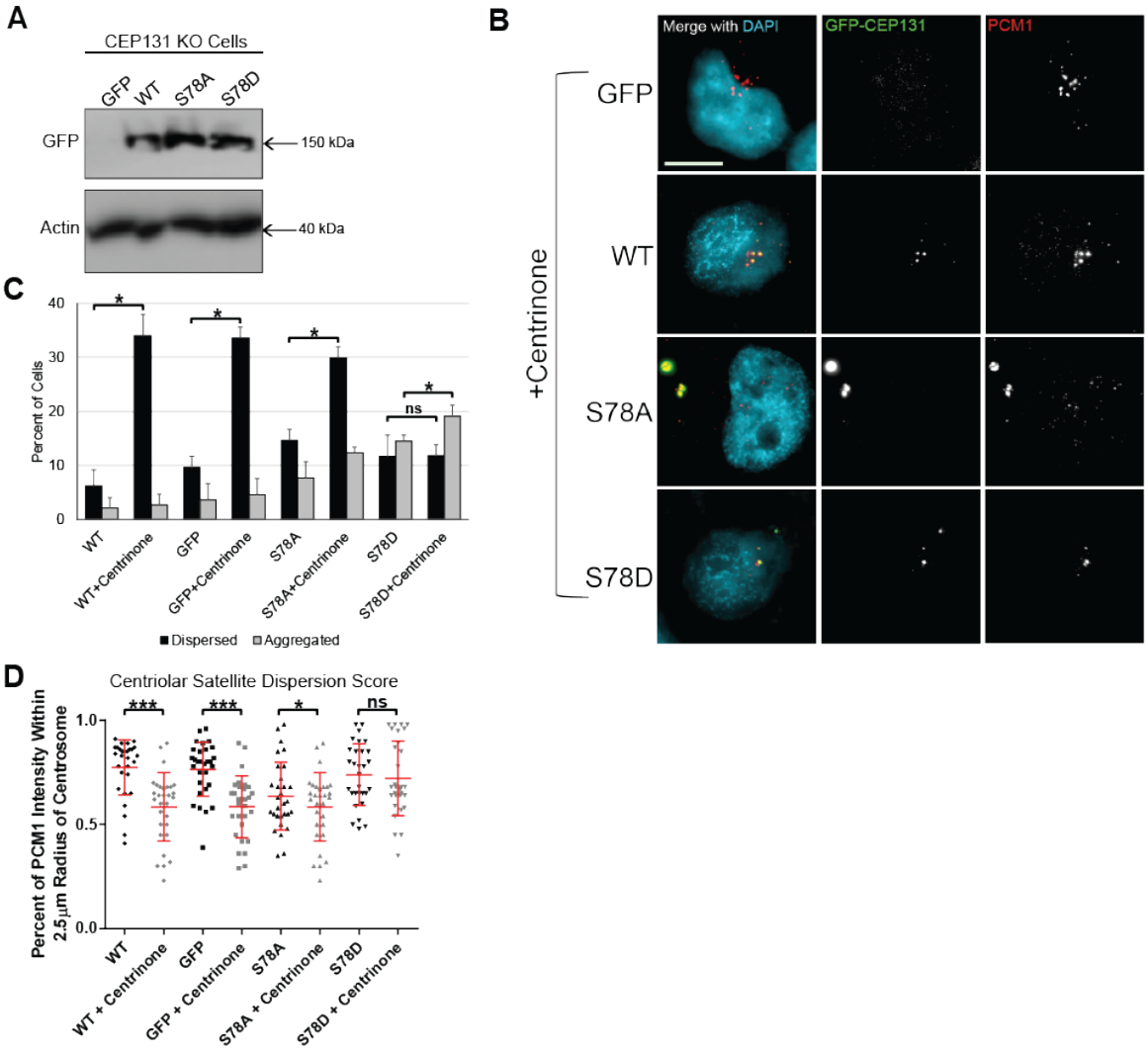
A
CEP131 KO Cells
GFP
WT
S78A
S78D
GFP
150 kDa
Actin
40 kDa
B
Merge with DAPI
GFP-CEP131
PCM1
+Centrinone
GFP
WT
S78A
S78D
C
Percent of Cells
40
30
20
10
0
*
*
*
*
ns
WT
WT+Centrinone
GFP
GFP+Centrinone
S78A
S78A+Centrinone
S78D
S78D+Centrinone
Dispersed
Aggregated
D
Centriolar Satellite Dispersion Score
Percent of PCM1 Intensity Within 2.5μm Radius of Centrosome
1.0
0.5
0.0
***
***
*
ns
WT
WT + Centrinone
GFP
GFP + Centrinone
S78A
S78A + Centrinone
S78D
S78D + Centrinone

Figure 7-7

PLK4 phosphorylation of CEP131 cooperates with its phosphorylation of PCM1.

(A) Western blotting demonstrating transfection efficiency of GFP-PCM1 and FLAG-CEP131 constructs. **(B)** Images of centriolar satellites in the transfected cell before and after PLK4 inhibition with centrinone B. Scale bar = 10µm. **(C)** Quantification of dispersed and aggregated centriolar satellites. *P value < 0.05. **(D)** Diagram summarizing the regulation of centriolar satellite integrity by PLK4 phosphorylation of CEP131 and PCM1.

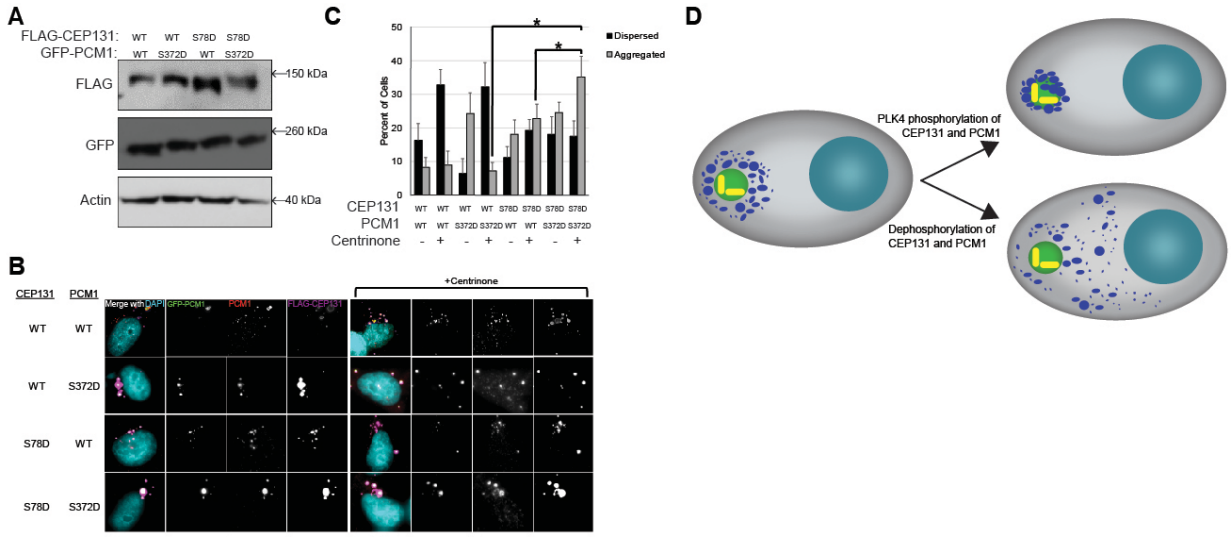

Supplemental Table 7-1

Sequences of peptides used in kinase assays.

Centrosome protein used in kinase assay	Phosphosite	Sequence of purified protein	Phosphorylated by PLK4 in our kinase assays?
CEP131	S78	NLRRSNsTTQVSQ	Yes
CEP131	S78A	NLRRSNATTQVSQ	No
CEP131	S89	SQPRSGsPRPTEP	No
CEP215	S1238	NKFRDLsPPRYDS	No
CEP350	S1648	RGHHDDsDEEASP	No
STIL (positive control)	S1108	RSTVGLsLISPNN	Yes

Supplemental Table 7-2

Primers utilized for qRT-PCR.

Gene	**Forward Primer (5'-3')**	**Reverse Primer (5'-3')**
CEP131 endogenous	CAAGGCCAACAATACTGGTGG	GCTCGGGGCCATCATCTC
GFP	GCATCGACTTCAAGGAGGACG	GTGTTCTGCTGGTAGTGGTCGG
RRN18S	GTAACCCGTTGAACCCCATT	CCATCCAATCGGTAGTAGCG
GAPDH	GGAGCGAGATCCCTCCAAAAT	GGCTGTTGTCATACTTCTCATGG
ACTB	CATGTACGTTGCTATCCAGGC	CTCCTTAATGTCACGCACGAT

Supplemental Figure 7-1

Validation of PLK4 conditional knockout system.

(A) Schematic of the PLK4 gene demonstrating the targeting vector and primer sets used to screen clones. **(B)** PCR reactions using the two primer sets diagrammed in (A). **(C)** Two cell lines of genotype fn/f were treated with AdCre and fixed 14 days later. To assess for centrioles and centrosomes, the cells were probed with the indicated antibodies, and counterstained with DAPI. **(D)** The indicated centrosome markers were counted in the same cells used in C to assess the efficiency of centriole loss after AdCre treatment. **(E)** Proliferation was assessed in these $PLK4^{floxneo/flox}$ cell lines by crystal violet staining. The indicated number of cells were plated and treated with adenovirus expressing Cre recombinase (AdCre) or GFP control (AdGFP). Staining was performed 5 days later. **(F)** The genotype of the PLK4 AS line was validated by PCR screening using the indicated primers. **(G)** Surface representations for crystal structures of PLK4 (PDB: 4YUR) were visualized using PyMol software where nitrogen, oxygen, sulfur, and carbon atoms are shown in dark blue, red, yellow, and light blue or green respectively. The mutagenesis function of PyMol was used to model the effects of a glycine substitution at leucine 89 on the surface of the ATP binding pocket. Where the carbon atoms of L89 are colored in green, changing that residue to a glycine, shown in light blue, enlarges the exposed surface area.

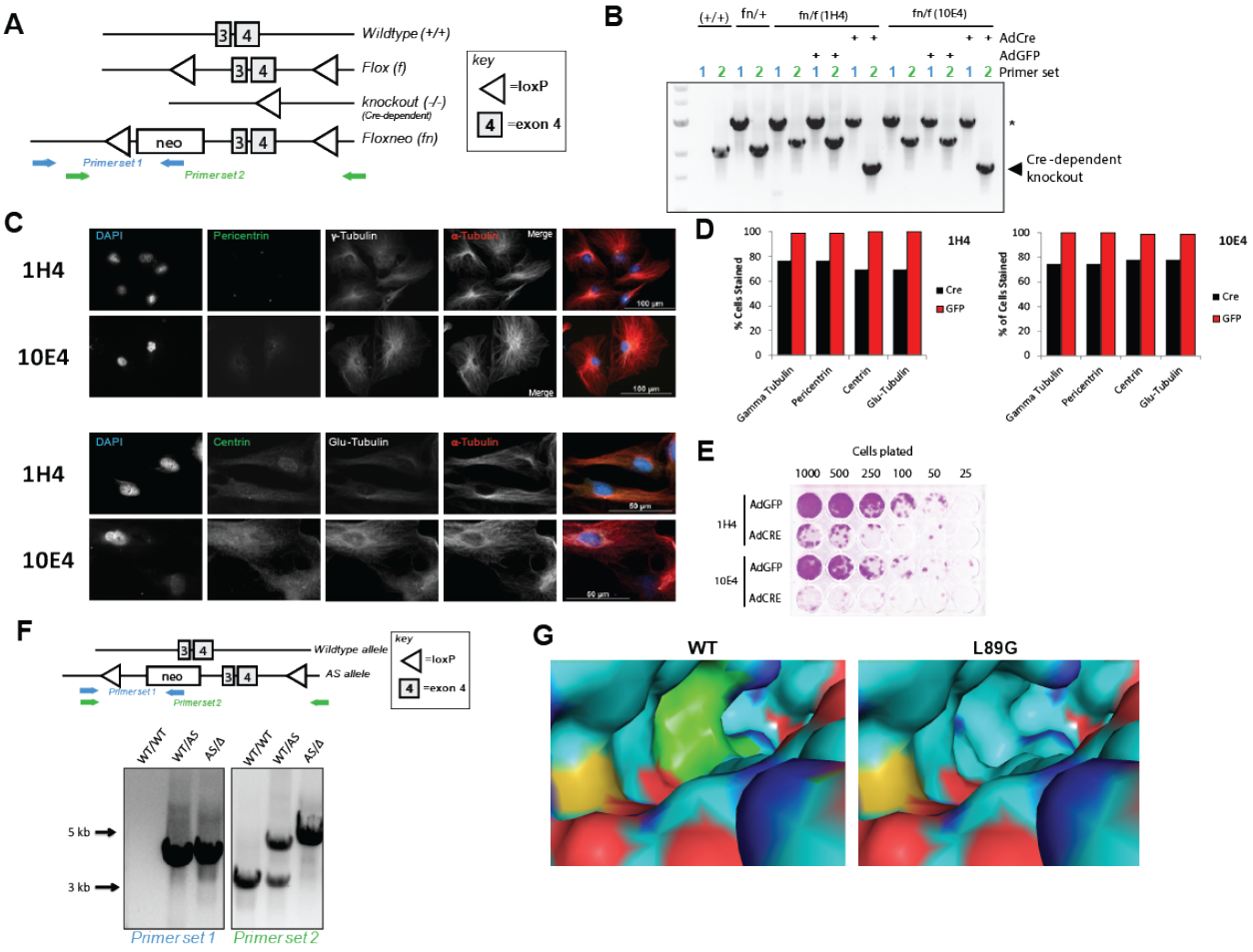
A
Wildtype (+/+)
Flox (fl)
knockout (-/-)
(Cre-dependent)
Floxneo (fn)
neo
Primer set 1
Primer set 2
key
=loxP
=exon 4
B
(+/+)
fn/+
fn/f (1H4)
fn/f (10E4)
AdCre
AdGFP
Primer set
Cre-dependent knockout
C
1H4
10E4
DAPI
Pericentrin
γ-Tubulin
α-Tubulin
Merge
Centrin
Glu-Tubulin
D
1H4
10E4
% Cells Stained
Cre
GFP
Gamma Tubulin
Pericentrin
Centrin
Glu-Tubulin
E
Cells plated
1000 500 250 100 50 25
AdGFP
AdCRE
F
Wildtype allele
AS allele
WT/WT
WT/AS
AS/Δ
5 kb
3 kb
Primer set 1
Primer set 2
G
WT
L89G

Supplemental Figure 7-2

PLK4 activity is required for centriole duplication, centriolar satellite integrity, and ciliogenesis.

(A) Representative images of AS and HeLa cells with and without PLK4 inhibition. AS cells were treated with 3-MB-PP1, and HeLa cells were treated with centrinone B. Blue = DAPI, green = centrin. Centrosomes are enlarged in the inset images. **(B)** Quantification of cells. Each dot represents an independent experiment with at least 50 cells per experiment. Bars represent means ±SEM. **(C)** Representative images of ciliated and non-ciliated AS and HeLa cells. Blue = DAPI, green = γ-tubulin (centrosome marker), red = acetylated tubulin (primary cilium marker). **(D)** Quantification of primary cilia formation. Cells were treated with serum-free media for 48 hours and subsequently fixed, stained, and assessed for primary cilia formation. 3-MB-PP1 and centrinone were added at the time of serum-free media addition. Cells with complete media (10% serum) were used as negative controls. Each dot represents an independent experiment with at least 100 cells per experiment. Bars represent means ±SEM. **(E)** Representative images of centriolar satellites (PCM1). **(F)** Quantification of the percent of cells with dispersed or aggregated centriolar satellites. *P value < 0.05; **P value < 0.01; *** P value < 0.0001.

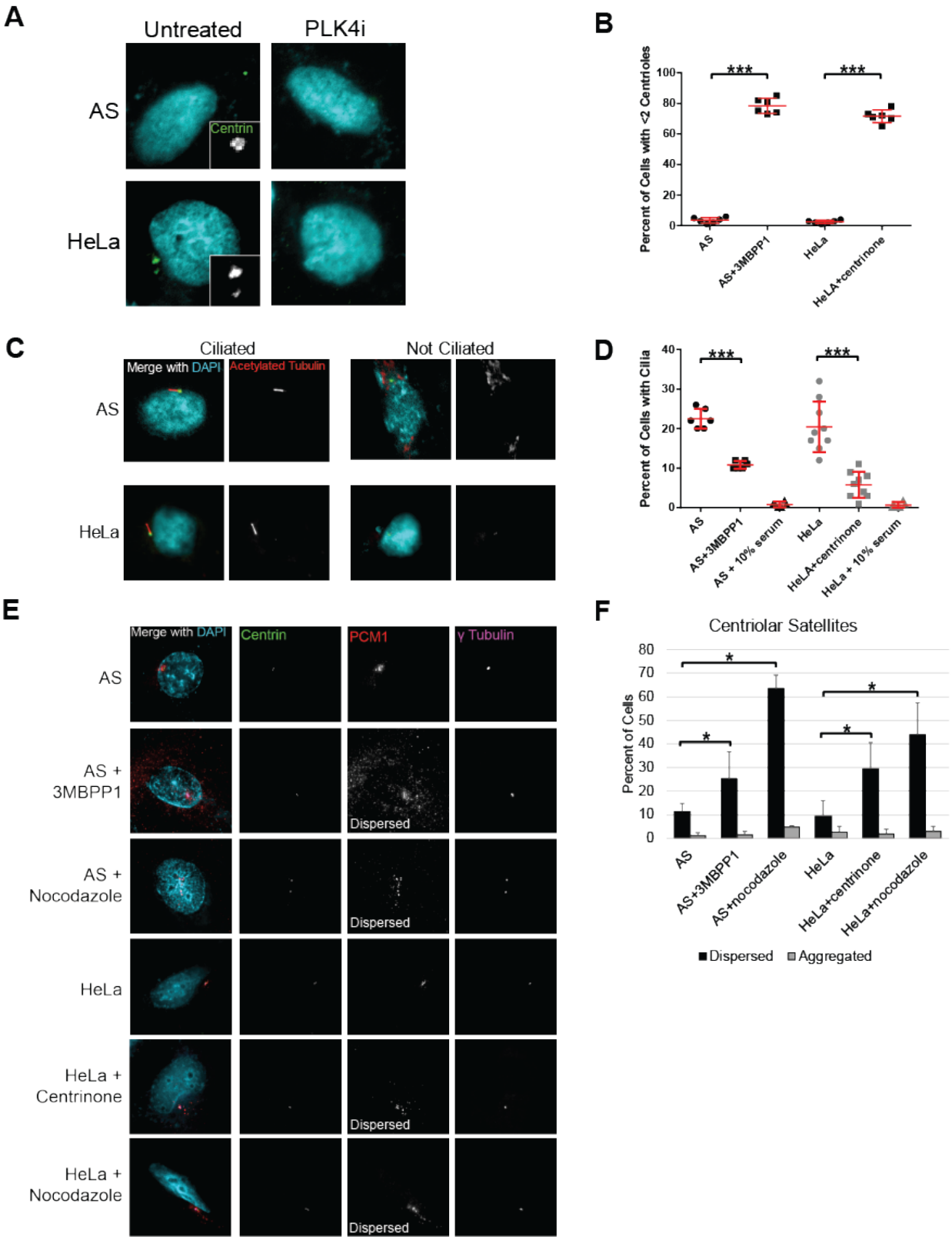
A
Untreated
PLK4i
AS
HeLa
Centrin
B
Percent of Cells with <2 Centrioles
***
***
AS
AS+3MBPP1
HeLa
HeLA+centrinone
C
Ciliated
Not Ciliated
Merge with DAPI
Acetylated Tubulin
AS
HeLa
D
Percent of Cells with Cilia
***
***
AS
AS+3MBPP1
AS + 10% serum
HeLa
HeLA+centrinone
HeLa + 10% serum
E
Merge with DAPI
Centrin
PCM1
γ Tubulin
AS
AS + 3MBPP1
AS + Nocodazole
HeLa
HeLa + Centrinone
HeLa + Nocodazole
Dispersed
F
Centriolar Satellites
Percent of Cells
AS
AS+3MBPP1
AS+nocodazole
HeLa
HeLa+centrinone
HeLa+nocodazole
Dispersed
Aggregated

Supplemental Figure 7-3

PLK4 activity is not required for centriolar satellite remodeling in response to UV.

(A) Representative images of centriolar satellites (PCM1 staining) in HeLa cells under the indicated conditions. The p38 inhibitor (p38i) utilized was SB203580. Scale bar = 10 μm. **(B)** Quantification of centriolar satellites as aggregated or dispersed. Bars represent averages ±SD for 1 independent experiment. *P value < 0.05; ns = not significant. Scale bar = 5 μm.

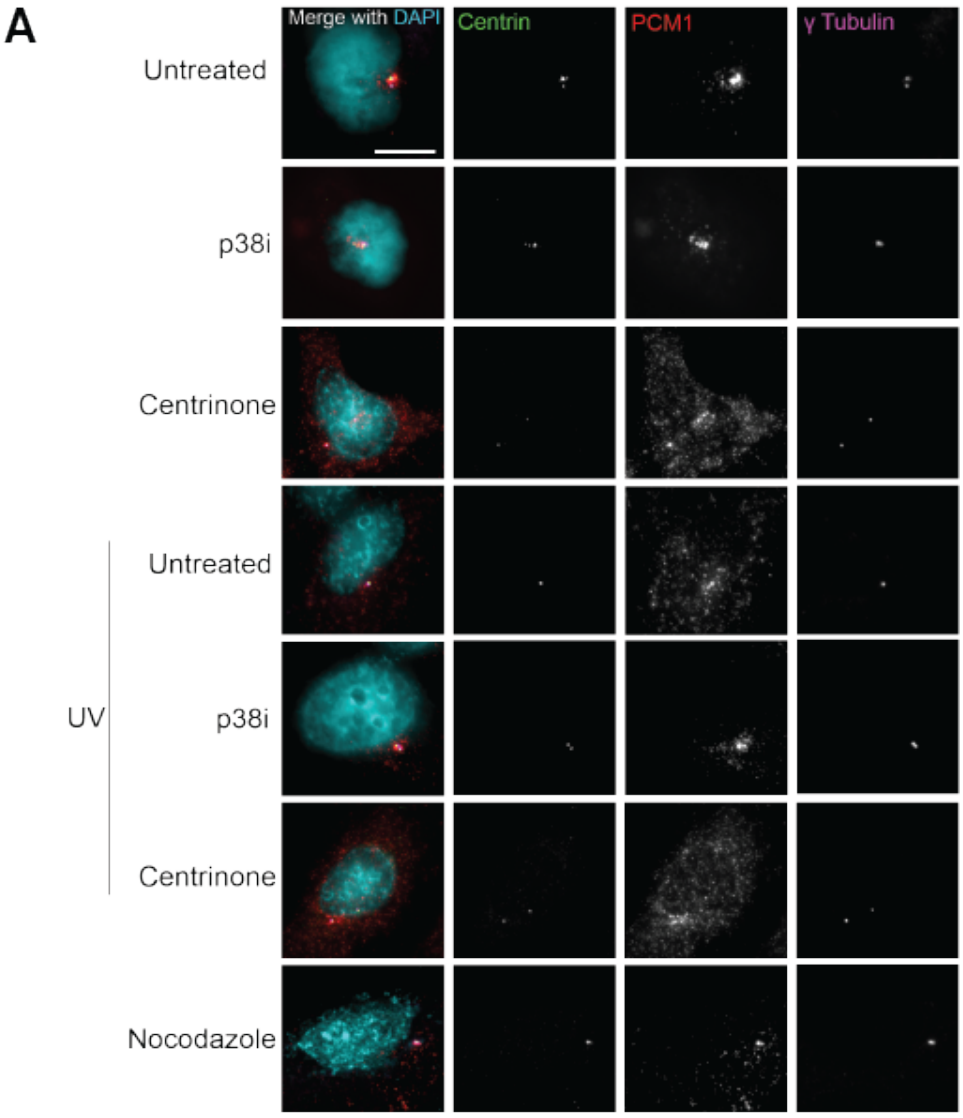
A
Merge with DAPI
Centrin
PCM1
γ Tubulin
Untreated
p38i
Centrinone
UV
Untreated
p38i
Centrinone
Nocodazole

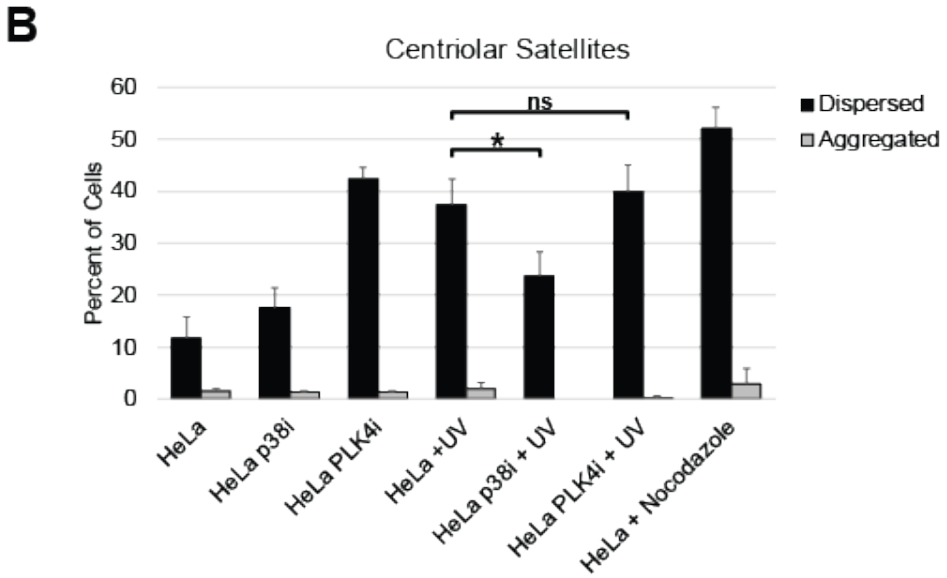
B
Centriolar Satellites
Percent of Cells
60
50
40
30
20
10
0
ns
*
Dispersed
Aggregated
HeLa
HeLa p38i
HeLa PLK4i
HeLa +UV
HeLa p38i + UV
HeLa PLK4i + UV
HeLa + Nocodazole

Supplemental Figure 7-4

Effects of S78A and S78D mutations on CEP131 interactions with previously reported interactors.

(A) HeLa cells were simultaneously transfected with CEP131 siRNA and the indicated GFP-tagged CEP131 construct. Cells were then fixed and stained for CEP152. The amount of CEP152 at the centrosome was quantified and is shown in the adjacent dotplot. Insets on CEP152 images show magnified CEP152 at the centrosome. **(B)** WT HeLa cells and CEP131 knockout cell lines (KO4E and KO9) were stained for CEP152, and the amount of CEP152 at the centrosome was quantified. Insets show magnifications of the centrosome. Each dot represents a single cell. Bars represent means ±SD. Scale bars = 10μm. *** P value < 0.0001; ns = not significant.

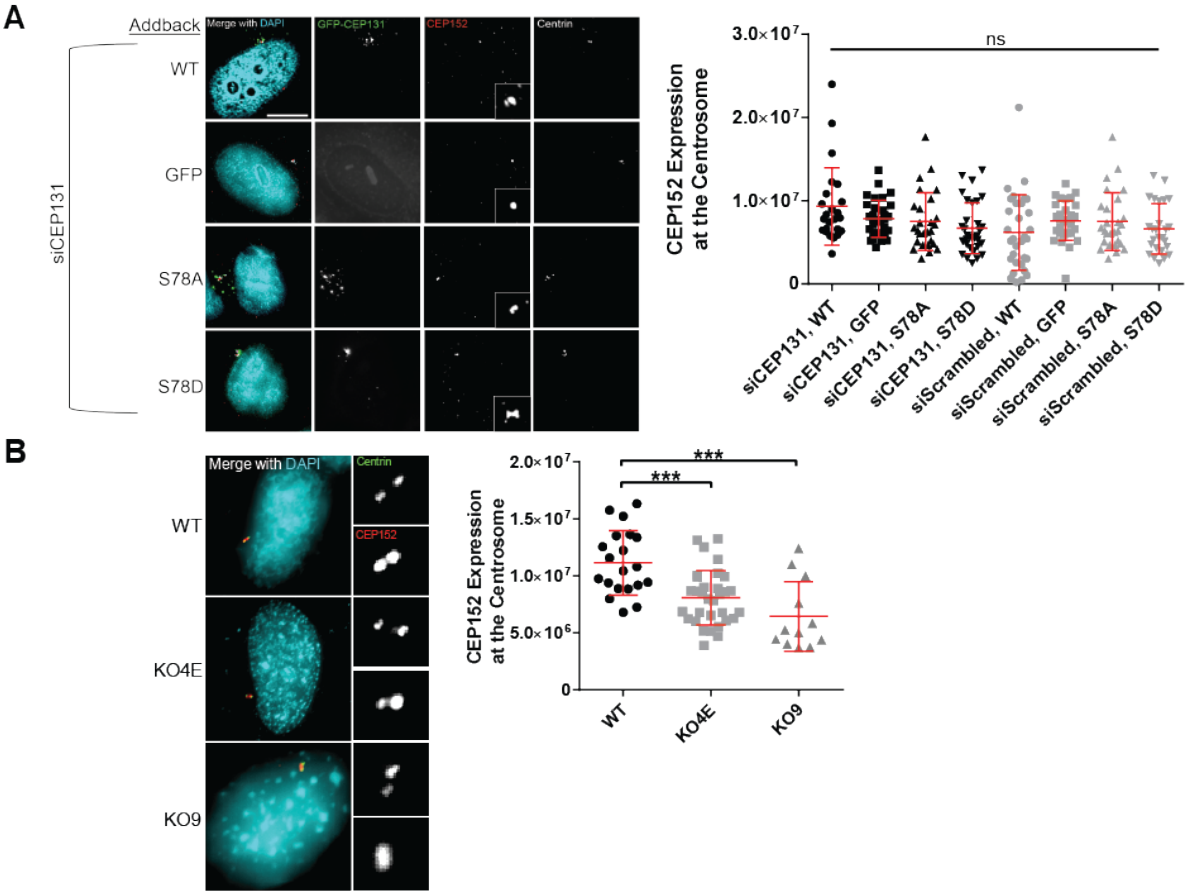

Supplemental Figure 7-5

Dynein is required for satellite aggregation with CEP131 S78D phosphomimetic.

(A) Representative images of HeLa cells treated with nocodazole and the dynein inhibitor ciliobrevin D. **(B)** Quantification of centriolar satellites (PCM1 staining) in the conditions shown in panel A. **(C)** Representative images of WT HeLa cells transfected with CEP131 S78D and treated with ciliobrevin D. **(D)** Quantification of centriolar satellites (PCM1 staining) in the conditions shown in panel C. Bars represent means ±SD from three replicates. Scale bars = 10µm. At least 300 cells were analyzed for each condition. *P value < 0.05.

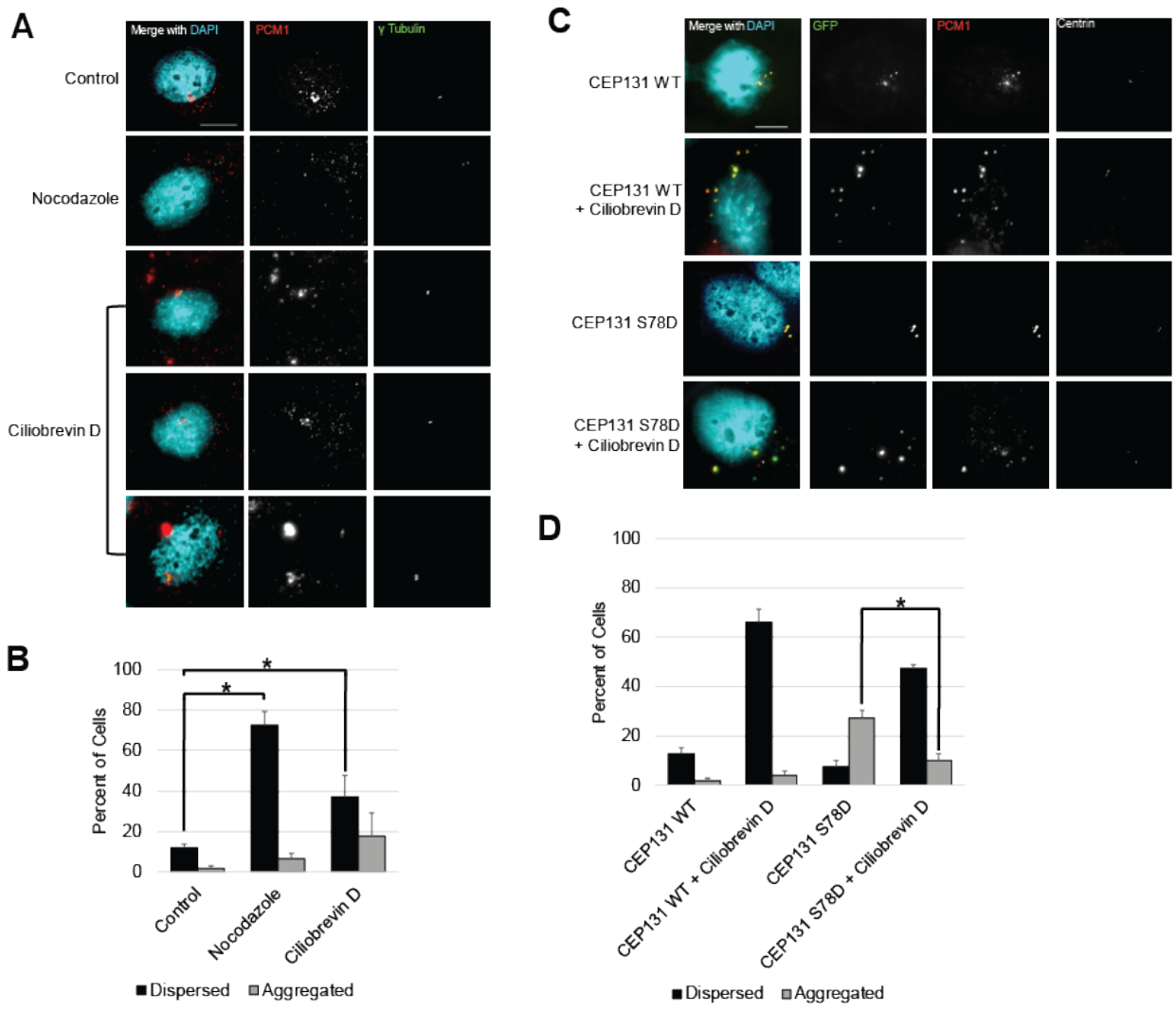

Acknowledgements

This project is supported by R01 GM097245 to MEB, F30CA203271 to RAD, the National Center for Quantitative Biology of Complex Systems (P41 GM108538 to JJC), and University of Wisconsin Carbone Cancer Center Support Grant P30 CA014520. RAD is in the University of Wisconsin Medical Scientist Training Program (T32GM008692) and an ICTR TL1 trainee (supported under NIH awards UL1TR000427 and TL1TR000429). The content is the responsibility of the authors and does not necessarily represent the views of the NIH. The authors thank Drs. Spencer Collis (University of Sheffield), Katie Myers (University of Sheffield), Tim Miller (University of Wisconsin), Takashi Toda (Hiroshima University), Jun Wan (University of Wisconsin), and Beth Weaver (University of Wisconsin) for reagents and formative discussions; Roshan Norman (University of Wisconsin) for assistance with determination of homology/conservation; and Rob Lera for critical review of the manuscript.

CHAPTER 8: Pericentriolar material 1 (PCM1) is a novel tumor suppressor that maintains genomic integrity

Work in this chapter is in preparation for submission:

Pericentriolar material 1 (PCM1) is a novel tumor suppressor that maintains genomic integrity

Ryan A. Denu, Andrew R. Lynch, Mark E. Burkard

Abstract

Centriolar satellites are granular, fibrous structures that surround the centrosome and regulate movement of proteins to and from the centrosome. Their role in human cancer has not been reported. We analyzed genomic and transcriptomic alterations in the 44 genes known to localize to the centriolar satellites. Notably, genomic deletion of pericentriolar material 1 (PCM1) occurs in up to 15% of human cancers, depending on the disease site. We used CRISPR genome editing to knockout PCM1 in HeLa and RPE cells. Interestingly, we find that PCM1 deletion increases the incidence of multipolar spindles in metaphase and anaphase in cells with mutant p53, suggesting that loss of PCM1 in human cancer drives carcinogenesis by increasing the incidence of multipolar spindles. To identify potential novel therapeutic strategies to treat PCM1-deleted cancers, we screened a panel of drugs in our PCM1 knockout cell lines. Interestingly, PCM1-deleted cells were more sensitive to autophagy inhibition, consistent with previous findings that chromosomal instability and aneuploidy increase the cell's dependence on autophagy and sensitizes cells to inhibition of autophagy. Taken together, these findings suggest that PCM1-deleted cancers are more chromosomally unstable, are more dependent on autophagy, and are sensitized to autophagy inhibitors.

Introduction

Centriolar satellites are protein-rich, electron-dense regions that surround the centrosome and regulate movement of protein to and from the centrosome.[24,442] They are important for recruiting factors involved in microtubule nucleation, ciliogenesis, and centriole duplication.[25,26] Centriolar satellites disassemble during mitosis and reassemble when cells entered interphase.[27-29] Pericentriolar material 1 (PCM1) forms the major structural platform of centriolar satellites and has been used by many to define centriolar satellites.[25,27,30,31] PCM1 is conserved in mammals and zebrafish, but analogs are not seen in *Drosophila* or *C. elegans*. Deletion of PCM1 eliminates and/or disperses centriolar satellites,[25,28] as assessed by immunofluorescent staining of CEP131, CEP290, CEP90, and MIB1.[443] Furthermore, depletion of PCM1 reduces targeting of centrin, pericentrin, ninein, and PLK1 to the centrosome (but not γ-tubulin or dynactin),[25,444] reduces microtubule anchoring and radial organization at the centrosome,[25] and reduces ciliogenesis.[103,426] Additional studies of PCM1 depletion demonstrated a G1 arrest in RPE1 cells,[445] which was similarly found in primary human fibroblasts (MRC-5)[446] and when injecting anti-PCM1 antibodies into mouse embryos.[447] Furthermore, PCM1 depletion in *g*lioblastoma cells sensitizes them to temozolomide.[428]

Accumulating evidence suggests that centriolar satellites are also important for maintaining genomic stability. PCM1 is involved in spindle pole integrity during metaphase[448]. Additionally, depletion of other centriolar satellite proteins causes mitotic errors. For example, depletion of CEP131,[416] CEP72,[449] CEP90,[450] and PAR6α[451] result in increased multipolar spindles. Lastly, depletion of centriolar satellite component OFD1 does not increase mitotic errors,[28,75] but it was identified in whole genome screen as being important for mitotic fidelity.[452] However, the role of PCM1 in mitotic fidelity has not been assessed.

Chromosomal instability (CIN) refers to an increased rate of chromosome missegregation due to erroneous mitoses that can lead to aneuploidy, the state of gain or loss of whole chromosomes.[453] There are many potential causes of CIN, including multipolar spindles, improper chromosome condensation or cohesion, inefficient chromosome congression, defects in mitotic spindle assembly, defective mitotic checkpoint, and improper kinetochore-microtubule attachments.[454] Furthermore, aneuploidy itself may make cells more chromosomally unstable; evidence for this notion comes from studies of aneuploid yeast,[455] cells derived from humans with inherited aneuploidy disorders (e.g. Down syndrome),[456] and experiments involving microcell-mediated chromosome transfer.[457]

To our knowledge, there have been no reports of centriolar satellite biology in human cancer. Herein, we describe a bioinformatic screen of alterations in the 44 known centriolar satellite proteins and identify PCM1 deletions to be common in human cancer, and that deletion of PCM1 increases CIN.

Results

Bioinformatic screen of centriolar satellite genes in human cancer

Centriolar satellites regulate movement of proteins to and from the centrosome and may coordinate processes such as centriole duplication and microtubule nucleation. Given that centriole duplication and microtubule nucleation can go awry in human cancer, we asked whether centrioles are dysregulated in human cancer. To our knowledge, 44 proteins have been identified to localize to the centriolar satellites. We examined TCGA data sets to assess potential genomic and transcriptomic alterations in centriolar satellite components. In general, there was a relative dearth of genomic alterations, similar to the relative dearth of genomic alterations in mitosis genes in human cancer.[274] However, we observed that PCM1 genomic deletions are relatively common in human cancer, occurring in up to 15% of cancers depending on the cancer site (Figure 8-1A). Heterozygous PCM1 deletions are more common than homozygous PCM1 deletions (Figure 8-1B). PCM1 is the major defining protein of centriolar satellites. We then explored the impact of these PCM1 deletions on survival in the cohorts with the highest incidence of PCM1 deletion (endometrial, prostate, bladder, colorectal). There is a general trend toward worse overall survival and disease-free survival in all cohorts, with statistically significant survival differences seen in endometrial cancer OS and PFS and bladder cancer DFS (Figure 8-1C). Cox proportional hazards modeling revealed that PCM1 deletion was an independent predictor of PFS in bladder cancer, but it was not an independent predictor of OS or DFS for endometrial, prostate, and colorectal cancer datasets when stage, age, and Gleason score (for prostate dataset only) were included in the model (Supplemental Table 8-1).

PCM1 deletion causes multipolar mitotic spindles

Next, we sought to explore the mechanism by which PCM1 deletion could negatively impact cancer patient survival. Therefore, we used CRISPR/Cas9 genome engineering to create PCM1 knockout cells using HeLa cells, which were validated by immunofluorescent staining (Figure 8-2A) and western blotting (Figure 8-2B) for PCM1. First we examined the proliferation of our knockouts compared to the wild type cells. Interestingly, PCM1 knockout cells proliferate slower than their wild type counterparts (Figure 8-3A). Therefore, we asked whether this is due to a delay or errors in mitosis. We assessed errors in metaphase and anaphase by fixed cell immunofluorescence (Figure 8-3B). Strikingly, PCM1 knockout cells exhibited a greater incidence of multipolar metaphases (Figure 8-3C) and lagging chromosomes and/or chromosome bridges in anaphase (Figure 8-3C).

We then assessed the mechanism by which PCM1 knockout increases multipolar spindles. The potential mechanisms leading to multipolarity that we tested included the following: centrosome amplification (due to either centriole overduplication or cytokinesis failure), centriole disengagement, PCM fragmentation, loss of spindle pole integrity in response to spindle and/or chromosomal forces, lack of spindle pole resistance to traction forces, and depletion of ninein.[131,448,458]

To confirm the finding that PCM1 deletion increases multipolar spindles, we employed a different PCM1 deleted cell line, RPE1, which we validated by immunofluorescent staining (Figure 8-4A) and western blotting (Figure 8-4B) for PCM1. Consistent with our observations in HeLa cells, RPE1 PCM1 knockout cells demonstrate a proliferative defect (Figure 8-4C). However, when analyzing mitotic cells, we did not observe nearly the same magnitude of an increase in multipolar metaphases (Figure 8-4D) or chromosome missegregation in anaphase (Figure 8-4E). Since HeLa cells lack functional p53 while RPE1 cells have functional p53, we

hypothesize that the observed inconsistency between HeLa and RPE1 metaphase cells is due to p53 status. Previous work has demonstrated that loss of p53 is permissive of more mitotic errors induced by depletion of various mitosis genes.[285]

PCM1 deletion causes chromosomal instability in human cancer

To see whether PCM1 deleted tumors have greater CIN, TCGA data were assessed. We calculated the CIN70 gene score, a previously validated method of assessing CIN,[459] and tested whether these gene scores were higher in PCM1 deleted tumors versus non-deleted tumors. Interestingly, PCM1 deleted tumors show a trend toward higher CIN70 gene scores (Figure 8-4).

PCM1 deletion sensitizes cells to autophagy inhibitors

Lastly, we asked whether PCM1 deletion sensitizes cells to cancer drugs. Since PCM1 deleted cells demonstrate greater CIN, we hypothesized that these PCM1 deleted cells would be more sensitive to drugs that induce CIN, such as paclitaxel.[460] Interestingly, it appears that PCM1 deleted cells are more resistant to many anti-mitotic drugs, such as microtubule poisons and PLK1 inhibitors. However, this is likely an artifact of their reduced proliferative rate, thereby making them less susceptible to anti-mitotic drugs. Similar findings have been reported in drug screens of cells with centrosome amplification.[379] Consistent with previous reports demonstrating that PCM1 depleted cells are more sensitive to nutrient stresses, we find that PCM1 knockout cells are more sensitive to serum deprivation (Figure 8-5). We have previously shown that deletion of another centriolar satellite protein, CEP131, sensitizes cells to nutrient deprivation (Chapter 7).

Interestingly, PCM1 deleted cells are more sensitive to the autophagy inhibitors bafilomycin A1 and chloroquine (Figure 8-5). Previously, chromosome 8p deletion has been shown to increase autophagosomes and increase sensitivity to inhibitors of autophagy.[291] Our findings suggest that PCM1 deletion may be responsible for this increased reliance on autophagy.

Discussion

In this investigation of PCM1 deletion in human cancer, we find that loss of PCM1 increases CIN, resulting in an autophagic stress response, increased reliance on autophagy, and increased sensitivity to inhibitors of autophagy. Our results suggest a potential novel strategy to specifically target PCM1 deleted tumors with autophagy inhibitors.

PCM1 alterations have been reported in human cancer. In thyroid cancer, there are genomic rearrangements involving the RET tyrosine kinase domain and the 5' portion of PCM1.[461] Immunohistochemical analysis of PCM1 in these tumors demonstrated that PCM1 protein level was drastically decreased and its subcellular localization was altered in papillary thyroid tumor tissue with respect to normal thyroid.[461] Furthermore, PCM1 loss of heterozygosity has been reported in hepatocellular carcinomas, colorectal cancers, and non-small-cell lung cancers.[462] In addition, PCM1 is on chromosome 8p, and chromosome 8p deletions are common in human cancer, especially breast and prostate cancer.[218,288,291] Chromosome 8p deletion has previously been shown to increase autophagosomes and increase sensitivity to inhibitors of autophagy.[291] Herein, we have provided evidence that one of the contributors to the malignant phenotype associated with loss of chromosome 8p depends on loss of PCM1 driving CIN. CIN is a fundamental characteristic of solid tumors[321] and is known to increase carcinogenesis[322,323] and promote tumor evolution, malignant phenotypes, and resistance to therapy.[463,464]

Furthermore, we provide evidence that the increased reliance on autophagy and increased sensitivity to inhibitors of autophagy reported previously in 8p-deleted cancers[291] is conferred by loss of PCM1. We hypothesize that this increased reliance on autophagy is due to PCM1 deletion causing CIN, which generates aneuploid cells with unbalanced karyotypes, resulting in

aberrations in chromosomes, gene expression, and protein complex stoichiometry. Chromosome missegregation and aneuploidy have previously been shown to generate an autophagic stress response characterized by an accumulation of autophagosomes and autophagic cargo in autophagosomes.[374]

It is thought that hemizygous focal deletions, which often contain no known tumor suppressors, contain high densities of "STOP" genes, which negatively regulate proliferation, and that hemizygous deletion of these STOP genes maximizes proliferative fitness.[465] many of these stop genes are involved in cell cycle regulation, apoptosis, and autophagy. Increased frequencies of deletions with clusters of STOP genes may occur because the cell has many opportunities to lose the second allele of a recessive tumor suppressor gene or because of combined haploinsufficiencies.[465] These recurrently deleted regions tend to have a relative dearth of essential genes (e.g. DNA replication, spliceosome, ribosome genes).[465] given that these focal deletions tend to occur hemizygously, it is likely that haploinsuffienncy is likely operating. There are reports of unequal distribution of expression between the 2 alleles of a gene,[466] so perhaps this monoallelelic deletion is acting more like a biallelic deletion.

This study also uncovers additional findings regarding the basic biology of centriolar satellites. Firstly, are centriolar satellites required for centriole duplication? Previous reports have demonstrated that depletion of several satellite components, including PCM1, reduces the recruitment of crucial mediators of centriole duplication, but few have demonstrated how this affects centriole number.[467] Herein, we find that PCM1 knockout cells can still duplicate their centrioles, suggesting that either PCM1 and/or centriolar satellites are not required for centriole duplication, or that they can adapt to chronic depletion of PCM1 and recruit the centriole duplication machinery to the centrosome. Secondly, are centriolar satellites important for

mitosis? Previous work has demonstrated that depletion of the centriolar satellite components causes mitotic errors. PCM1 reportedly is involved in spindle pole integrity during metaphase.[448] CEP131 depletion increases multipolar spindles.[416] CEP72 depletion causes multipolar spindles.[449] CEP90 depletion increases monopolar and multipolar spindles and chromosome misalignment in metaphase.[450] The polarity gene Par6α also turned out to be a satellite protein, and its knock-down in human HeLa cells results in severe mitotic defects and frequently assembling multipolar spindles.[451] Lastly, depletion of centriolar satellite component OFD1 does not increase mitotic errors,[28,75] but it was identified in whole genome screen as being important for mitotic fidelity.[452] We conclude that centriolar satellites are important for mitotic fidelity.

An interesting remaining question to be answered in the field of CIN and carcinogenesis is what compensatory changes have to be made to allow cancer cells to exist with CIN. We see time and again that cell lines with CIN proliferate more slowly (e.g. CEP170 KO, PCM1 KO, CA), so in and of itself, CIN is not necessarily an advantage to the tumor. However, the results of CIN can be quite advantageous to the tumor. The very presence of CIN is tumor promoting, and CIN is thought to allow tumors to continue to evolve over time and become resistant to therapy. The compensatory changes necessary to increase the fitness of these cells remain to be completely uncovered.

Chromosome 8p deletions are common in human cancer[286,287] and are occasionally associated with gains of chromosome 8q.[218] This is likely to be an initiating event, as it is detected at early stages of breast cancer.[288,289] Furthermore, heterozygous loss of chromosome 8p using TALEN-based genomic engineering caused changes in fatty acid and ceramide metabolism and increased autophagy leading to increased invasiveness.[291] In this study, MCF10A with 8p deletion were more sensitive to the autophagy inhibitor mefloquine and more resistant to

increasing doses of microtubule inhibitors, such as paclitaxel, consistent with our observations in PCM1 knockout cells. Herein we provide evidence that the likely gene responsible for the increased reliance on autophagy is PCM1.

In conclusion, we surveyed genomic alterations in the 44 known centriolar satellite genes, finding that the most commonly described centriolar satellite gene, PCM1, is commonly deleted in human cancer. Deletion of PCM1 causes CIN and increases the reliance on autophagy. This study suggests a novel therapeutic strategy to treat chromosome 8p-deleted cancers with autophagy inhibitors.

Materials and Methods

Bioinformatic screen of centriolar satellite components

Centriolar satellite components were pooled from an extensive literature search.[442,468] Furthermore, we supplemented with Uniprot reviewed proteins that localize to centriolar satellites. This yielded a total of 44 centriolar satellite genes. We used cBioPortal to query 21 TCGA datasets.[196,301] We analyzed genomic (mutations and copy number variations) and transcriptomic changes in these centriolar satellite genes in all TCGA datasets. Genomic deletion of PCM1 was most common in bladder, colorectal, and prostate cancers, so these datasets were further analyzed. We compared survival of patients with tumors with loss of PCM1 versus wild type PCM1 using the Kaplan Meier method and log rank tests to determine significance. Cox proportional hazards modeling was performed to assess whether loss of PCM1 independently predicted survival. Stage (for all datasets) and Gleason score (for prostate dataset only) were also included in the model. Multivariate cox proportional hazard analysis was performed using the survival package in R.

Cell Culture

All cell lines were grown at 37 °C in 5% CO_2. RPE-1-derived cell lines (ATCC) were grown in a 1:1 mixture of DMEM and Ham's F-12 medium supplemented with 2.5 mm l-glutamine, with 10% fetal bovine serum and 100 units/mL penicillin-streptomycin. RPE1 PCM1 knockout cells were kindly provided by Brian Dynlacht.[443] HeLa cell lines (ATCC) were grown in high glucose DMEM supplemented with 2.5 mm l-glutamine, with 10% fetal bovine serum and 100 units/mL penicillin-streptomycin.

For stable retroviral transduction, constructs were co-transfected with a VSV-G envelope plasmid into Phoenix cells. Fresh medium was applied at 24 hours post-transfection, harvested 24 hours later, clarified by centrifugation and filtration through a 0.45 μm membrane to remove cell debris, and diluted 1:1 with complete medium containing 10 μg/mL polybrene. Target cells were infected at 40-60% confluence for 24 hours. Polyclonal transductants were further purified by limiting dilution to obtain individual clones.

Immunofluorescence

Immunofluorescence and imaging were carried out as previously described [194,195,208]. Cells were seeded on glass coverslips in 24-well plates and fixed with 100% ice-cold methanol for 30 minutes. Fixed cells were then blocked for 30 minutes in 3% bovine serum albumin (BSA) and 0.1% triton X-100 in PBS (PBSTx + BSA). Primary antibodies were incubated in PBSTx + BSA for 1 hour at room temperature and washed three times in PBSTx, followed by secondary antibody incubation in PBSTx + BSA for 30 minutes at room temperature and two washes with PBSTx. Cells were counterstained with DAPI and mounted on glass slides with Prolong Gold antifade medium (Invitrogen). Image acquisition was performed on a Nikon Eclipse Ti inverted microscope equipped with 10x, 20x, 40x, and 100x objectives; a temperature-controlled motorized stage with 5% CO_2 support (In Vivo Scientific); and CoolSNAP HQ2 charge-coupled device camera (Photometrics). Where indicated in the figure legends, optical sections were taken at 0.2-μm intervals and deconvolved using Nikon Elements. Where appropriate, the observer was blinded to treatment condition during image acquisition and analysis. Images were processed and analyzed using Nikon Elements.

Qualitative analysis of centriolar satellites was performed by categorizing cells as either normal, dispersed, or aggregated, as previously described.[103] Further, quantitative analysis of centriolar satellites was performed by taking Z stack images, deconvolving, and quantifying the percentage of PCM1 or CEP72 intensity within a 2.5 μm radius of the center of the centrosome.

Primary antibodies used were: CEP131 (Thermo, PA5-38978, 1:500), CEP72 (Proteintech, 19928-1-AP, 1:500), alpha tubulin (DSHB, 12G10, 1:1000), acetylated tubulin (Santa Cruz, sc-23950, 1:1000), pericentrin (Abcam, ab4448, 1:1000), PCM1 (Cell Signaling, 5259, 1:500), p62/SQSTM1 (Santa Cruz, SC-28359, 1:1000), LC3B (Cell Signaling Technology, 2775, 1:500) centrin (Millipore, 04-1624, 1:500), gamma tubulin (Abcam, ab27074, 1:1000), beta actin (Abcam, ab6276, 1:5000), FLAG (Sigma, F1804, 1:1000), GFP (Invitrogen, A-11120, 1:1000). Alexa Fluor-conjugated secondary antibodies were used at 1:350 (Invitrogen).

Western Blotting

Cells were lysed in buffer (50 mM HEPES, pH 7.5, 100 mM NaCl, 0.5% NP-40, 10% glycerol) containing phosphatase inhibitors (10 mm sodium pyrophosphate, 5 mM β-glycerol phosphate, 50 mm NaF, 0.3 mm Na_3VO_4), 1 mM PMSF, protease inhibitor cocktail (Thermo Scientific), and 1 mm dithiothreitol. Samples were sonicated and heated in SDS buffer. Proteins were separated by SDS-PAGE (8% acrylamide for PCM1 blots, 12% acrylamide for LC3 blots, 10% for all others), transferred to PVDF membrane (Millipore), and blocked for at least 30 minutes in 5% milk and 0.1% Tween 20 in Tris-buffered saline, pH 7.4 (TBST + milk). Membranes were incubated 1 hour at room temperature or overnight at 4° C with primary antibodies diluted in TBST + 5% milk, washed three times with TBST, and incubated for 1 hour at room temperature in secondary antibodies conjugated to horseradish peroxidase in TBST +

5% milk. Membranes were washed and developed with luminol/peroxide (Millipore) and visualized with film.

Antibodies utilized for immunoblotting include: beta actin (DSHB, JLA20, 1:1000), FLAG (Sigma, F1804, 1:5000), GFP (Invitrogen, A-11120, 1:1000), PCM1 (Cell Signaling Technology, 5259, 1:500), LC3B (Cell Signaling Technology, 2775, 1:1000), p62/SQSTM1 (Santa Cruz, SC-28359, 1:1000), and alpha tubulin (DSHB, 12G10, 1:1000). HRP-conjugated secondary antibodies were used (Jackson, 1:5000). Relative intensities of bands were calculated using ImageJ from scanned images and normalized to their respective loading control intensity.

CRISPR/Cas9 Gene Editing

CRISPR/Cas9 was used to create PCM1 knockout cell lines in HeLa cells. Two gRNAs targeting PCM1 (ATTTCTCCGGAGTCGTCACCAGG and CTACTGTGTGGGAACGTATGTGG) were cloned into PX459 (pSpCas9(BB)-2A-Puro, from Feng Zhang, Addgene plasmid # 48139) [302], and the cutting efficiency of each guide was assessed by surveyor assay (IDT, 706025) following nested PCR of 1000bp and then 500bp fragments from genomic DNA encompassing the guide RNA locus using the following primers: 1000F: CGTACTGACTTTATAGGAGATCGGTAA; 1000R: GGAAATGTGTGTGTCTCTATGACATATAG; 500F: GTCTCTAGGAGTATAAGTCTGTCAAAAATG; 500R: CACTTGAGTTAGTCATATAACATAGTATAAAGTCC.. PX459 vectors were transfected into HeLa cells using Fugene (Promega). Prior to transfection, media was replaced with serum- and antibiotic-free media. 24 hours after transfection, cells were selected with puromycin (1µg/mL) for 72 hours, then allowed to recover for 24 hours in fresh media. The guide RNA

yielding the greatest cutting by surveryor assay (IDT, 706025) was transfected again into HeLa cells, which were then subcloned by limiting dilution. Colonies were selected and screened by PCR of the region flanking the cut site and sequencing. Verification of knockout lines was performed with PCM1 western blotting and immunofluorescence.

Statistics

Statistical evaluations were performed using Prism software (GraphPad). Two-tailed t-tests and one-way ANOVA were used for comparisons. Tukey's correction was made for multiple comparisons. P-values <0.05 were considered significant for all tests, and designations are made in the figures for statistical significance.

Table 8-1

Summary of common alterations in centriolar satellite genes in human cancer.

Centriolar Satellite Gene	Other names	Mutations	CNVs	Pursue? Why?
ALDOB		not common	not common	No
BBS1		not common	not common	No
BBS2		not common	not common	No
BBS4		not common	not common	No
BBS5		not common	not common	No
BBS7		not common	not common	No
BBS8	TTC8	not common	not common	No
BBS9	PTHB1	not common	not common	No
C2CD3		7 mutations, AA Change: I477*/Nfs*12	not common	No
CAMK2B		not common	not common	No
CCDC11	CFAP53	7 mutations, AA Change: D326E/H/Y	not common	No
CCDC113		not common	not common	No
CCDC13		not common	not common	No
CCDC14		not common	not common	No
CCDC66		13 mutations, AA Change: L3LG*AX/fs	not common	No
CEP131		not common	not common	No

CEP135		5 mutations, AA Change: S997L	not common	No
CEP152		7 mutations, AA Change: I1277Lfs*20/N	not common	No
CEP290		18 mutations, AA Change: N212Tfs*14; 17 mutations, AA Change: I556Ffs*17/N/Nfs*20	not common	No
CEP63		not common	not common	No
CEP72		not common	not common	No
CETN1		not common	not common	No
DISC1		not common	amplifications, especially breast	No
FOPNL	FOR20	8 mutations, AA Change: K18Rfs*4	not common	No
HAP1		not common	not common	No
HOOK3		not common	not common	No
HTT		14 mutations, AA Change: P49dup	not common	No
MIB1		not common	not common	No
MOONR	KIAA0753, moonraker, MNR	not common	not common	No
NEK2		8 mutations, AA Change: S296L	Amplifications	No

NIN		13 mutations, AA Change: N435Mfs*19	not common	No
ODF2L	BCAP	10 mutations, AA Change: K407Nfs*22/ Q408Tfs*6	not common	No
OFD1		6 mutations, AA Change: K237Sfs*6/ Y238Vfs*2	not common	No
PARD6A	PAR6alpha	not common	not common	No
PCM1		10 mutations, AA Change: A262T	Deletions	Yes, major satellite platform/scaffold
PCNT	Pericentrin	7 mutations, AA Change: P3251Qfs*39/T3252Nfs*84	not common	No
PIBF1	CEP90	8 mutations, AA Change: R408fs/X408_splice	not common	No
PLK1		9 mutations, AA Change: S326L	not common	No
SPAG5		5 mutations, AA Change: Q766del	not common	No
SSX2IP		not common	not common	No
TALPID3	KIAA0586	not common	not common	No
WDR62		not common	Amplifications	No
WDR8	WRAP73	not common	not common	No

ZMYND10		not common	not common	No

Figure 8-1

Survey of alterations in centriolar satellite genes in human cancer.

(A) Graphical demonstration of the percent of tumors within each tumor site that harbor deletions (blue), amplifications (red), or mutations (green). **(B)** Incidence of heterozygous versus homozygous deletion of PCM1 in endometrial, bladder, colorectal, and prostate cancers. **(C)** Kaplan Meier curves demonstrating overall survival (OS) or disease-free survival (DFS) in endometrial, bladder, colorectal, and prostate cancers (some of the tumor sites where PCM1 deletion is most common and where patient number is sufficiently high to draw conclusions about survival).

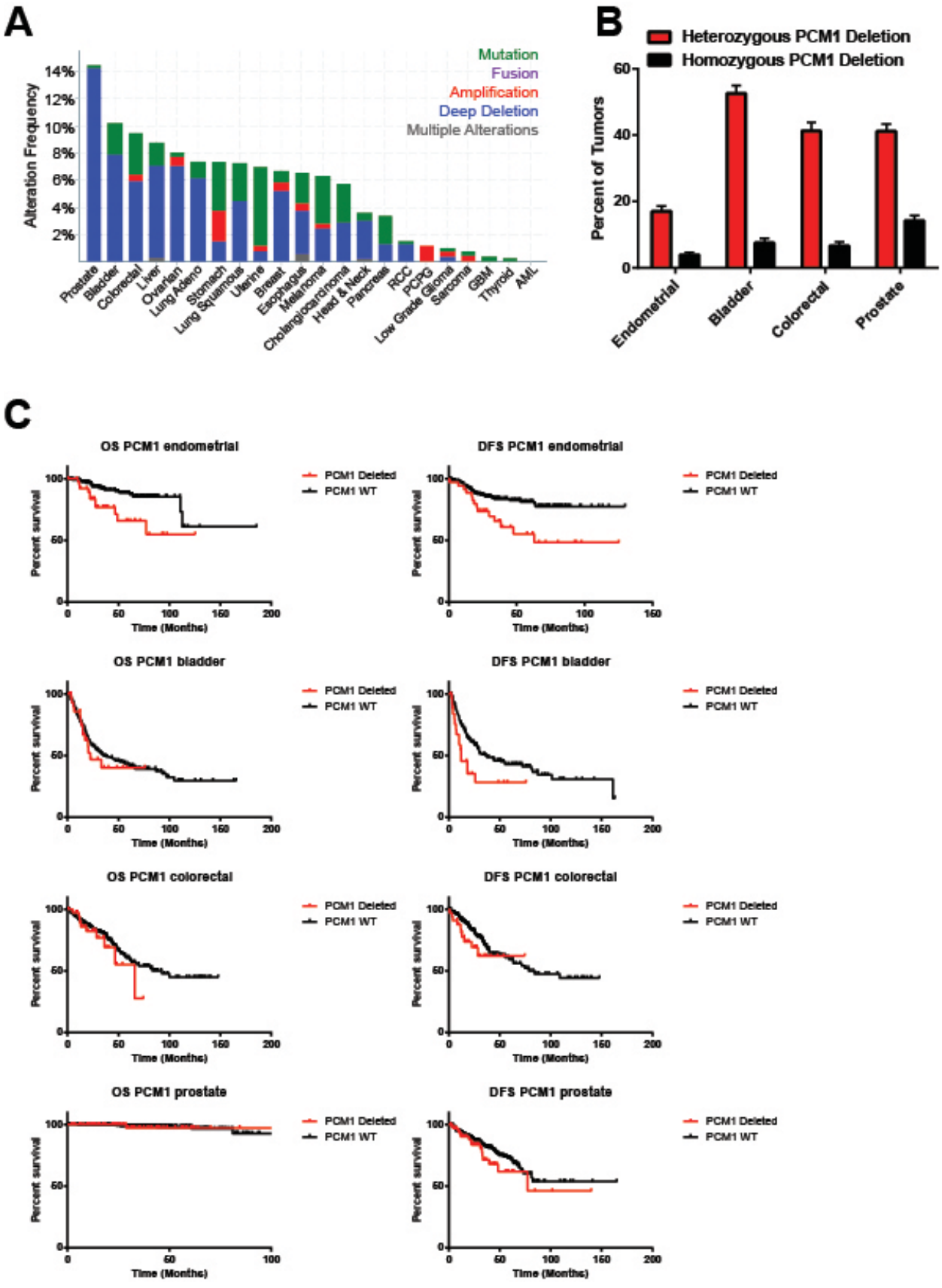
A
Alteration Frequency
14%
12%
10%
8%
6%
4%
2%
Mutation
Fusion
Amplification
Deep Deletion
Multiple Alterations
Prostate
Bladder
Colorectal
Liver
Ovarian
Lung Adeno
Stomach
Lung Squamous
Uterine
Breast
Esophagus
Melanoma
Cholangiocarcinoma
Head & Neck
Pancreas
RCC
PCPG
Low Grade Glioma
Sarcoma
GBM
Thyroid
AML
B
Heterozygous PCM1 Deletion
Homozygous PCM1 Deletion
Percent of Tumors
60
40
20
0
Endometrial
Bladder
Colorectal
Prostate
C
OS PCM1 endometrial
DFS PCM1 endometrial
OS PCM1 bladder
DFS PCM1 bladder
OS PCM1 colorectal
DFS PCM1 colorectal
OS PCM1 prostate
DFS PCM1 prostate
Percent survival
Time (Months)
PCM1 Deleted
PCM1 WT

Figure 8-2

PCM1 knockout HeLa cells display increased multipolar mitotic spindles.

(A) Representative images of PCM1 knockout HeLa cells. KO1 and KO2 are the two monoclonal knockout cell lines. **(B)** Western blotting for PCM1 with alpha tubulin loading control. **(C)** Cell counts over time. **(D)** Representative images of the metaphase and anaphase phenotypes that were quantified. **(E)** Quantification of metaphase cells. **(F)** Quantification of anaphase cells. Bars represent means ±SEM from 3 independent experiments. Scale bars = 10µm. *P value < 0.05 and indicates a statistically significant difference compared to WT.

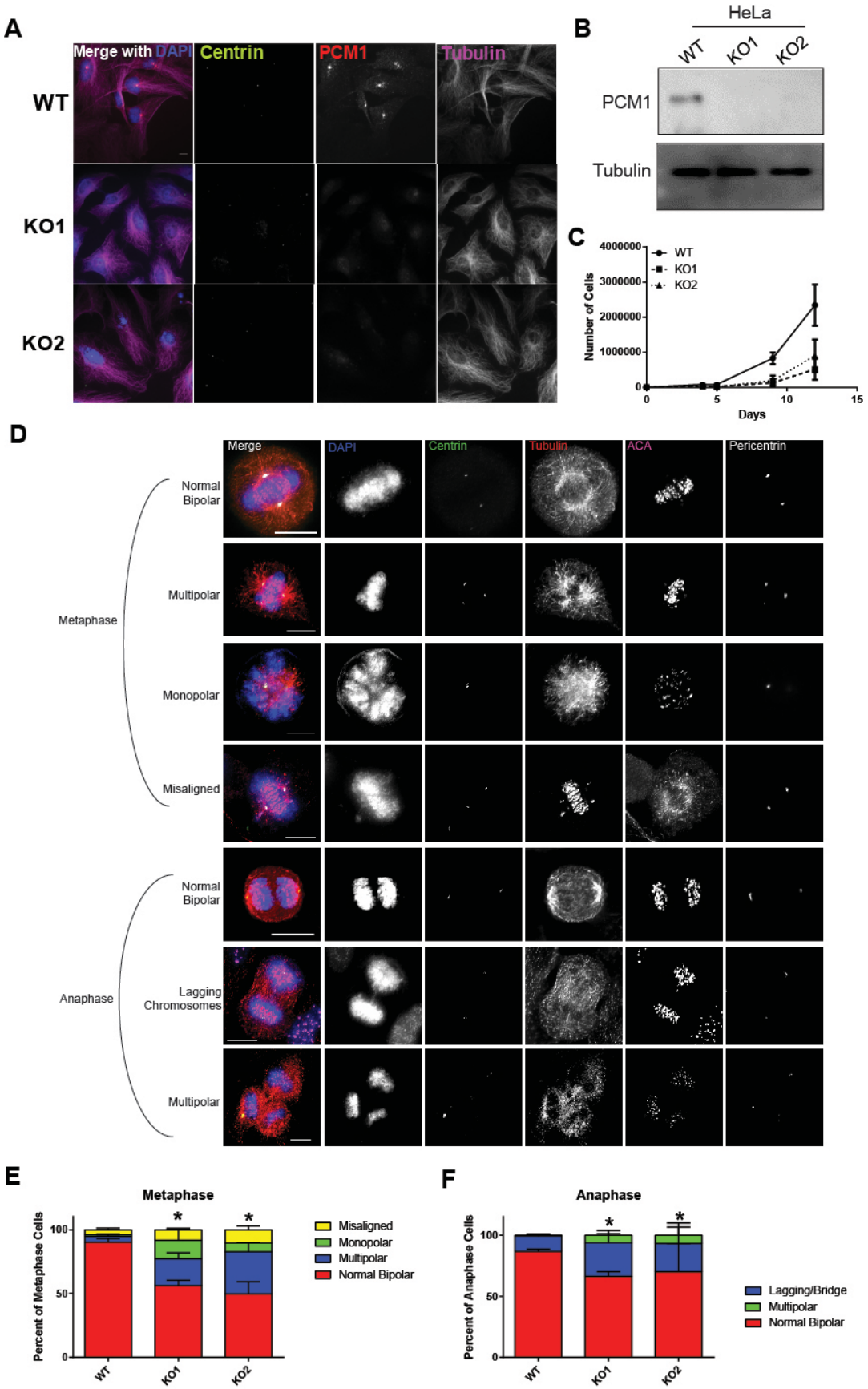
A
Merge with DAPI
Centrin
PCM1
Tubulin
WT
KO1
KO2
B
HeLa
WT
KO1
KO2
PCM1
Tubulin
C
Number of Cells
4000000
3000000
2000000
1000000
0
WT
KO1
KO2
0
5
10
15
Days
D
Merge
DAPI
Centrin
Tubulin
ACA
Pericentrin
Metaphase
Normal Bipolar
Multipolar
Monopolar
Misaligned
Anaphase
Normal Bipolar
Lagging Chromosomes
Multipolar
E
Metaphase
Percent of Metaphase Cells
100
50
0
WT
KO1
KO2
Misaligned
Monopolar
Multipolar
Normal Bipolar
F
Anaphase
Percent of Anaphase Cells
100
50
0
WT
KO1
KO2
Lagging/Bridge
Multipolar
Normal Bipolar

Figure 8-3

Loss of p53 is required for increased multipolar spindles in PCM1 knockout RPE1 cells.

(A) Representative images of PCM1 knockout RPE1 cells. Smaller images on the right are enlargements of the centrosome. **(B)** Western blotting for PCM1. **(C)** Cell counts over time in WT versus PCM1 knockout RPE1 cells. **(D)** Quantification of metaphase cells. **(E)** Quantification of anaphase cells. Bars represent means ±SEM from 3 independent experiments.

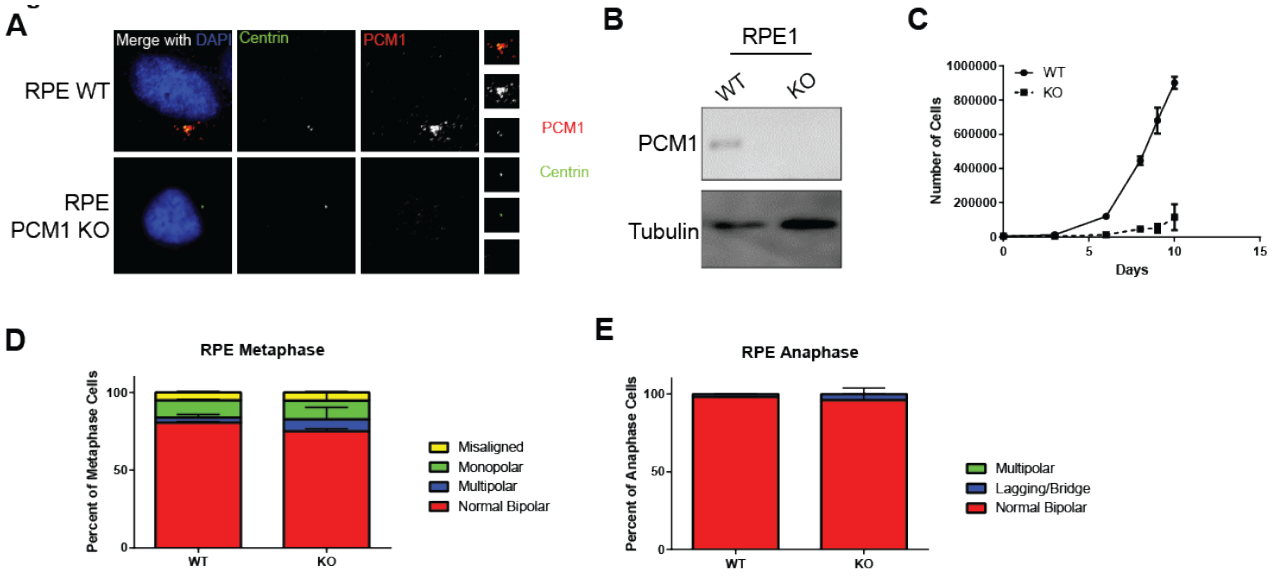

Figure 8-4

Higher CIN gene scores in PCM1 deleted human tumors.

CIN70 gene scores were determined for each tumor and compared based on whether the tumor also had a homozygous or heterozygous PCM1 deletion or no PCM1 deletion. Bars represent means ±SD. **P value < 0.01, ***P value < 0.001.

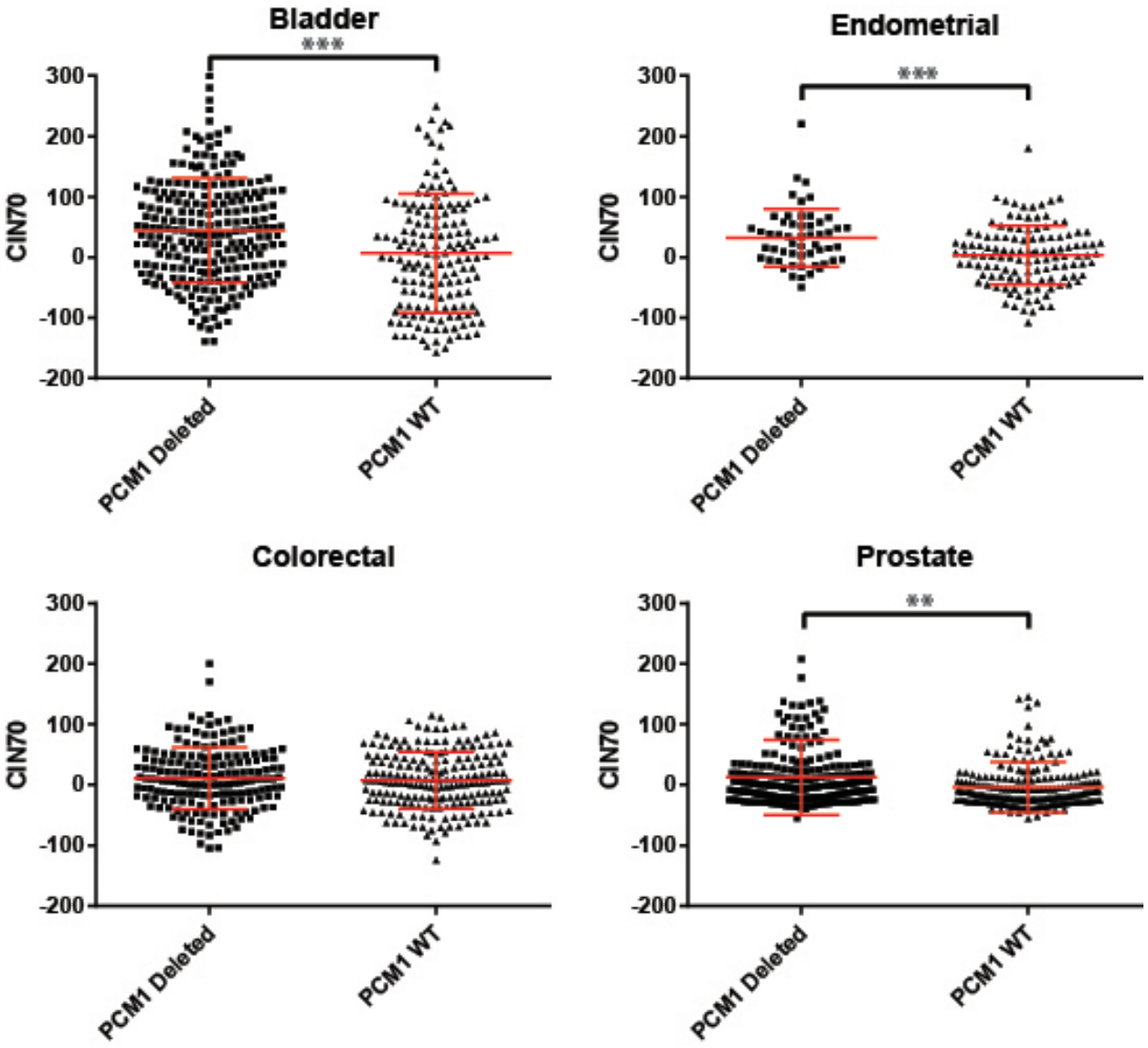

Figure 8-5

PCM1 knockout cells are more sensitive to autophagy inhibitors.

The indicated HeLa cell lines were exposed to three different concentrations of the indicated drugs. Cell viability was assessed on day 4 by Vita Orange (CCK-8) staining. Viability values are normalized to the untreated control for each different cell line.

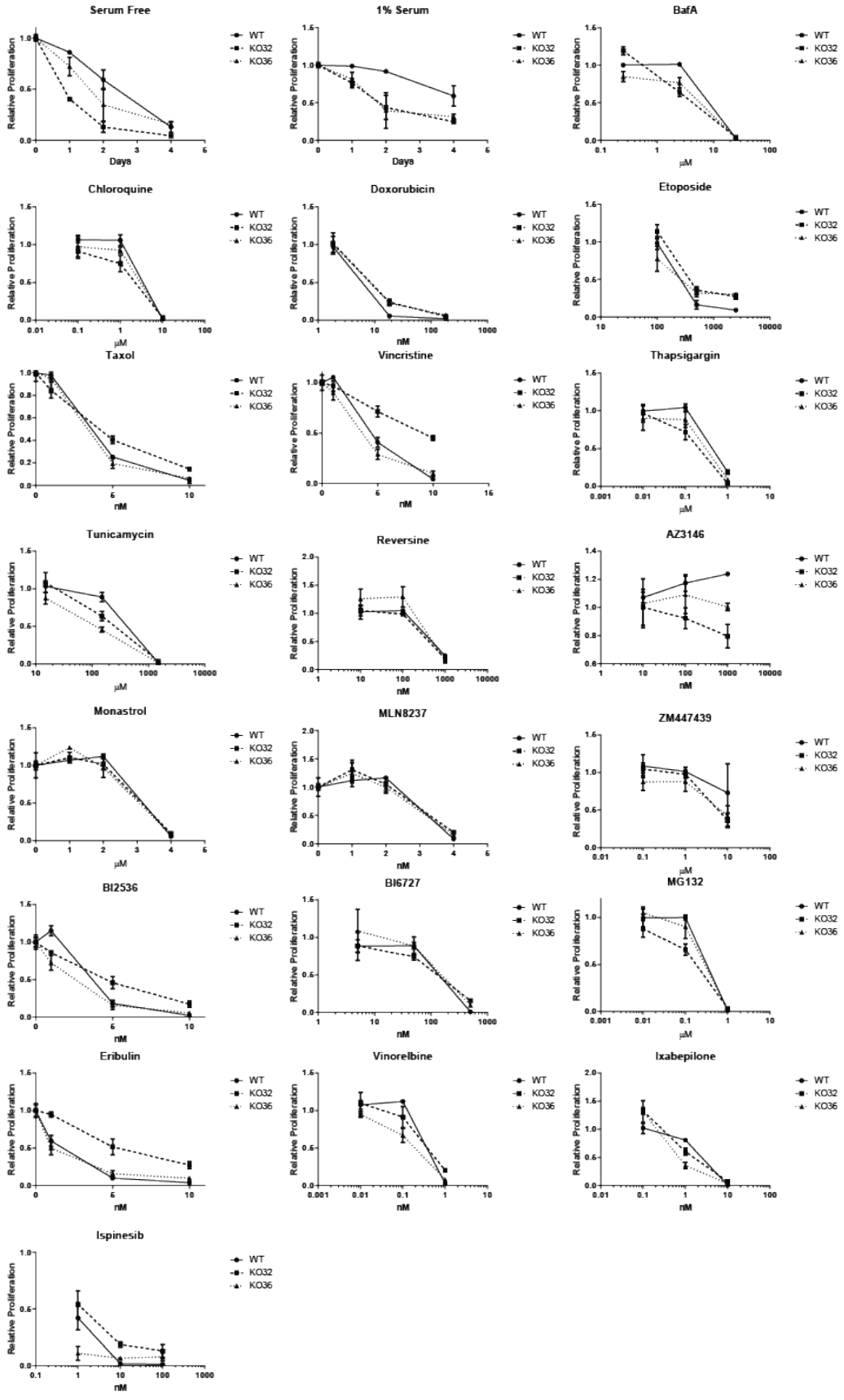
Serum Free
1% Serum
BafA
Chloroquine
Doxorubicin
Etoposide
Taxol
Vincristine
Thapsigargin
Tunicamycin
Reversine
AZ3146
Monastrol
MLN8237
ZM447439
BI2536
BI6727
MG132
Eribulin
Vinorelbine
Ixabepilone
Ispinesib
Relative Proliferation
Days
µM
nM
WT
KO32
KO36

Supplemental Table 8-1

Hazard ratios from multivariate survival analysis.

Endometrial

	OS		**DFS**	
	HR	**P-Value**	**HR**	**P-Value**
PCM1 deletion	2.70 (1.29-5.67)	0.009	1.83 (0.94-3.56)	0.076
Stage	1.15 (1.09-1.21)	<0.001	1.55 (1.18-2.03)	0.002

Prostate

	OS		**DFS**	
	HR	**P-Value**	**HR**	**P-Value**
PCM1 deletion	1.57 (0.31-7.90)	0.583	1.47 (0.85-2.53)	0.168
Stage	0.97 (0.19-4.87)	0.968	1.67 (1.05-2.66)	0.031
Gleason	2.41 (0.98-5.92)	0.056	1.98 (1.57-2.50)	<0.001

Colorectal

	OS		**DFS**	
	HR	**P-Value**	**HR**	**P-Value**
PCM1 deletion	0.89 (0.45-1.78)	0.751	1.19 (0.60-2.36)	0.619
Stage	2.12 (1.72-2.62)	<0.001	2.03 (1.65-2.50)	<0.001

Bladder

	OS		**DFS**	
	HR	**P-Value**	**HR**	**P-Value**
PCM1 deletion	1.13 (0.64-1.99)	0.674	2.13 (1.26-3.60)	0.005
Stage	1.73 (1.43-2.09)	<0.001	1.79 (1.45-2.20)	<0.001

Acknowledgements

The authors thank: Brian Dynlacht and Lei Wang (NYU) for cell lines; Takashi Toda (Hiroshima University) for reagents; Jun Wan and Beth Weaver (University of Wisconsin-Madison) for reagents; the University of Wisconsin Translational Initiatives in Pathology (TRIP) Laboratory; the University of Wisconsin Small Molecule Screening and Synthesis Facility; the University of Wisconsin Carbone Cancer Center Flow Cytometry Laboratory. This project is supported by R01 GM097245 to MEB, F30CA203271 to RAD, and University of Wisconsin Carbone Cancer Center Support Grant P30 CA014520. RAD is in the University of Wisconsin Medical Scientist Training Program (T32GM008692). The content is the responsibility of the authors and does not necessarily represent the views of the NIH.

CHAPTER 9: Perspectives

The centrosome is the major microtubule organizer of human cells. Polo-like kinase 4 (PLK4) is the master regulator of centriole duplication; however, the phosphoproteome of PLK4 has not been entirely mapped. One focus of this thesis was to probe the phosphoproteome of PLK4 and identify potential novel substrates and functions. Centrosome amplification (CA), or a numerical increase in centrosomes, is common in human cancer, causes mitotic errors and chromosomal instability (CIN), and correlates with worse patient outcomes. However, the causes and consequences of CA in human cancer have not been fully elucidated. The focus of this thesis was to further identify the causes and consequences of CA using unbiased approaches, and then to narrow in on the specific molecular underpinnings of the causes and consequences of CA. Here, I highlight several important findings from my work and suggest potential avenues for future work.

Canonical and non-canonical roles of PLK4

A number of centrosomal PLK4 substrates relevant to highly regulated centriole duplication are known. Most notably, PLK4 autophosphorylation results in ubiquitination by the βTrCP E3 ubiquitin ligase complex and subsequent proteasomal degradation,[66,67,70,100] which is critical for limiting PLK4-mediated centriole duplication to once per cell cycle. Effectors such as FBXW5,[94] GCP6,[95] CP110,[98] SAS6,[93] ECT2,[319] and STIL/Ana2 [64,91,92] are important for the centriole duplication. PLK4 phosphorylation of PCM1 is important for controlling the integrity of centriolar satellites.[103] Other genes, such as CEP152,[91,408] CDC25C,[409] CHK2,[410] ARP2,[168] and HAND1,[407] have been identified as PLK4 substrates, but the function of these phosphorylation events is not well understood. Three previous studies have reported mass

spectrometry (MS)-based screens to identify PLK4 substrates and/or interactors. One study purified Plx4 from *Xenopus* egg extracts by affinity chromatography and analyzed its associated binding partners by MS,[408] the second study performed PLK4 BioID to identify proximity interactions,[411] and the third study immunoprecipitated tagged PLK4 from HeLa cells and examined binding partners by MS.[91] To our knowledge, there has not been reported an unbiased MS-based analysis of PLK4 phosphorylation targets. In this thesis, a chemical genetic system was utilized to perform an unbiased MS-based analysis of PLK4 phosphorylation targets in non-transformed human cells to discover novel substrates of PLK4. We identify CEP131 as a novel substrate of PLK4, and that PLK4 phosphorylation of CEP131 is an important contributor to maintaining centriolar satellite integrity.

This work also identified CEP170 and CDK5RAP2 to be substrates of PLK4. Future work will be needed to assess the potential cellular functions of these phosphorylation events. Additionally, future work is needed to test other potential substrates that were identified in our phosphoproteomic screen.

Causes of centrosome amplification in human cancer

Many previous studies have identified ways to amplify centrioles *in cellulo*, such as overexpression of pericentrin,[185] PLK4,[126] SASS6,[183] CEP57,[198] PIM1,[199] CEP70,[200] γ-tubulin, CEP152,[201] MPS1,[202,203] cyclin A,[204] cyclin E,[243,270,271] SIRT2,[205] MOB1A/B,[206] STIL,[184] Aurora A,[207] Aurora B[207], PLK1,[207] among others.[114] However, the clinical relevance of these mechanisms is unclear and has not been demonstrated. To address this question, I analyzed genomic and transcriptomic alterations in the 366 centrosome proteins using TCGA data from 9555 patients representing 21 of the most common tumor sites. I then identified a short list of

centrosome proteins that are most frequently altered in cancer, then tested them *in cellulo* to determine the predominant causes of CA in cancer. This work identified MCPH1 deletion to be a common and penetrant cause of CA in human cancer (Chapter 4).

My work has demonstrated that approximately 35% of cancers have CA, defined as having an average of greater than 2 centrosomes per cell (Chapter 2). Of this 35%, most (approximately 80%, Chapter 3) of CA is due to centriole overduplication, while a smaller fraction (approximately 20%) is due to cell doubling (Chapter 3). Viral causes (e.g. EBV, HPV) likely account for 10%, cyclin E amplification accounts for 15%, and we estimate that MCPH1 deletion accounts for 30%. This leaves unexplained an additional 45% of cases of centriole overduplication.

Future work will be necessary to identify this remaining 45% of centriole overduplication in human cancer. One way to do this would be to assess genomic, transcriptomic, and proteomic changes in centrosome genes and centriole duplication regulators in the breast tumors we identified to have CA. Similar analyses could be done using NCI-60 cell lines, as recent data have been reported on centrosome abnormalities (both centriole number and length) in these NCI-60 cell lines.[209]

In addition, the major causes of cell doubling events (e.g. cytokinesis failure) remain unclear and are a necessary avenue of future investigation.

Consequences of centrosome amplification in human cancer

CA has a number of consequences, including chromosomal instability, high-grade phenotypes, and cellular invasiveness.[108,109,123,124,126,134,165,179,197] Understanding the causes and consequences of CA can help us identify therapeutic strategies to treat cancer. Herein, I have

identified additional consequences of CA. I confirm the finding that CA causes multipolar spindles and lagging chromosomes (Chapter 5). Furthermore, I identify autophagy to be altered in cells with CA and find that cells with CA are more sensitive to autophagy inhibition (Chapter 6).

The multipolar divisions seen in cells with CA and the resulting CIN can impair cell viability, frequently leading to cell death.[134,322] Prior work has demonstrated that cells with CA rely on centrosome clustering for survival, and this clustering was found to be dependent on HSET/KIFC1.[36,137,458] Other mediators of centrosome clustering include: PI3K through regulation of the actin cytoskeleton; NEK6;[469] and Hsp72.[469] HSET inhibitors have been developed, including AZ82,[470] which blocks the ATP binding pocket, and CW069,[471] which binds to an allosteric site. Clinical trials involving these or future agents represent attractive areas of future investigation.

Because CA is a prognostic and potentially a predictive biomarker, it will be important to develop a translatable, high throughout method to quantify centrosomes in human cancer. This could enable CA to be used as a prognostic and/or predictive biomarker for cancer.

Biologic functions of centriolar satellites

Centriolar satellites are a relatively understudied cellular structure. This thesis serendipitously wandered into the realm of centriolar satellites after the discovery of CEP131, a centriolar satellite component, as a substrate of PLK4 (Chapter 7). Centriolar satellites are protein-rich, electron-dense regions that surround the centrosome and regulate movement of proteins to and from the centrosome.[24,442] They are important for recruiting factors involved in microtubule nucleation, ciliogenesis, and centriole duplication.[25,26] Accumulating evidence

suggests that centriolar satellites are also important for maintaining genomic stability. PCM1 is involved in spindle pole integrity during metaphase.[448] Additionally, depletion of other centriolar satellite proteins causes mitotic errors. For example, depletion of CEP131,[416] CEP72,[449] CEP90,[450] and PAR6A[451] result in increased multipolar spindles. The work in this thesis also found that PCM1 deletion is common in human cancer and causes multipolar spindles, likely leading to CIN and aneuploidy (Chapter 8). Further work will be necessary to continue to learn about all the functions of centriolar satellites, including their role in human cancer.

Chromosomal instability as a predictive biomarker for autophagy inhibitors

In this thesis, I have reported two different mechanisms of CIN (CA and PCM1 deletion) that cause an increased reliance on autophagy and sensitivity to autophagy inhibitors. Furthermore, generation of CIN by inhibiting the mitotic checkpoint kinase MPS1 has been reported to generate a TFEB-mediated autophagic stress response.[374] The exact mechanism by which CIN causes an accumulation of autophagosomes and increased sensitivity to autophagy inhibitors remains unclear and will need to be determined. The leading hypothesis is that CIN generates aneuploidy, which causes a stoichiometric imbalance in chromosome number and therefore a stoichiometric imbalance in the transcriptome and proteome. This is thought to cause aberrant protein complex formation, causing an increased reliance on autophagy to clear these aberrant protein complexes.[376,377,383,384] Taken together, these results suggest that cancers with high CIN may be sensitized to autophagy inhibition.

Future work will be necessary to further substantiate CIN as a predictive biomarker for autophagy inhibitors. Several different mechanisms of CIN should be tested in mouse xenograft experiments treated with autophagy inhibitors. Furthermore, development of more specific

autophagy inhibitors will be necessary; many clinical trials are utilizing non-specific autophagy inhibitors such as hydroxychloroquine.[472,473] Newer, more specific inhibitors, such as ULK1 inhibitors, have been developed.[474] To date, cancer clinical trials involving autophagy inhibitors have been largely unsuccessful. Perhaps one of the reasons for this is lack of tailoring these inhibitors to the patients that will benefit the most, such as patients with high-CIN cancers.

Additionally, since MCPH1 and PCM1 are both located on chromosome 8p and because chromosome 8p deletions are common in human cancer, chromosome 8p deletion may be a predictive biomarker for autophagy inhibitors. Additional preclinical models of chromosome 8p-deleted tumors and subsequent prospective clinical trials with autophagy inhibitors will be necessary to substantiate this potential therapeutic strategy.

Conclusion

This thesis has contributed to our understanding of the causes and consequences of CA in human cancer. The major findings include: (1) CA is prognostic of worse patient survival in breast cancer; (2) CA is predominantly caused by centriole overduplication versus cell doubling (e.g. cytokinesis failure); (3) genomic deletion of MCPH1 is a common and penetrant cause of centriole overduplication in human cancer; (4) loss of centrioles may occur in a small subset of human cancers; (5) centrosome-mediated microtubule nucleation is important for autophagy; (6) CA causes an increased reliance on autophagy and sensitizes cells to autophagy inhibition; (7) mapping of the PLK4 phosphoproteome reveals CEP131 to be a substrate of PLK4, and this phosphorylation event is important for the organization of centriolar satellites; (8) PLK4 phosphorylates CEP170 and CDK5RAP2; (9) CEP170 is a centriolar subdistal appendage protein that is important for genomic stability; (10) centriolar satellites are important for

chromosomal stability; and (11) PCM1 deletion is common in human cancer, results in CIN, and causes an increased reliance on autophagy. Our unbiased phosphoproteomic experiment has the potential to reveal additional substrates of PLK4 and potentially novel roles of PLK4. In addition, our findings suggest that CIN may be a predictive biomarker for autophagy inhibitors in human cancer, and further study is warranted.

REFERENCES

1. Wunderlich V. JMM—past and present. Chromosomes and cancer: Theodor Boveri's predictions 100 years later. *J Mol Med (Berl)*. 2002;80:545–548.

2. Boveri T. Concerning the origin of malignant tumours by Theodor Boveri. Translated and annotated by Henry Harris. *J Cell Sci*. 2008;121 Suppl 1:1-84.

3. Azimzadeh J. Exploring the evolutionary history of centrosomes. *Philos Trans R Soc Lond B Biol Sci*. 2014;369(1650).

4. Carvalho-Santos Z, Azimzadeh J, Pereira-Leal JB, Bettencourt-Dias M. Evolution: Tracing the origins of centrioles, cilia, and flagella. *J Cell Biol*. 2011;194(2):165-175.

5. Bornens M, Azimzadeh J. Origin and evolution of the centrosome. *Adv Exp Med Biol*. 2007;607:119-129.

6. Mitchell DR. The evolution of eukaryotic cilia and flagella as motile and sensory organelles. *Adv Exp Med Biol*. 2007;607:130-140.

7. Mitchell DR. Evolution of Cilia. *Cold Spring Harb Perspect Biol*. 2017;9(1).

8. Gupta A, Kitagawa D. Ultrastructural diversity between centrioles of eukaryotes. *J Biochem*. 2018.

9. Jaspersen SL, Winey M. The budding yeast spindle pole body: structure, duplication, and function. *Annu Rev Cell Dev Biol*. 2004;20:1-28.

10. Conduit PT, Wainman A, Raff JW. Centrosome function and assembly in animal cells. *Nat Rev Mol Cell Biol*. 2015;16(10):611-624.

11. Azimzadeh J, Marshall WF. Building the centriole. *Curr Biol*. 2010;20(18):R816-825.

12. Wloga D, Dave D, Meagley J, Rogowski K, Jerka-Dziadosz M, Gaertig J. Hyperglutamylation of tubulin can either stabilize or destabilize microtubules in the same cell. *Eukaryot Cell*. 2010;9(1):184-193.

13. Bobinnec Y, Moudjou M, Fouquet JP, Desbruyères E, Eddé B, Bornens M. Glutamylation of centriole and cytoplasmic tubulin in proliferating non-neuronal cells. *Cell Motil Cytoskeleton*. 1998;39(3):223-232.

14. Kitagawa D, Vakonakis I, Olieric N, et al. Structural basis of the 9-fold symmetry of centrioles. *Cell*. 2011;144(3):364-375.

15. van Breugel M, Hirono M, Andreeva A, et al. Structures of SAS-6 suggest its organization in centrioles. *Science*. 2011;331(6021):1196-1199.

16. González C, Tavosanis G, Mollinari C. Centrosomes and microtubule organisation during Drosophila development. *J Cell Sci*. 1998;111 (Pt 18):2697-2706.

17. LEVINE RP, EBERSOLD WT. The genetics and cytology of Chlamydomonas. *Annu Rev Microbiol*. 1960;14:197-216.

18. Tanos BE, Yang HJ, Soni R, et al. Centriole distal appendages promote membrane docking, leading to cilia initiation. *Genes Dev*. 2013;27(2):163-168.

19. Bornens M. Centrosome composition and microtubule anchoring mechanisms. *Curr Opin Cell Biol*. 2002;14(1):25-34.

20. Dictenberg JB, Zimmerman W, Sparks CA, et al. Pericentrin and gamma-tubulin form a protein complex and are organized into a novel lattice at the centrosome. *J Cell Biol*. 1998;141(1):163-174.

21. Young A, Dictenberg JB, Purohit A, Tuft R, Doxsey SJ. Cytoplasmic dynein-mediated assembly of pericentrin and gamma tubulin onto centrosomes. *Mol Biol Cell*. 2000;11(6):2047-2056.

22. Lüders J, Stearns T. Microtubule-organizing centres: a re-evaluation. *Nat Rev Mol Cell Biol*. 2007;8(2):161-167.

23. Raynaud-Messina B, Merdes A. Gamma-tubulin complexes and microtubule organization. *Curr Opin Cell Biol*. 2007;19(1):24-30.

24. Hori A, Toda T. Regulation of centriolar satellite integrity and its physiology. *Cell Mol Life Sci*. 2016.

25. Dammermann A, Merdes A. Assembly of centrosomal proteins and microtubule organization depends on PCM-1. *J Cell Biol*. 2002;159(2):255-266.

26. Kodani A, Yu TW, Johnson JR, et al. Centriolar satellites assemble centrosomal microcephaly proteins to recruit CDK2 and promote centriole duplication. *Elife*. 2015;4.

27. Balczon R, Bao L, Zimmer WE. PCM-1, A 228-kD centrosome autoantigen with a distinct cell cycle distribution. *J Cell Biol*. 1994;124(5):783-793.

28. Lopes CA, Prosser SL, Romio L, et al. Centriolar satellites are assembly points for proteins implicated in human ciliopathies, including oral-facial-digital syndrome 1. *J Cell Sci*. 2011;124(Pt 4):600-612.

29. Hori A, Ikebe C, Tada M, Toda T. Msd1/SSX2IP-dependent microtubule anchorage ensures spindle orientation and primary cilia formation. *EMBO Rep*. 2014;15(2):175-184.

30. Balczon R, West K. The identification of mammalian centrosomal antigens using human autoimmune anticentrosome antisera. *Cell Motil Cytoskeleton*. 1991;20(2):121-135.

31. Kubo A, Tsukita S. Non-membranous granular organelle consisting of PCM-1: subcellular distribution and cell-cycle-dependent assembly/disassembly. *J Cell Sci*. 2003;116(Pt 5):919-928.

32. Farina F, Gaillard J, Guérin C, et al. The centrosome is an actin-organizing centre. *Nat Cell Biol*. 2016;18(1):65-75.

33. Tanaka T, Serneo FF, Higgins C, Gambello MJ, Wynshaw-Boris A, Gleeson JG. Lis1 and doublecortin function with dynein to mediate coupling of the nucleus to the centrosome in neuronal migration. *J Cell Biol*. 2004;165(5):709-721.

34. Tsai JW, Bremner KH, Vallee RB. Dual subcellular roles for LIS1 and dynein in radial neuronal migration in live brain tissue. *Nat Neurosci*. 2007;10(8):970-979.

35. Mahjoub MR. The importance of a single primary cilium. *Organogenesis*. 2013;9(2):61-69.

36. Basto R, Lau J, Vinogradova T, et al. Flies without centrioles. *Cell*. 2006;125(7):1375-1386.

37. Bettencourt-Dias M, Glover DM. Centrosome biogenesis and function: centrosomics brings new understanding. *Nat Rev Mol Cell Biol*. 2007;8(6):451-463.

38. Debec A, Sullivan W, Bettencourt-Dias M. Centrioles: active players or passengers during mitosis? *Cell Mol Life Sci*. 2010;67(13):2173-2194.

39. Azimzadeh J, Wong ML, Downhour DM, Sánchez Alvarado A, Marshall WF. Centrosome loss in the evolution of planarians. *Science*. 2012;335(6067):461-463.

40. Canning EU, Curry A, Hill SL, Okamura B. Ultrastructure of Buddenbrockia allmani n. sp. (Myxozoa, Malacosporea), a parasite of Lophopus crystallinus (Bryozoa, Phylactolaemata). *J Eukaryot Microbiol*. 2007;54(3):247-262.

41. Debec A, Abbadie C. The acentriolar state of the Drosophila cell lines 1182. *Biol Cell*. 1989;67(3):307-311.

42. Calarco-Gillam PD, Siebert MC, Hubble R, Mitchison T, Kirschner M. Centrosome development in early mouse embryos as defined by an autoantibody against pericentriolar material. *Cell*. 1983;35(3 Pt 2):621-629.

43. Rodrigues-Martins A, Riparbelli M, Callaini G, Glover DM, Bettencourt-Dias M. From centriole biogenesis to cellular function: centrioles are essential for cell division at critical developmental stages. *Cell Cycle*. 2008;7(1):11-16.

44. Dzafic E, Strzyz PJ, Wilsch-Bräuninger M, Norden C. Centriole Amplification in Zebrafish Affects Proliferation and Survival but Not Differentiation of Neural Progenitor Cells. *Cell Rep*. 2015;13(1):168-182.

45. Nigg EA, Raff JW. Centrioles, centrosomes, and cilia in health and disease. *Cell*. 2009;139(4):663-678.

46. Thornton GK, Woods CG. Primary microcephaly: do all roads lead to Rome? *Trends Genet*. 2009;25(11):501-510.

47. Higginbotham HR, Gleeson JG. The centrosome in neuronal development. *Trends Neurosci*. 2007;30(6):276-283.

48. Sir JH, Pütz M, Daly O, et al. Loss of centrioles causes chromosomal instability in vertebrate somatic cells. *J Cell Biol*. 2013;203(5):747-756.

49. Nigg EA, Stearns T. The centrosome cycle: Centriole biogenesis, duplication and inherent asymmetries. *Nat Cell Biol*. 2011;13(10):1154-1160.

50. Bettencourt-Dias M, Hildebrandt F, Pellman D, Woods G, Godinho SA. Centrosomes and cilia in human disease. *Trends Genet*. 2011;27(8):307-315.

51. Vaughan S, Dawe HR. Common themes in centriole and centrosome movements. *Trends Cell Biol*. 2011;21(1):57-66.

52. Strnad P, Gönczy P. Mechanisms of procentriole formation. *Trends Cell Biol*. 2008;18(8):389-396.

53. O'Connell KF, Caron C, Kopish KR, et al. The C. elegans zyg-1 gene encodes a regulator of centrosome duplication with distinct maternal and paternal roles in the embryo. *Cell*. 2001;105(4):547-558.

54. Leidel S, Delattre M, Cerutti L, Baumer K, Gönczy P. SAS-6 defines a protein family required for centrosome duplication in C. elegans and in human cells. *Nat Cell Biol*. 2005;7(2):115-125.

55. Kirkham M, Müller-Reichert T, Oegema K, Grill S, Hyman AA. SAS-4 is a C. elegans centriolar protein that controls centrosome size. *Cell*. 2003;112(4):575-587.

56. Dammermann A, Müller-Reichert T, Pelletier L, Habermann B, Desai A, Oegema K. Centriole assembly requires both centriolar and pericentriolar material proteins. *Dev Cell*. 2004;7(6):815-829.

57. Leidel S, Gönczy P. SAS-4 is essential for centrosome duplication in C elegans and is recruited to daughter centrioles once per cell cycle. *Dev Cell*. 2003;4(3):431-439.

58. Kemp CA, Kopish KR, Zipperlen P, Ahringer J, O'Connell KF. Centrosome maturation and duplication in C. elegans require the coiled-coil protein SPD-2. *Dev Cell*. 2004;6(4):511-523.

59. Pelletier L, Ozlü N, Hannak E, et al. The Caenorhabditis elegans centrosomal protein SPD-2 is required for both pericentriolar material recruitment and centriole duplication. *Curr Biol*. 2004;14(10):863-873.

60. Delattre M, Leidel S, Wani K, et al. Centriolar SAS-5 is required for centrosome duplication in C. elegans. *Nat Cell Biol*. 2004;6(7):656-664.

61. Sánchez I, Dynlacht BD. Cilium assembly and disassembly. *Nat Cell Biol*. 2016;18(7):711-717.

62. Bettencourt-Dias M, Rodrigues-Martins A, Carpenter L, et al. SAK/PLK4 is required for centriole duplication and flagella development. *Curr Biol*. 2005;15(24):2199-2207.

63. Habedanck R, Stierhof YD, Wilkinson CJ, Nigg EA. The Polo kinase Plk4 functions in centriole duplication. *Nat Cell Biol*. 2005;7(11):1140-1146.

64. Moyer TC, Clutario KM, Lambrus BG, Daggubati V, Holland AJ. Binding of STIL to Plk4 activates kinase activity to promote centriole assembly. *J Cell Biol*. 2015;209(6):863-878.

65. Guichard P, Hamel V, Le Guennec M, et al. Cell-free reconstitution reveals centriole cartwheel assembly mechanisms. *Nat Commun*. 2017;8:14813.

66. Guderian G, Westendorf J, Uldschmid A, Nigg EA. Plk4 trans-autophosphorylation regulates centriole number by controlling betaTrCP-mediated degradation. *J Cell Sci*. 2010;123(Pt 13):2163-2169.

67. Holland AJ, Fachinetti D, Zhu Q, et al. The autoregulated instability of Polo-like kinase 4 limits centrosome duplication to once per cell cycle. *Genes Dev*. 2012;26(24):2684-2689.

68. Holland AJ, Lan W, Niessen S, Hoover H, Cleveland DW. Polo-like kinase 4 kinase activity limits centrosome overduplication by autoregulating its own stability. *J Cell Biol*. 2010;188(2):191-198.

69. Rogers GC, Rusan NM, Roberts DM, Peifer M, Rogers SL. The SCF Slimb ubiquitin ligase regulates Plk4/Sak levels to block centriole reduplication. *J Cell Biol*. 2009;184(2):225-239.

70. Sillibourne JE, Tack F, Vloemans N, et al. Autophosphorylation of polo-like kinase 4 and its role in centriole duplication. *Mol Biol Cell*. 2010;21(4):547-561.

71. Kohlmaier G, Loncarek J, Meng X, et al. Overly long centrioles and defective cell division upon excess of the SAS-4-related protein CPAP. *Curr Biol*. 2009;19(12):1012-1018.

72. Schmidt TI, Kleylein-Sohn J, Westendorf J, et al. Control of centriole length by CPAP and CP110. *Curr Biol*. 2009;19(12):1005-1011.

73. Tang CJ, Fu RH, Wu KS, Hsu WB, Tang TK. CPAP is a cell-cycle regulated protein that controls centriole length. *Nat Cell Biol*. 2009;11(7):825-831.

74. Azimzadeh J, Hergert P, Delouvée A, et al. hPOC5 is a centrin-binding protein required for assembly of full-length centrioles. *J Cell Biol*. 2009;185(1):101-114.

75. Singla V, Romaguera-Ros M, Garcia-Verdugo JM, Reiter JF. Ofd1, a human disease gene, regulates the length and distal structure of centrioles. *Dev Cell*. 2010;18(3):410-424.

76. Kleylein-Sohn J, Westendorf J, Le Clech M, Habedanck R, Stierhof YD, Nigg EA. Plk4-induced centriole biogenesis in human cells. *Dev Cell*. 2007;13(2):190-202.

77. Spektor A, Tsang WY, Khoo D, Dynlacht BD. Cep97 and CP110 suppress a cilia assembly program. *Cell*. 2007;130(4):678-690.

78. Lee K, Rhee K. PLK1 phosphorylation of pericentrin initiates centrosome maturation at the onset of mitosis. *J Cell Biol*. 2011;195(7):1093-1101.

79. Lane HA, Nigg EA. Antibody microinjection reveals an essential role for human polo-like kinase 1 (Plk1) in the functional maturation of mitotic centrosomes. *J Cell Biol*. 1996;135(6 Pt 2):1701-1713.

80. Joukov V, Walter JC, De Nicolo A. The Cep192-organized aurora A-Plk1 cascade is essential for centrosome cycle and bipolar spindle assembly. *Mol Cell*. 2014;55(4):578-591.

81. Mayor T, Stierhof YD, Tanaka K, Fry AM, Nigg EA. The centrosomal protein C-Nap1 is required for cell cycle-regulated centrosome cohesion. *J Cell Biol*. 2000;151(4):837-846.

82. Meraldi P, Nigg EA. Centrosome cohesion is regulated by a balance of kinase and phosphatase activities. *J Cell Sci*. 2001;114(Pt 20):3749-3757.

83. Tsou MF, Wang WJ, George KA, Uryu K, Stearns T, Jallepalli PV. Polo kinase and separase regulate the mitotic licensing of centriole duplication in human cells. *Dev Cell*. 2009;17(3):344-354.

84. Arquint C, Nigg EA. STIL microcephaly mutations interfere with APC/C-mediated degradation and cause centriole amplification. *Curr Biol*. 2014;24(4):351-360.

85. Wang WJ, Soni RK, Uryu K, Tsou MF. The conversion of centrioles to centrosomes: essential coupling of duplication with segregation. *J Cell Biol*. 2011;193(4):727-739.

86. Novak ZA, Wainman A, Gartenmann L, Raff JW. Cdk1 Phosphorylates Drosophila Sas-4 to Recruit Polo to Daughter Centrioles and Convert Them to Centrosomes. *Dev Cell*. 2016;37(6):545-557.

87. de Cárcer G, Manning G, Malumbres M. From Plk1 to Plk5: functional evolution of polo-like kinases. *Cell Cycle*. 2011;10(14):2255-2262.

88. Fode C, Binkert C, Dennis JW. Constitutive expression of murine Sak-a suppresses cell growth and induces multinucleation. *Mol Cell Biol*. 1996;16(9):4665-4672.

89. Slevin LK, Nye J, Pinkerton DC, Buster DW, Rogers GC, Slep KC. The structure of the plk4 cryptic polo box reveals two tandem polo boxes required for centriole duplication. *Structure*. 2012;20(11):1905-1917.

90. Leung GC, Hudson JW, Kozarova A, Davidson A, Dennis JW, Sicheri F. The Sak polo-box comprises a structural domain sufficient for mitotic subcellular localization. *Nat Struct Biol*. 2002;9(10):719-724.

91. Kratz AS, Bärenz F, Richter KT, Hoffmann I. Plk4-dependent phosphorylation of STIL is required for centriole duplication. *Biol Open*. 2015;4(3):370-377.

92. Dzhindzhev NS, Tzolovsky G, Lipinszki Z, et al. Plk4 phosphorylates Ana2 to trigger Sas6 recruitment and procentriole formation. *Curr Biol*. 2014;24(21):2526-2532.

93. Kitagawa D, Busso C, Flückiger I, Gönczy P. Phosphorylation of SAS-6 by ZYG-1 is critical for centriole formation in C. elegans embryos. *Dev Cell*. 2009;17(6):900-907.

94. Puklowski A, Homsi Y, Keller D, et al. The SCF-FBXW5 E3-ubiquitin ligase is regulated by PLK4 and targets HsSAS-6 to control centrosome duplication. *Nat Cell Biol*. 2011;13(8):1004-1009.

95. Bahtz R, Seidler J, Arnold M, et al. GCP6 is a substrate of Plk4 and required for centriole duplication. *J Cell Sci*. 2012;125(Pt 2):486-496.

96. Galletta BJ, Fagerstrom CJ, Schoborg TA, et al. A centrosome interactome provides insight into organelle assembly and reveals a non-duplication role for Plk4. *Nat Commun*. 2016;7:12476.

97. Chang J, Cizmecioglu O, Hoffmann I, Rhee K. PLK2 phosphorylation is critical for CPAP function in procentriole formation during the centrosome cycle. *EMBO J*. 2010;29(14):2395-2406.

98. Lee M, Seo MY, Chang J, Hwang DS, Rhee K. PLK4 phosphorylation of CP110 is required for efficient centriole assembly. *Cell Cycle*. 2017;16(12):1225-1234.

99. Xu X, Huang S, Zhang B, et al. DNA replication licensing factor Cdc6 and Plk4 kinase antagonistically regulate centrosome duplication via Sas-6. *Nat Commun*. 2017;8:15164.

100. Cunha-Ferreira I, Bento I, Pimenta-Marques A, et al. Regulation of autophosphorylation controls PLK4 self-destruction and centriole number. *Curr Biol*. 2013;23(22):2245-2254.

101. Martin CA, Ahmad I, Klingseisen A, et al. Mutations in PLK4, encoding a master regulator of centriole biogenesis, cause microcephaly, growth failure and retinopathy. *Nat Genet*. 2014;46(12):1283-1292.

102. Wheway G, Schmidts M, Mans DA, et al. An siRNA-based functional genomics screen for the identification of regulators of ciliogenesis and ciliopathy genes. *Nat Cell Biol*. 2015;17(8):1074-1087.

103. Hori A, Barnouin K, Snijders AP, Toda T. A non-canonical function of Plk4 in centriolar satellite integrity and ciliogenesis through PCM1 phosphorylation. *EMBO Rep*. 2016;17(3):326-337.

104. Giansanti MG, Gatti M, Bonaccorsi S. The role of centrosomes and astral microtubules during asymmetric division of Drosophila neuroblasts. *Development*. 2001;128(7):1137-1145.

105. Lancaster MA, Knoblich JA. Spindle orientation in mammalian cerebral cortical development. *Curr Opin Neurobiol*. 2012;22(5):737-746.

106. Chen JF, Zhang Y, Wilde J, Hansen KC, Lai F, Niswander L. Microcephaly disease gene Wdr62 regulates mitotic progression of embryonic neural stem cells and brain size. *Nat Commun*. 2014;5:3885.

107. Chan JY. A clinical overview of centrosome amplification in human cancers. *Int J Biol Sci*. 2011;7(8):1122-1144.

108. Pihan GA, Purohit A, Wallace J, et al. Centrosome defects and genetic instability in malignant tumors. *Cancer Res*. 1998;58(17):3974-3985.

109. Denu RA, Zasadil LM, Kanugh C, Laffin J, Weaver BA, Burkard ME. Centrosome amplification induces high grade features and is prognostic of worse outcomes in breast cancer. *BMC Cancer*. 2016;16(1):47.

110. Lingle WL, Salisbury JL. Altered centrosome structure is associated with abnormal mitoses in human breast tumors. *Am J Pathol*. 1999;155(6):1941-1951.

111. Lingle WL, Lutz WH, Ingle JN, Maihle NJ, Salisbury JL. Centrosome hypertrophy in human breast tumors: implications for genomic stability and cell polarity. *Proc Natl Acad Sci U S A*. 1998;95(6):2950-2955.

112. Krämer A, Neben K, Ho AD. Centrosome aberrations in hematological malignancies. *Cell Biol Int*. 2005;29(5):375-383.

113. Giehl M, Fabarius A, Frank O, et al. Centrosome aberrations in chronic myeloid leukemia correlate with stage of disease and chromosomal instability. *Leukemia*. 2005;19(7):1192-1197.

114. Godinho SA, Pellman D. Causes and consequences of centrosome abnormalities in cancer. *Philos Trans R Soc Lond B Biol Sci*. 2014;369(1650).

115. Pihan GA, Wallace J, Zhou Y, Doxsey SJ. Centrosome abnormalities and chromosome instability occur together in pre-invasive carcinomas. *Cancer Res*. 2003;63(6):1398-1404.

116. Kronenwett U, Huwendiek S, Ostring C, et al. Improved grading of breast adenocarcinomas based on genomic instability. *Cancer Res*. 2004;64(3):904-909.

117. D'Assoro AB, Barrett SL, Folk C, et al. Amplified centrosomes in breast cancer: a potential indicator of tumor aggressiveness. *Breast Cancer Res Treat*. 2002;75(1):25-34.

118. Schneeweiss A, Sinn HP, Ehemann V, et al. Centrosomal aberrations in primary invasive breast cancer are associated with nodal status and hormone receptor expression. *Int J Cancer*. 2003;107(3):346-352.

119. Bagheri-Yarmand R, Biernacka A, Hunt KK, Keyomarsi K. Low molecular weight cyclin E overexpression shortens mitosis, leading to chromosome missegregation and centrosome amplification. *Cancer Res*. 2010;70(12):5074-5084.

120. Guo HQ, Gao M, Ma J, et al. Analysis of the cellular centrosome in fine-needle aspirations of the breast. *Breast Cancer Res*. 2007;9(4):R48.

121. Pannu V, Mittal K, Cantuaria G, et al. Rampant centrosome amplification underlies more aggressive disease course of triple negative breast cancers. *Oncotarget*. 2015;6(12):10487-10497.

122. Levine MS, Bakker B, Boeckx B, et al. Centrosome Amplification Is Sufficient to Promote Spontaneous Tumorigenesis in Mammals. *Dev Cell*. 2017;40(3):313-322.e315.

123. Ghadimi BM, Sackett DL, Difilippantonio MJ, et al. Centrosome amplification and instability occurs exclusively in aneuploid, but not in diploid colorectal cancer cell lines, and correlates with numerical chromosomal aberrations. *Genes Chromosomes Cancer*. 2000;27(2):183-190.

124. Lingle WL, Barrett SL, Negron VC, et al. Centrosome amplification drives chromosomal instability in breast tumor development. *Proc Natl Acad Sci U S A*. 2002;99(4):1978-1983.

125. Mahjoub MR, Stearns T. Supernumerary centrosomes nucleate extra cilia and compromise primary cilium signaling. *Curr Biol*. 2012;22(17):1628-1634.

126. Godinho SA, Picone R, Burute M, et al. Oncogene-like induction of cellular invasion from centrosome amplification. *Nature*. 2014;510(7503):167-171.

127. Salisbury JL, D'Assoro AB, Lingle WL. Centrosome amplification and the origin of chromosomal instability in breast cancer. *J Mammary Gland Biol Neoplasia*. 2004;9(3):275-283.

128. Schvartzman JM, Sotillo R, Benezra R. Mitotic chromosomal instability and cancer: mouse modelling of the human disease. *Nat Rev Cancer*. 2010;10(2):102-115.

129. Nicholson JM, Cimini D. How mitotic errors contribute to karyotypic diversity in cancer. *Adv Cancer Res*. 2011;112:43-75.

130. Mitelman F, Johansson B, Mertens F. Mitelman Database of Chromosome Aberrations and Gene Fusions in Cancer; 2012.

131. Maiato H, Logarinho E. Mitotic spindle multipolarity without centrosome amplification. *Nat Cell Biol*. 2014;16(5):386-394.

132. Hanks S, Coleman K, Reid S, et al. Constitutional aneuploidy and cancer predisposition caused by biallelic mutations in BUB1B. *Nat Genet*. 2004;36(11):1159-1161.

133. Quintyne NJ, Reing JE, Hoffelder DR, Gollin SM, Saunders WS. Spindle multipolarity is prevented by centrosomal clustering. *Science*. 2005;307(5706):127-129.

134. Ganem NJ, Godinho SA, Pellman D. A mechanism linking extra centrosomes to chromosomal instability. *Nature*. 2009;460(7252):278-282.

135. Brenton JD, Carey LA, Ahmed AA, Caldas C. Molecular classification and molecular forecasting of breast cancer: ready for clinical application? *J Clin Oncol*. 2005;23(29):7350-7360.

136. Ring D, Hubble R, Kirschner M. Mitosis in a cell with multiple centrioles. *J Cell Biol*. 1982;94(3):549-556.

137. Kwon M, Godinho SA, Chandhok NS, et al. Mechanisms to suppress multipolar divisions in cancer cells with extra centrosomes. *Genes Dev*. 2008;22(16):2189-2203.

138. Wolff A, de Néchaud B, Chillet D, et al. Distribution of glutamylated alpha and beta-tubulin in mouse tissues using a specific monoclonal antibody, GT335. *Eur J Cell Biol*. 1992;59(2):425-432.

139. Dewhurst SM, McGranahan N, Burrell RA, et al. Tolerance of whole-genome doubling propagates chromosomal instability and accelerates cancer genome evolution. *Cancer Discov*. 2014;4(2):175-185.

140. Difilippantonio MJ, Ghadimi BM, Howard T, et al. Nucleation capacity and presence of centrioles define a distinct category of centrosome abnormalities that induces multipolar mitoses in cancer cells. *Environ Mol Mutagen*. 2009;50(8):672-696.

141. Ganem NJ, Cornils H, Chiu SY, et al. Cytokinesis failure triggers hippo tumor suppressor pathway activation. *Cell*. 2014;158(4):833-848.

142. Kumar A, Gao H, Xu J, Reuben J, Yu D, Mehta K. Evidence that aberrant expression of tissue transglutaminase promotes stem cell characteristics in mammary epithelial cells. *PLoS One*. 2011;6(6):e20701.

143. Al-Hajj M, Wicha MS, Benito-Hernandez A, Morrison SJ, Clarke MF. Prospective identification of tumorigenic breast cancer cells. *Proc Natl Acad Sci U S A*. 2003;100(7):3983-3988.

144. Ricardo S, Vieira AF, Gerhard R, et al. Breast cancer stem cell markers CD44, CD24 and ALDH1: expression distribution within intrinsic molecular subtype. *J Clin Pathol*. 2011;64(11):937-946.

145. Sheridan C, Kishimoto H, Fuchs RK, et al. CD44+/CD24- breast cancer cells exhibit enhanced invasive properties: an early step necessary for metastasis. *Breast Cancer Res*. 2006;8(5):R59.

146. Alge CS, Suppmann S, Priglinger SG, et al. Comparative proteome analysis of native differentiated and cultured dedifferentiated human RPE cells. *Invest Ophthalmol Vis Sci*. 2003;44(8):3629-3641.

147. Kivelä T, Uusitalo M. Structure, development and function of cytoskeletal elements in non-neuronal cells of the human eye. *Prog Retin Eye Res*. 1998;17(3):385-428.

148. McKechnie NM, Boulton M, Robey HL, Savage FJ, Grierson I. The cytoskeletal elements of human retinal pigment epithelium: in vitro and in vivo. *J Cell Sci*. 1988;91 (Pt 2):303-312.

149. Sheridan C, Hiscott P, Grierson I. Retinal Pigment Epithelium Differentiation and Dedifferentiation. In: Kirchhof B, Wong D, eds. Vitreo-retinal Surgery; 2005:101-119.

150. Simpson JF, Gray R, Dressler LG, et al. Prognostic value of histologic grade and proliferative activity in axillary node-positive breast cancer: results from the Eastern Cooperative Oncology Group Companion Study, EST 4189. *J Clin Oncol*. 2000;18(10):2059-2069.

151. Elston CW, Ellis IO. Pathological prognostic factors in breast cancer. I. The value of histological grade in breast cancer: experience from a large study with long-term follow-up. *Histopathology*. 1991;19(5):403-410.

152. Basto R, Brunk K, Vinadogrova T, et al. Centrosome amplification can initiate tumorigenesis in flies. *Cell*. 2008;133(6):1032-1042.

153. Shimomura A, Miyoshi Y, Taguchi T, Tamaki Y, Noguchi S. Association of loss of BRCA1 expression with centrosome aberration in human breast cancer. *J Cancer Res Clin Oncol*. 2009;135(3):421-430.

154. Brinkley BR. Managing the centrosome numbers game: from chaos to stability in cancer cell division. *Trends Cell Biol*. 2001;11(1):18-21.

155. Mason JM, Lin DC, Wei X, et al. Functional Characterization of CFI-400945, a Polo-like Kinase 4 Inhibitor, as a Potential Anticancer Agent. *Cancer Cell*. 2014;26(2):163-176.

156. Sampson PB, Liu Y, Forrest B, et al. The discovery of Polo-like kinase 4 inhibitors: identification of (1R,2S).2-(3-((E).4-(((cis).2,6-dimethylmorpholino)methyl)styryl). 1H.indazol-6-yl)-5□'-methoxyspiro[cyclopropane-1,3□'-indolin]-2□'-one (CFI-400945) as a potent, orally active antitumor agent. *J Med Chem*. 2015;58(1):147-169.

157. Wong YL, Anzola JV, Davis RL, et al. Reversible centriole depletion with an inhibitor of Polo-like kinase 4. *Science*. 2015.

158. Wang L, Zhao Z, Meyer MB, et al. CARM1 methylates chromatin remodeling factor BAF155 to enhance tumor progression and metastasis. *Cancer Cell*. 2014;25(1):21-36.

159. Nahta R, O'Regan RM. Therapeutic implications of estrogen receptor signaling in HER2-positive breast cancers. *Breast Cancer Res Treat*. 2012;135(1):39-48.

160. Pietras RJ, Arboleda J, Reese DM, et al. HER-2 tyrosine kinase pathway targets estrogen receptor and promotes hormone-independent growth in human breast cancer cells. *Oncogene*. 1995;10(12):2435-2446.

161. Doxsey SJ, Stein P, Evans L, Calarco PD, Kirschner M. Pericentrin, a highly conserved centrosome protein involved in microtubule organization. *Cell*. 1994;76(4):639-650.

162. A C, B Z, F LR, et al. Identification of selective lead compounds for treatment of high-ploidy breast cancer. *Submitted*. 2015.

163. Choudhary A, Lera RF, Martowicz ML, et al. Interphase cytofission maintains genomic integrity of human cells after failed cytokinesis. *Proc Natl Acad Sci U S A*. 2013;110(32):13026-13031.

164. Livak KJ, Schmittgen TD. Analysis of relative gene expression data using real-time quantitative PCR and the 2(-Delta Delta C(T)) Method. *Methods*. 2001;25(4):402-408.

165. Nigg EA. Origins and consequences of centrosome aberrations in human cancers. *Int J Cancer*. 2006;119(12):2717-2723.

166. Holland AJ, Lan W, Cleveland DW. Centriole duplication: A lesson in self-control. *Cell Cycle*. 2010;9(14):2731-2736.

167. Coelho PA, Bury L, Shahbazi MN, et al. Over-expression of Plk4 induces centrosome amplification, loss of primary cilia and associated tissue hyperplasia in the mouse. *Open Biol*. 2015;5(12):150209.

168. Kazazian K, Go C, Wu H, et al. Plk4 Promotes Cancer Invasion and Metastasis through Arp2/3 Complex Regulation of the Actin Cytoskeleton. *Cancer Res*. 2017;77(2):434-447.

169. Dominguez-Brauer C, Thu KL, Mason JM, Blaser H, Bray MR, Mak TW. Targeting Mitosis in Cancer: Emerging Strategies. *Mol Cell*. 2015;60(4):524-536.

170. Macmillan JC, Hudson JW, Bull S, Dennis JW, Swallow CJ. Comparative expression of the mitotic regulators SAK and PLK in colorectal cancer. *Ann Surg Oncol*. 2001;8(9):729-740.

171. Marina M, Saavedra HI. Nek2 and Plk4: prognostic markers, drivers of breast tumorigenesis and drug resistance. *Front Biosci (Landmark Ed)*. 2014;19:352-365.

172. Li Z, Dai K, Wang C, et al. Expression of Polo-Like Kinase 4(PLK4) in Breast Cancer and Its Response to Taxane-Based Neoadjuvant Chemotherapy. *J Cancer*. 2016;7(9):1125-1132.

173. Siegel RL, Miller KD, Jemal A. Cancer Statistics, 2017. *CA Cancer J Clin*. 2017;67(1):7-30.

174. Zhang L, Shi R, He C, et al. Oncogenic B-Raf(V600E) abrogates the AKT/B-Raf/Mps1 interaction in melanoma cells. *Cancer Lett*. 2013;337(1):125-132.

175. Cui Y, Borysova MK, Johnson JO, Guadagno TM. Oncogenic B-Raf(V600E) induces spindle abnormalities, supernumerary centrosomes, and aneuploidy in human melanocytic cells. *Cancer Res*. 2010;70(2):675-684.

176. Charters GA, Stones CJ, Shelling AN, Baguley BC, Finlay GJ. Centrosomal dysregulation in human metastatic melanoma cell lines. *Cancer Genet*. 2011;204(9):477-485.

177. Guarguaglini G, Duncan PI, Stierhof YD, Holmström T, Duensing S, Nigg EA. The forkhead-associated domain protein Cep170 interacts with Polo-like kinase 1 and serves as a marker for mature centrioles. *Mol Biol Cell*. 2005;16(3):1095-1107.

178. Chng WJ, Ahmann GJ, Henderson K, et al. Clinical implication of centrosome amplification in plasma cell neoplasm. *Blood*. 2006;107(9):3669-3675.

179. Chng WJ, Braggio E, Mulligan G, et al. The centrosome index is a powerful prognostic marker in myeloma and identifies a cohort of patients that might benefit from aurora kinase inhibition. *Blood*. 2008;111(3):1603-1609.

180. Ogden A, Rida PC, Aneja R. Prognostic value of CA20, a score based on centrosome amplification-associated genes, in breast tumors. *Sci Rep*. 2017;7(1):262.

181. Li JJ, Weroha SJ, Lingle WL, Papa D, Salisbury JL, Li SA. Estrogen mediates Aurora-A overexpression, centrosome amplification, chromosomal instability, and breast cancer in female ACI rats. *Proc Natl Acad Sci U S A*. 2004;101(52):18123-18128.

182. Ahmed AA, Mills AD, Ibrahim AE, et al. The extracellular matrix protein TGFBI induces microtubule stabilization and sensitizes ovarian cancers to paclitaxel. *Cancer Cell*. 2007;12(6):514-527.

183. Shinmura K, Kato H, Kawanishi Y, et al. SASS6 overexpression is associated with mitotic chromosomal abnormalities and a poor prognosis in patients with colorectal cancer. *Oncol Rep*. 2015;34(2):727-738.

184. Tang CJ, Lin SY, Hsu WB, et al. The human microcephaly protein STIL interacts with CPAP and is required for procentriole formation. *EMBO J*. 2011;30(23):4790-4804.

185. Loncarek J, Hergert P, Magidson V, Khodjakov A. Control of daughter centriole formation by the pericentriolar material. *Nat Cell Biol*. 2008;10(3):322-328.

186. Korzeniewski N, Hohenfellner M, Duensing S. CAND1 promotes PLK4-mediated centriole overduplication and is frequently disrupted in prostate cancer. *Neoplasia*. 2012;14(9):799-806.

187. Sredni ST, Tomita T. The polo-like kinase 4 gene (PLK4) is overexpressed in pediatric medulloblastoma. *Childs Nerv Syst*. 2017;33(7):1031.

188. Young SK, Wek RC. Upstream Open Reading Frames Differentially Regulate Gene-specific Translation in the Integrated Stress Response. *J Biol Chem*. 2016;291(33):16927-16935.

189. Holland AJ. Molecular control of centrosome duplication. EMBO Conference - Centrosomes and Spindle Pole Bodies. Heidelberg; 2017.

190. Kazazian K, Go CD, Wu H, et al. Plk4 promotes cancer invasion and metastasis through Arp2/3 complex regulation of the actin cytoskeleton. *Cancer Res*. 2016.

191. Bedard PL, Cescon DW, Fletcher G, et al. First-in-human phase I trial of the oral PLK4 inhibitor CFI-400945 in patients with advanced solid tumors. American Association for Cancer Research Annual Meeting. New Orleans; 2016.

192. Wilking MJ, Singh C, Nihal M, Zhong W, Ahmad N. SIRT1 deacetylase is overexpressed in human melanoma and its small molecule inhibition imparts anti-proliferative response via p53 activation. *Arch Biochem Biophys*. 2014;563:94-100.

193. Wang X, Spandidos A, Wang H, Seed B. PrimerBank: a PCR primer database for quantitative gene expression analysis, 2012 update. *Nucleic Acids Res*. 2012;40(Database issue):D1144-1149.

194. Lasek AL, McPherson BM, Trueman NG, Burkard ME. The Functional Significance of Posttranslational Modifications on Polo-Like Kinase 1 Revealed by Chemical Genetic Complementation. *PLoS One*. 2016;11(2):e0150225.

195. Lera RF, Burkard ME. High mitotic activity of Polo-like kinase 1 is required for chromosome segregation and genomic integrity in human epithelial cells. *J Biol Chem*. 2012;287(51):42812-42825.

196. Gao J, Aksoy BA, Dogrusoz U, et al. Integrative analysis of complex cancer genomics and clinical profiles using the cBioPortal. *Sci Signal*. 2013;6(269):pl1.

197. Silkworth WT, Nardi IK, Scholl LM, Cimini D. Multipolar spindle pole coalescence is a major source of kinetochore mis-attachment and chromosome mis-segregation in cancer cells. *PLoS One*. 2009;4(8):e6564.

198. Cuevas R, Korzeniewski N, Tolstov Y, Hohenfellner M, Duensing S. FGF-2 disrupts mitotic stability in prostate cancer through the intracellular trafficking protein CEP57. *Cancer Res*. 2013;73(4):1400-1410.

199. Roh M, Gary B, Song C, et al. Overexpression of the oncogenic kinase Pim-1 leads to genomic instability. *Cancer Res*. 2003;63(23):8079-8084.

200. Xie S, Qin J, Liu S, et al. Cep70 overexpression stimulates pancreatic cancer by inducing centrosome abnormality and microtubule disorganization. *Sci Rep*. 2016;6:21263.

201. Dzhindzhev NS, Yu QD, Weiskopf K, et al. Asterless is a scaffold for the onset of centriole assembly. *Nature*. 2010;467(7316):714-718.

202. Pike AN, Fisk HA. Centriole assembly and the role of Mps1: defensible or dispensable? *Cell Div*. 2011;6:9.

203. Fisk HA, Winey M. The mouse Mps1p-like kinase regulates centrosome duplication. *Cell*. 2001;106(1):95-104.

204. Balczon RC. Overexpression of cyclin A in human HeLa cells induces detachment of kinetochores and spindle pole/centrosome overproduction. *Chromosoma*. 2001;110(6):381-392.

205. Zhou X, Fan LX, Li K, Ramchandran R, Calvet JP, Li X. SIRT2 regulates ciliogenesis and contributes to abnormal centrosome amplification caused by loss of polycystin-1. *Hum Mol Genet*. 2014;23(6):1644-1655.

206. Hergovich A, Kohler RS, Schmitz D, Vichalkovski A, Cornils H, Hemmings BA. The MST1 and hMOB1 tumor suppressors control human centrosome duplication by regulating NDR kinase phosphorylation. *Curr Biol*. 2009;19(20):1692-1702.

207. Meraldi P, Honda R, Nigg EA. Aurora-A overexpression reveals tetraploidization as a major route to centrosome amplification in p53-/- cells. *EMBO J*. 2002;21(4):483-492.

208. Denu RA, Shabbir M, Nihal M, et al. Centriole Overduplication is the Predominant Mechanism Leading to Centrosome Amplification in Melanoma. *Mol Cancer Res*. 2018.

209. Marteil G, Guerrero A, Vieira AF, et al. Over-elongation of centrioles in cancer promotes centriole amplification and chromosome missegregation. *Nat Commun*. 2018;9(1):1258.

210. Andersen JS, Wilkinson CJ, Mayor T, Mortensen P, Nigg EA, Mann M. Proteomic characterization of the human centrosome by protein correlation profiling. *Nature*. 2003;426(6966):570-574.

211. Arquint C, Cubizolles F, Morand A, Schmidt A, Nigg EA. The SKP1-Cullin-F-box E3 ligase βTrCP and CDK2 cooperate to control STIL abundance and centriole number. *Open Biol*. 2018;8(2).

212. Peel N, Iyer J, Naik A, Dougherty MP, Decker M, O'Connell KF. Protein Phosphatase 1 Down Regulates ZYG-1 Levels to Limit Centriole Duplication. *PLoS Genet*. 2017;13(1):e1006543.

213. Győrffy B, Surowiak P, Budczies J, Lánczky A. Online survival analysis software to assess the prognostic value of biomarkers using transcriptomic data in non-small-cell lung cancer. *PLoS One*. 2013;8(12):e82241.

214. Fava LL, Schuler F, Sladky V, et al. The PIDDosome activates p53 in response to supernumerary centrosomes. *Genes Dev*. 2017;31(1):34-45.

215. Lawrence MS, Stojanov P, Polak P, et al. Mutational heterogeneity in cancer and the search for new cancer-associated genes. *Nature*. 2013;499(7457):214-218.

216. Klatte T, Kroeger N, Rampersaud EN, et al. Gain of chromosome 8q is associated with metastases and poor survival of patients with clear cell renal cell carcinoma. *Cancer*. 2012;118(23):5777-5782.

217. Kang JU. Chromosome 8q as the most frequent target for amplification in early gastric carcinoma. *Oncol Lett*. 2014;7(4):1139-1143.

218. El Gammal AT, Brüchmann M, Zustin J, et al. Chromosome 8p deletions and 8q gains are associated with tumor progression and poor prognosis in prostate cancer. *Clin Cancer Res*. 2010;16(1):56-64.

219. Ribeiro FR, Jerónimo C, Henrique R, et al. 8q gain is an independent predictor of poor survival in diagnostic needle biopsies from prostate cancer suspects. *Clin Cancer Res*. 2006;12(13):3961-3970.

220. Steiner T, Junker K, Burkhardt F, Braunsdorf A, Janitzky V, Schubert J. Gain in chromosome 8q correlates with early progression in hormonal treated prostate cancer. *Eur Urol*. 2002;41(2):167-171.

221. Weber RG, Pietsch T, von Schweinitz D, Lichter P. Characterization of genomic alterations in hepatoblastomas. A role for gains on chromosomes 8q and 20 as predictors of poor outcome. *Am J Pathol*. 2000;157(2):571-578.

222. van Beek JG, Koopmans AE, Vaarwater J, et al. The prognostic value of extraocular extension in relation to monosomy 3 and gain of chromosome 8q in uveal melanoma. *Invest Ophthalmol Vis Sci*. 2014;55(3):1284-1291.

223. Schleicher C, Poremba C, Wolters H, Schäfer KL, Senninger N, Colombo-Benkmann M. Gain of chromosome 8q: a potential prognostic marker in resectable adenocarcinoma of the pancreas? *Ann Surg Oncol*. 2007;14(4):1327-1335.

224. Han S, Park K, Shin E, Kim HJ, Kim JY, Gwak G. Genomic change of chromosome 8 predicts the response to taxane-based neoadjuvant chemotherapy in node-positive breast cancer. *Oncol Rep*. 2010;24(1):121-128.

225. Furge KA, Chen J, Koeman J, et al. Detection of DNA copy number changes and oncogenic signaling abnormalities from gene expression data reveals MYC activation in high-grade papillary renal cell carcinoma. *Cancer Res*. 2007;67(7):3171-3176.

226. Alderton GK, Galbiati L, Griffith E, et al. Regulation of mitotic entry by microcephalin and its overlap with ATR signalling. *Nat Cell Biol*. 2006;8(7):725-733.

227. Rai R, Dai H, Multani AS, et al. BRIT1 regulates early DNA damage response, chromosomal integrity, and cancer. *Cancer Cell*. 2006;10(2):145-157.

228. Zhou L, Bai Y, Li Y, et al. Overexpression of MCPH1 inhibits uncontrolled cell growth by promoting cell apoptosis and arresting the cell cycle in S and G2/M phase in lung cancer cells. *Oncol Lett*. 2016;11(1):365-372.

229. Mai L, Yi F, Gou X, et al. The overexpression of MCPH1 inhibits cell growth through regulating cell cycle-related proteins and activating cytochrome c-caspase 3 signaling in cervical cancer. *Mol Cell Biochem*. 2014;392(1-2):95-107.

230. Jo YS, Kim SS, Kim MS, Yoo NJ, Lee SH. Candidate tumor suppressor gene MCPH1 is mutated in colorectal and gastric cancers. *Int J Colorectal Dis*. 2017;32(1):161-162.

231. Zhong X, Pfeifer GP, Xu X. Microcephalin encodes a centrosomal protein. *Cell Cycle*. 2006;5(4):457-458.

232. Jeffers LJ, Coull BJ, Stack SJ, Morrison CG. Distinct BRCT domains in Mcph1/Brit1 mediate ionizing radiation-induced focus formation and centrosomal localization. *Oncogene*. 2008;27(1):139-144.

233. Liu X, Zong W, Li T, et al. The E3 ubiquitin ligase APC/CCdh1 degrades MCPH1 after MCPH1-βTrCP2-Cdc25A-mediated mitotic entry to ensure neurogenesis. *EMBO J*. 2017;36(24):3666-3681.

234. Jackson AP, Eastwood H, Bell SM, et al. Identification of microcephalin, a protein implicated in determining the size of the human brain. *Am J Hum Genet*. 2002;71(1):136-142.

235. Rai R, Phadnis A, Haralkar S, et al. Differential regulation of centrosome integrity by DNA damage response proteins. *Cell Cycle*. 2008;7(14):2225-2233.

236. Brown JA, Bourke E, Liptrot C, Dockery P, Morrison CG. MCPH1/BRIT1 limits ionizing radiation-induced centrosome amplification. *Oncogene*. 2010;29(40):5537-5544.

237. Antonczak AK, Mullee LI, Wang Y, et al. Opposing effects of pericentrin and microcephalin on the pericentriolar material regulate CHK1 activation in the DNA damage response. *Oncogene*. 2015.

238. Bhattacharya N, Mukherjee N, Singh RK, et al. Frequent alterations of MCPH1 and ATM are associated with primary breast carcinoma: clinical and prognostic implications. *Ann Surg Oncol*. 2013;20 Suppl 3:S424-432.

239. Brunk K, Vernay B, Griffith E, et al. Microcephalin coordinates mitosis in the syncytial Drosophila embryo. *J Cell Sci*. 2007;120(Pt 20):3578-3588.

240. Graser S, Stierhof YD, Lavoie SB, et al. Cep164, a novel centriole appendage protein required for primary cilium formation. *J Cell Biol*. 2007;179(2):321-330.

241. Bourke E, Brown JA, Takeda S, Hochegger H, Morrison CG. DNA damage induces Chk1-dependent threonine-160 phosphorylation and activation of Cdk2. *Oncogene*. 2010;29(4):616-624.

242. Bourke E, Dodson H, Merdes A, et al. DNA damage induces Chk1-dependent centrosome amplification. *EMBO Rep*. 2007;8(6):603-609.

243. Hinchcliffe EH, Li C, Thompson EA, Maller JL, Sluder G. Requirement of Cdk2-cyclin E activity for repeated centrosome reproduction in Xenopus egg extracts. *Science*. 1999;283(5403):851-854.

244. Lacey KR, Jackson PK, Stearns T. Cyclin-dependent kinase control of centrosome duplication. *Proc Natl Acad Sci U S A*. 1999;96(6):2817-2822.

245. Matsumoto Y, Hayashi K, Nishida E. Cyclin-dependent kinase 2 (Cdk2) is required for centrosome duplication in mammalian cells. *Curr Biol*. 1999;9(8):429-432.

246. Meraldi P, Lukas J, Fry AM, Bartek J, Nigg EA. Centrosome duplication in mammalian somatic cells requires E2F and Cdk2-cyclin A. *Nat Cell Biol*. 1999;1(2):88-93.

247. Chen Z, Indjeian VB, McManus M, Wang L, Dynlacht BD. CP110, a cell cycle-dependent CDK substrate, regulates centrosome duplication in human cells. *Dev Cell*. 2002;3(3):339-350.

248. Adon AM, Zeng X, Harrison MK, et al. Cdk2 and Cdk4 regulate the centrosome cycle and are critical mediators of centrosome amplification in p53-null cells. *Mol Cell Biol*. 2010;30(3):694-710.

249. Arquint C, Sonnen KF, Stierhof YD, Nigg EA. Cell-cycle-regulated expression of STIL controls centriole number in human cells. *J Cell Sci*. 2012;125(Pt 5):1342-1352.

250. Strnad P, Leidel S, Vinogradova T, Euteneuer U, Khodjakov A, Gönczy P. Regulated HsSAS-6 levels ensure formation of a single procentriole per centriole during the centrosome duplication cycle. *Dev Cell*. 2007;13(2):203-213.

251. Trimborn M, Bell SM, Felix C, et al. Mutations in microcephalin cause aberrant regulation of chromosome condensation. *Am J Hum Genet*. 2004;75(2):261-266.

252. Arroyo M, Kuriyama R, Trimborn M, et al. MCPH1, mutated in primary microcephaly, is required for efficient chromosome alignment during mitosis. *Sci Rep*. 2017;7(1):13019.

253. Trimborn M, Richter R, Sternberg N, et al. The first missense alteration in the MCPH1 gene causes autosomal recessive microcephaly with an extremely mild cellular and clinical phenotype. *Hum Mutat*. 2005;26(5):496.

254. Tibelius A, Marhold J, Zentgraf H, et al. Microcephalin and pericentrin regulate mitotic entry via centrosome-associated Chk1. *J Cell Biol*. 2009;185(7):1149-1157.

255. Lin SY, Rai R, Li K, Xu ZX, Elledge SJ. BRIT1/MCPH1 is a DNA damage responsive protein that regulates the Brca1-Chk1 pathway, implicating checkpoint dysfunction in microcephaly. *Proc Natl Acad Sci U S A*. 2005;102(42):15105-15109.

256. Messina M, Diena D, Dellepiane S, et al. Long-Term Outcomes and Discard Rate of Kidneys by Decade of Extended Criteria Donor Age. *Clin J Am Soc Nephrol*. 2016.

257. Novorol C, Burkhardt J, Wood KJ, et al. Microcephaly models in the developing zebrafish retinal neuroepithelium point to an underlying defect in metaphase progression. *Open Biol*. 2013;3(10):130065.

258. Yun C, Cho H, Kim SJ, Lee JH, Park SY, Chan GK. Mitotic aberration coupled with centrosome amplification is induced by hepatitis B virus X oncoprotein via the Ras-mitogen-activated protein/extracellular signal-regulated kinase-mitogen-activated protein pathway. *Mol Cancer Res*. 2004;2(3):159-169.

259. Zhang WY, Cai N, Ye LH, Zhang XD. Transformation of human liver L-O2 cells mediated by stable HBx transfection. *Acta Pharmacol Sin*. 2009;30(8):1153-1161.

260. Fujii R, Zhu C, Wen Y, et al. HBXIP, cellular target of hepatitis B virus oncoprotein, is a regulator of centrosome dynamics and cytokinesis. *Cancer Res*. 2006;66(18):9099-9107.

261. Wen Y, Golubkov VS, Strongin AY, Jiang W, Reed JC. Interaction of hepatitis B viral oncoprotein with cellular target HBXIP dysregulates centrosome dynamics and mitotic spindle formation. *J Biol Chem*. 2008;283(5):2793-2803.

262. Korzeniewski N, Treat B, Duensing S. The HPV-16 E7 oncoprotein induces centriole multiplication through deregulation of Polo-like kinase 4 expression. *Mol Cancer*. 2011;10:61.

263. Duensing A, Chin A, Wang L, Kuan SF, Duensing S. Analysis of centrosome overduplication in correlation to cell division errors in high-risk human papillomavirus (HPV)-associated anal neoplasms. *Virology*. 2008;372(1):157-164.

264. Nitta T, Kanai M, Sugihara E, et al. Centrosome amplification in adult T-cell leukemia and human T-cell leukemia virus type 1 Tax-induced human T cells. *Cancer Sci*. 2006;97(9):836-841.

265. Shumilov A, Tsai MH, Schlosser YT, et al. Epstein-Barr virus particles induce centrosome amplification and chromosomal instability. *Nat Commun*. 2017;8:14257.

266. Koopal S, Furuhjelm JH, Järviluoma A, et al. Viral oncogene-induced DNA damage response is activated in Kaposi sarcoma tumorigenesis. *PLoS Pathog*. 2007;3(9):1348-1360.

267. Verschuren EW, Klefstrom J, Evan GI, Jones N. The oncogenic potential of Kaposi's sarcoma-associated herpesvirus cyclin is exposed by p53 loss in vitro and in vivo. *Cancer Cell*. 2002;2(3):229-241.

268. Pan H, Zhou F, Gao SJ. Kaposi's sarcoma-associated herpesvirus induction of chromosome instability in primary human endothelial cells. *Cancer Res*. 2004;64(12):4064-4068.

269. Si H, Robertson ES. Kaposi's sarcoma-associated herpesvirus-encoded latency-associated nuclear antigen induces chromosomal instability through inhibition of p53 function. *J Virol*. 2006;80(2):697-709.

270. Mussman JG, Horn HF, Carroll PE, et al. Synergistic induction of centrosome hyperamplification by loss of p53 and cyclin E overexpression. *Oncogene*. 2000;19(13):1635-1646.

271. Kawamura K, Izumi H, Ma Z, et al. Induction of centrosome amplification and chromosome instability in human bladder cancer cells by p53 mutation and cyclin E overexpression. *Cancer Res*. 2004;64(14):4800-4809.

272. Nelsen CJ, Kuriyama R, Hirsch B, et al. Short term cyclin D1 overexpression induces centrosome amplification, mitotic spindle abnormalities, and aneuploidy. *J Biol Chem*. 2005;280(1):768-776.

273. Hanashiro K, Kanai M, Geng Y, Sicinski P, Fukasawa K. Roles of cyclins A and E in induction of centrosome amplification in p53-compromised cells. *Oncogene*. 2008;27(40):5288-5302.

274. Pérez de Castro I, de Cárcer G, Malumbres M. A census of mitotic cancer genes: new insights into tumor cell biology and cancer therapy. *Carcinogenesis*. 2007;28(5):899-912.

275. Lambrus BG, Uetake Y, Clutario KM, et al. p53 protects against genome instability following centriole duplication failure. *J Cell Biol*. 2015;210(1):63-77.

276. Ko MA, Rosario CO, Hudson JW, et al. Plk4 haploinsufficiency causes mitotic infidelity and carcinogenesis. *Nat Genet*. 2005;37(8):883-888.

277. Swallow CJ, Ko MA, Siddiqui NU, Hudson JW, Dennis JW. Sak/Plk4 and mitotic fidelity. *Oncogene*. 2005;24(2):306-312.

278. Brüning-Richardson A, Bond J, Alsiary R, et al. ASPM and microcephalin expression in epithelial ovarian cancer correlates with tumour grade and survival. *Br J Cancer*. 2011;104(10):1602-1610.

279. Wang N, Lu H, Chen W, et al. Primary microcephaly gene MCPH1 shows a novel molecular biomarker of human renal carcinoma and is regulated by miR-27a. *Int J Clin Exp Pathol*. 2014;7(8):4895-4903.

280. Zhang J, Wu XB, Fan JJ, et al. MCPH1 Protein Expression in Normal and Neoplastic Lung Tissues. *Asian Pac J Cancer Prev*. 2013;14(12):7295-7300.

281. Venkatesh T, Nagashri MN, Swamy SS, Mohiyuddin SM, Gopinath KS, Kumar A. Primary microcephaly gene MCPH1 shows signatures of tumor suppressors and is regulated by miR-27a in oral squamous cell carcinoma. *PLoS One*. 2013;8(3):e54643.

282. Richardson J, Shaaban AM, Kamal M, et al. Microcephalin is a new novel prognostic indicator in breast cancer associated with BRCA1 inactivation. *Breast Cancer Res Treat*. 2011;127(3):639-648.

283. Liang Y, Gao H, Lin SY, et al. BRIT1/MCPH1 is essential for mitotic and meiotic recombination DNA repair and maintaining genomic stability in mice. *PLoS Genet*. 2010;6(1):e1000826.

284. Xu X, Lee J, Stern DF. Microcephalin is a DNA damage response protein involved in regulation of CHK1 and BRCA1. *J Biol Chem*. 2004;279(33):34091-34094.

285. McKinley KL, Cheeseman IM. Large-Scale Analysis of CRISPR/Cas9 Cell-Cycle Knockouts Reveals the Diversity of p53-Dependent Responses to Cell-Cycle Defects. *Dev Cell*. 2017;40(4):405-420.e402.

286. Birnbaum D, Adélaïde J, Popovici C, Charafe-Jauffret E, Mozziconacci MJ, Chaffanet M. Chromosome arm 8p and cancer: a fragile hypothesis. *Lancet Oncol*. 2003;4(10):639-642.

287. Xue W, Krasnitz A, Lucito R, et al. DLC1 is a chromosome 8p tumor suppressor whose loss promotes hepatocellular carcinoma. *Genes Dev*. 2008;22(11):1439-1444.

288. Yaremko ML, Recant WM, Westbrook CA. Loss of heterozygosity from the short arm of chromosome 8 is an early event in breast cancers. *Genes Chromosomes Cancer*. 1995;13(3):186-191.

289. Amari M, Suzuki A, Moriya T, et al. LOH analyses of premalignant and malignant lesions of human breast: frequent LOH in 8p, 16q, and 17q in atypical ductal hyperplasia. *Oncol Rep*. 1999;6(6):1277-1280.

290. Xue W, Kitzing T, Roessler S, et al. A cluster of cooperating tumor-suppressor gene candidates in chromosomal deletions. *Proc Natl Acad Sci U S A*. 2012;109(21):8212-8217.

291. Cai Y, Crowther J, Pastor T, et al. Loss of Chromosome 8p Governs Tumor Progression and Drug Response by Altering Lipid Metabolism. *Cancer Cell*. 2016;29(5):751-766.

292. Ostergaard GZ, Tommerup N. The 8p-syndrome. *Ann Genet*. 1989;32(2):87-91.

293. Mantel C, Braun SE, Reid S, et al. p21(cip-1/waf-1) deficiency causes deformed nuclear architecture, centriole overduplication, polyploidy, and relaxed microtubule damage checkpoints in human hematopoietic cells. *Blood*. 1999;93(4):1390-1398.

294. Lambrus BG, Daggubati V, Uetake Y, et al. A USP28-53BP1-p53-p21 signaling axis arrests growth after centrosome loss or prolonged mitosis. *J Cell Biol*. 2016;214(2):143-153.

295. Fukasawa K, Choi T, Kuriyama R, Rulong S, Vande Woude GF. Abnormal centrosome amplification in the absence of p53. *Science*. 1996;271(5256):1744-1747.

296. Al-Romaih K, Bayani J, Vorobyova J, et al. Chromosomal instability in osteosarcoma and its association with centrosome abnormalities. *Cancer Genet Cytogenet*. 2003;144(2):91-99.

297. Li J, Tan M, Li L, Pamarthy D, Lawrence TS, Sun Y. SAK, a new polo-like kinase, is transcriptionally repressed by p53 and induces apoptosis upon RNAi silencing. *Neoplasia*. 2005;7(4):312-323.

298. Marthiens V, Rujano MA, Pennetier C, Tessier S, Paul-Gilloteaux P, Basto R. Centrosome amplification causes microcephaly. *Nat Cell Biol*. 2013;15(7):731-740.

299. Schnerch D, Nigg EA. Structural centrosome aberrations favor proliferation by abrogating microtubule-dependent tissue integrity of breast epithelial mammospheres. *Oncogene*. 2016;35(21):2711-2722.

300. Loncarek J, Hergert P, Khodjakov A. Centriole reduplication during prolonged interphase requires procentriole maturation governed by Plk1. *Curr Biol*. 2010;20(14):1277-1282.

301. Cerami E, Gao J, Dogrusoz U, et al. The cBio cancer genomics portal: an open platform for exploring multidimensional cancer genomics data. *Cancer Discov*. 2012;2(5):401-404.

302. Ran FA, Hsu PD, Wright J, Agarwala V, Scott DA, Zhang F. Genome engineering using the CRISPR-Cas9 system. *Nat Protoc*. 2013;8(11):2281-2308.

303. Shalata A, Ramirez MC, Desnick RJ, et al. Morbid obesity resulting from inactivation of the ciliary protein CEP19 in humans and mice. *Am J Hum Genet*. 2013;93(6):1061-1071.

304. Lüddecke S, Ertych N, Stenzinger A, et al. The putative oncogene CEP72 inhibits the mitotic function of BRCA1 and induces chromosomal instability. *Oncogene*. 2016;35(18):2398-2406.

305. Tsang WY, Spektor A, Vijayakumar S, et al. Cep76, a centrosomal protein that specifically restrains centriole reduplication. *Dev Cell*. 2009;16(5):649-660.

306. Bahmanyar S, Kaplan DD, Deluca JG, et al. beta-Catenin is a Nek2 substrate involved in centrosome separation. *Genes Dev*. 2008;22(1):91-105.

307. Mbom BC, Nelson WJ, Barth A. β-catenin at the centrosome: discrete pools of β-catenin communicate during mitosis and may co-ordinate centrosome functions and cell cycle progression. *Bioessays*. 2013;35(9):804-809.

308. Mbom BC, Siemers KA, Ostrowski MA, Nelson WJ, Barth AI. Nek2 phosphorylates and stabilizes β-catenin at mitotic centrosomes downstream of Plk1. *Mol Biol Cell*. 2014;25(7):977-991.

309. Bahmanyar S, Guiney EL, Hatch EM, Nelson WJ, Barth AI. Formation of extra centrosomal structures is dependent on beta-catenin. *J Cell Sci*. 2010;123(Pt 18):3125-3135.

310. Li J, Kim S, Kobayashi T, et al. Neurl4, a novel daughter centriole protein, prevents formation of ectopic microtubule organizing centres. *EMBO Rep*. 2012;13(6):547-553.

311. Croessmann S, Wong HY, Zabransky DJ, et al. NDRG1 links p53 with proliferation-mediated centrosome homeostasis and genome stability. *Proc Natl Acad Sci U S A*. 2015;112(37):11583-11588.

312. Wang W, Budhu A, Forgues M, Wang XW. Temporal and spatial control of nucleophosmin by the Ran-Crm1 complex in centrosome duplication. *Nat Cell Biol*. 2005;7(8):823-830.

313. Goto M, O'Brien DA, Eddy EM. Speriolin is a novel human and mouse sperm centrosome protein. *Hum Reprod*. 2010;25(8):1884-1894.

314. Feldman JL, Marshall WF. ASQ2 encodes a TBCC-like protein required for mother-daughter centriole linkage and mitotic spindle orientation. *Curr Biol*. 2009;19(14):1238-1243.

315. André J, Harrison S, Towers K, et al. The tubulin cofactor C family member TBCCD1 orchestrates cytoskeletal filament formation. *J Cell Sci*. 2013;126(Pt 23):5350-5356.

316. Fode C, Motro B, Yousefi S, Heffernan M, Dennis JW. Sak, a murine protein-serine/threonine kinase that is related to the Drosophila polo kinase and involved in cell proliferation. *Proc Natl Acad Sci U S A*. 1994;91(14):6388-6392.

317. Liu L, Zhang CZ, Cai M, Fu J, Chen GG, Yun J. Downregulation of polo-like kinase 4 in hepatocellular carcinoma associates with poor prognosis. *PLoS One*. 2012;7(7):e41293.

318. Pellegrino R, Calvisi DF, Ladu S, et al. Oncogenic and tumor suppressive roles of polo-like kinases in human hepatocellular carcinoma. *Hepatology*. 2010;51(3):857-868.

319. Rosario CO, Ko MA, Haffani YZ, et al. Plk4 is required for cytokinesis and maintenance of chromosomal stability. *Proc Natl Acad Sci U S A*. 2010;107(15):6888-6893.

320. Meitinger F, Anzola JV, Kaulich M, et al. 53BP1 and USP28 mediate p53 activation and G1 arrest after centrosome loss or extended mitotic duration. *J Cell Biol*. 2016;214(2):155-166.

321. Lengauer C, Kinzler KW, Vogelstein B. Genetic instabilities in human cancers. *Nature*. 1998;396(6712):643-649.

322. Weaver BA, Silk AD, Montagna C, Verdier-Pinard P, Cleveland DW. Aneuploidy acts both oncogenically and as a tumor suppressor. *Cancer Cell*. 2007;11(1):25-36.

323. Weaver BA, Silk AD, Cleveland DW. Low rates of aneuploidy promote tumorigenesis while high rates of aneuploidy cause cell death and tumor suppression. *Cell Oncol*. 2008;30(5):453.

324. Khodjakov A, Cole RW, Oakley BR, Rieder CL. Centrosome-independent mitotic spindle formation in vertebrates. *Curr Biol*. 2000;10(2):59-67.

325. Hornick JE, Mader CC, Tribble EK, et al. Amphiastral mitotic spindle assembly in vertebrate cells lacking centrosomes. *Curr Biol*. 2011;21(7):598-605.

326. Khodjakov A, Rieder CL. Centrosomes enhance the fidelity of cytokinesis in vertebrates and are required for cell cycle progression. *J Cell Biol*. 2001;153(1):237-242.

327. Siller KH, Doe CQ. Spindle orientation during asymmetric cell division. *Nat Cell Biol*. 2009;11(4):365-374.

328. Tang N, Marshall WF. Centrosome positioning in vertebrate development. *J Cell Sci*. 2012;125(Pt 21):4951-4961.

329. Magdalena J, Millard TH, Machesky LM. Microtubule involvement in NIH 3T3 Golgi and MTOC polarity establishment. *J Cell Sci*. 2003;116(Pt 4):743-756.

330. Bobinnec Y, Khodjakov A, Mir LM, Rieder CL, Eddé B, Bornens M. Centriole disassembly in vivo and its effect on centrosome structure and function in vertebrate cells. *J Cell Biol*. 1998;143(6):1575-1589.

331. Flanagan AM, Stavenschi E, Basavaraju S, Gaboriau D, Hoey DA, Morrison CG. Centriole splitting caused by loss of the centrosomal linker protein C-NAP1 reduces centriolar satellite density and impedes centrosome amplification. *Mol Biol Cell*. 2017.

332. Tapley EC, Starr DA. Connecting the nucleus to the cytoskeleton by SUN-KASH bridges across the nuclear envelope. *Curr Opin Cell Biol*. 2013;25(1):57-62.

333. Guo Y, Zheng Y. Lamins position the nuclear pores and centrosomes by modulating dynein. *Mol Biol Cell*. 2015.

334. Shinmura K, Kurabe N, Goto M, et al. PLK4 overexpression and its effect on centrosome regulation and chromosome stability in human gastric cancer. *Mol Biol Rep*. 2014.

335. Maniotis A, Schliwa M. Microsurgical removal of centrosomes blocks cell reproduction and centriole generation in BSC-1 cells. *Cell*. 1991;67(3):495-504.

336. Uetake Y, Loncarek J, Nordberg JJ, et al. Cell cycle progression and de novo centriole assembly after centrosomal removal in untransformed human cells. *J Cell Biol*. 2007;176(2):173-182.

337. Fong CS, Mazo G, Das T, et al. 53BP1 and USP28 mediate p53-dependent cell cycle arrest in response to centrosome loss and prolonged mitosis. *Elife*. 2016;5.

338. Avidor-Reiss T, Gopalakrishnan J. Building a centriole. *Curr Opin Cell Biol*. 2013;25(1):72-77.

339. Gopalakrishnan J, Mennella V, Blachon S, et al. Sas-4 provides a scaffold for cytoplasmic complexes and tethers them in a centrosome. *Nat Commun*. 2011;2:359.

340. Abal M, Keryer G, Bornens M. Centrioles resist forces applied on centrosomes during G2/M transition. *Biol Cell*. 2005;97(6):425-434.

341. Kuriyama R, Bettencourt-Dias M, Hoffmann I, Arnold M, Sandvig L. Gamma-tubulin-containing abnormal centrioles are induced by insufficient Plk4 in human HCT116 colorectal cancer cells. *J Cell Sci*. 2009;122(Pt 12):2014-2023.

342. Rosario CO, Kazazian K, Zih FS, et al. A novel role for Plk4 in regulating cell spreading and motility. *Oncogene*. 2014.

343. Wakida NM, Botvinick EL, Lin J, Berns MW. An intact centrosome is required for the maintenance of polarization during directional cell migration. *PLoS One*. 2010;5(12):e15462.

344. Vinogradova T, Paul R, Grimaldi AD, et al. Concerted effort of centrosomal and Golgi-derived microtubules is required for proper Golgi complex assembly but not for maintenance. *Mol Biol Cell*. 2012;23(5):820-833.

345. Kushner EJ, Ferro LS, Liu JY, et al. Excess centrosomes disrupt endothelial cell migration via centrosome scattering. *J Cell Biol*. 2014;206(2):257-272.

346. Yvon AM, Wadsworth P, Jordan MA. Taxol suppresses dynamics of individual microtubules in living human tumor cells. *Mol Biol Cell*. 1999;10(4):947-959.

347. Berdougo E, Terret ME, Jallepalli PV. Functional dissection of mitotic regulators through gene targeting in human somatic cells. *Methods Mol Biol*. 2009;545:21-37.

348. Burkard ME, Randall CL, Larochelle S, et al. Chemical genetics reveals the requirement for Polo-like kinase 1 activity in positioning RhoA and triggering cytokinesis in human cells. *Proc Natl Acad Sci U S A*. 2007;104(11):4383-4388.

349. Klionsky DJ, Abdelmohsen K, Abe A, et al. Guidelines for the use and interpretation of assays for monitoring autophagy (3rd edition). *Autophagy*. 2016;12(1):1-222.

350. Klionsky DJ. Autophagy: from phenomenology to molecular understanding in less than a decade. *Nat Rev Mol Cell Biol*. 2007;8(11):931-937.

351. Janku F, McConkey DJ, Hong DS, Kurzrock R. Autophagy as a target for anticancer therapy. *Nat Rev Clin Oncol*. 2011;8(9):528-539.

352. Duffy A, Le J, Sausville E, Emadi A. Autophagy modulation: a target for cancer treatment development. *Cancer Chemother Pharmacol*. 2015;75(3):439-447.

353. Seglen PO, Bohley P. Autophagy and other vacuolar protein degradation mechanisms. *Experientia*. 1992;48(2):158-172.

354. Amaya C, Fader CM, Colombo MI. Autophagy and proteins involved in vesicular trafficking. *FEBS Lett*. 2015;589(22):3343-3353.

355. Fass E, Shvets E, Degani I, Hirschberg K, Elazar Z. Microtubules support production of starvation-induced autophagosomes but not their targeting and fusion with lysosomes. *J Biol Chem*. 2006;281(47):36303-36316.

356. Mackeh R, Perdiz D, Lorin S, Codogno P, Poüs C. Autophagy and microtubules - new story, old players. *J Cell Sci*. 2013;126(Pt 5):1071-1080.

357. Bonifacino JS, Neefjes J. Moving and positioning the endolysosomal system. *Curr Opin Cell Biol*. 2017;47:1-8.

358. Rubinsztein DC, Codogno P, Levine B. Autophagy modulation as a potential therapeutic target for diverse diseases. *Nat Rev Drug Discov*. 2012;11(9):709-730.

359. Gutierrez MG, Munafó DB, Berón W, Colombo MI. Rab7 is required for the normal progression of the autophagic pathway in mammalian cells. *J Cell Sci*. 2004;117(Pt 13):2687-2697.

360. Tanaka Y, Guhde G, Suter A, et al. Accumulation of autophagic vacuoles and cardiomyopathy in LAMP-2-deficient mice. *Nature*. 2000;406(6798):902-906.

361. Köchl R, Hu XW, Chan EY, Tooze SA. Microtubules facilitate autophagosome formation and fusion of autophagosomes with endosomes. *Traffic*. 2006;7(2):129-145.

362. Aplin A, Jasionowski T, Tuttle DL, Lenk SE, Dunn WA. Cytoskeletal elements are required for the formation and maturation of autophagic vacuoles. *J Cell Physiol*. 1992;152(3):458-466.

363. Fengsrud M, Roos N, Berg T, Liou W, Slot JW, Seglen PO. Ultrastructural and immunocytochemical characterization of autophagic vacuoles in isolated hepatocytes: effects of vinblastine and asparagine on vacuole distributions. *Exp Cell Res*. 1995;221(2):504-519.

364. Punnonen EL, Reunanen H. Effects of vinblastine, leucine, and histidine, and 3-methyladenine on autophagy in Ehrlich ascites cells. *Exp Mol Pathol*. 1990;52(1):87-97.

365. Seglen PO, Berg TO, Blankson H, Fengsrud M, Holen I, Strømhaug PE. Structural aspects of autophagy. *Adv Exp Med Biol*. 1996;389:103-111.

366. Klionsky DJ, Abdalla FC, Abeliovich H, et al. Guidelines for the use and interpretation of assays for monitoring autophagy. *Autophagy*. 2012;8(4):445-544.

367. Hanada T, Noda NN, Satomi Y, et al. The Atg12-Atg5 conjugate has a novel E3-like activity for protein lipidation in autophagy. *J Biol Chem*. 2007;282(52):37298-37302.

368. Tanida I, Ueno T, Kominami E. LC3 conjugation system in mammalian autophagy. *Int J Biochem Cell Biol*. 2004;36(12):2503-2518.

369. Kabeya Y, Mizushima N, Ueno T, et al. LC3, a mammalian homologue of yeast Apg8p, is localized in autophagosome membranes after processing. *EMBO J*. 2000;19(21):5720-5728.

370. Mizushima N. Methods for monitoring autophagy. *Int J Biochem Cell Biol*. 2004;36(12):2491-2502.

371. Kimura S, Noda T, Yoshimori T. Dissection of the autophagosome maturation process by a novel reporter protein, tandem fluorescent-tagged LC3. *Autophagy*. 2007;3(5):452-460.

372. Pankiv S, Clausen TH, Lamark T, et al. p62/SQSTM1 binds directly to Atg8/LC3 to facilitate degradation of ubiquitinated protein aggregates by autophagy. *J Biol Chem*. 2007;282(33):24131-24145.

373. Mizushima N, Yoshimori T, Levine B. Methods in mammalian autophagy research. *Cell*. 2010;140(3):313-326.

374. Santaguida S, Vasile E, White E, Amon A. Aneuploidy-induced cellular stresses limit autophagic degradation. *Genes Dev*. 2015;29(19):2010-2021.

375. Krämer A, Maier B, Bartek J. Centrosome clustering and chromosomal (in)stability: a matter of life and death. *Mol Oncol*. 2011;5(4):324-335.

376. Santaguida S, Amon A. Aneuploidy triggers a TFEB-mediated lysosomal stress response. *Autophagy*. 2015;11(12):2383-2384.

377. Santaguida S, Amon A. Short- and long-term effects of chromosome mis-segregation and aneuploidy. *Nat Rev Mol Cell Biol*. 2015;16(8):473-485.

378. Balczon R, Bao L, Zimmer WE, Brown K, Zinkowski RP, Brinkley BR. Dissociation of centrosome replication events from cycles of DNA synthesis and mitotic division in hydroxyurea-arrested Chinese hamster ovary cells. *J Cell Biol*. 1995;130(1):105-115.

379. Konotop G, Bausch E, Nagai T, et al. Pharmacological Inhibition of Centrosome Clustering by Slingshot-Mediated Cofilin Activation and Actin Cortex Destabilization. *Cancer Res*. 2016.

380. Stingele S, Stoehr G, Peplowska K, Cox J, Mann M, Storchova Z. Global analysis of genome, transcriptome and proteome reveals the response to aneuploidy in human cells. *Mol Syst Biol*. 2012;8:608.

381. Pavelka N, Rancati G, Zhu J, et al. Aneuploidy confers quantitative proteome changes and phenotypic variation in budding yeast. *Nature*. 2010;468(7321):321-325.

382. Torres EM, Dephoure N, Panneerselvam A, et al. Identification of aneuploidy-tolerating mutations. *Cell*. 2010;143(1):71-83.

383. Oromendia AB, Dodgson SE, Amon A. Aneuploidy causes proteotoxic stress in yeast. *Genes Dev*. 2012;26(24):2696-2708.

384. Oromendia AB, Amon A. Aneuploidy: implications for protein homeostasis and disease. *Dis Model Mech*. 2014;7(1):15-20.

385. Stingele S, Stoehr G, Storchova Z. Activation of autophagy in cells with abnormal karyotype. *Autophagy*. 2013;9(2):246-248.

386. Joachim J, Razi M, Judith D, et al. Centriolar Satellites Control GABARAP Ubiquitination and GABARAP-Mediated Autophagy. *Curr Biol*. 2017;27(14):2123-2136.e2127.

387. Watanabe Y, Honda S, Konishi A, et al. Autophagy controls centrosome number by degrading Cep63. *Nat Commun*. 2016;7:13508.

388. White E. The role for autophagy in cancer. *J Clin Invest*. 2015;125(1):42-46.

389. Qu X, Yu J, Bhagat G, et al. Promotion of tumorigenesis by heterozygous disruption of the beclin 1 autophagy gene. *J Clin Invest*. 2003;112(12):1809-1820.

390. Yue Z, Jin S, Yang C, Levine AJ, Heintz N. Beclin 1, an autophagy gene essential for early embryonic development, is a haploinsufficient tumor suppressor. *Proc Natl Acad Sci U S A*. 2003;100(25):15077-15082.

391. Laddha SV, Ganesan S, Chan CS, White E. Mutational landscape of the essential autophagy gene BECN1 in human cancers. *Mol Cancer Res*. 2014;12(4):485-490.

392. Yang S, Wang X, Contino G, et al. Pancreatic cancers require autophagy for tumor growth. *Genes Dev*. 2011;25(7):717-729.

393. Liu J, Debnath J. The Evolving, Multifaceted Roles of Autophagy in Cancer. *Adv Cancer Res*. 2016;130:1-53.

394. Amaravadi R, Kimmelman AC, White E. Recent insights into the function of autophagy in cancer. *Genes Dev*. 2016;30(17):1913-1930.

395. Lebovitz CB, Robertson AG, Goya R, et al. Cross-cancer profiling of molecular alterations within the human autophagy interaction network. *Autophagy*. 2015;11(9):1668-1687.

396. Adams O, Dislich B, Berezowska S, et al. Prognostic relevance of autophagy markers LC3B and p62 in esophageal adenocarcinomas. *Oncotarget*. 2016.

397. Choudhary A, Zachek B, Lera RF, et al. Identification of Selective Lead Compounds for Treatment of High-Ploidy Breast Cancer. *Mol Cancer Ther*. 2016;15(1):48-59.

398. N'Diaye EN, Kajihara KK, Hsieh I, Morisaki H, Debnath J, Brown EJ. PLIC proteins or ubiquilins regulate autophagy-dependent cell survival during nutrient starvation. *EMBO Rep*. 2009;10(2):173-179.

399. Chinnadurai R, Copland IB, Ng S, et al. Mesenchymal Stromal Cells Derived From Crohn's Patients Deploy Indoleamine 2,3-dioxygenase-mediated Immune Suppression, Independent of Autophagy. *Mol Ther*. 2015;23(7):1248-1261.

400. Toepfer N, Childress C, Parikh A, Rukstalis D, Yang W. Atorvastatin induces autophagy in prostate cancer PC3 cells through activation of LC3 transcription. *Cancer Biol Ther*. 2011;12(8):691-699.

401. Spandidos A, Wang X, Wang H, Seed B. PrimerBank: a resource of human and mouse PCR primer pairs for gene expression detection and quantification. *Nucleic Acids Res*. 2010;38(Database issue):D792-799.

402. Toops KA, Tan LX, Jiang Z, Radu RA, Lakkaraju A. Cholesterol-mediated activation of acid sphingomyelinase disrupts autophagy in the retinal pigment epithelium. *Mol Biol Cell*. 2015;26(1):1-14.

403. Holland AJ, Fachinetti D, Da Cruz S, et al. Polo-like kinase 4 controls centriole duplication but does not directly regulate cytokinesis. *Mol Biol Cell*. 2012;23(10):1838-1845.

404. Sonnen KF, Gabryjonczyk AM, Anselm E, Stierhof YD, Nigg EA. Human Cep192 and Cep152 cooperate in Plk4 recruitment and centriole duplication. *J Cell Sci*. 2013;126(Pt 14):3223-3233.

405. Kim TS, Park JE, Shukla A, et al. Hierarchical recruitment of Plk4 and regulation of centriole biogenesis by two centrosomal scaffolds, Cep192 and Cep152. *Proc Natl Acad Sci U S A*. 2013;110(50):E4849-4857.

406. Fırat-Karalar EN, Stearns T. The centriole duplication cycle. *Philos Trans R Soc Lond B Biol Sci*. 2014;369(1650).

407. Martindill DM, Risebro CA, Smart N, et al. Nucleolar release of Hand1 acts as a molecular switch to determine cell fate. *Nat Cell Biol*. 2007;9(10):1131-1141.

408. Hatch EM, Kulukian A, Holland AJ, Cleveland DW, Stearns T. Cep152 interacts with Plk4 and is required for centriole duplication. *J Cell Biol*. 2010;191(4):721-729.

409. Bonni S, Ganuelas ML, Petrinac S, Hudson JW. Human Plk4 phosphorylates Cdc25C. *Cell Cycle*. 2008;7(4):545-547.

410. Petrinac S, Ganuelas ML, Bonni S, Nantais J, Hudson JW. Polo-like kinase 4 phosphorylates Chk2. *Cell Cycle*. 2009;8(2):327-329.

411. Firat-Karalar EN, Rauniyar N, Yates JR, Stearns T. Proximity interactions among centrosome components identify regulators of centriole duplication. *Curr Biol*. 2014;24(6):664-670.

412. Merrill AE, Coon JJ. Quantifying proteomes and their post-translational modifications by stable isotope label-based mass spectrometry. *Curr Opin Chem Biol*. 2013;17(5):779-786.

413. Richards AL, Merrill AE, Coon JJ. Proteome sequencing goes deep. *Curr Opin Chem Biol*. 2015;24:11-17.

414. Riley NM, Coon JJ. Phosphoproteomics in the Age of Rapid and Deep Proteome Profiling. *Anal Chem*. 2016;88(1):74-94.

415. Riley NM, Hebert AS, Coon JJ. Proteomics Moves into the Fast Lane. *Cell Syst*. 2016;2(3):142-143.

416. Staples CJ, Myers KN, Beveridge RD, et al. The centriolar satellite protein Cep131 is important for genome stability. *J Cell Sci*. 2012;125(Pt 20):4770-4779.

417. Mori Y, Inoue Y, Tanaka S, et al. Cep169, a Novel Microtubule Plus-End-Tracking Centrosomal Protein, Binds to CDK5RAP2 and Regulates Microtubule Stability. *PLoS One*. 2015;10(10):e0140968.

418. Korzeniewski N, Cuevas R, Duensing A, Duensing S. Daughter centriole elongation is controlled by proteolysis. *Mol Biol Cell*. 2010;21(22):3942-3951.

419. Hall EA, Keighren M, Ford MJ, et al. Acute versus chronic loss of mammalian Azi1/Cep131 results in distinct ciliary phenotypes. *PLoS Genet*. 2013;9(12):e1003928.

420. Ai R, Sun Y, Guo Z, et al. NDRG1 overexpression promotes the progression of esophageal squamous cell carcinoma through modulating Wnt signaling pathway. *Cancer Biol Ther*. 2016;17(9):943-954.

421. Kubo A, Sasaki H, Yuba-Kubo A, Tsukita S, Shiina N. Centriolar satellites: molecular characterization, ATP-dependent movement toward centrioles and possible involvement in ciliogenesis. *J Cell Biol*. 1999;147(5):969-980.

422. Tollenaere MA, Villumsen BH, Blasius M, et al. p38- and MK2-dependent signalling promotes stress-induced centriolar satellite remodelling via 14-3-3-dependent sequestration of CEP131/AZI1. *Nat Commun*. 2015;6:10075.

423. Blomen VA, Májek P, Jae LT, et al. Gene essentiality and synthetic lethality in haploid human cells. *Science*. 2015;350(6264):1092-1096.

424. Villumsen BH, Danielsen JR, Povlsen L, et al. A new cellular stress response that triggers centriolar satellite reorganization and ciliogenesis. *EMBO J*. 2013;32(23):3029-3040.

425. Balczon R, Varden CE, Schroer TA. Role for microtubules in centrosome doubling in Chinese hamster ovary cells. *Cell Motil Cytoskeleton*. 1999;42(1):60-72.

426. Baron Gaillard CL, Pallesi-Pocachard E, Massey-Harroche D, et al. Hook2 is involved in the morphogenesis of the primary cilium. *Mol Biol Cell*. 2011;22(23):4549-4562.

427. Liu XH, Yang YF, Fang HY, Wang XH, Zhang MF, Wu DC. CEP131 indicates poor prognosis and promotes cell proliferation and migration in hepatocellular carcinoma. *Int J Biochem Cell Biol*. 2017.

428. Hoang-Minh LB, Deleyrolle LP, Nakamura NS, et al. PCM1 Depletion Inhibits Glioblastoma Cell Ciliogenesis and Increases Cell Death and Sensitivity to Temozolomide. *Transl Oncol*. 2016;9(5):392-402.

429. Bedard PL, Cescon DW, Fletcher G, et al. First-in-human phase I trial of the oral PLK4 inhibitor

CFI-400945 in patients with advanced solid tumors. American Association for Cancer Research Annual Meeting. New Orleans; 2016.

430. Li X, Song N, Liu L, et al. USP9X regulates centrosome duplication and promotes breast carcinogenesis. *Nat Commun*. 2017;8:14866.

431. Sanjana NE, Shalem O, Zhang F. Improved vectors and genome-wide libraries for CRISPR screening. *Nat Methods*. 2014;11(8):783-784.

432. Shalem O, Sanjana NE, Hartenian E, et al. Genome-scale CRISPR-Cas9 knockout screening in human cells. *Science*. 2014;343(6166):84-87.

433. Wenger CD, Phanstiel DH, Lee MV, Bailey DJ, Coon JJ. COMPASS: a suite of pre- and post-search proteomics software tools for OMSSA. *Proteomics*. 2011;11(6):1064-1074.

434. Taus T, Köcher T, Pichler P, et al. Universal and confident phosphorylation site localization using phosphoRS. *J Proteome Res*. 2011;10(12):5354-5362.

435. Klebba JE, Buster DW, Nguyen AL, et al. Polo-like kinase 4 autodestructs by generating its Slimb-binding phosphodegron. *Curr Biol*. 2013;23(22):2255-2261.

436. Carvalho-Santos Z, Machado P, Branco P, et al. Stepwise evolution of the centriole-assembly pathway. *J Cell Sci*. 2010;123(Pt 9):1414-1426.

437. D'Angiolella V, Donato V, Vijayakumar S, et al. SCF(Cyclin F) controls centrosome homeostasis and mitotic fidelity through CP110 degradation. *Nature*. 2010;466(7302):138-142.

438. Franz A, Roque H, Saurya S, Dobbelaere J, Raff JW. CP110 exhibits novel regulatory activities during centriole assembly in Drosophila. *J Cell Biol*. 2013;203(5):785-799.

439. Cizmecioglu O, Arnold M, Bahtz R, et al. Cep152 acts as a scaffold for recruitment of Plk4 and CPAP to the centrosome. *J Cell Biol*. 2010;191(4):731-739.

440. Le Clech M. Role of CAP350 in centriolar tubule stability and centriole assembly. *PLoS One*. 2008;3(12):e3855.

441. Pihan GA. Centrosome dysfunction contributes to chromosome instability, chromoanagenesis, and genome reprograming in cancer. *Front Oncol*. 2013;3:277.

442. Tollenaere MA, Mailand N, Bekker-Jensen S. Centriolar satellites: key mediators of centrosome functions. *Cell Mol Life Sci*. 2015;72(1):11-23.

443. Wang L, Lee K, Malonis R, Sanchez I, Dynlacht BD. Tethering of an E3 ligase by PCM1 regulates the abundance of centrosomal KIAA0586/Talpid3 and promotes ciliogenesis. *Elife*. 2016;5.

444. Wang G, Chen Q, Zhang X, et al. PCM1 recruits Plk1 to the pericentriolar matrix to promote primary cilia disassembly before mitotic entry. *J Cell Sci*. 2013;126(Pt 6):1355-1365.

445. Mikule K, Delaval B, Kaldis P, Jurcyzk A, Hergert P, Doxsey S. Loss of centrosome integrity induces p38-p53-p21-dependent G1-S arrest. *Nat Cell Biol*. 2007;9(2):160-170.

446. Srsen V, Gnadt N, Dammermann A, Merdes A. Inhibition of centrosome protein assembly leads to p53-dependent exit from the cell cycle. *J Cell Biol*. 2006;174(5):625-630.

447. Balczon R, Simerly C, Takahashi D, Schatten G. Arrest of cell cycle progression during first interphase in murine zygotes microinjected with anti-PCM-1 antibodies. *Cell Motil Cytoskeleton*. 2002;52(3):183-192.

448. Logarinho E, Maffini S, Barisic M, et al. CLASPs prevent irreversible multipolarity by ensuring spindle-pole resistance to traction forces during chromosome alignment. *Nat Cell Biol*. 2012;14(3):295-303.

449. Oshimori N, Li X, Ohsugi M, Yamamoto T. Cep72 regulates the localization of key centrosomal proteins and proper bipolar spindle formation. *EMBO J*. 2009;28(14):2066-2076.

450. Kim K, Rhee K. The pericentriolar satellite protein CEP90 is crucial for integrity of the mitotic spindle pole. *J Cell Sci*. 2011;124(Pt 3):338-347.

451. Kodani A, Tonthat V, Wu B, Sütterlin C. Par6 alpha interacts with the dynactin subunit p150 Glued and is a critical regulator of centrosomal protein recruitment. *Mol Biol Cell*. 2010;21(19):3376-3385.

452. Neumann B, Walter T, Hériché JK, et al. Phenotypic profiling of the human genome by time-lapse microscopy reveals cell division genes. *Nature*. 2010;464(7289):721-727.

453. Geigl JB, Obenauf AC, Schwarzbraun T, Speicher MR. Defining 'chromosomal instability'. *Trends Genet*. 2008;24(2):64-69.

454. Giam M, Rancati G. Aneuploidy and chromosomal instability in cancer: a jackpot to chaos. *Cell Div*. 2015;10:3.

455. Sheltzer JM, Blank HM, Pfau SJ, et al. Aneuploidy drives genomic instability in yeast. *Science*. 2011;333(6045):1026-1030.

456. Reish O, Regev M, Kanesky A, Girafi S, Mashevich M. Sporadic aneuploidy in PHA-stimulated lymphocytes of trisomies 21, 18, and 13. *Cytogenet Genome Res*. 2011;133(2-4):184-189.

457. Kost-Alimova M, Fedorova L, Yang Y, Klein G, Imreh S. Microcell-mediated chromosome transfer provides evidence that polysomy promotes structural instability in tumor cell chromosomes through asynchronous replication and breakage within late-replicating regions. *Genes Chromosomes Cancer*. 2004;40(4):316-324.

458. Leber B, Maier B, Fuchs F, et al. Proteins required for centrosome clustering in cancer cells. *Sci Transl Med*. 2010;2(33):33ra38.

459. Carter SL, Eklund AC, Kohane IS, Harris LN, Szallasi Z. A signature of chromosomal instability inferred from gene expression profiles predicts clinical outcome in multiple human cancers. *Nat Genet*. 2006;38(9):1043-1048.

460. Zasadil LM, Andersen KA, Yeum D, et al. Cytotoxicity of paclitaxel in breast cancer is due to chromosome missegregation on multipolar spindles. *Sci Transl Med*. 2014;6(229):229ra243.

461. Corvi R, Berger N, Balczon R, Romeo G. RET/PCM-1: a novel fusion gene in papillary thyroid carcinoma. *Oncogene*. 2000;19(37):4236-4242.

462. Ohata H, Fujiwara Y, Koyama K, Nakamura Y. Mapping of the human autoantigen pericentriolar material 1 (PCM1) gene to chromosome 8p21.3-p22. *Genomics*. 1994;24(2):404-406.

463. Negrini S, Gorgoulis VG, Halazonetis TD. Genomic instability--an evolving hallmark of cancer. *Nat Rev Mol Cell Biol*. 2010;11(3):220-228.

464. Lee AJ, Endesfelder D, Rowan AJ, et al. Chromosomal instability confers intrinsic multidrug resistance. *Cancer Res*. 2011;71(5):1858-1870.

465. Solimini NL, Xu Q, Mermel CH, et al. Recurrent hemizygous deletions in cancers may optimize proliferative potential. *Science*. 2012;337(6090):104-109.

466. Zwemer LM, Zak A, Thompson BR, et al. Autosomal monoallelic expression in the mouse. *Genome Biol*. 2012;13(2):R10.

467. Vladar EK, Stearns T. Molecular characterization of centriole assembly in ciliated epithelial cells. *J Cell Biol*. 2007;178(1):31-42.

468. Conkar D, Culfa E, Odabasi E, Rauniyar N, Yates JR, Firat-Karalar EN. The centriolar satellite protein CCDC66 interacts with CEP290 and functions in cilium formation and trafficking. *J Cell Sci*. 2017;130(8):1450-1462.

469. Sampson J, O'Regan L, Dyer MJ, Bayliss R, Fry AM. Hsp72 and Nek6 cooperate to cluster amplified centrosomes in cancer cells. *Cancer Res*. 2017.

470. Yang B, Lamb ML, Zhang T, et al. Discovery of potent KIFC1 inhibitors using a method of integrated high-throughput synthesis and screening. *J Med Chem*. 2014;57(23):9958-9970.

471. Watts CA, Richards FM, Bender A, et al. Design, synthesis, and biological evaluation of an allosteric inhibitor of HSET that targets cancer cells with supernumerary centrosomes. *Chem Biol*. 2013;20(11):1399-1410.

472. Levy JMM, Towers CG, Thorburn A. Targeting autophagy in cancer. *Nat Rev Cancer*. 2017;17(9):528-542.

473. Towers CG, Thorburn A. Therapeutic Targeting of Autophagy. *EBioMedicine*. 2016;14:15-23.

474. Egan DF, Chun MG, Vamos M, et al. Small Molecule Inhibition of the Autophagy Kinase ULK1 and Identification of ULK1 Substrates. *Mol Cell*. 2015;59(2):285-297.

475. Mullee LI, Morrison CG. Centrosomes in the DNA damage response-the hub outside the centre. *Chromosome Res*. 2015.

476. Doxsey S, McCollum D, Theurkauf W. Centrosomes in cellular regulation. *Annu Rev Cell Dev Biol*. 2005;21:411-434.

477. Zhang S, Hemmerich P, Grosse F. Centrosomal localization of DNA damage checkpoint proteins. *J Cell Biochem*. 2007;101(2):451-465.

478. Fletcher L, Muschel RJ. The centrosome and the DNA damage induced checkpoint. *Cancer Lett*. 2006;243(1):1-8.

479. Oricchio E, Saladino C, Iacovelli S, Soddu S, Cundari E. ATM is activated by default in mitosis, localizes at centrosomes and monitors mitotic spindle integrity. *Cell Cycle*. 2006;5(1):88-92.

480. Brown CR, Doxsey SJ, White E, Welch WJ. Both viral (adenovirus E1B) and cellular (hsp 70, p53) components interact with centrosomes. *J Cell Physiol*. 1994;160(1):47-60.

481. Augustin A, Spenlehauer C, Dumond H, et al. PARP-3 localizes preferentially to the daughter centriole and interferes with the G1/S cell cycle progression. *J Cell Sci*. 2003;116(Pt 8):1551-1562.

482. Ciciarello M, Mangiacasale R, Casenghi M, et al. p53 displacement from centrosomes and p53-mediated G1 arrest following transient inhibition of the mitotic spindle. *J Biol Chem*. 2001;276(22):19205-19213.

483. Takada S, Kelkar A, Theurkauf WE. Drosophila checkpoint kinase 2 couples centrosome function and spindle assembly to genomic integrity. *Cell*. 2003;113(1):87-99.

484. Golan A, Pick E, Tsvetkov L, Nadler Y, Kluger H, Stern DF. Centrosomal Chk2 in DNA damage responses and cell cycle progression. *Cell Cycle*. 2010;9(13):2647-2656.

485. Lukinavičius G, Lavogina D, Gönczy P, Johnsson K. Commercial Cdk1 antibodies recognize the centrosomal protein Cep152. *Biotechniques*. 2013;55(3):111-114.

486. Douthwright S, Sluder G. Link between DNA damage and centriole disengagement/reduplication in untransformed human cells. *J Cell Physiol*. 2014;229(10):1427-1436.

487. Löffler H, Fechter A, Liu FY, Poppelreuther S, Krämer A. DNA damage-induced centrosome amplification occurs via excessive formation of centriolar satellites. *Oncogene*. 2013;32(24):2963-2972.

488. Dinçer T, Yorgancıoğlu-Budak G, Ölmez A, et al. Analysis of centrosome and DNA damage response in PLK4 associated Seckel syndrome. *Eur J Hum Genet*. 2017.

489. Tritarelli A, Oricchio E, Ciciarello M, et al. p53 localization at centrosomes during mitosis and postmitotic checkpoint are ATM-dependent and require serine 15 phosphorylation. *Mol Biol Cell*. 2004;15(8):3751-3757.

490. Kong D, Farmer V, Shukla A, et al. Centriole maturation requires regulated Plk1 activity during two consecutive cell cycles. *J Cell Biol*. 2014;206(7):855-865.

491. Ishikawa K, Nagase T, Nakajima D, et al. Prediction of the coding sequences of unidentified human genes. VIII. 78 new cDNA clones from brain which code for large proteins in vitro. *DNA Res*. 1997;4(5):307-313.

492. Santamaria A, Wang B, Elowe S, et al. The Plk1-dependent phosphoproteome of the early mitotic spindle. *Mol Cell Proteomics*. 2011;10(1):M110.004457.

493. Hutchins JR, Toyoda Y, Hegemann B, et al. Systematic analysis of human protein complexes identifies chromosome segregation proteins. *Science*. 2010;328(5978):593-599.

494. Welburn JP, Cheeseman IM. The microtubule-binding protein Cep170 promotes the targeting of the kinesin-13 depolymerase Kif2b to the mitotic spindle. *Mol Biol Cell*. 2012;23(24):4786-4795.

495. Pillai S, Nguyen J, Johnson J, Haura E, Coppola D, Chellappan S. Tank binding kinase 1 is a centrosome-associated kinase necessary for microtubule dynamics and mitosis. *Nat Commun*. 2015;6:10072.

496. Leung GC, Ho CS, Blasutig IM, Murphy JM, Sicheri F. Determination of the Plk4/Sak consensus phosphorylation motif using peptide spots arrays. *FEBS Lett*. 2007;581(1):77-83.

497. Silk AD, Zasadil LM, Holland AJ, Vitre B, Cleveland DW, Weaver BA. Chromosome missegregation rate predicts whether aneuploidy will promote or suppress tumors. *Proc Natl Acad Sci U S A*. 2013;110(44):E4134-4141.

498. Graser S, Stierhof YD, Nigg EA. Cep68 and Cep215 (Cdk5rap2) are required for centrosome cohesion. *J Cell Sci*. 2007;120(Pt 24):4321-4331.

499. Bahe S, Stierhof YD, Wilkinson CJ, Leiss F, Nigg EA. Rootletin forms centriole-associated filaments and functions in centrosome cohesion. *J Cell Biol*. 2005;171(1):27-33.

500. Mundy GR. Metastasis to bone: causes, consequences and therapeutic opportunities. *Nat Rev Cancer*. 2002;2(8):584-593.

501. Janni WJ, Rack B, Terstappen LW, et al. Pooled Analysis of the Prognostic Relevance of Circulating Tumor Cells in Primary Breast Cancer. *Clin Cancer Res*. 2016;22(10):2583-2593.

502. Bidard FC, Peeters DJ, Fehm T, et al. Clinical validity of circulating tumour cells in patients with metastatic breast cancer: a pooled analysis of individual patient data. *Lancet Oncol*. 2014;15(4):406-414.

503. Pukazhendhi G, Glück S. Circulating tumor cells in breast cancer. *J Carcinog*. 2014;13:8.

504. de Bono JS, Scher HI, Montgomery RB, et al. Circulating tumor cells predict survival benefit from treatment in metastatic castration-resistant prostate cancer. *Clin Cancer Res*. 2008;14(19):6302-6309.

505. Okegawa T, Nutahara K, Higashihara E. Immunomagnetic quantification of circulating tumor cells as a prognostic factor of androgen deprivation responsiveness in patients with hormone naive metastatic prostate cancer. *J Urol*. 2008;180(4):1342-1347.

506. Fukasawa K. Centrosome amplification, chromosome instability and cancer development. *Cancer Lett*. 2005;230(1):6-19.

507. Sperger JM, Strotman LN, Welsh A, et al. Integrated Analysis of Multiple Biomarkers from Circulating Tumor Cells Enabled by Exclusion-Based Analyte Isolation. *Clin Cancer Res*. 2016.

508. Shono M, Sato N, Mizumoto K, et al. Stepwise progression of centrosome defects associated with local tumor growth and metastatic process of human pancreatic carcinoma cells transplanted orthotopically into nude mice. *Lab Invest*. 2001;81(7):945-952.

APPENDICES

Appendix A. Transcriptome analysis in cells with centrosome amplification

The goal of this project was to perform an unbiased look at changes in gene expression in cells with centrosome amplification (CA) to identify possible therapeutic targets for cancer. We utilized doxycycline-inducible Polo-like kinase 4 (PLK4) cell lines (RPE1 and MCF10A) to model centrosome amplification. PLK4 is the master regulator of centriole duplication, and overexpression has been shown to cause CA. The following conditions were performed in duplicate: RPE PLK4 WT + doxycycline; RPE PLK4 608 + doxycycline; MCF10A PLK4 WT + doxycycline; MCF10A PLK4 608 + doxycycline. The PLK4 WT cell lines express the full-length PLK4, while the PLK4 608 cell lines express a truncated form of PLK4 (amino acids 608) that lacks a crucial C-terminal localization domain and does not cause CA.[126]

Cells were treated with 2ug/ml doxycycline, then harvested. RNA was isolated using the Qiagen RNeasy Mini kit. RNA samples were processed by the University of Wisconsin-Madison Gene Expression Center. We used Affymetrix Human Transciptome Array 2.0 under the manufacturer's protocols.

We identified genes differentially expressed in cells with CA versus controls (Figure A-1A, Table A-1, Table A-2). Interestingly, three of the top hits that are overexpressed in cells with CA are involved in migration; CA has previously been shown to enhance migration and invasion.[121,126] To validate these findings, we performed qRT-PCR to assess gene expression changes. Interestingly, cells with CA demonstrate increased CEMIP, RAB25, and RAB31 transcript levels. We hypothesize that CA may upregulate these genes to cause increased cellular invasiveness.

Figure A-1. Genes differentially expressed in centrosome-amplified cells.

(A) Volcano plot demonstrating differences in gene expression in cells with CA versus controls. Data from both RPE and MCF10A cell lines are combined. Dotted lines indicate cutoffs for significance and fold change. **(B)** qRT-PCR data demonstrating the fold increase in CEMIP, RAB25, and RAB31 mRNA in cells with CA compared to controls.

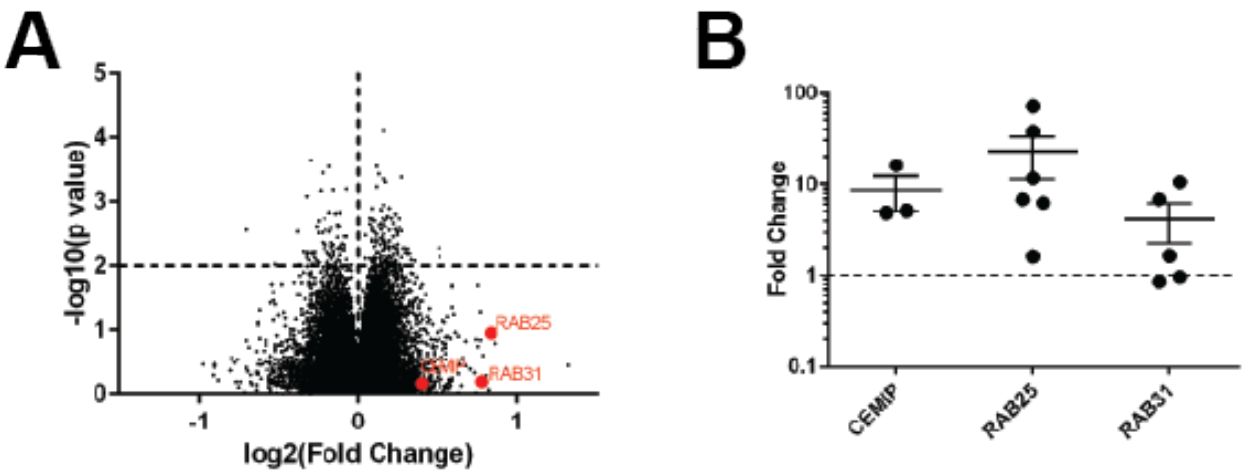

Table A-1. Genes differentially expressed in RPE1 cells with centrosome amplification.

Transcript Cluster ID	Gene Symbol	Description	Fold Change With CA	P Value
TC15000752.hg.1	CEMIP; KIAA1199	cell migration inducing protein, hyaluronan binding; KIAA1199	2.8	0.025801
TC01003671.hg.1	MIR181B1	microRNA 181b-1	2.61	0.017594
TC08002503.hg.1	FBXO32	F-box protein 32	2.45	0.012157
TC08001590.hg.1	FBXO32	F-box protein 32	2.43	0.033135
TC06004064.hg.1	HIST1H3H; HIST1H3A; HIST1H3D; HIST1H3C; HIST1H3E; HIST1H3I; HIST1H3G; HIST1H3J; HIST1H3B; HIST1H3F	histone cluster 1, H3h; histone cluster 1, H3a; histone cluster 1, H3d; histone cluster 1, H3c; histone cluster 1, H3e; histone cluster 1, H3i; histone cluster 1, H3g; histone cluster 1, H3j; histone cluster 1, H3b; histone cluster 1, H3f	-2.04	0.017953
TC01001749.hg.1	G0S2	G0/G1 switch 2; G0/G1switch 2	-2.5	0.030071

Table A-2. Genes differentially expressed in MCF10A cells with centrosome amplification

Transcript Cluster ID	Gene Symbol	Description	Fold Change With CA	P Value
TC01001311.hg.1	RAB25	RAB25, member RAS oncogene family	8.19	0.001387
TC18000047.hg.1	RAB31	RAB31, member RAS oncogene family	4.05	0.005797
TC0X001551.hg.1	CLIC2	chloride intracellular channel 2	3.26	0.004609
TC02001750.hg.1	CYP1B1	cytochrome P450, family 1, subfamily B, polypeptide 1	2.24	0.023501
TC12001804.hg.1	DCN	decorin	2.11	0.026697
TC14001319.hg.1	RNU4ATAC14P	RNA, U4atac small nuclear 14, pseudogene	-2.34	0.007346

Acknowledgements

Thank you to Nelson Wayne Davis at the Gene Expression Center at the University of Wisconsin-Madison for assistance with microarray analysis.

Appendix B. Centrioles are not required for the DNA damage response pathway

The centrosome, comprised of two orthogonally positioned centrioles surrounded by a matrix of proteins, is the microtubule organizing center of animal cells. A role for centrosomes in the DNA damage response has been hypothesized, and an entire review has been written on this topic;[475] however, this question has not been adequately addressed experimentally. There are many reports of DNA damage proteins localizing to the centrosome (e.g. ATM, BRCA1, BRCA2, CHK1, CHK2, p53, PARPs),[476-482] and Chk2 has been shown to localize to the centrosome after DNA damage.[483,484] However, some of these findings have been disproven by the observation that the antibodies used were cross-reacting with centrosome proteins, such as Chk1 antibodies cross-reacting with Cep152.[485] Another link between centrosomes and DNA damage has been suggested by studies demonstrating that treating cells with DNA damaging agents result in centriole splitting and centrosome amplification.[486] One report suggests that this may be dependent on excess formation of centriolar satellites.[487] Additionally, fibroblasts derived from individuals with Seckel syndrome due to inherited PLK4 mutation are deficient in DNA damage repair, as assessed by decreased Chk1 and Chk2 phosphorylation in hydroxyurea-treated cells compared to WT fibroblasts treated with hydroxyurea.[488] Several interesting questions remain. First, is the centrosome truly required for the DNA damage response? Second, do these proteins need to localize to centrosomes, and is that required for adequate DNA damage response?

To address these questions, we utilized a chemical genetic system where the ATP binding pocket of polo-like kinase 4 (PLK4), the master regulator of centrosome duplication, is enlarged by mutating the gatekeeper residue (L89G mutation) in the immortalized, non-transformed

human epithelial cell line RPE-1. This renders the kinase susceptible to inhibition with the bulky ATP analog 3-MB-PP1 and results in loss of centrosomes with centrioles after several days of inhibition (Figure B-1). The genotype is AS/Δ. To control for potential AS cell line-specific effects, we used AS+DMSO as a control. To control or haploinsufficiency of PLK4 (because the genotype of the AS cell line is AS/Δ) and off-target effects of the chemical, we used WT/Δ+3MBPP1 as a control. We then challenged these centrosome-less cells with doxorubicin to assess their response to DNA damage, as assessed by γH2AX immunofluorescent staining. We observed no difference in the DNA damage response in centrosome-less compared to controls (Figure B-2 A-B). We conclude that centrosomes are not required for an adequate DNA damage response.

Next, we asked whether *recovery* from DNA damage is impaired in the absence of centrosomes. Centrosome-less cells were treated with doxorubicin overnight, which was washed out and replaced with fresh media to allow the cells to recover. Cells were fixed at various time points and then stained for γH2AX. We observed no difference in γH2AX foci in centrosome-less cells versus controls. We conclude that centrosomes are not required for recovery from DNA damage.

Additionally, we assessed the viability of centrosome-less cells in response to the DNA damaging agents doxorubicin and hydroxyurea. We observed no significant differences in sensitivity of our centrosome-less cells compared to controls (Figure B-2 E-F).

Lastly, we assessed whether p53 localizes to the centrosome at baseline or under different experimental conditions. Previous reports have demonstrated that p53 localizes to the centrosome at different points in the cell cycle or after exposure to DNA damaging stimuli. This localization is lost with nocodazole treatment.[482] Additionally, p53 has been shown to

centrosomes during mitosis in an ATM-dependent manner[479,489] ATM is activated at each mitotic onset and phosphorylates p53 at Ser15 so as to keep p53 inactive at centrosomes when the spindle is correctly in place or, in case of inactivation of the mitotic spindle, to maintain the memory of a perturbed mitosis.[479] This activated p53 will be present in the daughter cell after an aberrant mitosis and result in apoptosis. However, there is controversy over whether or not p53 localizes to centrosomes, and whether this localization is required for the DNA damage response. We assessed p53 localization using 4 different p53 antibodies in 4 cell lines (RPE, MCF10A, HCT116, HeLa) under 3 different conditions: untreated cells and treatment with either doxorubicin or nocodazole (Figure B-3). Additionally, we assessed whether or not p53 localizes to centrosomes during mitosis, and did not find any evidence of this (Figure B-4).

Our data are supported by other reports of centrosome-less cells having robust DNA damage response, as assessed by γH2AX staining[157] and sensitivity to DNA damaging agents such as cisplatin and irradiation [48]. Furthermore, proteomic analysis of purified centrosomes has failed to identify DNA damage proteins.[210] We conclude that centrosomes are not required for the DNA damage response or recovery from DNA damage.

Figure B-1. Validation of PLK4 analog sensitive cell line.

(A) PLK4 analog sensitive (AS) cells were engineered to enlarge the ATP binding pocket of the kinase (L89G mutation) and render susceptible to a bulky ATP analog, 3MBPP1. The other endogenous locus was deleted, so the genotype is AS/Δ. To control for potential AS cell line-specific effects, we used AS+DMSO as a control. To control or haploinsufficiency of PLK4 and off-target effects of the chemical, we used WT/Δ+3MBPP1 as a control. Scale bar = 10 μm. (B) Quantification of the percent of cells in each condition containing centrosomes with centrioles, as indicated by the overlap of pericentrin (pericentriolar material marker, green) and centrin (centriole marker, red), with the indicated length of exposure to 3MBPP1/DMSO in days.

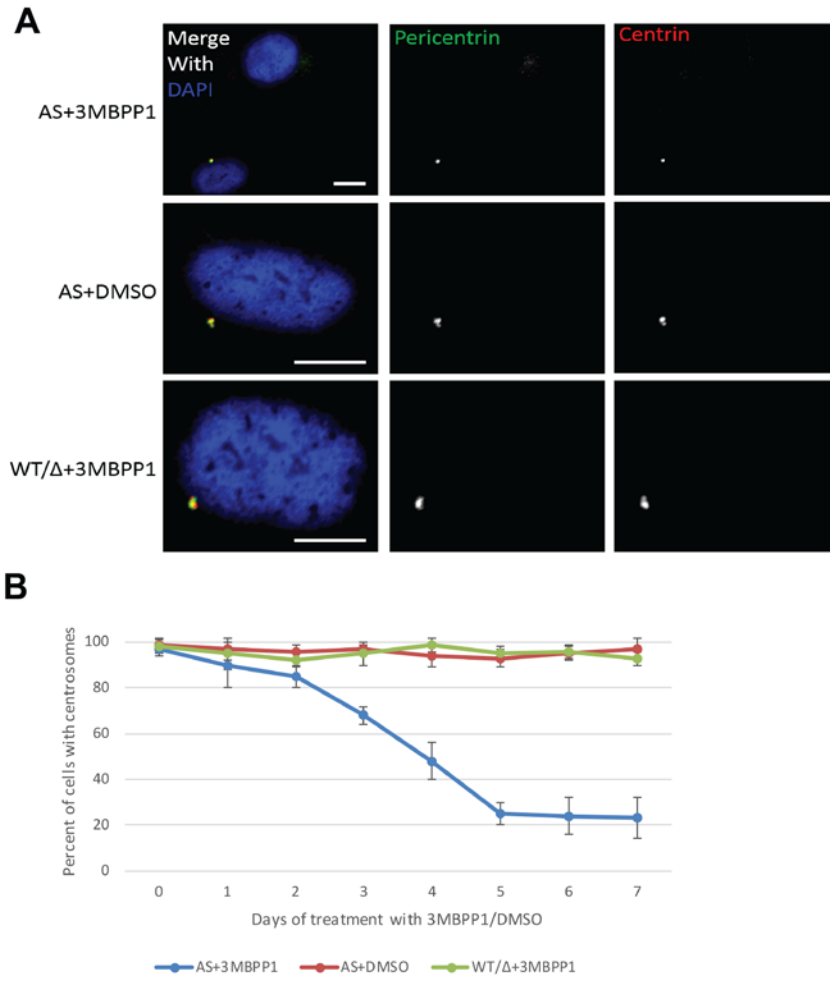

Figure B-2. Centrosomes are not required for the DNA damage response.

(A) PLK4 analog sensitive (AS) cells were pre-treated for 5 days with 3-MB-PP1 (10 μM) to induce loss of centrioles, then were challenged with doxorubicin (400nM) for up to 5 hours, then fixed and labeled by immunofluorescence. Representative images of AS cells treated with 3-MB-PP1 are shown, and each image includes one cell with centrosome(s), as pointed out by the white arrow, and one cell without centrosomes. Scale bars = 10 μm. (B) Quantification of γH2AX foci in RPE cells per condition for each time point. Time points represent number of hours after exposure to doxorubicin. N=50 cells for each condition and time point. Points represent means ±SEM. (C) PLK4 AS cells pre-treated treated for 5 days with 3-MB-PP1 (10 μM) to induce loss of centrioles, then were challenged with doxorubicin (400nM) for 12 hours. Doxorubicin was washed out 3 times with HBSS, then cells were allowed to recover for the indicated time points in normal media, then fixed and labeled by immunofluorescence. As in (A), representative images of AS cells treated with 3-MB-PP1 are shown, and each image includes one cell with centrosome(s), as pointed out by the white arrow, and one cell without centrosomes. (D) Quantification of γH2AX foci in cells from the experiment described in C. Time points represent the number of hours after washout of doxorubicin. N=50 cells for each condition and time point. Points represent means ±SEM. (E) To examine sensitivity of centrosome-less cells to DNA damaging agents, AS cells were pre-treated for 5 days with 3-MB-PP1 (10 μM) to induce loss of centrioles, then were challenged with the indicated concentrations of doxorubicin for 5 days. Cell viability was assessed by Cell Titer Glo luminescence assay (Promega). (F) Same experiment as in E, except with hydroxyurea, another DNA damaging agent.

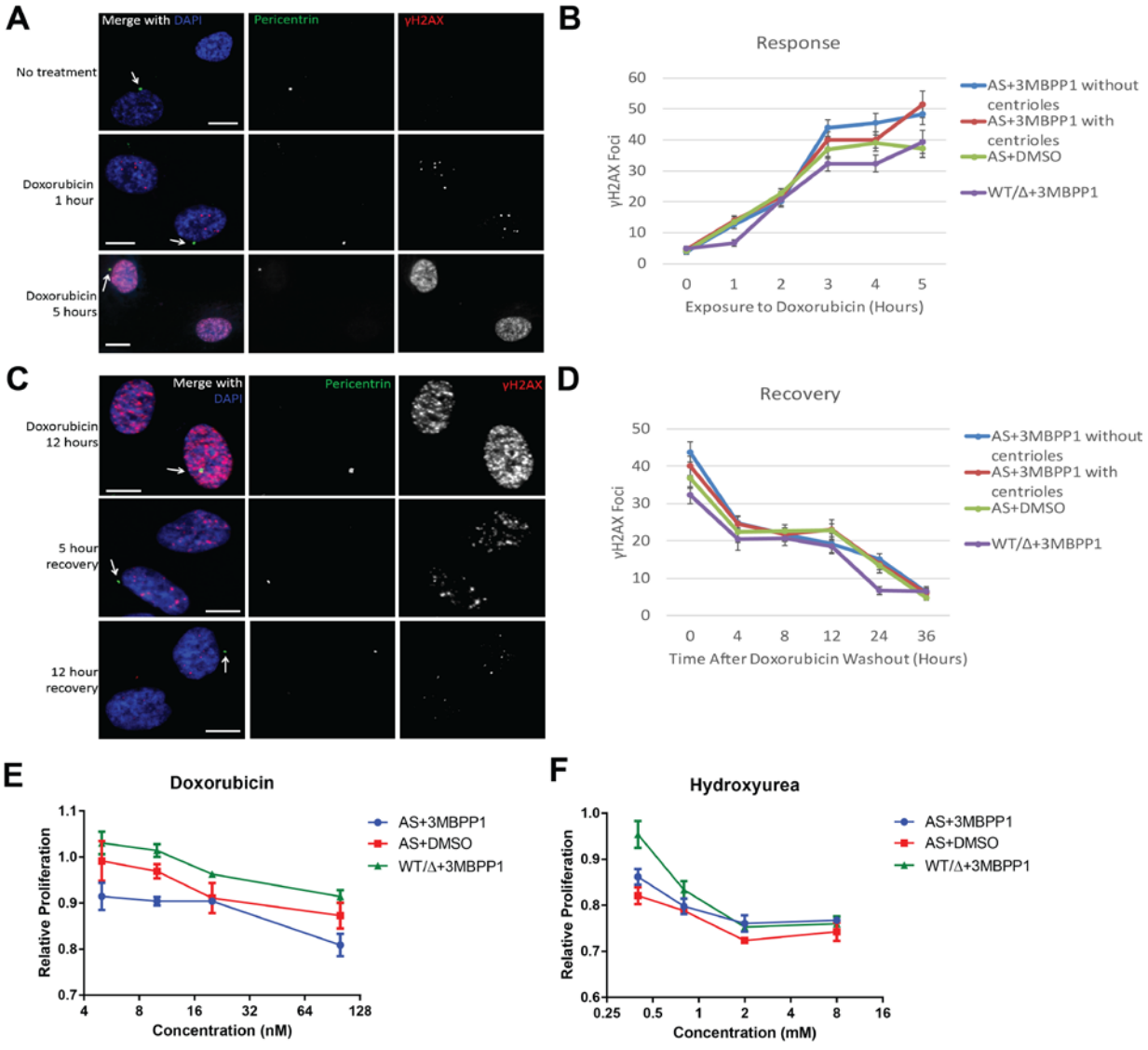
A
Merge with DAPI
Pericentrin
γH2AX
No treatment
Doxorubicin 1 hour
Doxorubicin 5 hours
B
Response
γH2AX Foci
Exposure to Doxorubicin (Hours)
AS+3MBPP1 without centrioles
AS+3MBPP1 with centrioles
AS+DMSO
WT/Δ+3MBPP1
C
Merge with DAPI
Pericentrin
γH2AX
Doxorubicin 12 hours
5 hour recovery
12 hour recovery
D
Recovery
γH2AX Foci
Time After Doxorubicin Washout (Hours)
AS+3MBPP1 without centrioles
AS+3MBPP1 with centrioles
AS+DMSO
WT/Δ+3MBPP1
E
Doxorubicin
Relative Proliferation
Concentration (nM)
AS+3MBPP1
AS+DMSO
WT/Δ+3MBPP1
F
Hydroxyurea
Relative Proliferation
Concentration (mM)
AS+3MBPP1
AS+DMSO
WT/Δ+3MBPP1

Figure B-3. P53 does not localize to the centrosome.

RPE, MCF10A, HCT116, and HeLa cells were probed for p53 (red), pericentrin (green), and centrin (white). At least 100 cells were examined per cell line, both before and after treatment with doxorubicin (40 nM for 5 hours) and nocodazole (0.7 μM for 16 hours to arrest cells in mitosis). Immunofluorescence was performed with 4 different p53 antibodies (Cell Signaling 9282, Cell Signaling 2527, Santa Cruz DO-1/SC126, DSHB PCRP-TP53-1F7). Representative images of the 4 cell lines are shown stained with (A) Cell Signaling 2527 or (B) DSHB PCRP-TP53-1F7. We probed for p53 (red), pericentrin (green), and counterstained with DAPI (blue). Insets show enlarged images of the centrosome(s) in each cell. Scale bars = 5 μm.

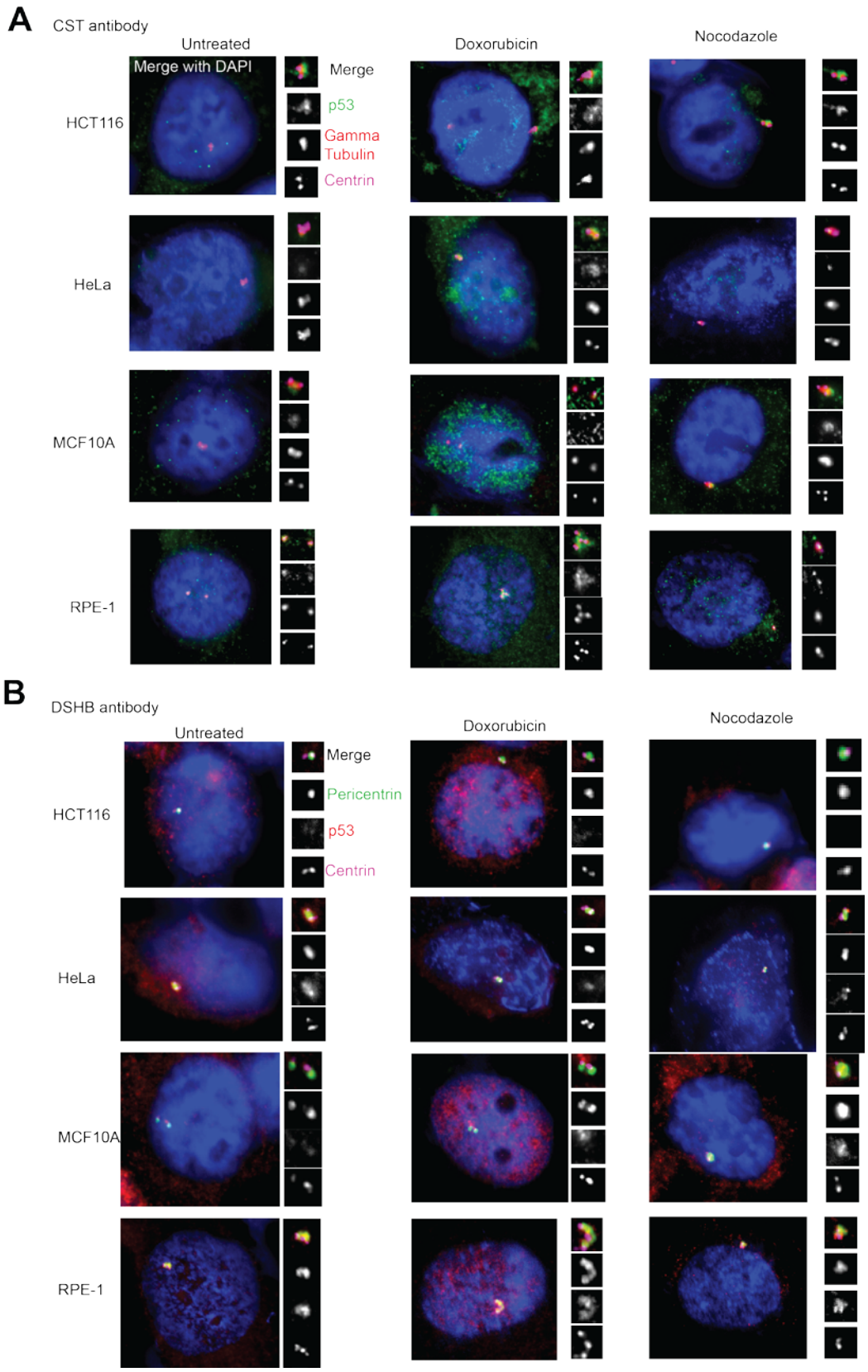
A
CST antibody
Untreated
Doxorubicin
Nocodazole
Merge with DAPI
Merge
p53
Gamma Tubulin
Centrin
HCT116
HeLa
MCF10A
RPE-1
B
DSHB antibody
Untreated
Doxorubicin
Nocodazole
Merge
Pericentrin
p53
Centrin
HCT116
HeLa
MCF10A
RPE-1

Figure B-4. P53 does not localize to the centrosome in mitosis.

The same cell lines and staining protocols were followed as in Supplemental Figure 2. Representative images of interphase and mitotic HCT116 cells are shown. We probed for p53 (red; Cell Signaling 2527), pericentrin (green), and counterstained with DAPI (blue). Additional images focusing on the centrosome(s) in each cell are shown on the right. Scale bars = 5 µm.

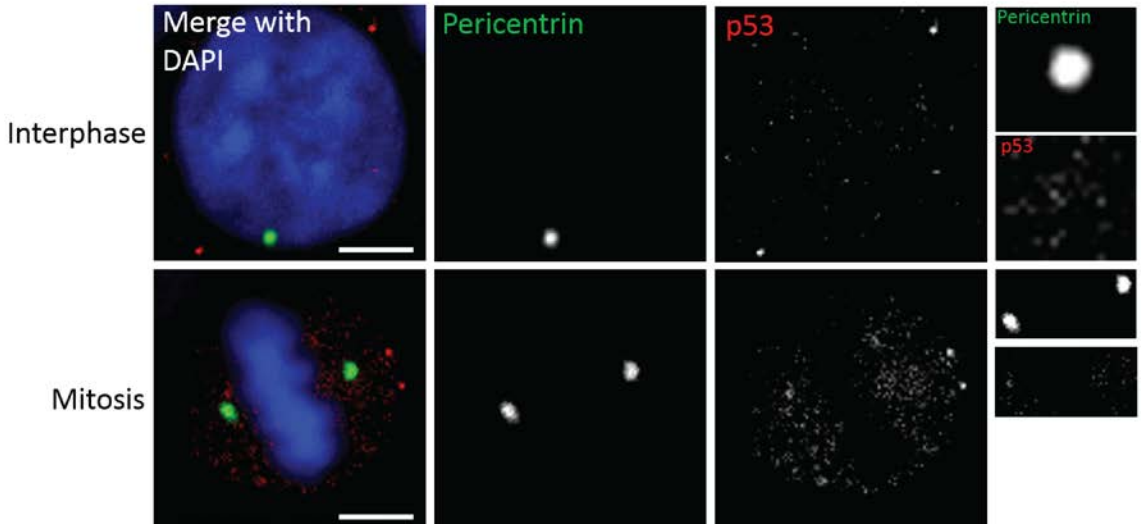

Appendix C. PLK4 phosphorylates CEP170

The following individuals contributed to the work in this Appendix:

Madilyn M. Sass, University of Wisconsin-Madison

ABSTRACT

Polo-like kinase 4 (PLK4) is the master regulator of centriole duplication in human cancer. However, recent evidence suggests that PLK4 may have other functions, including organization of centriolar satellites, actin organization, and regulation of migration. Interestingly, even though centriole duplication occurs in early S phase, PLK4 levels and activity reach their peak in mitosis, yet a role for PLK4 in mitosis has not been described. Herein, we perform a screen of potential PLK4 substrates identified in a previous phosphoproteomic experiment. We identify CEP170 as a substrate of PLK4 and map the phosphosites to S1436 and S1441. CEP170 is a subdistal centriole appendage protein. We generated HeLa CEP170 knockout cell lines to interrogate the functions of CEP170. We find that loss of CEP170 causes an increase in mitotic aberrations, namely lagging chromosomes and chromosome bridges in anaphase. We also observe an increase in centrosome amplification due to cytokinesis failure. Future work will assess the functional consequences of PLK4 phsophorylation of S1436 and S1441.

INTRODUCTION

The centrosome is the major microtubule organizing center in animal cells and consists of two orthogonally oriented centrioles surrounded by a structured protein matrix called the pericentriolar material (PCM) [37]. Centriole number is tightly controlled in human cells, and disruptions in centriole duplication can have several consequences, including mitotic errors and disrupted cilia formation and signaling [37,61]. Centriole duplication is regulated by Polo-like kinase 4 (PLK4) [62,63]. In late G1 and early S phase, CEP152 and CEP192 recruit PLK4 to the proximal end of the parent centriole. PLK4 then recruits and phosphorylates STIL, which allows SAS6 recruitment.[64] The nine-fold symmetry of centrioles is conferred by nine homodimers of SAS6.[14,15,65] PLK4 exists as a homodimer and engages in trans-autophosphorylation, causing SCF-βTrCP-mediated ubiquitination and subsequent degradation. The nascent centrioles then elongate, which is dependent on CPAP and limited by CP110,[76] and more PCM proteins are recruited as the cell nears M phase, which is dependent on PLK1[78,79] and Aurora A.[80] At the end of M phase, separase cleaves pericentrin to allow for centriole disengagement [83], and the cartwheel is removed from the procentriole, a process dependent on CDK1;[84] these events relieve the block to reduplication of the parental centriole. The procentrioles also depends on PLK1 and CDK1 to become competent for centriole duplication.[85,86]

Mature centriole markers, such as distal and subdistal appendage proteins, are loaded onto the mother centriole in late G2 and/or M phases, and this process is controlled by PLK1.[490] One such subdistal appendage protein is CEP170, a forkhead-associated domain protein.[177] We previously identified CEP170 as a potential substrate of PLK4. CEP170 is on chromosome 1 [491] and was originally identified in a yeast-two-hybrid screen of PLK1 interactors, and it is indeed a PLK1 substrate.[492] In addition to its mother centriole localization, during mitosis CEP170 also

localizes to spindle microtubules, and in early telophase, strong CEP170 staining is observed at astral microtubules.[177,493] In late telophase, CEP170 reassociates with centrosomes.[177] The C-terminal half of CEP170 is sufficient to confer localization to both centrosomes and microtubules, and specifically amino acids 1015–1460 are sufficient for centrosome localization. CEP170 associates with the microtubule depolymerase Kif2b,[494] Interestingly, western blotting using extracts from G1/S or M phase-arrested HeLa cells revealed little difference in abundance of CEP170 throughout the cell cycle but a striking change in mobility in M phase, suggesting a mitosis-specific posttranslational modification. In addition to phosphorylation by PLK1, CEP170 is phosphorylated by Tank binding kinase 1 (TBK1).[495] TBK1 phosphorylates 12 serine residues and a threonine residue (S767, S768, S783, T793, S832, S835, S841, S844, S1025, S1144, S1238, S1436, S1441 of Uniprot isoform 2) of CEP170 and is necessary for CEP170 centrosomal localization and binding to the microtubule depolymerase Kif2b.[495] Finally, selective disruption of the TBK1-CEP170 complex augments microtubule stability and triggers defects in mitosis, implicating TBK1 phosphorylation of CEP170 in microtubule dynamics and mitosis.[495]

Although centriole duplication occurs in early S phase, PLK4 levels actually do not reach their peak until anaphase. However, a role of PLK4 in mitosis has not been described. Herein, we screen additional potential PLK4 substrates revealed by a previous phosphoproteomic screen and identify CEP170 as a novel substrate of PLK4.

MATERIALS AND METHODS

Cell Culture

All cell lines were propagated at 37 °C in 5% CO_2. RPE-1-derived cell lines were grown in a 1:1 mixture of DMEM and Ham's F-12 medium supplemented with 2.5 mm l-glutamine, with 10% fetal bovine serum and 100 units/mL penicillin-streptomycin. HeLa cell lines (ATCC) were grown in high glucose DMEM supplemented with 2.5 mm l-glutamine, with 10% fetal bovine serum and 100 units/mL penicillin-streptomycin. For stable retroviral transduction, constructs were co-transfected with a VSV-G envelope plasmid into Phoenix cells. Fresh medium was applied at 24 hours post-transfection, harvested 24 hours later, clarified by centrifugation and filtration through a 0.45 μm membrane to remove cell debris, and diluted 1:1 with complete medium containing 10 μg/mL polybrene. Target cells were infected at 40-60% confluence for 24 hours. Polyclonal transductants were further purified by limiting dilution to obtain individual clones.

Chemicals used in this study include centrinone B (Tocris), cytochalasin D (Thermo Fisher), doxycycline (Thermo Fisher), and puromycin (Thermo Fisher).

Immunofluorescence

IF and imaging were carried out as previously described [194,195]. Cells were seeded on glass coverslips in 24-well plates and fixed with 100% ice-cold methanol for 15 minutes. Fixed cells were then blocked for 30 minutes in 3% bovine serum albumin (BSA) and 0.1% triton X-100 in PBS (PBSTx + BSA). Primary antibodies were incubated in PBSTx + BSA for 1 hour at room temperature and washed three times in PBSTx, followed by secondary antibody incubation in PBSTx + BSA for 30 minutes at room temperature and two washes with PBSTx. Cells were

counterstained with DAPI and mounted on glass slides with Prolong Gold antifade medium (Invitrogen).

Primary antibodies used were: CEP170 (Life Technologies, 41-3200), pericentrin (Abcam, ab4448), α-tubulin (Abcam, ab4074), pericentrin (Abcam, ab4448), centrin (Millipore, 04-1624), and γ-tubulin (Abcam, ab27074). Alexa Fluor-conjugated secondary antibodies were used at 1:350 (Invitrogen).

Molecular Biology

The pEGFP-CEP170 vector was obtained from Addgene (kind gift of Erich Nigg, Addgene #41150). This cDNA corresponds to Uniprot isoform 2 (identifier Q5SW79-2). Site-directed mutagenesis was performed using Phusion polymerase (Thermo Fisher). The cDNAs for PLK4 substrates of interest were cloned into pGEX-6P-1 vector (GE Healthcare).

Kinase Assays

The PLK4 kinase domain (amino acids 1–390) of human PLK4 was cloned into pGEX-6P-1 vector (GE Healthcare). 15-amino acid fragments of the identified potential PLK4 substrates (putative phosphosite ±7 amino acids) were also cloned into pGEX-6P-1. Sequences of these peptides can be found in Supplemental Table 2. Protein was expressed in Rosetta DE3 bacteria, extracted with Glutathione Sepharose 4B (GE Healthcare, 17-0756-01), and eluted by addition of glutathione for the production of the intact GST fusion proteins.

All kinase assay reactions were incubated at 30°C for 30 minutes in buffer (50mM Tris-HCl, pH 7.5, 10mM $MgCl_2$, 0.1mM NaF, 10μM Na_3VO_4) with 1mM DTT, 1μM cold ATP, 2μCi [γ-^{32}P] ATP, 5μg substrate, and 100ng PLK4. Reactions were resolved by SDS-PAGE. Dried

gels were exposed to a storage phosphor screen (GE Healthcare), and γ-^{32}P incorporation was visualized by Typhoon TRIO imager (GE Healthcare).

To confirm that which potential phosphosites were substrates of PLK4, serines and threonines were mutated to alanines and valines, respectively, using Phusion site-directed mutagenesis, purified, and utilized in kinase assays, as described above. Silent mutations were made to either introduce or remove restriction sites to facilitate screening for successful clones.

CRISPR Gene Editing

The CRISPR/Cas9 system was used to create CEP170 knockout cell lines in HeLa cells. Three gRNAs targeting CEP170 were cloned into lentiCRISPRv2 [431,432], which was a gift from Feng Zhang (Addgene plasmid #52961). The three guides used were: ATGCCCTGCACCTGTTATAT, TGATGACAGTACCCCAGGGA, CATAGATGCCAAGCAAGTTG. Cutting efficiency of each guide was assessed by surveyor assay (IDT, 706025) after nested PCR amplification of 1000bp fragments and subsequent PCR amplification of 500bp fragments from these 1000bp fragments using the following primers: 1000F, CGACTTGAGAAGGGAGTTCATGG; 1000R, GGACATGGGCAGTGTAGCTTCC;; 500F, CGGAGTAGTACACATGGCCATTAC; 500R, CCCATAGCATTTGAGGAGGGT.

Statistical Analyses

Statistical evaluations were performed using Graphpad Prism (Graphpad Software, San Diego, CA) or Microsoft Excel (Office 2011, Microsoft). Two-tailed t-tests and one-way ANOVA were used for comparisons. P-values <0.05 were considered significant for all tests, and designations are made in the figures for statistical significance.

RESULTS

We previously reported a phosphoproteomic screen in which we utilized a PLK4 analog sensitive cell line in RPE1, an immortalized, non-transformed human cell line. We screened an additional set of potential substrates in which we observed many potential phosphosites distributed along the length of the proteins. Protein fragments covering the whole length of the following proteins were purified: CAMSAP2, CEP170, CEP41, NUMA1, POC5, SPICE1, and TP53BP1. We observed phosphorylation of CEP170, NUMA1 and TP53BP1 (Supplemental Figure C-1). It is unclear whether TP53BP1 even localizes to the centrosome, and the NUMA1 fragment identified to contain the phosphosite(s) contains a plethora of serines and threonines; for these reasons, we focused on CEP170. We observed that PLK4 phosphorylates the C terminus of CEP170, corresponding to amino acids 1110-1584 (Figure C-1A-B). We further fragmented this C-terminal quarter of CEP170 and identified amino acids 1366-1460 as the fragment containing the phosphosite(s) of interest (Figure C-1C).

We examined this C-terminal fragment for serines and threonines that might be phosphorylated by PLK4 (Figure C-1D). We examined which serines and threonines are conserved across mammals, which fit the consensus phosphorylation site of PLK4 (S/T followed by 2 large hydrophobic residues),[496] and which are identified on Phosphosite Plus. None of the potential serines and threonines fit all these criteria, so we broadened our criteria. We first purified fragments containing mutations in each of the 6 sites identified on Phosphosite Plus. This demonstrated that S1436 is a substrate of PLK4, but that other phosphosites likely exist (Figure C-1E). We then separately mutated all the additional serines and threonines in combination with the S1436A mutant and compared to a protein fragment containing all 12

serines and threonines to alanines and valines, respectively (labeled 12AV). This demonstrated that S1436 and S1441 are the substrates of PLK4 (Figure C-1F).

CEP170 knockout causes chromosomal instability

To examine the role of these phosphorylation events by PLK4, we engineered CEP170 knockout cell lines and planned to re-introduce wild type, non-phosphorylatable, and phosphor-mimetic CEP170 transgenes. CEP170 is not a lethal gene,[423], and we were able to recover knockout clones (Figure C-2). We engineered both HeLa and RPE knockout cells. We confirmed knockout by immunofluorescent staining for CEP170 (Figure C-2A), western blotting for CEP170 (Figure C-2B), and sequencing (Supplemental Figure C-2). Our two knockout lines are henceforth denoted KO1 and KO2.

We then examined the phenotypes of these CEP170 knockout lines. We first examined centrosome amplification in these cells by centrin staining. The CEP170 knockout cells demonstrate a significant increase in the percent of cells with centrosome amplification, as defined by greater than 4 centrioles (centrin foci). Centrosome amplification can occur by 2 major mechanisms: centriole overduplication or cell doubling (e.g. cytokinesis failure or cell-cell fusion). To determine the predominant cause of centrosome amplification in the CEP170 knockouts, we examined the percentage of centrioles co-staining with the mother/mature centriole marker CEP164, which is loaded onto the mother centriole in late G2 and is not affected by CEP170 depletion.[240] In cells with centrosome amplification due to centriole overduplication, fewer centrioles will co-stain with mother centriole markers. In contrast, cell doubling events are expected to yield a higher percentage of centrioles co-staining with the mother centriole, as has been demonstrated previously.[177,208,240] We find that the knockouts with

CA demonstrate an increased percentage of centrioles with CEP164 compared to wild type cells with centrosome amplification, suggesting that cell doubling events may explain the majority of centrosome amplification seen in the CEP170 knockouts. Further evidence is provided by the increase in average cell size (Figure C-2G) and the increase in multinucleated cells (Figure C-2H). In addition, we also found that CEP170 knockout cell lines demonstrated more micronuclei (Figure C-2H).

We next assessed mitotic fidelity by examining cells in metaphase and anaphase. Interestingly, the CEP170 knockouts demonstrated an increase in multipolar metaphases and lagging chromosomes or chromosome bridges in anaphase (Figure C-3). We conclude that CEP170 is required for mitotic fidelity.

As centrosome amplification is common in human cancer,[107,109,208] we analyzed potential genomic alterations in CEP170 in human cancer using TCGA data sets. The most common alterations observed are gene amplifications. We hypothesize that loss of CEP170 would be detrimental to the cancer cell by generating too much CIN, which has been shown to inhibit tumor initiation and progression.[322,323,497] In the METABRIC breast cancer database and TCGA breast database, 20-25% of breast cancers demonstrated CEP170 gene amplifications. However, patients with these amplifications did not demonstrate any significant differences in disease free survival or overall survival.

DISCUSSION

Accumulating evidence suggests that PLK4 may have roles outside of centriole duplication. PLK4 levels increase to their maximum in mitosis in Drosophila and human cells,[70] which is inconsistent with its canonical role in coordinating centriole duplication, which occurs in early S phase. Furthermore, other PLK4 substrates have been identified that have nothing to do with centriole duplication, such as phosphorylation of PCM1[103] and CEP131 (Chapter 7) to control centriolar satellite integrity. Additional evidence has found that PLK4 can localize to the distal end of the mother centriole close to the sub-distal and distal appendages,[70] which is where CEP170 localizes.

Interestingly, previous reports of CEP170 depletion demonstrated that the shape of HeLa cells changed from a typical epithelial (cobblestone) to a more fibroblastic (elongated) appearance,[177] consistent with our findings. Further, CEP170-depleted HeLa cultures did not show a change percentage of mitotic cells. In contrast, U2OS cells got bigger and less were in mitosis upon CEP170 depletion,[177] which we speculate may have been due to cytokinesis failure and subsequent cell cycle arrest. We also speculate that the difference seen between these two cell lines may involve the p53 status of these cell lines. We know HeLa cells have lost p53 (by virtue of the HPV E6 protein), but U2OS are p53 competent. Cytokinesis failure is known to cause a p53-mediated arrest via the Hippo pathway.[141]

Future work will assess the functional consequences of PLK4 phosphorylation of CEP170. We will test the following hypotheses about these phosphorylation events: (1) centriole amplification; (2) ciliogenesis; (3) mitotic fidelity; (4) Kif2b recruitment to the spindle; (5) microtubule polymerization and organization in both interphase and mitosis.

Figure C-1. PLK4 phosphorylates CEP170 S1436 and S1441.

(A) Kinase assays using purified GST-tagged proteins. STIL is a known substrate of PLK4 and was used as a positive control. Four fragments covering the whole length of PLK4 were purified and tested. **(B)** Diagram of the known domains of CEP170 and summary of which fragment was phosphorylated. **(C)** Kinase assays in which the C-terminal fragment of CEP170 (amino acids 1010-1460) was sub-fragmented into 5 smaller fragments. **(D)** Amino acids 1366-1460 were identified as containing the phosphosite of interest. The first row shows all the serines and threonines in this fragment; the second row shows the serines and threonines conserved across among *H. sapiens, M musculus, D. rerio, B. Taurus, X. tropicalis*; the third row shows the serines and threonines conserved among mammals (*H. sapiens, M musculus, B. Taurus*); the fourth row shows the serines and threonines that fit the PLK4 consensus sequence (S/T followed by 2 large hydrophobic amino acids: F, I, L, M, P, V, or W); and the fifth row shows the serines and threonines that have been documented on Phosphosite Plus. **(E)** Kinase assays in which the 6 sites found on Phosphosite Plus were mutated. **(F)** Quantification of the kinase assays in (E) by normalizing to protein expression (Coomassie intensity). **(G)** After identifying S1436 as a substrate of PLK4, we mutated the additional sites that were not mutated in (E) in the S1436A mutant. **(H)** Quantification of the kinase assays in (G) by normalizing to protein expression (Coomassie intensity). CBB = Coomassie brilliant blue.

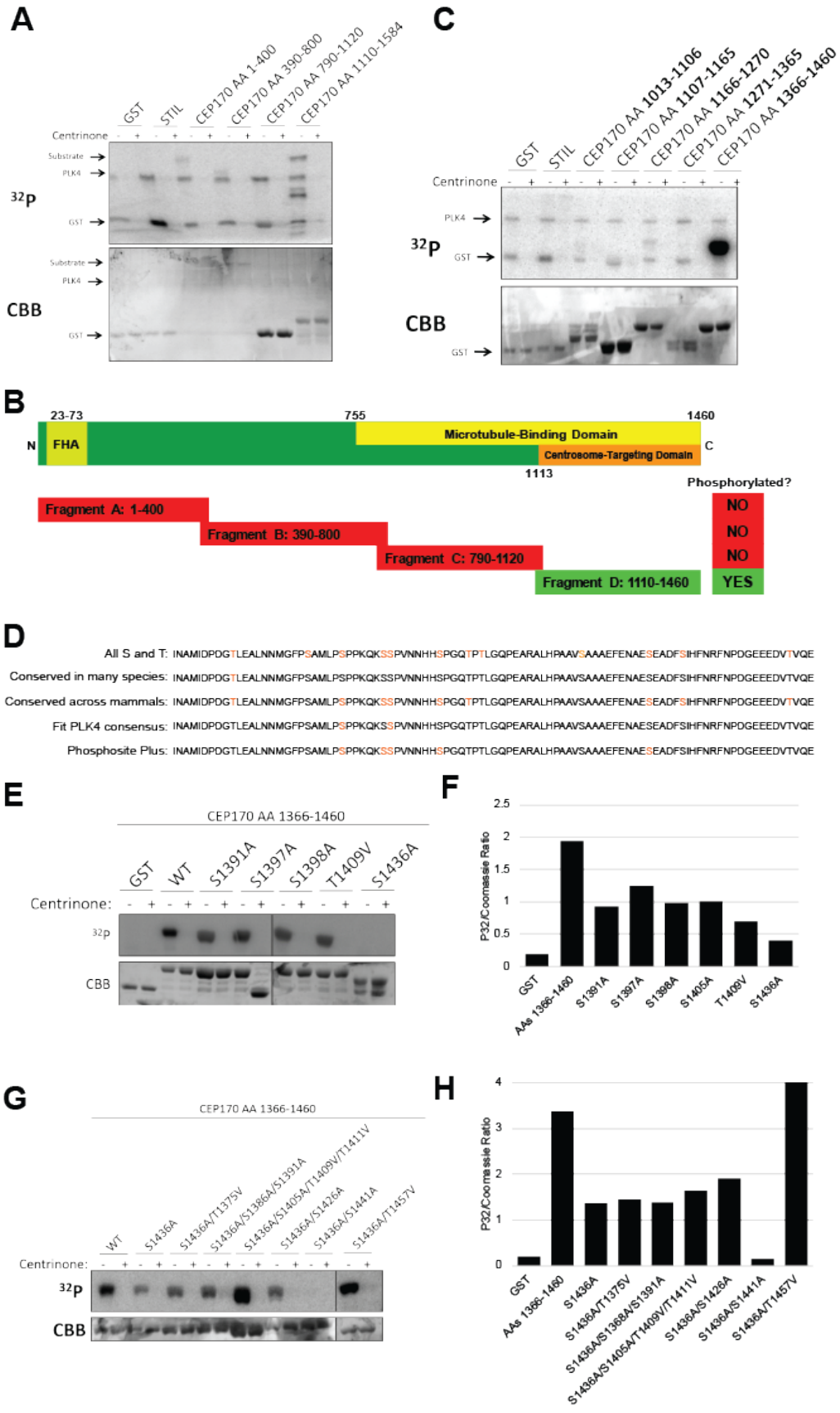
A
GST
STIL
CEP170 AA 1-400
CEP170 AA 390-800
CEP170 AA 790-1120
CEP170 AA 1110-1584
Centrinone
Substrate
PLK4
32P
GST
CBB
C
CEP170 AA 1013-1106
CEP170 AA 1107-1165
CEP170 AA 1166-1270
CEP170 AA 1271-1365
CEP170 AA 1366-1460
B
23-73
755
1460
N
FHA
Microtubule-Binding Domain
Centrosome-Targeting Domain
C
1113
Phosphorylated?
Fragment A: 1-400
Fragment B: 390-800
Fragment C: 790-1120
Fragment D: 1110-1460
NO
NO
NO
YES
D
All S and T: INAMIDPDGTLEALNNMGFPSAMLPSPPKQKSSPVNNHHSPGQTPTLGQPEARALHPAAVSAAAEFENAESEADFSIHFNRFNPDGEEEDVTVQE
Conserved in many species: INAMIDPDGTLEALNNMGFPSAMLPSPPKQKSSPVNNHHSPGQTPTLGQPEARALHPAAVSAAAEFENAESEADFSIHFNRFNPDGEEEDVTVQE
Conserved across mammals: INAMIDPDGTLEALNNMGFPSAMLPSPPKQKSSPVNNHHSPGQTPTLGQPEARALHPAAVSAAAEFENAESEADFSIHFNRFNPDGEEEDVTVQE
Fit PLK4 consensus: INAMIDPDGTLEALNNMGFPSAMLPSPPKQKSSPVNNHHSPGQTPTLGQPEARALHPAAVSAAAEFENAESEADFSIHFNRFNPDGEEEDVTVQE
Phosphosite Plus: INAMIDPDGTLEALNNMGFPSAMLPSPPKQKSSPVNNHHSPGQTPTLGQPEARALHPAAVSAAAEFENAESEADFSIHFNRFNPDGEEEDVTVQE
E
CEP170 AA 1366-1460
GST
WT
S1391A
S1397A
S1398A
T1409V
S1436A
Centrinone:
32p
CBB
F
P32/Coomassie Ratio
2.5
2
1.5
1
0.5
0
GST
AAs 1366-1460
S1391A
S1397A
S1398A
S1405A
T1409V
S1436A
G
CEP170 AA 1366-1460
WT
S1436A
S1436A/T1375V
S1436A/S1386A/S1391A
S1436A/S1405A/T1409V/T1411V
S1436A/S1426A
S1436A/S1441A
S1436A/T1457V
Centrinone:
32P
CBB
H
P32/Coomassie Ratio
4
3
2
1
0
GST
AAs 1366-1460
S1436A
S1436A/T1375V
S1436A/S1386A/S1391A
S1436A/S1405A/T1409V/T1411V
S1436A/S1426A
S1436A/S1441A
S1436A/T1457V

Figure C-2. Description of HeLa CEP170 knockout cell lines.

(A) Representative micrographs of WT and knockout (KO1 and KO2) HeLa cell lines. Insets are enlarged to better view the centrosome. **(B)** Western blotting for CEP170 with actin loading control. **(C)** Representative images of centrioles with CEP164 staining for mature/mother centrioles. If centriole overduplication is the predominant mechanism leading to centrosome amplification, then a lower percentage of CEP164+ centrioles is expected. Conversely, if cell doubling (e.g. cytokinesis failure) is predominant, then a higher percentage of CEP164+ centrioles is expected. Cytokinesis failure induced by cytochalasin D was used to model cell doubling, and PLK4 overexpression was used to model centriole overduplication. **(D)** Quantification of centrioles in each cell. Dots represent individual cells and bars represent means ±SD. **(E)** Quantification of the percent of cells with centrosome amplification, defined as greater than 4 centrioles. Dots represent different experiments and bars represent means ±SEM. **(F)** Quantification of the percentage of centrioles staining positive for CEP164. **(G)** Average cell diameter. **(H)** Representative histograms of propidium iodide flow cytometry to assess DNA content. The percentage of diploid (~2N) and tetraploid (~4N) cells is displayed. **(I)** Assessment of cell proliferation by cell counts. **(J)** Representative image of a CEP170 knockout cell that is multinucleated and has a micronucleus. **(K)** Quantification of the percentage of cells with multiple nuclei or micronuclei. Scale bars = 10μm.

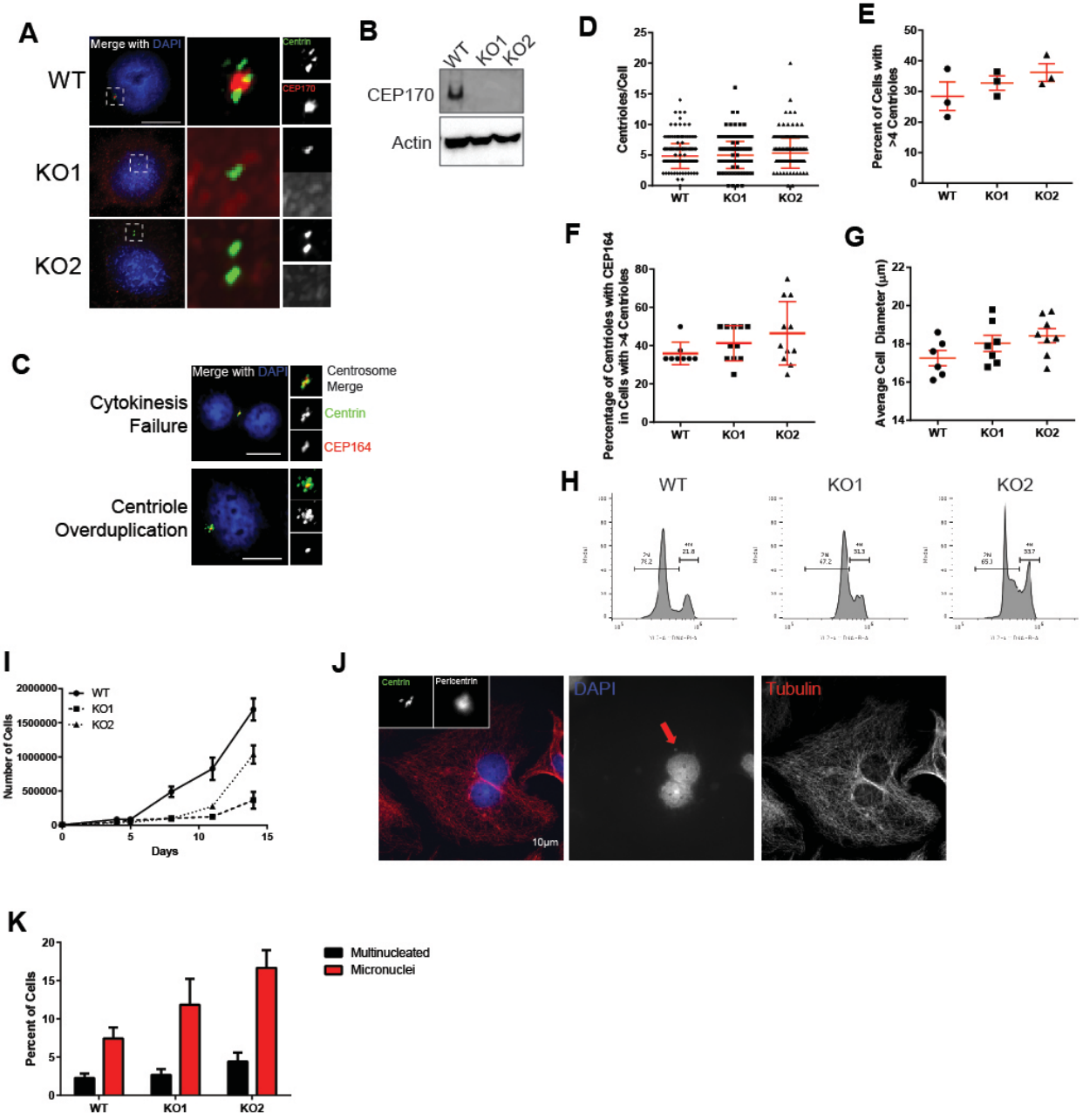
A
Merge with DAPI
Centrin
CEP170
WT
KO1
KO2
B
WT
KO1
KO2
CEP170
Actin
C
Merge with DAPI
Centrosome
Merge
Centrin
CEP164
Cytokinesis
Failure
Centriole
Overduplication
D
Centrioles/Cell
WT
KO1
KO2
E
Percent of Cells with
>4 Centrioles
F
Percentage of Centrioles with CEP164
in Cells with >4 Centrioles
G
Average Cell Diameter (µm)
H
WT
KO1
KO2
I
Number of Cells
Days
WT
KO1
KO2
J
Centrin
Pericentrin
DAPI
Tubulin
10µm
K
Percent of Cells
Multinucleated
Micronuclei

Figure C-3. CEP170 deletion causes chromosomal instability.

(A) Representative micrographs of the phenotypes in metaphase and anaphase cells that were assessed. **(B)** Quantification of metaphase cells. **(C)** Quantification of anaphase cells.

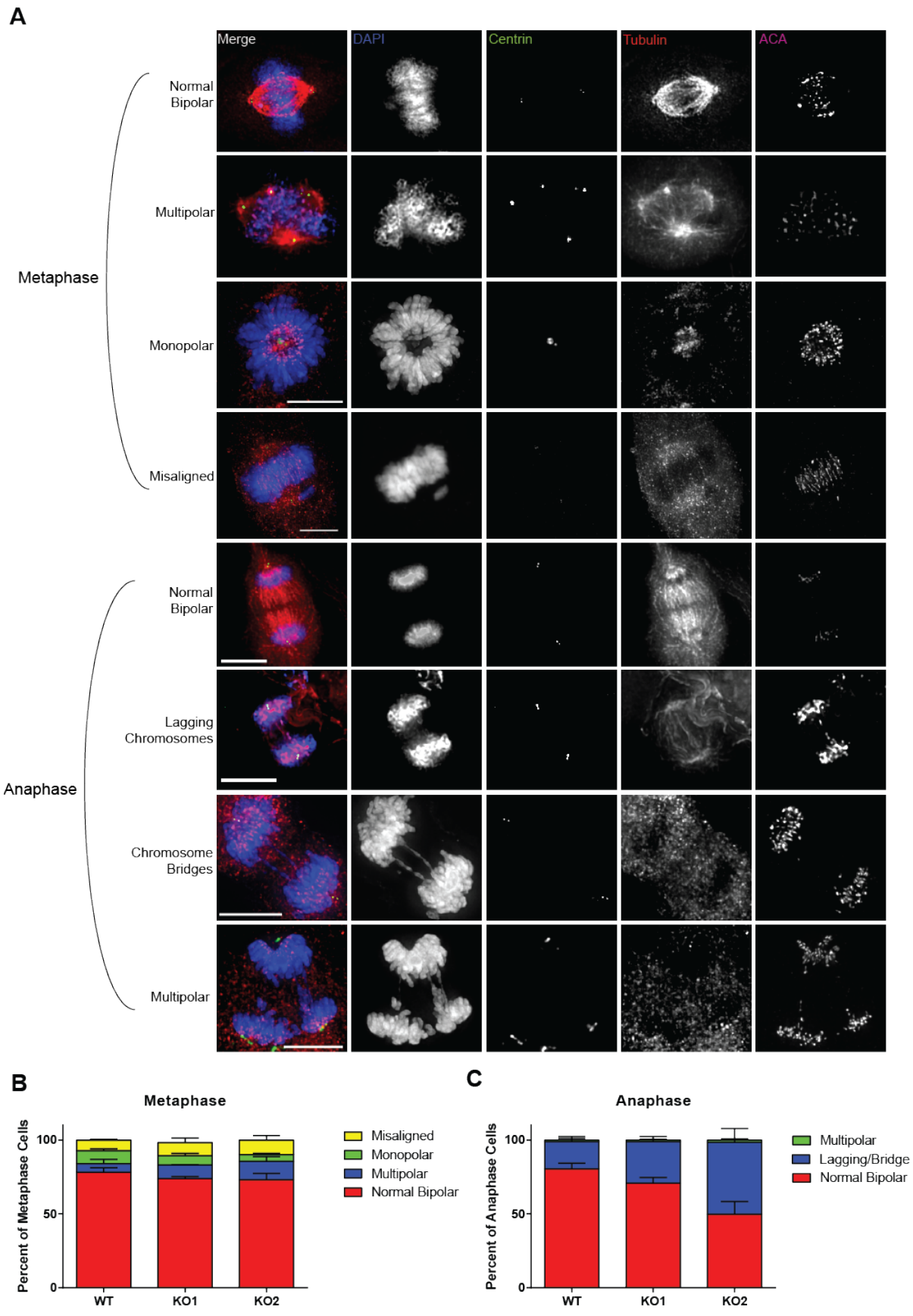
A
Merge
DAPI
Centrin
Tubulin
ACA
Metaphase
Normal Bipolar
Multipolar
Monopolar
Misaligned
Anaphase
Normal Bipolar
Lagging Chromosomes
Chromosome Bridges
Multipolar
B
Metaphase
Percent of Metaphase Cells
100
50
0
WT
KO1
KO2
Misaligned
Monopolar
Multipolar
Normal Bipolar
C
Anaphase
Percent of Anaphase Cells
100
50
0
WT
KO1
KO2
Multipolar
Lagging/Bridge
Normal Bipolar

Supplemental Figure C-1. Screening for potential substrates of PLK4.

The following substrates/peptides were purified and screened by kinase assay: NUMA1, CAMSAP2, SPICE1, TP53BP1, POC5, and CEP41. AA = amino acids; CBB = Coomassie brilliant blue. Centrinone is an inhibitor of PLK4.

NUMA1

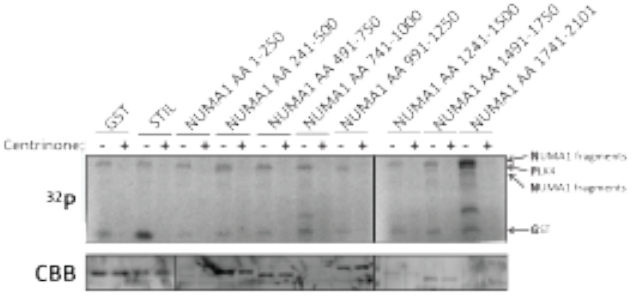

CAMSAP2

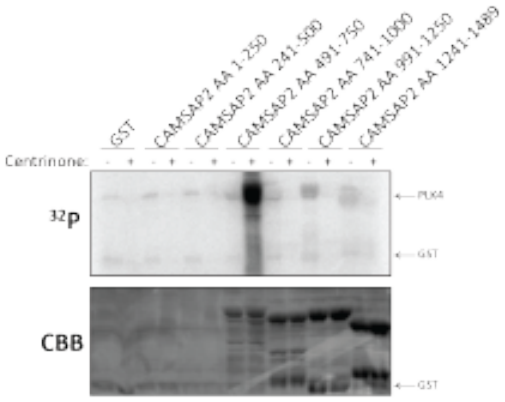

SPICE1

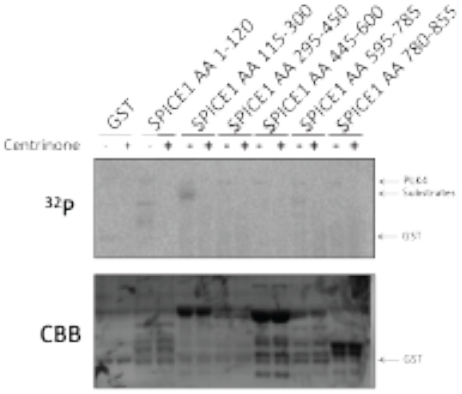

TP53BP1

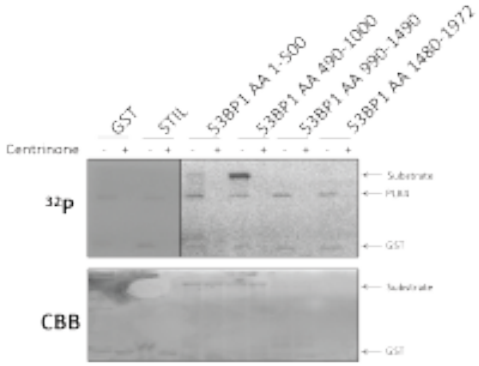

POC5 and CEP41

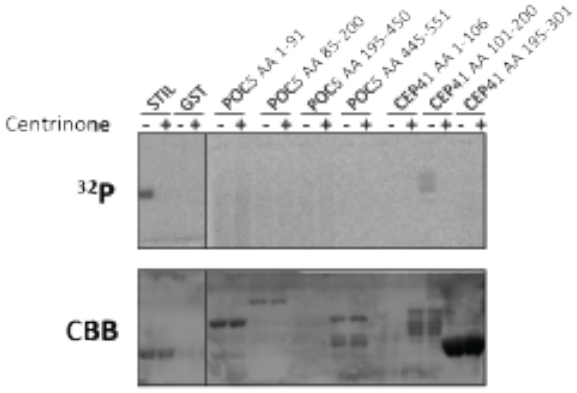

Supplemental Figure C-2. Sequencing of CEP170 knockout lines.

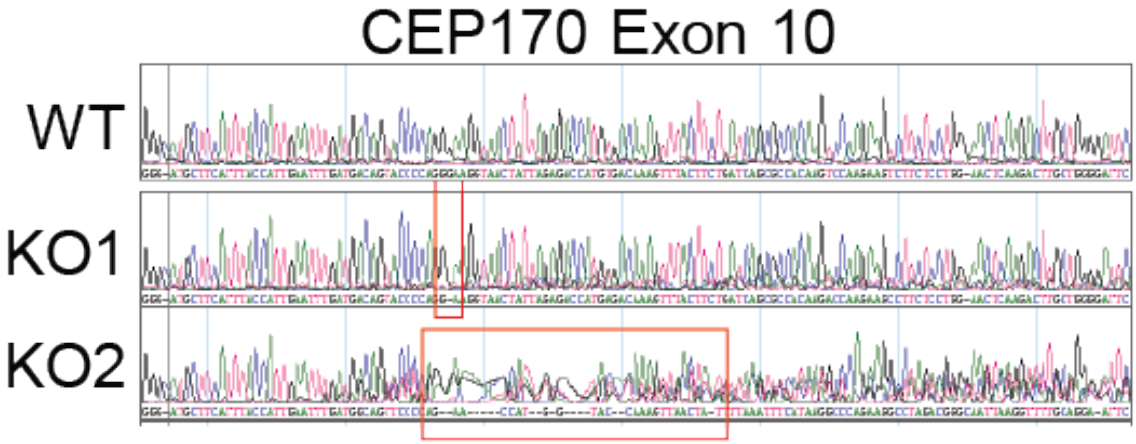

Supplemental Figure C-3. CEP170 is required for ciliation.

(A) Representative images of ciliated and non-ciliated cells. Blue = DNA, green = pericentrin, red = acetylated tubulin (to mark cilia). **(B)** Quantification of the percent of cells with a primary cilium. Each dot represents an individual experiment of at least 300 cells. Bars represent means ±SD.

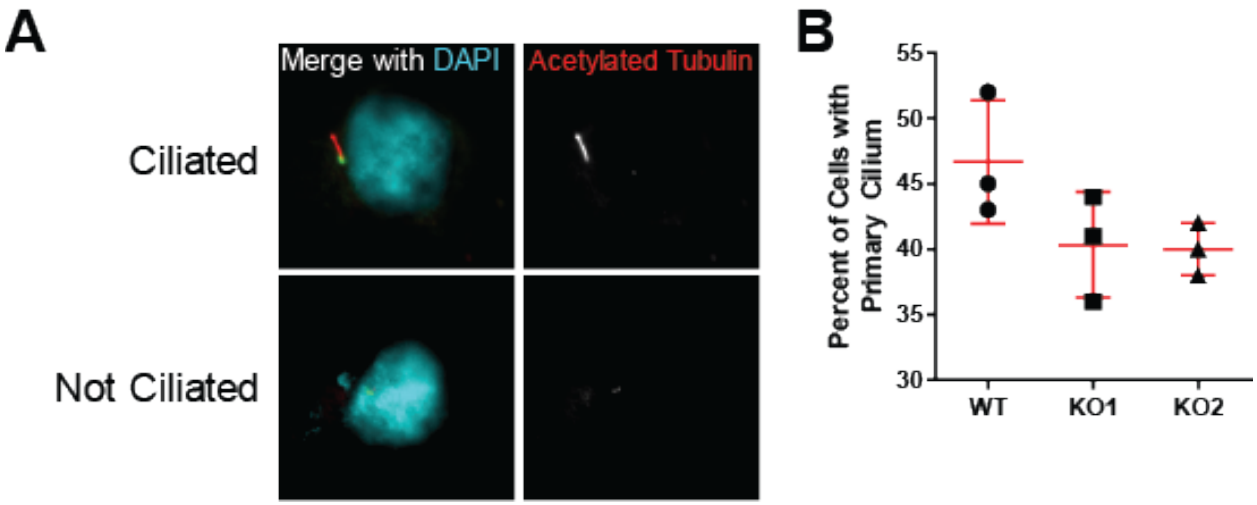

Supplemental Figure C-4. CEP170 gene amplifications in human cancer.

(A) Diagram of the alteration frequencies of mutations (green), gene amplifications (red), gene deletions (blue), or multiple alterations (gray) in CEP170 in TCGA cancer datasets. Data were queried with cBioPortal. **(B)** Kaplan Meier curves demonstrating overall survival (OS) in CEP170 amplified versus non-amplified tumors in the METABRIC dataset. (C) OS in tumors with high versus low mRNA expression in the METABRIC dataset. **(D)** OS in CEP170 amplified versus non-amplified tumors in the breast TCGA dataset. **(E)** OS in breast tumors with high versus low mRNA expression in the breast TCGA dataset. **(F)** DFS in CEP170 amplified versus non-amplified tumors in the breast TCGA dataset. **(G)** DFS in breast tumors with high versus low mRNA expression in the breast TCGA dataset. **(H-K)** Comparison of histologic subtype of breast cancer **(H)**, molecular subtype **(I)**, stage **(J)**, and grade **(K)** in the METABRIC dataset. **(L-M)** Comparison of histologic subtype of breast cancer **(L)** and molecular subtype **(M)** in the breast TCGA dataset.

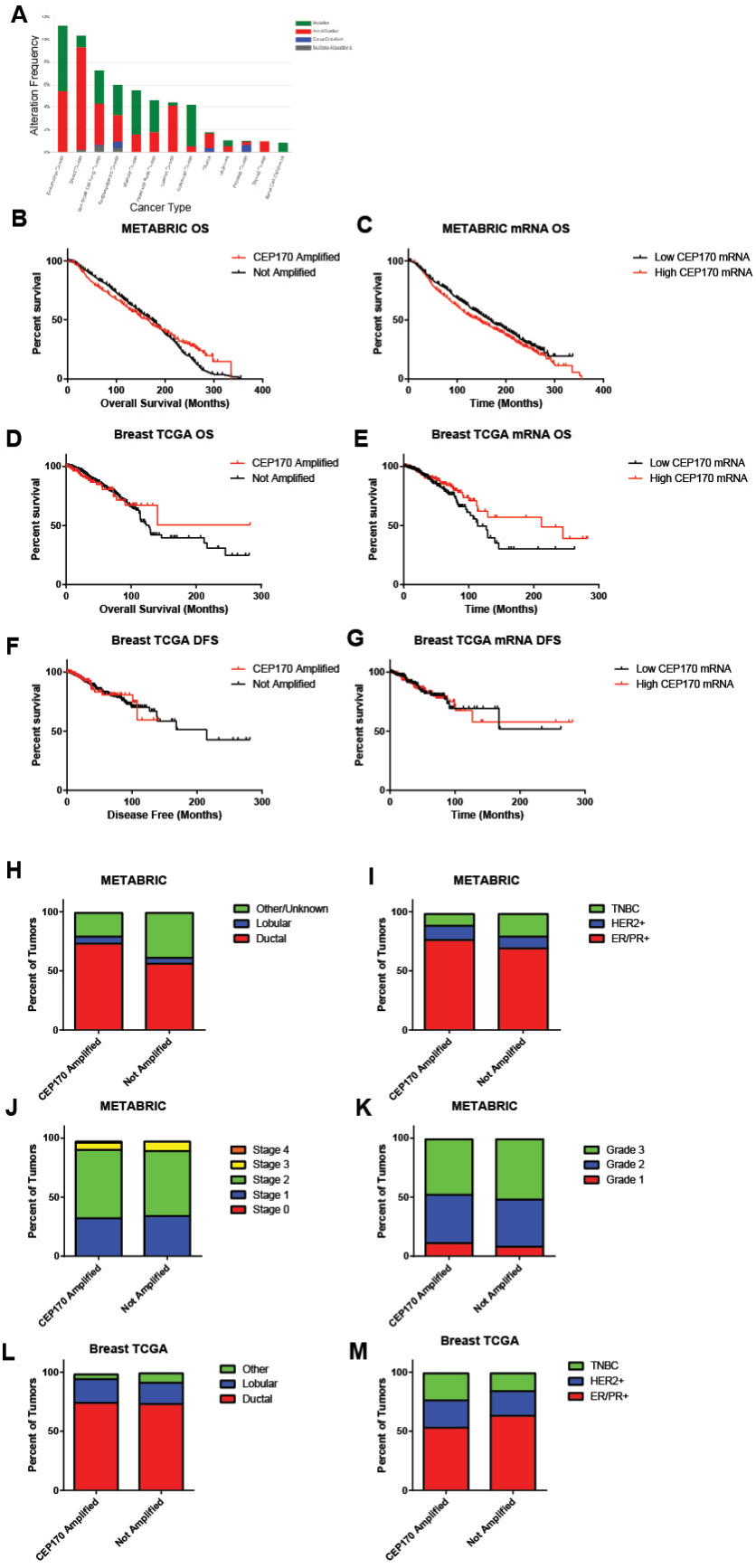
A
Alteration Frequency
Cancer Type
B
METABRIC OS
CEP170 Amplified
Not Amplified
Percent survival
Overall Survival (Months)
C
METABRIC mRNA OS
Low CEP170 mRNA
High CEP170 mRNA
Time (Months)
D
Breast TCGA OS
E
Breast TCGA mRNA OS
F
Breast TCGA DFS
Disease Free (Months)
G
Breast TCGA mRNA DFS
H
METABRIC
Other/Unknown
Lobular
Ductal
Percent of Tumors
I
TNBC
HER2+
ER/PR+
J
Stage 4
Stage 3
Stage 2
Stage 1
Stage 0
K
Grade 3
Grade 2
Grade 1
L
Breast TCGA
Other
M

Appendix D. PLK4 phosphorylates CDK5RAP2.

The following individuals contributed to the work in this Appendix:

Roshan X. Norman

McKenna S. Wenzel

ABSTRACT

Polo-like kinase 4 (PLK4) is the master regulator of centriole duplication. Many substrates of PLK4 have been identified, however the entire mechanism of PLK4-mediated centriole duplication has not been fully elucidated. Centrosome amplification (CA) is a hallmark of cancer, is prognostic of more aggressive breast cancers in humans, and is dependent on PLK4 activity; therefore, it is critical to learn more about the pathway driving centriole duplication. CDK5RAP2 (CEP215) was identified as a possible substrate of PLK4 through an unbiased phosphoproteomic experiment (Chapter 7), and it is known to play a role in centriole cohesion and regulation of centriole duplication. The goal of this project is to determine if PLK4 phosphorylates CDK5RAP2, and if so, how does that phosphorylation event impact centriole duplication. Through *in vitro* kinase assays, we determined that CDK5RAP2 is a substrate of PLK4 and mapped the phosphosite to S1368. To assess the function of this phosphorylation, we are using CRISPR gene editing to knock out CDK5RAP2 and will reintroduce S1368A non-phosphorylatable and S1368D phospho-mimetic mutants. We will test the hypothesis that PLK4 phosphorylation of CDK5RAP2 is important for separating the centrioles to license them for duplication each cell cycle.

INTRODUCTION

The centrosome is the cell's microtubule organizing center and is important for organization of the spindle fibers during mitosis. Polo-like kinase 4 (PLK4) is the principal kinase that regulates centriole duplication.[62,403] Overexpression of PLK4 leads to centriole overduplication, while inhibition or loss of PLK4 leads to centriole depletion, either of which can lead to chromosome missegregation, resulting in aneuploidy and/or chromosomal instability (Chapter 5). Several substrates of PLK4 have been elucidated (Table 7-1); however, the entire mechanism of PLK4-mediated centriole duplication has not been determined. Our goal is to learn more about how PLK4 is controlling centriole duplication, which we hope will tell us more about the development of CA in cancer cells.

To accomplish this, we previously performed an unbiased phosphoproteomic experiment using analog sensitive PLK4 cells (Chapter 7). CEP215 was chosen for further testing because it is required for centriole duplication.[498] Further, CEP215 is involved in centriole cohesion.[498] CEP215 is known to localize to the centrosome in all stages of the cell cycle, and when overexpressed assembles a subset of centrosomal proteins, such as y-tubulin, onto the centrosomes. Further, CEP215 is involved in centriole cohesion.[498] Centrioles must physically separate in order to be licensed for duplication. There is evidence that premature separation can cause early licensing and lead to centriole overduplication.[499] Since we know that CEP215 is important for centriole cohesion, we hypothesize that depletion of CEp215 would lead to early separation in licensure of centrioles. Disrupting CEP215 function is expected to increase the space between centrioles and negatively affect centriole duplication, possibly leading to centriole overduplication and improper mitosis.

We hypothesized CEP215 is phosphorylated by PLK4 and allows for centriole disengagement and licenses centrioles for duplication. Herein, we used purified proteins to perform *in vitro* kinase assays to demonstrate whether PLK4 phosphorylates CEP215 and narrow down the exact phosphosite.

METHODS

Molecular Biology

To assess whether or not CDK5RAP2 is a substrate of PLK4 we fragmented the whole length of CDK5RAP2. CDK5RAP2 cDNA was acquired from transOMIC (corresponding to Uniprot isoform 4), split into nine fragments to simplify protein purification and to help narrow down the location of the phosphorylation event. These fragments were amplified via PCR, run out on a 2% agarose gel, cut out, purified, and then utilized for Gibson assembly with the vector pGEX-6P-1 (GE Healthcare). The resulting nine plasmids were transformed into Rosetta bacteria and proteins were pulled out of the bacterial lysates with Glutathione Sepharose 4B beads (GE Healthcare). Protein expression and purification were assessed by SDS-PAGE and Coomassie staining.

After we found that fragment 7 (amino acids 1201-1400) was phosphorylated by PLK4, we further divided this fragment into 5 smaller fragments, which were similarly cloned into pGEX-6P-1 and purified from bacteria. We identified amino acids 1357-1375 to be phosphorylated by PLK4. This site contained 5 serines and theronines, all of which were mutated separately to alanines or valines, respectively. As a negative control, all 5 serines and threonines were mutated (5AV mutant).

Kinase Assays

For kinase assays, PLK4 kinase domain (amino acids 1–390) of human PLK4 was cloned into pGEX-6P-1 vector (GE Healthcare) and purified. All kinase assay reactions were incubated at 30°C for 30 minutes in buffer (50mM Tris-HCl, pH 7.5, 10mM $MgCl_2$, 0.1mM NaF, 10μM Na_3VO_4) with 1mM DTT, 1μM cold ATP, 2μCi [γ-^{32}P] ATP, 5μg substrate, and 200ng PLK4.

Centrinone B is a specific PLK4 inhibitor and was used to help us confirm that the phosphorylations we are seeing are dependent on PLK4 activity. Reactions were resolved by SDS-PAGE. Dried gels were exposed to a storage phosphor screen (GE Healthcare), and γ-^{32}P incorporation was visualized by Typhoon TRIO imager (GE Healthcare).

Mutagenesis

After identifying the phosphorylation site to be S1368, S1368A non-phosphorylatable and S1368D phosphomimetic mutants were made. Mutagenesis reactions were performed with Phusion polymerase (Thermo). PCR was performed with primers containing the mutation of interest and silent mutations to introduce restriction enzyme sites for later screening. Next, Dpn1 digestion was performed to digest any methylated and therefore presumably non-mutated plasmid. The DNA was cleaned up and transformed into DH10B bacteria. Clones were screened by restriction enzyme digest.

RESULTS

We previously identified CDK5RAP2 in an unbiased phosphoproteomic experiment of PLK4 substrates (Chapter 7). To test whether CDK5RAP2 is phosphorylated by PLK4 in vitro, we fragmented CDK5RAP2 into 9 fragments, purified from bacteria, and tested by in vitro kinase assay. We identified amino acids 1201-1400 to be phosphorylated by PLK4 (Figure D-1A). To further narrow down the phosphosite, we sub-fragmented this fragment into 5 sub-fragments. We identified amino acids 1357-1375 to be phosphorylated by PLK4 (Figure D-1B). Amino acids 1357-1375 contain 5 serines and threonines. Each of these was mutated (serines to alanines and threonines to valines). A protein containing all 5 mutations (5AV) was used as a negative control. We identified S1386 to be the phosphosite (Figure D-1C-D).

DISCUSSION

Herein, we have identified CDK5RAP2 S1386 to be phosphorylated by PLK4. Future work will elucidate the potential function of this phosphorylation event. We will test the hypothesis that PLK4 phosphorylation of CDK5RAP2 is important for disrupting centriole cohesion and licensing centrioles for duplication. To test this hypothesis, we will use CRISPR/Cas9 to generate CDK5RAP2 knockout cell lines. Then we will add back wild type CDK5RAP2, non-phosphorylatable CDK5RAP2 (S1368A), and phospho-mimetic CDK5RAP2 (S1386D). These conditions will be assessed for centriole number and distance between centrioles.

Figure D-1. PLK4 phosphorylates CDK5RAP2 S1386.

(A) Kinase assay testing 9 fragments representing the entire length of CDK5RAP2. GST was used as a negative control, and STIL (amino acids 1102-1114; S1108 is a previously reported substrate) was used as a positive control. **(B)** Amino acids 1201-1400 were further fragmented into 5 sub-fragments. **(C)** The CDK5RAP2 fragment consistent of amino acids 1357-1375 contains 5 serines and threonines, each of which were mutated. This fragment was also mutated at all 5 serines and threonines (5AV) as a negative control. **(D)** Quantification of ^{32}P signal relative to protein expression (Coomassie quantification). CBB = Coomassie brilliant blue.

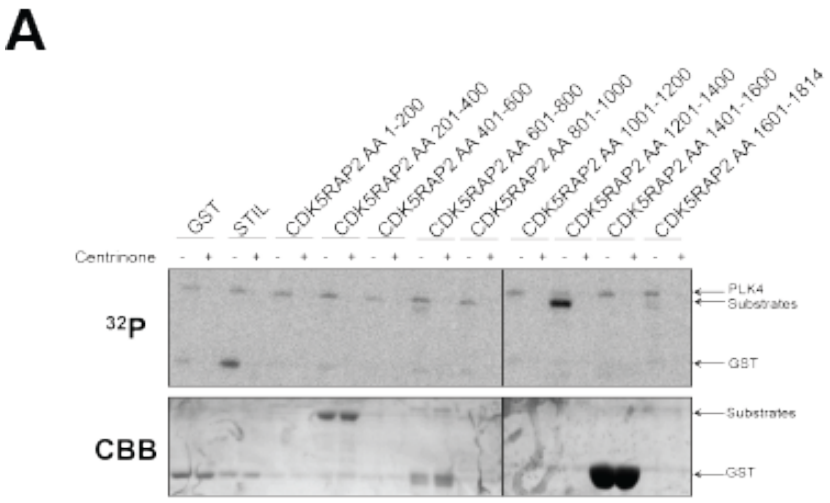
A
GST
STIL
CDK5RAP2 AA 1-200
CDK5RAP2 AA 201-400
CDK5RAP2 AA 401-600
CDK5RAP2 AA 601-800
CDK5RAP2 AA 801-1000
CDK5RAP2 AA 1001-1200
CDK5RAP2 AA 1201-1400
CDK5RAP2 AA 1401-1600
CDK5RAP2 AA 1601-1814
Centrinone
32P
PLK4
Substrates
GST
CBB
Substrates
GST

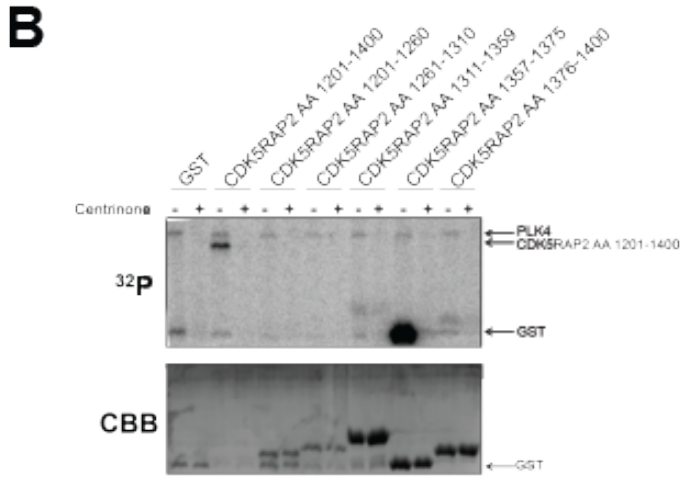
B
GST
CDK5RAP2 AA 1201-1400
CDK5RAP2 AA 1201-1260
CDK5RAP2 AA 1261-1310
CDK5RAP2 AA 1311-1359
CDK5RAP2 AA 1357-1375
CDK5RAP2 AA 1376-1400
Centrinone
32P
PLK4
CDK5RAP2 AA 1201-1400
GST
CBB
GST

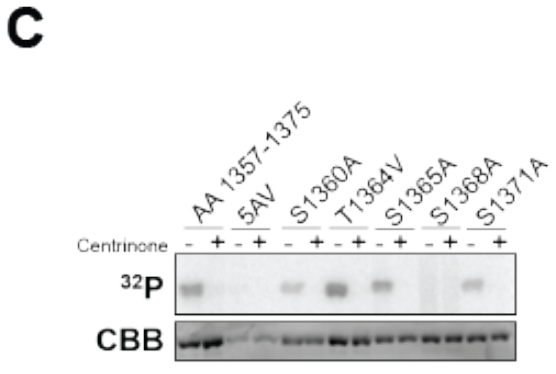
C
AA 1357-1375
5AV
S1360A
T1364V
S1365A
S1368A
S1371A
Centrinone
32P
CBB

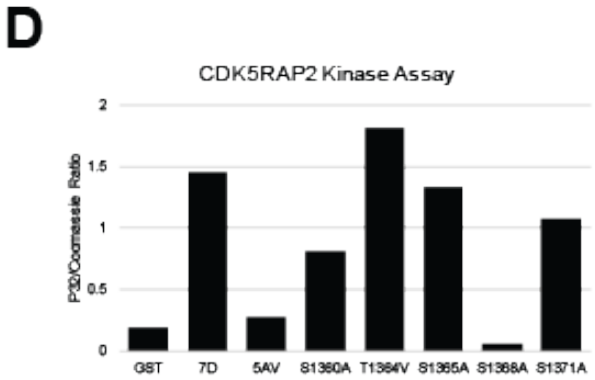
D
CDK5RAP2 Kinase Assay
P32/Coomassie Ratio
2
1.5
1
0.5
0
GST
7D
5AV
S1360A
T1364V
S1365A
S1368A
S1371A

Appendix E. Centrosome amplification occurs in circulating tumor cells from metastatic cancer patients.

The following individuals contributed to the work in this Appendix:

Ashok Singh

Jamie M. Sperger

Josh M. Lang

ABSTRACT

Metastatic cancer remains largely incurable and accounts for at least 90% of cancer-related mortality. Circulating tumor cells (CTCs) are a rare population of tumor cells released into peripheral circulation from primary and metastatic tumor sites that may both contribute to the development of metastatic disease and reflect the heterogeneity that likely exists between various tumor deposits. Centrosome amplification (CA), or a numerical increase in centrosomes, has been reported in virtually all human cancers and has been shown to make cells more invasive. We therefore hypothesized that CTCs are more likely to have CA than the primary tumor from which they are derived. There have been no reports of CA or description of centrosomes in CTCs. In this study, we develop an assay to detect CA in CTCs. We find that CA is prevalent in CTCs from metastatic breast, prostate, and lung cancer patients. Future work will assess whether CA in CTCs is a prognostic and/or predictive biomarker (e.g. for response to taxanes). Furthermore, we will compare CA in CTCs to the matched primary tumor tissue from that patient.

INTRODUCTION

Despite major advances in understanding the genetic, molecular, and cellular underpinnings of human cancer, metastatic disease remains largely incurable and accounts for at least 90% of cancer-related mortality.

Circulating tumor cells (CTCs) are a rare population of tumor cells released into peripheral circulation from primary and metastatic tumor sites that may both contribute to the development of metastatic disease and reflect the heterogeneity that likely exists between various tumor deposits.[500] Further, the number of CTCs in peripheral blood has been shown to have prognostic information in both early and advanced disease,[501,502] and these cells are thought to be at least in part responsible for metastasis and resistance to chemotherapy.[503,504] Specific to prostate cancer, number of CTCs in metastatic hormone sensitive prostate cancer predicts duration of androgen responsiveness.[505] Despite advances in detection and treatment strategies, most cancer-related deaths are due to metastatic growth. Therefore, it is important to learn more about CTCs and their potential predictive information.

Genomic instability and evolution of cancers is linked to chemotherapy sensitivity and resistance in patients with metastatic cancer. Taxane-based chemotherapies have been shown to promote chromosomal instability (CIN) by increasing multipolar mitoses. Breast tumors with CIN are more sensitive to paclitaxel compared to tumors without CIN. There is a critical need for new biomarkers focused on biological evaluation of mechanisms of response and resistance to chemotherapies in metastatic cancer. Centrosome amplification (CA) is a common mechanism that increases CIN in cancer. CA is a numerical increase in centrosomes and has been reported in virtually all human tumors.[107] CA increases the frequency of multipolar cell divisions and

merotelic attachments, leading to aneuploidy and chromosomal instability (CIN) [506]. Furthermore, CA makes cells more invasive.[126]

There have been no reports of CA or description of centrosomes in CTCs. In this study, we develop an assay to detect CA in CTCs that may serve as a minimally invasive tool to evaluate sensitivity to taxane-based chemotherapies.

MATERIALS AND METHODS

Isolation of circulating tumor cells

Blood samples from patients with metastatic breast and prostate cancer were collected and processed for nucleated cells using a Ficoll gradient and magnetic depletion of CD45-positive cells. EpCAM-positive CTCs were captured using an exclusion-based sample preparation technology known as the VERSA (Versatile Exclusion-based Rare Sample Analysis) platform.[507] CTCs were defined as cells positive for Hoechst, cytokeratin and negative for multiple immune and endothelial cell markers (CD45/CD11b/CD14 and CD34). EpCAM-captured CTCs cells were also stained with pericentrin and centrin to identify CA and evaluated for pericentrin (whole centrosome marker) and centrin (centriole marker) protein staining intensity, number and size.

Cell Culture

RPE1 doxycycline-inducible PLK4 cell lines were kindly provided by Dr. David Pellman (Harvard). RPE-1-derived cell lines were grown in a 1:1 mixture of DMEM and Ham's F-12 medium supplemented with 2.5 mm l-glutamine, with 10% fetal bovine serum and 100 units/mL penicillin-streptomycin. Cells were treated with 2 µg/mL doxycycline (Fisher, BP26531) for 24 hours, then captured with the VERSA device as described above.

Immunofluorescence

For analysis of centrioles, CTCs were captured by exclusion of CD45+ cells and inclusion of EPCAM+ cells, then cells were cytospun (1000g for 5 minutes) onto number 1.5, 13mm coverslips pre-treated with poly-L-lysine (1mg/mL poly-L-lysine, Sigma, for 1 hour, then washed 5 times with deionized water and allowed to dry) and fixed with 100% ice-cold methanol

for 15 minutes. Fixed cells were then blocked for 30 minutes in 3% bovine serum albumin (BSA) and 0.1% triton X-100 in PBS (PBSTx + BSA). Primary antibodies were incubated in PBSTx + BSA for 1 hour at room temperature and washed three times in PBSTx, followed by secondary antibody incubation in PBSTx + BSA for 30 minutes at room temperature and two washes with PBSTx. Cells were counterstained with DAPI and mounted on glass slides with Prolong Gold antifade medium (Invitrogen). Cells were stained for centrin (Millipore, 04-1624, 1:500), pan-cytokeratin, CD14, CD34, CD45, CD116. Alexa Fluor-conjugated secondary antibodies were used at 1:350 (Invitrogen). Cells were counted as CTCs if they exceeded a pre-set threshold for cytokeratins and fell below a pre-set threshold for the dump channel (combination of CD14, CD34, CD45, CD116).

Statistical Analysis

Assuming an average of 1.8 and standard deviation of 0.8 from previous data,[109] to detect a difference between 1.8 and 2.5 centrosomes/cell in primary tumor and CTCs, respectively, a sample size of 21 patients is needed.

RESULTS

To validate our method of capturing CTCs and staining centrioles, we utilized an RPE1 cell line with doxycycline-inducible PLK4. PLK4 is the master regulator of centriole duplication, and overexpression causes CA. We harvested these cells by capturing Epcam-positive cells and excluding CD45-positive cells using the VERSA technology. Half of the cells were kept in the VERSA device for staining for pericentrin; the other half of the cells were cytospun onto coverslips for centriole analysis. We quantified the number of pericentrin foci per cell, the pericentrin intensity per cell, and the size of the pericentrin foci per cell. Furthermore, we demonstrated that the number of centrioles is correlated positively and significantly with pericentrin intensity (Figure E-1).

CA was detected in a subset of CTCs from patients with metastatic breast, prostate, and lung cancer patients (Figure E-2). As a control, centrosomes were also analyzed in matched peripheral blood mononuclear cells from the same patients. CA was heterogeneous with 100% of patients demonstrating some degree of CA (>4 centrioles), ranging from 15-48% of CTCs.

DISCUSSION

Evidence for or against CA being more prevalent in metastatic foci versus primary tumor. In Suit-2 human pancreatic carcinoma cell xenograft into nude mice, CA is more prevalent in metastatic foci than the original xenograft.[508]

In conclusion, we report the presence of CA in EpCAM-captured CTCs from metastatic cancer patients. Evaluation of CA in CTCs using pericentrin and centrin staining may serve as a predictive biomarker of taxane based chemotherapy response and resistance. We are recruiting taxane-naïve metastatic cancer patients to test the hypothesis that CA and/or CIN predict taxane sensitivity.

Figure E-1. Validation of method to quantify centrosome amplification.

(A) RPE1 cells with doxycycline-inducible PLK4 were captured with the VERSA chip. Representative images of RPE cells are shown. **(B)** Quantification of the number of pericentrin foci per cell. **(C)** Quantification of the pericentrin intensity in each cell. **(D)** Quantification of centrosome size. **(E)** Quantification of the number of centrin foci in RPE cells after cytospinning and staining. **(F)** Correlation of pericentrin intensity with centriole number (centrin foci) in RPE cells after cytospinning and staining. Each dot represents a single cell. Bars represent means ± SD.

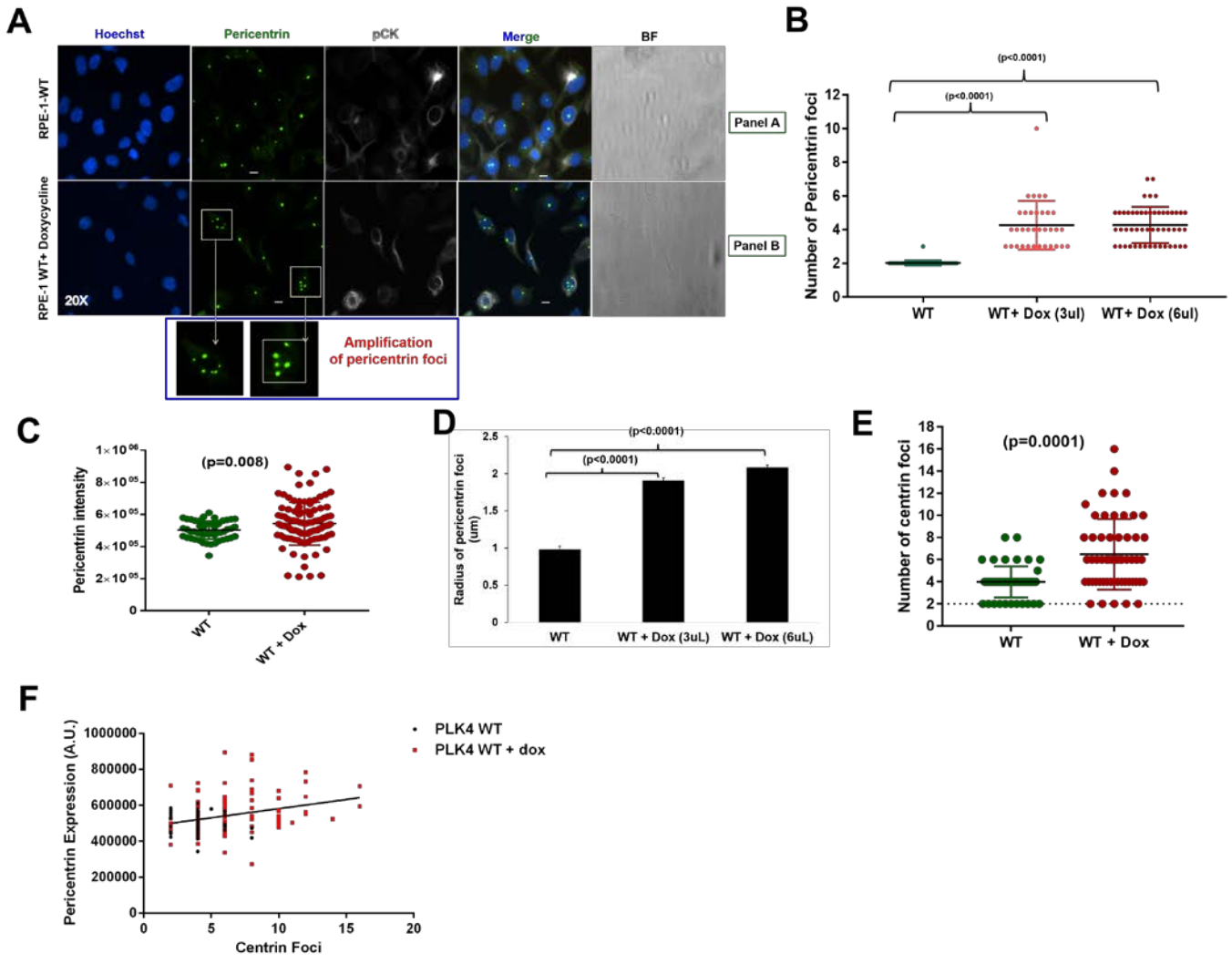

Figure E-2. Analysis of centrioles in circulating tumor cells.

Quantification of centrioles in non-CTCs versus CTCs in each patient analyzed. BC = breast cancer; PC = prostate cancer; LC = lung cancer. Each number represents a different patient.